PROCEEDINGS

of the

Eighth International Conference on the Ultrasonic Measurement and Imaging of Tissue Elasticity©

Vlissingen, Zeeland, The Netherlands
September 14 – 17, 2009

PROCEEDINGS

of the
Eighth International Conference
on the Ultrasonic Measurement and Imaging
of Tissue Elasticity©

Vlissingen, Zeeland, The Netherlands
September 14 – 17, 2009

Table of Contents

QUESTIONS OR COMMENTS ARE WELCOME AT ANY TIME AT <elasticity.conference@uth.tmc.edu>

WELCOME

Dear Conference Delegate:

It is a great pleasure to welcome to Vlissingen all scientific participants, exhibitors, spouses and guests of the Eighth International Conference on the Ultrasonic Measurement and Imaging of Tissue Elasticity©. This is the third time that the meeting is being held outside the United States, and, based on the number of participants, you are greatly supporting this initiative. We are delighted that so many of you have chosen to attend the meeting, share your latest findings and discuss the future of this exciting field of research. We hope that our choice of venue, Hotel Westduin in the Province of Zeeland will provide you an exciting flavor of the Netherlands. It was chosen for its attractive seaside location, and its facilities are excellent for stimulating interaction among the delegates. Zeeland is located in the southwest of the Netherlands and is famous for its battle against the sea. In 1953, a large part of the islands were flooded. To prevent future flooding, the 'Deltaworks', an ensemble of dunes, dikes, dams and other ingenious construction, was build. The 'Oosterschelde Kering' is the most famous dam preserving tidal movement in the Oosterschelde.

Vlissingen is a harbor city with long history. In the 16th century, ships of the 'Vereenigde Oostindische Compagnie' (VOC) sailed from this harbor for the East. Furthermore, the famous Dutch Admiral Michiel de Ruijter was born here. Wednesday night might be a nice opportunity to visit to the harbor site with its many restaurants. To help you explore the area, which has much to offer in terms of history and culture, the Tourists' Information Office (VVV) will have a "Tourists' Briefing" in the Westduin Hotel on Tuesday, September 15 at 9:00 am to which all delegates and guests are warmly invited. The Dutch flavor is also reflected in the mug and bag that are collector's items since the first meeting in Niagara Falls.

I would also like to thank all members of the groups in Houston and Rochester for their hard work. We started the organization with a visit by Jonathan and Karen in September, 2008. From that first day, we had a very pleasant collaboration to achieve our goal: together organizing the best International Tissue Elasticity Conference ever.

As always, there are no parallel sessions to increase interaction among the delegates. Due to the large number of papers, timing will be very tight for presentations and refreshment breaks. Especially to benefit the new format of the Formal Poster Session, we will keep the time allotted for the presentations very strict. So, please, be prepared for methods that go far beyond the usual colored light indicators on the podium.

Without the help of my "Dream-Team" at the Clinical Physics Laboratory, it would never have been possible to organize this meeting. First of all, I would like to thank Sonja van de Ven for her great help; Han Thijssen for his enthusiastic support and hosting Jonathan and Karen; Jan Menssen and Gert Weijers for handling the AV; Maartje Nillesen and Han Thijssen for their musical input; and Rik and Richard for their…?

I hope that you will enjoy a walk along the beach or a cultural visit to Vlissingen or Middelburg. Finally, thank you all for coming. Have a wonderful, beneficial experience and, when the time comes, a safe journey home!

Chris L. de Korte
Chair of the Local Organizing Team
14 September 2009

FOREWORD

Dear Conference Delegate:
Welcome to the 8th annual International Conference on the Ultrasonic Measurement and Imaging of Tissue Elasticity©.

The international participation in the Conference includes virtually all global entities engaged in research, development, commercialization and practice in the field. This year, the meeting is hosted by Dr Chris de Korte from the Radboud University Nijmegen Medical Center, the Netherlands, and takes place on the North Sea coast of Zeeland at the Golden Tulip Westduin Hotel in Vlissingen.

Last year's Conference feedback was again unanimous in the desire for continuation of the tutorial series. We are pleased that Drs. Tim Hall (USA) and Ralph Sinkus (France) have agreed to present this year's exciting tutorials on the basic science and instrumentation that are involved in imaging the elastic properties of tissue, geared primarily for clinicians. We are also continuing last year's popular format of the formal Poster Session, where each presenter has the opportunity to give a brief oral summary of his/her poster, and we thank Drs. Chris de Korte (the Netherlands) and Edoardo Mazza (Switzerland) for their enthusiastic leadership in conducting this event.

This year we have made extra efforts to attract a rapidly growing number of clinicians who are users of novel elasticity imaging equipment. We will, for the first time, have three clinical sessions and one cardiovascular session.

Due to the generous sponsorship from Ultrasonix Medical Corporation of Vancouver, Canada, the Conference will deliver Student Best Paper certificates and cash awards to the authors of papers that have been judged as most meritorious by three independent review cycles. On Monday afternoon, we will have a special session where the eight finalists will present their abstracts. The final awardees will be announced during the Conference dinner on Tuesday evening.

We would like to thank all the delegates, reviewers and session chairs for their continuing support of the Conference. Special thanks are in order to our enthusiastic support staff that has worked above and beyond. Dr. Chris de Korte, the local host and Ms. Sonja van deVen, his assistant, and the members of his "Dream-Team" who have handled the many local organizational arrangements in the Netherlands. Jonathan and Karen would like to thank Dr. Han and Loes Thijssen for their wonderful hospitality during our planning trip to the Netherlands in 2008. On the USA side, Ms. Christina Andrews of the Conference Secretariat's office has handled the correspondence and budgets on the US side; Ms. Karen Ophir volunteered to design the Conference's artwork, publications and web site, organize the scientific program and edit all abstracts and compile the Conference Proceedings; Ms. Charlene Waldron for assisting Karen with the Proceedings; and Ms. Elizabeth Marshall has constantly updated the Conference web site.

The Conference is conducted under the joint auspices of the University of Rochester Center for Biomedical Ultrasound and the Ultrasonics Laboratory in the Department of Diagnostic and Interventional Imaging at the University of Texas Health Science Center at Houston. These organizations have contributed in personnel, equipment and financial support. Most direct funding for the Conference is derived from registration fees, and, with your continued support in abstract submissions and attendance, we are committed to improve and expand the Conference in the years to come. We appreciate your written and oral feedback that always helps us in planning for future Conferences.

We hope that you will enjoy this year's scientific and social programs as well as the Westduin Hotel and the local environment.

J. Ophir and K.J. Parker
Conference Organizers
Vlissingen, The Netherlands,
September 14, 2009

2009 SPONSORS

The Conference Organizers wish to express appreciation
to the following companies
for providing donations in support of this year's Conference:

Ultrasonix Medical Corporation

On the Cover:
Antique map of Vlissingen by J. Blaeu
Vlissingen – J.Blaeu, 1649.

Copper engraving
Size: 41 x 51.5cm (16 x 20.1 inches)

From: Novum Ac Magnum Theatrum Urbium Belgicae Liberae Ac Foederatae.
Amsterdam, J. Blaeu, 1649. (Koeman, Bl62)

CONFERENCE–AT–A–GLANCE

Eighth International Conference on the Ultrasonic Measurement and Imaging of Tissue Elasticity©
Golden Tulip Westduin – Vlissingen, Zeeland, The Netherlands September 14 – 17, 2009

Monday, September 14		**9:00A – 8:00P**	
9:00A – 12:00P	**Set Up:**	Oral Presenters load presentations (CD/jump drive)	Lecture Hall
		Poster Presenters set up presentations	Conf Rm 2 & Lecture Hall
		Exhibitors set up exhibits	Conference Room 2
9:00A – 8:00P		Registration Desk Open	Conference Foyer
11:00A – 8:00P	**Session EEX:**	Equipment Exhibit *(during breaks & Reception)*	Conference Room 2
12:00P – 2:00P	**Session TUT:**	**Tutorials: Clinically Oriented Phys & Instrumentation**	Lecture Hall
2:00P – 2:30P		*Coffee Break*	Conference Foyer
2:30P – 4:30P	**Session SAS:**	**Oral Presentations of Finalists for Student Awards Session**	
		Sponsored by Ultrasonix Medical Corporation	Lecture Hall
4:30P – 5:00P		*Recess*	
5:00P – 6:00P	**Session POS:**	**Poster Session – Live Oral Summaries**	Lecture Hall & Conf Rm 2
6:00P – 8:00P		*Opening Dinner Reception*	Conference Room 2 & Foyer
Tuesday, September 15		**7:00A – 10:00P**	
7:00A – 8:00A		*Group Breakfast*	Restaurant
7:00A – 5:00P		Registration Desk Open	Conference Foyer
8:00A – 5:00P	**Session POS:**	Posters	Conference Room 2
8:00A – 5:00P	**Session EEX:**	Equipment Exhibit	Conference Room 2
9:00A – 9:30A		*Tourist Information*	To be announced
8:00A – 8:15A		Opening Remarks	Lecture Hall
8:15A – 10:00A	**Session CAA–1:**	**Clinical and Animal Applications – I**	Lecture Hall
10:00A – 10:30A		*Coffee Break*	Conference Foyer
10:30A – 11:30A	**Session FIP:**	**Forward and Inverse Problems**	Lecture Hall
11:30A – 1:00P		*Group Lunch*	Restaurant
1:00P – 3:00P	**Session MIP–1:**	**Methods for Imaging Elastic Tissue Properties – I**	Lecture Hall
3:00P – 3:30P		*Coffee Break*	Conference Foyer
3:30P – 5:00P	**Session INS:**	**Instrumentation**	Lecture Hall
7:00P – 10:00P		*Conference Dinner & Musical Event*	Lecture Hall
Wednesday, September 16		**7:00A – 6:30P**	
7:00A – 8:15A		*Group Breakfast*	Restaurant
7:00A – 5:30P		Registration Desk Open	Conference Foyer
8:15A – 5:30P	**Session POS:**	Posters	Conference Room 2
8:15A – 5:30P	**Session EEX:**	Equipment Exhibit	Conference Room 2
8:15A – 10:00A	**Session CVE:**	**Cardiovascular Elasticity**	Lecture Hall
10:00A – 10:30A		*Coffee Break*	Conference Foyer
10:30A – 11:45A	**Session SIP–1:**	**Signal and Image Processing – I**	Lecture Hall
11:45A – 1:15P		*Group Lunch*	Restaurant
1:15P – 2:30P	**Session MPT–1:**	**Mechanical Properties of Tissues – I**	Lecture Hall
2:30P – 3:45P	**Session MIP–2:**	**Methods for Imaging Elastic Tissue Properties – II**	Lecture Hall
3:45P – 4:15P		*Coffee Break*	Conference Foyer
4:15P – 5:30P	**Session CAA–2:**	**Clinical and Animal Applications – II**	Lecture Hall
5:30P – 6:30P		Group Photo	To be announced
Thursday, September 17		**7:00A – 10:00P**	
7:00A – 8:00A		*Group Breakfast*	Restaurant
7:00A – 3:45P		Registration Desk Open	Conference Foyer
8:00A – 3:45P	**Session POS:**	Posters	Conference Room 2
8:00A – 3:45P	**Session EEX:**	Equipment Exhibit	Conference Room 2
8:00A – 9:45A	**Session MIP–3:**	**Methods for Imaging Elastic Tissue Properties – III**	Lecture Hall
9:45A – 10:15A		*Coffee Break*	Conference Foyer
10:15A – 11:45A	**Session CAA–3:**	**Clinical and Animal Applications – III**	Lecture Hall
11:45A – 1:15P		*Group Lunch*	Restaurant
1:15P – 2:15P	**Session MPT–2:**	**Mechanical Properties of Tissues – II**	Lecture Hall
2:15P – 3:15P	**Session SIP–2:**	**Signal and Image Processing – II**	Lecture Hall
3:15P – 3:45P		*Coffee Break*	Conference Foyer
3:45P – 5:15P	**Session MIP–4:**	**Methods for Imaging Elastic Tissue Properties – IV**	Lecture Hall
7:00P – 10:00P		*Closing Dinner Reception*	To be announced

PROGRAM

Eighth International Conference
on the Ultrasonic Measurement and Imaging
of Tissue Elasticity©

Vlissingen, Zeeland, The Netherlands
September 14–17, 2009

Monday, September 14 9:00A – 8:00P

9:00A – 12:00P Presentation & Exhibit Set Up

All Oral Presenters load presentations onto Conference computers (CD/jump drive) Lecture Hall
Poster Presenters set up presentations Conference Room 2 & Lecture Hall
Exhibitors set up exhibits Conference Room 2

9:00A – 8:00P

Registration Desk Open Conference Foyer

11:00A – 12:00P 2:00P – 2:30P 4:30P – 5:00P 6:00P – 8:00P
Session EEX: Equipment Exhibit Conference Room 2

Monday 12:00P – 2:00P
Session TUT: Tutorials: Clinically Oriented Physics & Instrumentation

Chair: D Cosgrove, UK *Co-Chair: R Maurice, Canada* Lecture Hall

Page No.

12:00P – 12:45P

107 ELASTICITY IMAGING: TO BOLDLY MEASURE WHAT NO ONE HAS SHEARED BEFORE. 25
R Sinkus[1].*
[1]Laboratoire Ondes et Acoustique, ESPCI, Paris, FRANCE.

12:45P – 1:00P Discussion

1:00P – 1:45P

113 ELASTICITY IMAGING SYSTEMS: HOW DO THEY WORK AND WHERE ARE WE HEADED? 26
TJ Hall[1].*
[1]University of Wisconsin–Madison, Madison, WI, USA.

1:45P – 2:00P Discussion

2:00P – 2:30P

COFFEE BREAK Conference Foyer

Monday 2:30P – 4:30P
Session SAS: Oral Presentations of Finalists for Student Awards Session

Sponsored by Ultrasonix Medical Corporation, Vancouver, BC, Canada

Chair: KJ Parker, USA *Co-Chair: J Ophir, USA* Lecture Hall

Page No.

2:30P – 2:45P

016 RECENT CLINICAL RESULTS OF ACOUSTIC RADIATION FORCE IMPULSE IMAGING OF ABDOMINAL ABLATION. 27
DP Bradway[1], BJ Fahey[1], RC Nelson[1], GE Trahey[1].*
[1]Duke University, Durham, NC, USA.

2:45P – 3:00P

036 ON THE FEASIBILITY OF MONITORING CARDIAC HYPERTROPHY AND FIBROSIS USING BIPLANE ULTRASOUND STRAIN IMAGING. 28
RGP Lopata[1], MM Nillesen[1], L Kapusta[1], SK Singh[1], HB van Wetten[1], CN Verrijp[1], JAWN van der Laak[1], JM Thijssen[1], CL de Korte[1].*
[1]Radboud University Nijmegen Medical Center, Nijmegen, The NETHERLANDS.

3:00P – 3:15P

043 COMPLIANCE WEIGHTED IMAGING BASED ON HARMONIC SHEAR WAVE SCATTERING. 29
V Rengaraju[1,2], AFF da Silva[2], C Kargel[2], S Papazoglou[1], J Braun[1], I Sack[1].*
[1]Charité – University Medicine, Berlin, GERMANY; [2]Bundeswehr University, Munich, GERMANY.

3:15P – 3:30P

047 GENERATION AND TRACKING OF CIRCUMFERENTIALLY AND LONGITUDINALLY-PROPAGATING MECHANICAL WAVES USING A SINGLE TRANSDUCER: VASCULAR APPLICATIONS. 30
DM Dumont[1], ÁP Tierney[2], JJ Dahl[1], SJ Hsu[1], GE Trahey[1].*
[1]Duke University, Durham, NC, USA; [2] University of Limerick, Limerick, IRELAND.

3:30P – 3:45P

049 PARAMETRIC ANALYSIS OF MYOCARDIAL STIFFNESS CHANGES WITHIN THE CARDIAC CYCLE WITH ACOUSTIC RADIATION FORCE IMPULSE IMAGING. 31
SJ Hsu[1], PD Wolf[1], GE Trahey[1].*
[1]Duke University, Durham, NC, USA.

3:45P – 4:00P

057 REAL–TIME ELASTOGRAPHY OF THE BRAIN. 32
C Uff[1], L Garcia[1], J Fromageau[1], N Dorward[2], JC Bamber[1].*
[1]Institute of Cancer Research, Sutton, Surrey, England, UK; [2]Royal Free Hospital, London, England, UK.

4:00P – 4:15P

062 MEASURING MECHANICAL PROPERTIES OF GRAY AND WHITE MATTER *IN VIVO* USING MAGNETIC RESONANCE ELASTOGRAPHY. 33
AJ Pattison[1], SS Lollis[2], PR Perrinez[1], IM Perreard[2], MDJ McGarry[1], JB Weaver[1,2], KD Paulsen[1,3].*
[1]Dartmouth College, Hanover, NH, USA; [2]Dartmouth-Hitchcock Medical Center, Lebanon, NH, USA; [3]Norris Cotton Cancer Center, Lebanon, NH, USA.

4:15P – 4:30P

081 AUTOMATIC PROSTATE SEGMENTATION FROM TRANSRECTAL ULTRASOUND ELASTOGRAPHY IMAGES USING GEOMETRIC ACTIVE CONTOURS. 34
O Goksel[1], SE Salcudean[1].*
[1]University of British Columbia, Vancouver, BC, CANADA.

4:30P – 5:00P

Recess

Monday 5:00P – 6:00P

(Posters will be available for viewing and Coffee Break Discussion through Thursday, September 17, 3:45P)

Session POS: Poster Session – Live Oral Summaries

Chair: CL de Korte, The Netherlands *Co-Chair: E Mazza, Switzerland* Lecture Hall

5:00P – 5:02P

003 DEVELOPMENT OF A WEIGHTING SCHEME FOR STRAIN ESTIMATION. 35
L Chen[1], RJ Housden[1], GM Treece[1], AH Gee[1], RW Prager[1].*
[1]University of Cambridge, Cambridge, England, UK.

5:02P – 5:04P

022 BLOOD VESSEL STRAIN IMAGING USING LINEAR ARRAY TRANSDUCER WITH STEERING. 36
DK Ahn[1], MK Jeong[1], SJ Kwon[1], MH Bae[2].*
[1]Daejin University, Pocheon, Gyeonggi, KOREA; [2]Hallym University, Chuncheon, Gangweon, KOREA.

(Session POS continues on next page)

5:04P – 5:06P

5:06P – 5:08P

5:08P – 5:10P

5:10P – 5:12P

5:12P – 5:14P

5:14P – 5:16P

5:16P – 5:18P

5:18P – 5:20P

5:20P – 5:22P

5:22P – 5:24P

106 REAL TIME ULTRASOUND BREAST ELASTOGRAPHY – CLINICAL EXPERIENCE WITH DIFFERENT ULTRASOUND MANUFACTURERS' EQUIPMENT – WORK IN PROGRESS. 46
WE Svensson[1], R Williamson[1], N Zaman[1], L North[1], O Doryforou[1], S Putturaya[1].*
[1]Imperial College Healthcare NHS Trust, Charing Cross Hospital, London, England, UK.

5:24P – 5:26P

108 ELASTOGRAPHY ON GENERAL PURPOSE GRAPHICS PROCESSING UNIT (GPGPU) FOR REAL–TIME APPLICATIONS. 47
X Yang[1], S Deka[1], R Righetti[1].*
[1]Texas A&M University, College Station, TX, USA.

5:26P – 5:28P

109 PERFORMANCE ANALYSIS OF NEW LSE–BASED TIME CONSTANT ESTIMATORS FOR POROELASTOGRAPHY APPLICATIONS. 48
S Nair[1], TA Krouskop[2], R Righetti[1].*
[1]Texas A&M University, College Station, TX, USA; [2]National Center for Human Performance, Houston, TX, USA.

5:28P – 5:30P

110 THE FEASIBILITY OF USING ULTRASOUND ELASTOGRAPHY TECHNIQUES TO IMPROVE VISUALIZATION OF BONE STRUCTURE. 49
B Parmar[1], R Righetti[1], E Tasciotti[2], M Ferrari[2].*
[1]Texas A&M University, College Station, TX, USA; [2]The University of Texas Health Science Center at Houston, Houston, TX, USA.

5:30P – 5:32P

114 AXIAL–SHEAR STRAIN DISTRIBUTIONS IN BEEF MUSCLE SAMPLES UNDER LOAD: AN *IN VITRO* STUDY. 50
A Thitai Kumar[1], B Galaz[1], R Miller[2], J Ophir[1].*
[1]The University of Texas Health Science Center at Houston, Houston, TX, USA; [2]Texas A&M University, College Station, TX, USA.

040 IMPROVEMENT OF STRAIN UNIFORMITIES IN ELASTOGRAPHY BY INSERTION OF DAMPER. 51
T Sato[1], S Sato[1], Y Watanabe[1], S Goka[1], H Sekimoto[1].*
[1]Tokyo Metropolitan University, Hachioji, Tokyo, JAPAN.

087 2ND REPORT ON PROPER POINT SPREAD FUNCTION FOR LATERAL MODULATION. 52
C Sumi[1], K Shimizu[1], Y Takanashi[1], Y Tadokoro[1], Y Nozaki[1].*
[1]Sophia University, Chiyodaku, Tokyo, JAPAN.

105 IS REAL–TIME ELASTOGRAPHY TARGETED BIOPSY ABLE TO ENHANCE PROSTATE CANCER DETECTION? ANALYSIS OF DETECTION RATE BASED ON AN ELASTICITY SCORING SYSTEM. 53
L Pallwein[1], F Aigner[1], R Faschingbauer[1], E Pallwein[1], G Pinggera[1], G Bartsch[1], G Schaefer[1], P Struve[1], F Pedross[1], W Jaschke[1], F Frauscher[1].*
[1]Medical University Innsbruck, AUSTRIA.

5:32P – 6:00P **Discussion**

Monday 6:00P – 8:00P

Opening Dinner Reception *Proceedings Book Signing* Conference Room 2 & Foyer

Tuesday, September 15 7:00A – 10:00P

7:00A – 8:00A
GROUP BREAKFAST — Restaurant

7:00A – 5:00P
Registration Desk Open — Conference Foyer

8:00A – 5:00P **Session POS: Posters** — Conference Room 2
Session EEX: Equipment Exhibit — Conference Room 2

9:00A – 9:30A *Tourist Information* — To Be Announced

Tuesday 8:00A – 8:15A
OPENING REMARKS
KJ Parker, J Ophir, CL de Korte — Lecture Hall

Tuesday 8:15A – 10:00A
Session CAA–1: Clinical and Animal Applications – I
Chair: D Cosgrove, UK *Co-Chair: A Săftoiu, Romania* — Lecture Hall

* indicates Presenter

Page No.

9:45A – 10:00A

098 INTRAOPERATIVE CHARACTERIZATION OF THE MECHANICAL BEHAVIOR OF HUMAN LIVER. 60
M Hollenstein[1], M Jabareen[1,2], S Breitenstein[3], M Riener[3], PA Clavien[3], M Bajka[3], E Mazza[1].*
[1]Swiss Federal Institute of Technology, Zurich, SWITZERLAND; [2]Technion – Israel Institute of Technology, Haifa, ISRAEL; [3]University Hospital Zurich, Zurich, SWITZERLAND.

10:00A – 10:30A

COFFEE BREAK Conference Foyer

Tuesday 10:30A – 11:30A
Session FIP: Forward and Inverse Problems

Chair: I Sack, Germany *Co-Chair: T Alrefae, Kuwait* Lecture Hall

Page No.

10:30A – 10:45A

065 MODEL–BASED ESTIMATION OF WAVE SPEED FOR THE SCALAR WAVE EQUATION. 61
J Fehrenbach[1], V Miette[2], L Sandrin[2].*
[1]Institut de Mathematiques de Toulouse, Toulouse, FRANCE; [2]Echosens, Paris, FRANCE.

10:45A – 11:00A

010 VARIATIONAL MESH ADAPTION IN ELASTICITY IMAGING OF SOFT TISSUE. 62
A Arnold[1], OT Bruhns[1], J Mosler[2].*
[1]Ruhr–University Bochum, Bochum, GERMANY; [2]GKSS Research Centre Geesthacht, Geesthacht, GERMANY.

11:00A – 11:15A

061 THE EFFECTS OF THE BOUNDARY CONDITIONS AND SHAPE OF EXCITATION ON THE PHASE SPEED AND INVERSE PROBLEM SOLUTION. 63
A Baghani[1], SE Salcudean[1], R Rohling[1].*
[1]University of British Columbia, Vancouver, BC, CANADA.

11:15A – 11:30A

030 LINEAR ELASTIC MATERIAL RECONSTRUCTIONS OF NON–LINEARLY ELASTIC MRE PHANTOMS. 64
IM Perreard[1], AJ Pattison[2], MDJ McGarry[2], PR Perrinez[2], Z Barani[3], EEW Van Houten[3], JB Weaver[1], KD Paulsen[2].*
[1]Dartmouth–Hitchcock Medical Center, Lebanon, NH, USA; [2]Dartmouth College, Hanover, NH USA; [3]University of Canterbury, Christchurch, NEW ZEALAND.

11:30A – 1:00P

GROUP LUNCH Restaurant

Tuesday 1:00P – 3:00P
Session MIP–1: Methods for Imaging Elastic Tissue Properties – I

Chair: L Sandrin, France *Co-Chair: SA McAleavey, USA* Lecture Hall

Page No.

1:00P – 1:15P

017 ACCURACY OF ENDOSCOPIC ULTRASOUND ELASTOGRAPHY USED FOR THE DIFFERENTIAL DIAGNOSIS OF CHRONIC PANCREATITIS AND PANCREATIC CANCER: A MULTICENTRIC STUDY. 65
A Săftoiu[1], P Vilmann[2], F Gorunescu[1], U Will[3], M Giovannini[4], J Janssen[5], J Iglesias–Garcia[6], P Arcidiacono[7], M Hocke[8], C McKay[9], DI Gheonea[1].*
[1]University of Medicine and Pharmacy Craiova, Dolj, ROMÂNIA; [2]Gentofte University Hospital, Hellerup, DENMARK; [3]SRH Wald–Klinikum, Gera, GERMANY; [4]Paoli–Calmettes Institut, Marseilles, FRANCE; [5]HELIOS Klinikum, Wuppertal, GERMANY; [6]University Hospital, Santiago de Compostela, SPAIN; [7]University Vita–Salute San Raffaele, Milan, ITALY; [8]Friedrich–Schiller University, Jena, GERMANY; [9]Glasgow Royal Infirmary, Glasgow, Scotland, UK.

(Session MIP–1 continues on next page)

(Session MIP–1 continued from previous page) Page No.

1:15P – 1:30P

002 A HYBRID DISPLACEMENT ESTIMATION METHOD FOR STRAIN IMAGING. 66
L Chen[1], RJ Housden[1], GM Treece[1], AH Gee[1], RW Prager[1].*
[1]University of Cambridge, Cambridge, England, UK.

1:30P – 1:45P

013 ELASTICITY MAP RECONSTRUCTION OF ATHEROSCLEROTIC PLAQUES BASED ON A SEGMENTATION–DRIVEN OPTIMIZATION PROCEDURE USING STRAIN MEASUREMENTS. 67
J Ohayon[1,3], S Le Floc'h[1], P Tracqui[1], G Finet[2], AM Gharib[3], RL Maurice[4], G Cloutier[4], RI Pettigrew[3].*
[1]DynaCell, Grenoble, FRANCE; [2]INSERM, Lyon, FRANCE; [3]NIDDK, NIH, Bethesda, MD, USA; [4]University of Montréal Hospital Research Center, Montréal, Québec, CANADA.

1:45P – 2:00P

014 SIGNATURES OF MULTIPLE SHEAR WAVE SCATTERING IN BRAIN MRE WAVE IMAGES. 68
S Papazoglou[1], D Klatt[1], J Braun[1], I Sack[1].*
[1]Charité Berlin, Berlin, GERMANY.

2:00P – 2:15P

028 ESTIMATION OF DISPLACEMENT WAVEFORMS WITH TRANSIENT MR ELASTOGRAPHY. 69
R Souchon[1], R Salomir[1], D Lyonnet[2], JY Chapelon[1], O Rouvière[1,2].*
[1]INSERM, Lyon, FRANCE; [2]Hôpital E. Herriot, Lyon, FRANCE.

2:15P – 2:30P

032 NON INVASIVE ASSESSMENT OF COMPARTMENT PRESSURES BY ULTRASOUND: AN *IN VITRO* MODEL. 70
RM Sellei[1], SJ Hingmann[1], M Knobe[1], M de la Fuente[2], F Schmidt[2], K Radermacher[2], HC Pape[1].*
[1]University Hospital RWTH Aachen, Aachen, GERMANY; [2]Helmholtz Institute for Biomedical Engineering, Aachen, GERMANY.

2:30P – 2:45P

079 ELASTIC MODULUS IMAGING (EMI) FOR VISUALIZING THERMAL ABLATION ZONE: INITIAL EXPERIENCE IN A PORCINE MODEL. 71
J Jiang[1], C Brace[1], A Andreano[1], R DeWall[1], N Rubert[1], T Varghese[1], F Lee, Jr[1], TJ Hall[1].*
[1]University of Wisconsin–Madison, Madison, WI, USA

2:45P – 3:00P

037 PERFORMANCE OF RF–BASED 2D STRAIN IMAGING TECHNIQUES IN DEFORMING STRUCTURES WITH LARGE SHEARING AND ROTATIONAL MOVEMENT. 72
RGP Lopata[1], MM Nillesen[1], HHG Hansen[1], JM Thijssen[1], CL de Korte[1].*
[1]Radboud University Nijmegen Medical Center, Nijmegen, The NETHERLANDS.

3:00P – 3:30P

COFFEE BREAK Conference Foyer

Tuesday 3:30P – 5:00P
Session INS: Instrumentation

Chair: V Egorov, USA *Co-Chair: R Souchon, France* Lecture Hall

Page No.

3:30P – 3:45P

001 QUANTIFYING ACOUSTIC RADIATION FORCE IMPULSE-INDUCED DYNAMICS THROUGH OPTICAL METHODS: EXPERIMENTAL AND SIMULATION RESULTS. 73
RR Bouchard[1], JE Streeter[2,3], ML Palmeri[1], PA Dayton[2,3].*
[1]Duke University, Durham, NC, USA; [2]University of North Carolina at Chapel Hill, [3]North Carolina State University, Chapel Hill, NC, USA.

* *indicates Presenter*

Page No.

3:45P – 4:00P

038 3D RADIATION DOSIMETRY: DOSE READ–OUT OF GELS WITH SHEAR WAVE ELASTOGRAPHY. 74
RA Crescenti[1], JC Bamber[1], NL Bush[1], S Webb[1].*
[1]Institute of Cancer Research and Royal Marsden NHS Foundation Trust, Sutton, Surrey, UK.

4:00P – 4:15P

053 PHYSICAL BASIS FOR TYPICAL ELASTOGRAPHIC APPEARANCE OF CYSTIC LESIONS – PHANTOM BASED ANALYSIS. 75
K Kumar[1], [illegible][1], V Jayashankar[1], S Suresh[2], AK Mishra[1].*
[1]Indian Institute of Technology Madras, Chennai, Tamilnadu, INDIA, [2]Mediscan Systems, Chennai, Tamilnadu, INDIA.

CANCELLED

4:15P – 4:30P

060 A HIGH FRAME RATE ULTRASOUND SYSTEM FOR THE STUDY OF TISSUE MOTIONS. 76
A Baghani[1], SE Salcudean[1], R Rohling[1].*
[1]University of British Columbia, Vancouver, BC, CANADA.

4:30P – 4:45P

078 IMPROVED 2D MOTION TRACKING FOR ELASTOGRAPHY USING DUAL TRANSDUCERS. 77
JM Abeysekera[1], R Rohling[1].*
[1]University of British Columbia, Vancouver, British Columbia, CANADA.

4:45P – 5:00P

094 SIMULTANEOUS ULTRASOUND B–MODE IMAGING AND ELASTICITY MEASUREMENT USING VIBRATION BASED ON A CONVENTIONAL ULTRASOUND SCANNER. 78
YP Zheng[1], ZM Huang[1], YJ Zhou[1], JF He[1], JCW Cheung[1].*
[1]The Hong Kong Polytechnic University, Hong Kong, CHINA.

5:00P – 7:00P *No Conference Activities*

Tuesday 7:00P – 10:00P

Conference Dinner & Musical Event Lecture Hall
Proceedings Book Signing *Announcement of Student Best Paper Award Recipients*

Wednesday, September 16 7:00A – 6:30P

7:00A – 8:15A
GROUP BREAKFAST Restaurant

7:00A – 5:30P
Registration Desk Open Conference Foyer

8:15A – 5:30P **Session POS: Posters** Conference Room 2
Session EEX: Equipment Exhibit Conference Room 2

Wednesday 8:15A – 10:00A
Session CVE: Cardiovascular Elasticity

Chair: BS Garra, USA *Co-Chair: EE Konofagou, USA* Lecture Hall

Page No.

8:15A – 8:30A

009 A COMPENSATIVE MODEL FOR THE ANGLE DEPENDENCE OF MOTION ESTIMATES IN NON–INVASIVE VASCULAR ELASTOGRAPHY. 79
E Mercure[1], G Cloutier[1,2], RL Maurice[1,2].*
[1]University of Montréal Hospital Research Center, Montréal, Québec, CANADA; [2]University of Montréal, Montréal, Québec, CANADA.

(Session CVE continues on next page)

(Session CVE continued from previous page) Page No.

8:30A – 8:45A

039 LOCAL ARTERIAL STIFFNESS MEASUREMENT USING A HIGH FRAME RATE ULTRASOUND SYSTEM. 80
CZ Wang[1], YP Zheng[1].*
[1]Hong Kong Polytechnic University, Hong Kong, CHINA.

8:45A – 9:00A

041 3–D, HIGH VOLUME RATE, RAW AND DETECTED *IN VIVO* CARDIAC SPECKLE TRACKING: MOVEMENT TOWARDS OPTIMIZED STRAIN AND STRAIN RATE IMAGING. 81
BC Byram[1], G Holley[2], D Need[2], DM Giannantonio[1], GE Trahey[1].*
[1]Duke University, Durham, NC, USA; [2]Siemens Healthcare Sector, Mountain View, CA, USA.

9:00A – 9:15A

069 VALIDATION OF PULSE WAVE IMAGING (PWI) AS A QUANTITATIVE METHOD FOR MAPPING ARTERIAL ELASTICITY. 82
J Vappou[1], J Luo[1], EE Konofagou[1].*
[1]Columbia University, New York, NY, USA.

9:15A – 9:30A

064 *IN VIVO* DIFFERENTIATION OF MYOCARDIAL ABLATION LESIONS VIA A STIFFNESS RATIO WITH ACOUSTIC RADIATION FORCE IMPULSE IMAGING. 83
SA Eyerly[1], SJ Hsu[1], GE Trahey[1], PD Wolf[1].
[1]Duke University, Durham, NC, USA.

9:30A – 9:45A

103 MOTION TRACKING USING BINARY TECHNIQUES IN TMRI DATA. 84
T Alrefae[1], MD Alenezy[2].*
[1]Kuwait University, Khaldia, KUWAIT; [2]Universiy of Kansas, Lawrence, KS, USA.

9:45A – 10:00A

050 INCREASING THE ACCURACY OF NON–INVASIVE ESTIMATION OF SHEAR STRAIN IN THE ARTERIAL WALL. 85
T Idzenga[1], HHG Hansen[1], RGP Lopata[1], CL de Korte[1].*
[1]Radboud University Nijmegen Medical Center, Nijmegen, THE NETHERLANDS.

10:00A – 10:30A

COFFEE BREAK Conference Foyer

Wednesday 10:30A – 11:45A

Session SIP–1: Signal and Image Processing – I

Chair: GM Treece, UK *Co-Chair: JM Thijssen, The Netherlands* Lecture Hall

Page No.

10:30A – 10:45A

011 IMAGE REGISTRATION IN ELASTICITY IMAGING: A FEASABILITY STUDY. 86
A Costet[1], L Morris[2], WE Svensson[2], DW McRobbie[2].*
[1]Imperial College London, London, England, UK; [2]Imperial College Healthcare NHS Trust, London, England, UK.

10:45A – 11:00A

004 FREEHAND STRAIN IMAGE NORMALIZATION FOR CONVEX PROBES. 87
RJ Housden[1], AH Gee[1], GM Treece[1], RW Prager[1].*
[1]University of Cambridge, Cambridge, England, UK.

11:00A – 11:15A

019 METHODS FOR THE ESTIMATION OF SUB–SAMPLE MOTION USING DIGITIZED ULTRASOUND ECHO SIGNALS IN THREE DIMENSIONS. 88
R Zahiri–Azar[1], O Goksel[1], SE Salcudean[1].*
[1]The University of British Columbia, Vancouver, BC, CANADA.

* *indicates Presenter*

Page No.

11:15A – 11:30A

021 STRAIN IMAGING OF BREAST USING TWO LINEAR ARRAY TRANSDUCERS. 89
MK Jeong[1], SJ Kwon[1], MH Bae[2].*
[1]Daejin University, Pocheon, Gyeonggi, KOREA; [2]Hallym University, Chuncheon, Gangweon, KOREA.

11:30A – 11:45A

082 LIVE ESTIMATION AND VISUALIZATION OF 4D×3D ULTRASOUND MOTION VECTORS. 90
ER Pospisil[1], R Zahiri–Azar[1], R Rohling[1], SE Salcudean[1].*
[1]The University of British Columbia, Vancouver, BC, CANADA.

11:45A – 1:15P

GROUP LUNCH Restaurant

Wednesday 1:15P – 2:30P

Session MPT–1: Mechanical Properties of Tissues – I

Chair: G Cloutier, Canada *Co-Chair: R Sinkus, France* Lecture Hall

Page No.

1:15P – 1:30P

029 QUANTITATIVE CORNEA ELASTICITY MAPPING USING HIGH FREQUENCY SUPERSONIC SHEAR IMAGING. 91
M Tanter[1], JL Gennisson[1], D Touboul[3], TM Nguyen[1], J Bercoff[2], M Fink[1].*
[1]Laboratoire Ondes et Acoustique, ESPCI, Paris, FRANCE; [2]SuperSonic Imagine, Aix en Provence, FRANCE; [3]Hôpital Pellegrin, Bordeaux, FRANCE.

1:30P – 1:45P

096 BIAXIAL CHARACTERIZATION OF HUMAN FETAL MEMBRANES. 92
J Egger[1], A Mallik[2], C Haller[2], M Jabareen[3], A Zisch[2], E Mazza[1].*
[1]Swiss Federal Institute of Technology, Zurich, SWITZERLAND; [2]University Hospital, Zurich, SWITZERLAND; [3]Technion – Israel Institute of Technology, Haifa, ISRAEL.

1:45P – 2:00P

005 MEASURING THE NONLINEAR ELASTIC PROPERTIES OF LIVER TISSUES *IN VITRO* AND *EX VIVO*. 93
J Chenot[1,2], D Melodelima[1,2], JY Chapelon[1,2].*
[1]Inserm, U556, Lyon, FRANCE; [2]University of Lyon, Lyon, FRANCE.

2:00P – 2:15P

023 THERMAL EFFECTS ON MUSCULAR SHEAR MODULUS ASSESSED BY ULTRASOUND. 94
E Sapin[1], JL Gennisson[1], M Pernot[1], M Tanter[1], M Fink[1].*
[1]Laboratoire Ondes et Acoustique, ESPCI, Paris, FRANCE.

2:15P – 2:30P

093 MENSTRUAL CYCLE, SITE AND INDIVIDUAL DEPENDENCES OF BREAST ELASTICITY MEASURED *IN VIVO* USING ULTRASOUND INDENTATION. 95
JW Li[1], ST Chan[1], YP Huang[1], YP Zheng[1].*
[1]The Hong Kong Polytechnic University, Hong Kong, CHINA.

Wednesday 2:30P – 3:45P

Session MIP–2: Methods for Imaging Elastic Tissue Properties – II

Chair: TJ Hall, USA *Co-Chair: MM Doyley, USA* Lecture Hall

Page No.

2:30P – 2:45P

083 SHEAR MODULUS IMAGING OF LIVER USING SPATIALLY MODULATED ULTRASOUND RADIATION FORCE. 96
SA McAleavey[1], E Elegbe[1], M Menon[1].*
[1]University of Rochester, Rochester, NY, USA.

(Session MIP–2 continues on next page)

(Session MIP–2 continued from previous page) Page No.

2:45P – 3:00P

072 ON THE FEASIBILITY OF LONGITUDINAL WAVE VISCOELASTICITY IMAGING. 97
H Eskandari[1], A Baghani[1], SE Salcudean[1], R Rohling[1].*
[1]University of British Columbia, Vancouver, BC, CANADA.

3:00P – 3:15P

067 ON THE IMAGING OF SLIP BOUNDARIES USING 3D ELASTOGRAPHY. 98
L Garcia[1], C Uff[1], J Fromageau[1], J Bamber[1].*
[1]Institute of Cancer Research, Sutton, Surrey, England, UK.

3:15P – 3:30P

045 AXIAL–SHEAR STRAIN DISTRIBUTIONS IN AN ELLIPTICAL INCLUSION MODEL (PART I): A SIMULATION STUDY. 99
B Galaz[1], A Thitai Kumar[1], J Ophir[1].*
[1]The University of Texas Health Science Center Houston, Houston, TX, USA.

3:30P – 3:45P

046 AXIAL–SHEAR STRAIN DISTRIBUTIONS IN AN ELLIPTICAL INCLUSION MODEL (PART II): EXPERIMENTAL VALIDATION AND *IN VIVO* EXAMPLES WITH IMPLICATIONS TO BREAST TUMOR CLASSIFICATION. 100
A Thitai Kumar[1], B Galaz[1], J Ophir[1].*
[1]The University of Texas Health Science Center Houston, Houston, TX, USA.

3:45P – 4:15P

COFFEE BREAK Conference Foyer

Wednesday 4:15P – 5:30P

Session CAA–2: Clinical and Animal Applications – II

Chair: WE Svensson, UK *Co-Chair: H Feltovich, USA* Lecture Hall

Page No.

4:15P – 4:30P

044 DIFFERENTIATION OF BENIGN AND MALIGNANT BREAST LESIONS BY MECHANICAL IMAGING: CLINICAL RESULTS. 101
V Egorov[1], T Kearney[2], SB Pollak[3], C Rohatgi[4], N Sarvazyan[1], S Airapetian[1], S Browning[5], A Sarvazyan[1].*
[1]Artann Laboratories, Trenton, NJ, USA; [2]The Cancer Institute of New Jersey, New Brunswick, NJ, USA; [3]Mercy Medical Center, Rockville Centre, NY, USA; [4]The Breast Care Center & General Surgery Practice, Easton, PA, USA; [5]New Jersey Institute of Technology, University Heights, Newark, NJ, USA.

4:30P – 4:45P

008 VIBRO–ELASTOGRAPHY OF THE PROSTATE: METHOD EVALUATION. 102
SS Mahdavi[1], M Moradi[1], X Wen[1], WJ Morris[2], SE Salcudean[1].*
[1]University of British Columbia, Vancouver, BC, CANADA; [2]BC Cancer Agency, Vancouver, BC, CANADA.

4:45P – 5:00P

034 PERFORMANCE OF *EX VIVO* PROSTATE CANCER DETECTION USING 3D SONOELASTOGRAPHY. 103
B Castañeda[1,2], L An[2], J Yao[3], L Baxter[3], L Kushner[3], J Joseph[3], K Hoyt[4], J Strang[3], DJ Rubens[3], KJ Parker[2].*
[1]Pontificia Universidad Católica del Perú, Lima, PERÚ; [2]University of Rochester, Rochester, NY, USA; [3]University of Rochester Medical Center, Rochester, NY, USA; [4]University of Alabama at Birmingham, Birmingham, AL, USA.

5:00P – 5:15P

056 VIBROGRAPHY AND FREE HAND ELASTOGRAPHY FOR RESECTION OF GLIOMAS AND OTHER BRAIN TUMORS. 104
M Scholz[1], S Möller[1], J Thissen[1], C Löhnert[1], P Spangenberg[1], A Harders[1].*
[1]Ruhr–University Bochum, GERMANY.

* *indicates Presenter*

Page No.

5:15P – 5:30P

059 MONITORING DEMYELINATING PROCESSES BY HIGH RESOLUTION MAGNETIC RESONANCE ELASTOGRAPHY IN THE MOUSE BRAIN. 105
E Diguet[1], B Larrat[1], R Sinkus[1], M Fink[1].*
[1]Laboratoire Ondes et Acoustique, ESPCI, Paris, FRANCE.

Wednesday 5:30P – 6:30P

Group Photo TBA

After 6:30P *No Conference Activities*

Thursday, September 17 7:00A – 10:00P

7:00A – 8:00A
GROUP BREAKFAST Restaurant

7:00A – 3:45P
Registration Desk Open Conference Foyer

8:00A – 3:45P **Session POS: Posters** Conference Room 2
Session EEX: Equipment Exhibit Conference Room 2

Thursday 8:00A – 9:45A

Session MIP–3: Methods for Imaging Elastic Tissue Properties – III

Chair: JC Bamber, UK *Co-Chair: JL Gennisson, France* Lecture Hall

Page No.

8:00A – 8:15A

102 ARFI MEASUREMENTS ON THE HUMAN UTERINE CERVIX USING A NOVEL INTRACAVITARY TRANSDUCER. 106
H Feltovich[1], L Reusch[1], JJ Dahl[2], ML Palmeri[2], JM Harter[1], M Kliewer[1], TJ Hall[1].*
[1]University of Wisconsin–Madison, Madison, WI, USA; [2]Duke University, Durham, NC, USA.

8:15A – 8:30A

055 VALIDATION OF MAGNETIC RESONANCE ELASTOGRAPHY WITH DIRECT MECHANICAL MEASUREMENT. 107
P Debergue[1], P Latta[2], V Pazos[1], C Bowman[2].*
[1]National Research Council of Canada, Boucherville, Québec, CANADA; [2]National Research Council of Canada, Winnipeg, Manitoba, CANADA.

8:30A – 8:45A

068 DEMONSTRATING MAGNETIC OPTICAL COHERENCE ELASTOGRAPHY (M–OCE). 108
A Grimwood[1], L Garcia[2], J Bamber[2], Q Pankhurst[1], J Holmes[3].*
[1]Royal Institution of Great Britain, England, UK; [2]Institute of Cancer Research, Sutton, Surrey, England, UK; [3]Michelson Diagnostics Limited, Orpington, Kent, England, UK.

8:45A – 9:00A

070 DYNAMIC VISCOELASTIC PROPERTIES OF SOFT TISSUES MEASURED BY HARMONIC MOTION IMAGING (HMI): PRELIMINARY RESULTS OBTAINED ON NORMAL AND CANCEROUS BREAST TISSUES. 109
J Vappou[1], C Maleke[1], EE Konofagou[1].*
[1]Columbia University, New York, NY, USA.

9:00A – 9:15A

073 ITERAIVE RECONSTRUCTION OF TISSUE ELASTICITY AND VISCOSITY USING FINITE ELEMENTS. 110
H Eskandari[1], I Bell[1], SE Salcudean[1], R Rohling[1].*
[1]University of British Columbia, Vancouver, BC, CANADA.

(Session MIP–3 continues on next page)

(Session MIP–3 continued from previous page) Page No.

9:15A – 9:30A

018 THE ROLE OF REAL–TIME ELASTOGRAPHY IN THE NON–INVASIVE ASSESSMENT OF FIBROSIS IN DIFFUSE HEPATOPATHIES. 111
DI Gheonea[1], A Săftoiu[1], F Gorunescu[1], M Gorunescu[2], T Ciurea[1].*
[1]University of Medicine & Pharmacy, Craiova, Dolj, ROMÂNIA; [2]University of Craiova, Craiova, ROMÂNIA.

9:30A – 9:45A

024 ULTRASOUND TRANSIENT ELASTOGRAPHY OF THE BRAIN: AN *IN VIVO* FEASABILITY STUDY IN SMALL ANIMALS. 112
E Macé[1], I Cohen[2], JL Gennisson[1], R Miles[2], M Tanter[1], M Fink[1].*
[1]Laboratoire Ondes et Acoustique, ESPCI, Paris, FRANCE; [2]Cortex et Epilepsie, INSERM, Paris, FRANCE.

9:45A – 10:15A

COFFEE BREAK Conference Foyer

Thursday 10:15A – 11:45A

Session CAA–3: Clinical and Animal Applications – III

Chair: W Weitzel, USA *Co-Chair: M Szabunio, USA* Lecture Hall

Page No.

10:15A – 10:30A

015 INTRAVASCULAR ULTRASOUND PALPOGRAPHY AS AN IMAGING BIOMARKER IN CLINICAL TRIALS. 113
AFW van der Steen[1], JA Schaar[1], F Mastik[1], H Garcia[1], MG Danilouchkine[1], PW Serruys[1].*
[1]Erasmus Medical Center, Rotterdam, The NETHERLANDS.

10:30A – 10:45A

090 SONORHEOMETRY FOR CLINICAL ASSESSMENT OF HEMOSTASIS. 114
WF Walker[1,2], X Lin–Schmidt[1], FW Mauldin[1], MB Lawrence[1,2], F Viola[1,2].*
[1]University of Virginia, Charlottesville, VA, USA; [2]HemoSonics, Charlottesville, VA, USA.

10:45A – 11:00A

075 TUMOUR SIZE MEASUREMENT OF BREAST CANCER USING ULTRASOUND ELASTOGRAPHY: A CLINICAL STUDY. 115
J Li[1], JA Nob[illegible][1], Y Ch[illegible], RE English[2], RF Adams[2], V Paruleka[2], JE Baadwin[2].*
[1]University of Oxford, Oxford, England, UK; [2]Oxford Radcliffe Hospitals NHS Trust, Oxford, England, UK.

CANCELLED

11:00A – 11:15A

091 QUANTITATIVE VISUALIZATION OF MUSCLE MOTION USING ELASTOGRAPHY TECHNIQUE. 116
YJ Zhou[1], YP Zheng[1], JY Guo[1].*
[1]The Hong Kong Polytechnic University, Hong Kong, CHINA.

11:15A – 11:30A

097 MEASUREMENT OF THE MECHANICAL RESPONSE OF THE VAGINAL WALL. 117
B Röhrnbauer[1], M Bajka[2], C Betschart[2], D Peruncchini[2], D Fink[2], E Mazza[1], D Scheiner[2].*
[1]Swiss Federal Institute of Technology Zurich, Zurich, SWITZERLAND; [2]University Hospital of Zurich, Zurich, SWITZERLAND.

11:30A – 11:45A

048 CHARACTERIZATION OF STRAIN DURING SIMULATED ANGIOPLASTY USING ULTRASOUND ELASTOGRAPHY. 118
WF Weitzel[1], PP Patel[1], R Biswas[1], DW Park[1], TJ Cichonski[1], MS Richards[1], JM Rubin[1], SH Phan[1].*
[1]University of Michigan, Ann Arbor, MI, USA.

11:45A – 1:15P

GROUP LUNCH Restaurant

 ** indicates Presenter*

Thursday 1:15P – 2:15P
Session MPT–2: Mechanical Properties of Tissues – II

Chair: AFW van der Steen, The Netherlands Co-Chair: YP Zheng, China Lecture Hall

Page No.

1:15P – 1:30P

058 *IN VITRO* CHARACTERIZATION OF MECHANICAL PROPERTIES OF HUMAN MESENCHYMAL STEM CELLS BY TIME–RESOLVED ACOUSTIC MICROSCOPY. 119

C Hildebrandt[1], W Bost[1], H Thielecke[1], RM Lemor[1].*

[1]Fraunhofer Institut fuer Biomedizinische Technik, St. Ingbert, GERMANY.

1:30P – 1:45P

027 NON–INVASIVE LIVER FIBROSIS STAGING USING SUPERSONIC SHEAR IMAGING: A CLINICAL STUDY ON 150 PATIENTS. 120

E Bavu[1], JL Gennisson[1], BF Osmanski[2], J Bercoff[2], M Fink[1], V Mallet[3], P Sogni[3], A Vallet–Pichard[3], B Nalpas[3], M Tanter[1], S Pol[3].*

[1]Laboratoire Ondes et Acoustique, ESPCI, Paris, FRANCE; [2]SuperSonic Imagine, Aix en Provence, FRANCE; [3]Hôpital Cochin, Paris, FRANCE.

1:45P – 2:00P

099 CHANGES OF MECHANICAL PROPERTIES OF ARTICULAR CARTILAGE WITH ENZYMATICALLY–INDUCED DEGRADATION DETECTED USING AN OCT-BASED AIR JET INDENTATION *IN VITRO*. 121

SZ Wang[1], YP Huang[1], YP Zheng[1].*

[1]The Hong Kong Polytechnic University, Hong Kong, CHINA.

2:00P – 2:15P

100 *IN VIVO* MONITORING OF DIABETIC FOOT ULCER HEALING USING OCT AIR–JET INDENTATION. 122

CYL Chao[1,2], YP Zheng[2], YP Huang[2], GLY Cheing[2].*

[1]Queen Elizabeth Hospital, Hong Kong, CHINA; [2]The Hong Kong Polytechnic University, Hong Kong, CHINA.

Thursday 2:15P – 3:15P
Session SIP–2: Signal and Image Processing – II

Chair: SE Salcudean, Canada Co-Chair: WF Walker, USA Lecture Hall

Page No.

2:15P – 2:30P

071 THE IMPACT OF PHASE ENCODING ON LATERAL DISPLACEMENT ESTIMATES. 123

S Korukonda[1], MM Doyley[1].*

[1]University of Rochester, Rochester, NY, USA.

2:30P – 2:45P

086 APPLICATION OF 2D POLYNOMIAL FITTING TO BEAM STEERING FOR MOTION ESTIMATION WITH SUB–SAMPLE ACCURACY. 124

R Zahiri–Azar[1], O Goksel[1], SE Salcudean[1].*

[1]The University of British Columbia, Vancouver, BC, CANADA.

2:45P – 3:00P

088 PRELIMINARY EXPERIMENTS ON VIRTUAL SOURCE FOR LATERAL MODULATION. 125

C Sumi[1], N Matsui[1], K Shimizu[1], Y Takanashi[1].*

[1]Sophia University, Chiyodaku, Tokyo, JAPAN.

3:00P – 3:15P

095 COMPARATIVE ANALYSIS OF TWO COMPOUNDING TECHNIQUES FOR IVUS PALPOGRAPHY. 126

MG Danilouchkine[1], F Mastik[1], AFW van der Steen[1,2].*

[1]Erasmus Medical Center, Rotterdam, The NETHERLANDS; [2]Interuniversity Cardiology Institute of The Netherlands, Utrecht, The NETHERLANDS.

3:15P – 3:45P
COFFEE BREAK Conference Foyer

Thursday 3:45P – 5:15P
Session MIP–4: Methods for Imaging Elastic Tissue Properties – IV
Chair: A Sarvazyan, USA *Co-Chair: R Righetti, USA* Lecture Hall

Page No.

3:45P – 4:00P

042 STUDY OF CONTRAST DETAILS OF HETEROGENEOUS PHANTOMS BASED ON CRAWLING WAVE SONOELASTOGRAPHY. 127
L An[1], DJ Rubens[2], YT Cho[1], Z Hah[1], KJ Parker[1].*
[1]University of Rochester, Rochester, NY, USA; [2]University of Rochester Medical Center, Rochester, NY, USA.

4:00P – 4:15P

051 RADIATION FORCE INDUCED CRAWLING WAVES. 128
Z Hah[1], YT Cho[1], CR Hazard[2], DJ Rubens[1], KJ Parker[1].*
[1]University of Rochester, Rochester, NY, USA; [2]GE Global Research, Niskayuna, NY, USA.

4:15P – 4:30P

074 MEASURING THE EXTENT OF TIME–HARMONIC SHEAR DEFORMATION USING THE OCTAHEDRAL SHEAR STRAIN. 129
MDJ McGarry[1], EEW Van Houten[2], PR Perrinez[1], AJ Pattison[1], JB Weaver[1,3], KD Paulsen[1].*
[1]Dartmouth College, Hanover, NH, USA; [2]University of Canterbury, Christchurch, NEW ZEALAND; [3]Dartmouth–Hitchcock Medical Center, Lebanon, NH, USA.

4:30P – 4:45P

080 A ROBUST REAL–TIME SPECKLE TRACKING ALGORITHM FOR ULTRASONIC ELASTICITY IMAGING. 130
J Jiang[1], TJ Hall[1].*
[1]University of Wisconsin–Madison, Madison, WI, USA.

4:45P – 5:00P

076 HIGH QUALITY LATERAL STRAIN ESTIMATION USING TWO BEAM STEERING ANGLES. 131
HHG Hansen[1], RGP Lopata[1], T Idzenga[1], CL de Korte[1].*
[1]Radboud University Nijmegen Medical Center, Nijmegen, The NETHERLANDS.

5:00P – 5:15P

089 A STUDY ON REGULATION FOR RECONSTRUCTION OF PHYSICAL QUANTITIES – MECHANICAL SOURCE AND THERMAL SOURCE/PERFUSION. 132
C Sumi[1], Y Takanashi[1], K Shimizu[1], R Yamashita[1], Y Ishii[1].*
[1]Sophia University, Chiyodaku, Tokyo, JAPAN.

5:15P – 5:30P

Reprinted from 2008 Proceedings:

112 HEIGHT PROFILING AND DETERMINATION OF ELASTIC PROPERTIES OF LAYERED BIO–MATERIALS WITH VECTOR–CONTRAST SCANNING ACOUSTIC MICROSCOPY USING POLAR DIAGRAM IMAGE REPRESENTATION. 133
ET Ahmed Mohamed[1], A Kamanyi[1], M von Buttlar[1], R Wannemacher[1], K Hillmann[1], W Ngwa[2], W Grill[1].*
[1]University of Leipzig, Leipzig, Germany; [2]University of Central Florida, Orlando, FL, USA.

5:30P – 7:00P *No Conference Activities*

Thursday 7:00P – 10:00P
Closing Dinner Reception
Proceedings Book Signing TBA

Hitachi Medical Systems Ltd., Hitachi Medical Systems Europe Holding AG.
Kashiwa, JAPAN.

Kibero GmbH
Saarbruecken, Sarrland, GERMANY.

Siemens AG, Healthcare Sector
Erlangen, GERMANY.

AUTHOR INDEX

AUTHOR INDEX

Musical Events:

From Baroque to Rock-Pop:
A Time Warp

Maartje Nillesen (piano)
and
Johan Thijssen (recorders)

Maartje Nillesen *started playing piano when she was eight years old. During her school years, she started playing chamber music in a piano quartet. After finishing high school, she studied mathematics and music at the University of Leeds (UK) for one year. Returning to Holland, she continued studying piano at the School of Music in Groningen (NL) with Rob van Deinse.*
She also studied mathematics at the University of Groningen. Although playing the piano is still one of her favorite things, her professional career is dedicated to biomedical imaging, in which she is currently working on segmentation of echocardiographic images. Maartje also plays the viola and is a member of the Symphony Orchestra of Nijmegen and several chamber music ensembles.

Johan (Han) Thijssen *started recorder lessons in 1975. At first he preferred playing the Tenor recorder and later on he achieved the skills of playing also the Descant (soprano), Treble (alto) and Bass recorders. He formed an amateur ensemble of recorder players (4 to 7) and is still active in a recorder quartet presently. His music repertoire ranges from Renaissance to modern classical music and pop.*

Tonight's Program
Bits and pieces from

James Hook, England (1746-1827)
Sonata in G

Jean-Baptiste Loeillet, Belgium (1680-1730)
Sonata in F-dur, opus 2

A Song from The Beatles (1960-1970)

and a Musical Mystery Surprise...

ABSTRACTS

Eighth International Conference
on the Ultrasonic Measurement and Imaging
of Tissue Elasticity©
Vlissingen, Zeeland, The Netherlands
September 14 – 17, 2009

Session TUT: Tutorials: Clinically Oriented Physics & Instrumentation

Monday, September 14 12:00P – 2:00P

107 **ELASTICITY IMAGING: TO BOLDY MEASURE WHAT NO ONE HAS SHEARED BEFORE.**

R Sinkus[1].*
[1]Institut Langevin, CNRS UMR 7587, Univ. Paris 7, ESPCI Paristech, Laboratoire Ondes et Acoustique, 10 rue Vauquelin, 75005 Paris, FRANCE.

Elasticity imaging has gained significant interest in the medical community due to the availability of the required technology in the clinical environment.

Elasticity is the major physical parameter we experience from the very beginning of our life: we explore each object by touching and squeezing it in order to estimate its stiffness. Intuitively, we know that the more force we need in order to generate a certain amount of deformation, the stiffer we say the material is. This common sense idea is reflected in a basic physics law, i.e. in the Hookian law which states that the exerted pressure, σ, is proportional to the generated strain, ε, (relative deformation), i.e. $\sigma=E\varepsilon$ with E the Young's modulus.

Any general deformation can be decomposed in a **compressional part** where we try to change the volume of the material while maintaining its shape and a **shear part** where we try to change the shape of the material while maintaining its volume. Accordingly, we can attribute mechanical compressional and mechanical shear properties to each material. For instance, think about a balloon filled with water: the balloon's shape can easily be altered while it is impossible to change its volume. Since biological tissue consists of up to about 70% water, obviously tissue will behave similarly to water when examining its compressional properties. Therefore, we expect only little or no changes in terms of compressional properties when trying to differentiate tumors. However, by probing the shear properties of tissue, we examine the structural integrity of the solid matrix which is clearly altered in pathologies.
Therefore, elasticity imaging assesses the SHEAR properties via

1) the generation of mechanical waves/deformation on the surface or in the interior of the object,

and 2) the registration of the motion.

Let's start with the **static elastography** approach which uses a "quasi–static" deformation. Since it operates at 0Hz, there are no loss–effects involved. This advantage is counteracted by the fact that the resulting wavelength is quasi–infinite. Therefore, the wave "senses" the object in its totality, and boundary effects must be taken into account. This difficulty can be overcome by continuously vibrating at a finite frequency, for instance, 100Hz, which requires now loss–effects to be taken into account. Loss can be due to two effects:
a) true conversion of mechanical energy into heat and b) scattering.

This second effect leads to so–called **apparent viscosity**. It is important to realize that the measured values for stiffness and loss with this technique are independent of any *a priori* imposed mechanical (rheological) model.

A third approach to elasticity imaging measures the **shear wave speed** of a transient wave package consisting of several frequencies. However, speed is NOT a fundamental physical parameter but an effective parameter. Nature has added an additional complication: the mechanical properties of tissue also depend on the order of magnitude of displacement! Thus, when considering waves with amplitudes of ~1–100μm, all physical effects are so–called linear. When creating large deformations of the order of ~1mm, non–linear effects occur.

Altogether, elasticity imaging is a very rich field which is able to provide ABSOLUTE physical parameters to the physician in order to improve diagnosis.

113 **ELASTICITY IMAGING SYSTEMS: HOW DO THEY WORK AND WHERE ARE WE HEADED?**

TJ Hall[1]*.

[1]University of Wisconsin–Madison, Madison, WI, USA.

Efforts to estimate tissue elasticity using ultrasound have been under development for a few decades. Methods have progressed from simple M–mode data acquisition and simple motion tracking to sophisticated 3D/4D systems with quantitative estimates of elastic moduli on an absolute scale.

This presentation will parallel the joint tutorial on the physics of elasticity imaging (solid mechanics) by describing how each of the major elasticity imaging and non–imaging **systems** works and the kinds of information available from these approaches. This presentation also parallels last year's tutorial on "The Continuum of Elastic Responses from Compression to MRE" to illustrate the fact that the method of data acquisition affects the information available.

The **basic approach** for all ultrasound–based elasticity estimation methods is to acquire a map of anatomy before and after some type of tissue deformation. Therefore, fundamental to each approach is the method used for motion tracking. An overview of motion tracking will be provided along with relevant aspects of motion tracking for each elasticity imaging system (for example, the limitations in our ability to track motion). The clinical relevance of these methods and aspects will be highlighted.

This presentation will describe **representative examples** of each approach to ultrasound–based elasticity imaging or parameter estimation method. The goal of the tutorial is to inform the participants of the current state of the art in elasticity imaging and non–imaging systems and to provide a basic comparison with magnetic resonance elastography for reference. The presentation will conclude with some observations on current research.

016 **RECENT CLINICAL RESULTS OF ACOUSTIC RADIATION FORCE IMPULSE IMAGING OF ABDOMINAL ABLATION.**

David P. Bradway[1], Brian J. Fahey[1], Rendon C. Nelson[1], and Gregg E. Trahey[1].*
[1]Duke University, Durham, NC, USA.

Background: Radio–frequency (RF), cryo– and microwave ablation are minimally–invasive treatment options for malignant tissue in the liver or kidney. Ablative methods are often used for patients for whom surgical resection or other curative treatments are not feasible. Ablation planning, probe placement, procedure guidance and outcome assessment are performed under computed tomography (CT), magnetic resonance (MR) or ultrasound (US) imaging. In this work, we show recent results of using Acoustic Radiation Force Impulse (ARFI) imaging for abdominal ablations and liver lesion biopsies.

Aims: Demonstrate clinical utility of Acoustic Radiation Force Impulse (ARFI) imaging for use during abdominal ablation and liver lesion biopsy and describe recent developments in data processing.

Methods: To date, 33 cases have been completed, comprising 28 unique patients (15 male, 13 female) enrolled for image–guided liver biopsy (n=12), ablation of masses (n=17) or follow up appointments (n=4). Ablation patients were imaged immediately before or after their interventional procedures, which were performed under general anesthesia or conscious sedation. In addition to liver ablations, three cases of cryo–ablation of renal cell carcinoma have been included. For lesion biopsy cases, data were collected prior to biopsy. Also included were four follow–up cases of patients imaged during a previous ablation. The ultrasound scanner used in this study was a Siemens ACUSON AntaresTM Premium Edition (Siemens Medical Solutions, Ultrasound Division, Issaquah, WA, USA) that was modified for our research. A Siemens CH4–1 transducer was operated in the 2–3 MHz range and focused at depths ranging from 4–8 cm. All data were acquired during patient breath–hold (held inspiration) to decrease the impact of motion.

Results: In the ARFI images collected, primary liver tumors appear as relatively compliant structures surrounded by stiffer regional liver, whereas secondary liver tumors and thermal lesions appear as stiff regions of low displacement surrounded by more compliant regional liver tissue. Follow up cases suggest that ARFI may be a useful mechanism for early assessment of thermal lesions, while lesion biopsy cases demonstrate utility in lesion screening and biopsy guidance. Images from a typical case shown in Figure 1 include a lesion before RF ablation and a different thermal lesion that was ablated previously.

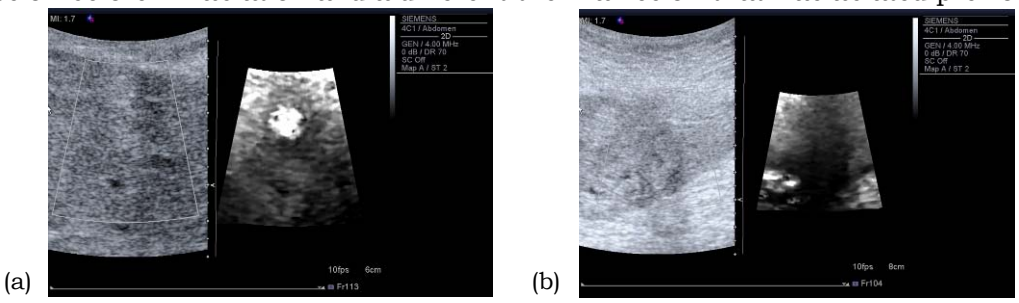

Figure 1: Results from a typical case are shown. In each image, matched B–mode (left) and ARFI displacement images (right) appear. (a) before RF ablation, a shallow liver lesion displayed a soft center and stiff capsule. (b) shows a deeper thermal lesion that was induced during a previous RFA procedure in the same patient The thermal lesion appeared extremely stiff, consistent with previous results.

Conclusions: Large displacement contrast was observed in ARFI images of both pre-ablation malignancies and post–ablation thermal lesions. Further investigations are required, but results are encouraging and demonstrate the clinical utility of the ARFI imaging method for use with abdominal ablation and liver lesion biopsy [1,2].

Acknowledgements: This work has been supported by NIH 5R01CA114093. We thank the Ultrasound Division at Siemens Medical Solutions, USA, Inc. for their technical and in–kind support.

References:

[1] BJ Fahey, RC Nelson, SJ Hsu, DP Bradway, DM Dumont, and GE Trahey, *In vivo* guidance and assessment of liver radio–frequency ablation with acoustic radiation force elastography, Ultrasound Med Biol, 34(10) 1590–603, Oct 2008.
[2] BJ Fahey, RC Nelson, SJ Hsu, DM Dumont, DP Bradway, and GE Trahey, *In vivo* visualization of abdominal malignancies with acoustic radiation force elastography, Phys Med Biol, 53 279–293, 2008.

036 **ON THE FEASIBILITY OF MONITORING CARDIAC HYPERTROPHY AND FIBROSIS USING BIPLANE ULTRASOUND STRAIN IMAGING.**

RGP Lopata[1], MM Nillesen[1], L Kapusta[2], SK Singh[3], HB van Wetten[3], CN Verrijp[4], JAWN van der Laak[4], JM Thijssen[1], CL de Korte[1].*

[1]Clinical Physics Laboratory, [2]Pediatric Cardiology, Pediatric Department, [3]Cardiothoracic Surgery Department, [4]Pathology Department, Radboud University Nijmegen Medical Center, Nijmegen, The NETHERLANDS.

Background: Congenital heart disease may lead to chronic heart failure in children. A frequent disorder is valvular aortic stenosis, where the stenotic valve results in an elevated trans–valvular pressure gradient. This will lead to hypertrophy of the heart muscle, and, finally, fibrotic tissue may result leading to heart failure. Hence, monitoring the development of hypertrophy is of great clinical value. 3D cardiac strain imaging seems promising considering the complex 3D structure and deformation of the heart. However, 3D ultrasound has limited temporal and spatial resolution.

Aims: This study focuses on BiPlane strain imaging of the myocardium and monitoring the development of hypertrophy and fibrosis in an animal model.

Methods: In an animal model, one of the three aortic valve cusps was surgically plicated which resulted in a valvular stenosis with subsequent hypertrophy of the left ventricle and in the long term development of fibrosis. BiPlane image sequences of the left ventricle were recorded during the cardiac cycle in four dogs (long– and short–axis view). Biplane image acquisition was performed at a relatively moderate frame rate (approximately 100 Hz) using a commercial platform (Philips SONOS 7500 with an X4 transducer) with a radio frequency (RF) interface. A 2D BiPlane strain imaging technique using RF ultrasound data was applied [1]. This RF–based method was adapted to reconstruct strain from inter–frame strain measurements and track the myocardium during the cardiac cycle [2]. Local displacements and accumulated displacements after tracking were estimated and subsequently the strain values were determined. Cumulative strain images as well as curves of the mean strain (and strain rate) vs. time were generated. Histometry was performed by staining the myocardial tissue after termination for identifying fibrotic tissue (Masson staining). Since the data was not normally distributed a log–conversion was applied. ANOVA was used with Dunnett post–hoc testing to study differences between different beagles.

Results: Initial results revealed the feasibility to measure large radial and circumferential/longitudinal cumulative strain (up to 70%) at the maximum available frame rate of 100 Hz. Results showed the feasibility and reproducibility of assessing these strains simultaneously in the long– and short–axis view of the infero–lateral wall. In this preliminary study, three beagles revealed an elevated pressure gradient over the aortic valve (Δp: 100–200 mmHg) and one dog did not develop any sign of hypertrophy (Δp = 20 mmHg). Histological and morphological findings showed a significant increase in fibrotic tissue for the hearts with larger pressure gradients. A negative correlation was found between the amount of fibrotic tissue and the measured strain and strain rate for all strain components. Hence, myocardial stiffening resulted in lower contractility of the heart muscle as revealed by the strain analysis. The results are in accordance with previous studies in humans [3].

Conclusions: This pilot study proved that a good animal model was achieved to monitor the development of hypertrophy and subsequent fibrosis with ultrasound strain imaging. Recently, a large–scale study has been initiated, using 3D full volume (strain) imaging.

Acknowledgements: The support of the Dutch Technology Foundation (STW; project 06466) is kindly acknowledged.

References:

[1] Lopata et al, Performance Evaluation of Methods for Two–Dimensional Displacement and Strain Estimation using Ultrasound Radio Frequency Data, Ultras Med Biol, 35(5), p.796–812, 2009.

[2] Lopata et al, 3D Cardiac Strain Imaging using a Novel Tracking Method, Proceedings eMBEC, Antwerp, Belgium, 2009 in press.

[3] Kowalski et al, One–dimensional Ultrasonic Strain and Strain Rate Imaging: A New Approach to the Quantification of regional myocardial function in Patients with Aortic Stenosis, Ultrasound Med Biol, 29(8), p.1085–1092, 2003.

* *indicates Presenter*

043 **COMPLIANCE WEIGHTED IMAGING BASED ON HARMONIC SHEAR WAVE SCATTERING.**

V. Rengaraju[1,2], A.F.F. da Silva[2], S. Papazoglou[1], J. Braun[3], C. Kargel[2], I. Sack[1].*
[1]Radiology Department, [3]Institute of Medical Informatics, Charité – University Medicine, Berlin, GERMANY; [2]Division of Sensor Technology and Measurement Systems, Bundeswehr University, Munich, GERMANY.

Background: Recovering elasticity maps from time–harmonic wave data remains a major issue in dynamic elastography. The calculation of spatially resolved elasticity parameters encounters ill–posed inverse problems due to noise and unknown boundary conditions. Therefore, compliance weighted imaging (CWI) was recently introduced in magnetic resonance elastography (MRE) [1].

Aims: To assess the ability of CWI for the detection and visualization of cylindrical inclusions in an ultrasound–based setting of dynamic elastography.

Methods: Simulations of wave amplitude and strain maps of refracted shear–horizontal (SH) waves in a cylindrical inclusion were performed using the eigenfunction expansion of the Helmholtz equation in cylindrical coordinates [2]. To verify the simulation results, a custom made agar phantom 10x10x10cm^3 (34kPa Young's modulus) with a hard cylindrical inclusion (181kPa Young's modulus, radius R = 6mm) was vibrated by 500Hz vertically polarized shear waves. Radiofrequency echo signals (7.3MHz center frequency, 30% FWHM bandwidth) were acquired in color flow mode using a commercial ultrasound scanner (Voluson 730 expert, GE Medical Systems, Kretztechnik, Austria) equipped with a digital research interface. From the shear vertical (SV) amplitude estimates $\hat{u}(x,y)$ [3] the complex wave image $\hat{u}(x,y,$ 500Hz$)$ was calculated. The CWI–map was derived by ¼ ($\hat{u}_x\hat{u}_x^*+\hat{u}_y\hat{u}_y^*$), with $\hat{u}_x$ and $\hat{u}_y$ as the spatial derivatives along rows (x) and columns (y) (* denotes the complex conjugate).

Results: The shear wave speed c_1 = 5.5m/s of the matrix material was significantly higher at the applied vibration frequency than predicted by static indentation measurements (3.4m/s). We failed to deduce the dynamic wave speed inside the inclusion due to low wave numbers. Transmission coefficients were measured to be $T_u \approx 0.3$ for amplitude and $T_\varepsilon \approx 0.1$ for strain. Simulation results consistently showed an increase in sensitivity to scattering by using strain instead of wave amplitudes. Moreover, both T_u and T_ε strongly depend on the wave number $k_1 = \omega/c_1$ of the matrix material and the radius R. With k_1R = 3.4, strain transmission can be approximated by $T_\varepsilon \approx c_1/c_2$ in our experiments (see Figure 1a). When assuming uniform mass density, T_ε^2 indicates the inverse stiffness ratio, i.e. the compliance ratio $(c_1/c_2)^2$ defined by the matrix and inclusion materials.

Conclusions: CWI is inherently more highly sensitive to stiffness changes than shear wave amplitudes. Quantification of stiffness ratios requires knowledge about the geometry of the inclusion and the elasticity of the matrix material. Therefore, CWI is intended as a qualitative method to display lesions by means of shear wave scattering. The method is limited in situations where strong wave damping and deviations from plane waves occur. The SH–wave model originally developed for MRE principally correlates with SV–wave data derived from ultrasound echo signals.

References:

[1] Papazoglou, et al., Scatter–based magnetic resonance elastography. Phys Med. Biol., 54, 2229–2241, 2009.
[2] Graff K.F., Wave motions in elastic solids, 1st ed., Dover, 1991.
[3] Eder, et al., Performance Evaluation of Displacement Estimators for Real–time Ultrasonic Strain and Blood Flow Imaging with Improved Spatial Resolution, IEEE Trans. Instr. Meas., 56, 4, 1275–84, 2007.

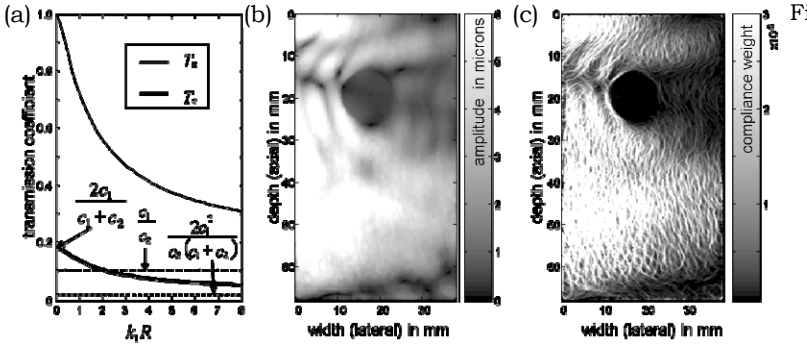

Figure1: Scatter–based elastography.
(a) Simulation results of SH–wave amplitude and strain transmission in a cylindrical inclusion (c_1=5.5m/s, c_2=55m/s, R=6mm). T_u at k_1R=3.4 is higher than observed in experiments which might be caused by a "higher efficiency" of SV–wave scattering in the experiments. Analytical limits of T_ε are given according to [1].
(b) SV–wave amplitude image of the phantom experiment,
(c) CWI–contrast of (b). Inclusion boundaries and contrast changes are more clearly pronounced than in (b). Shading caused by the inclusion is a limiting factor.

047 **GENERATION AND TRACKING OF CIRCUMFERENTIALLY AND LONGITUDINALLY-PROPAGATING MECHANICAL WAVES USING A SINGLE TRANSDUCER: VASCULAR APPLICATIONS.**

Douglas M. Dumont[1], Áine P. Tierney[2], Jeremy J. Dahl[1], Stephen J. Hsu[1] and Gregg E. Trahey[1].*
[1]Duke University, Durham, NC, 27008 USA; [2]University of Limerick, Limerick, IRELAND.

Aims: To generate and track Acoustic Radiation Force Impulse (ARFI)–induced elastic waves propagating in the longitudinal and circumferential direction in arterial phantoms with asymmetric and non–asymmetric material properties, as well as in *ex vivo* and *in vivo* vascular tissue using a single transducer.

Background: The generation of torsional and bending waves in arterial tissue using radiation force has been described by Zhang, et al. [1]. Previously, we have used radiation force to image the mechanical properties of carotid arteries [2]. In this presentation, we describe our technique for generating and tracking ARFI–induced mechanical waves in both the circumferential and longitudinal direction using a single transducer. ARFI–induced wave velocimetry is demonstrated for axisymmetric and non–axisymmetric cryogel phantoms, *ex vivo* porcine aortas and *in vivo* arterial tissue.

Methods: Axisymmetric and non–axisymmetric phantoms of varying moduli (20–120kPa) were constructed, mounted in a water–tank and pressurized with a gravity head. Circumferentially non–axisymmetric phantoms consisted of an approximately 45º arc composed of one modulus, and a 315º arc composed of another modulus. ARFI–induced mechanical waves were generated and tracked with the phantoms oriented both in the longitudinal and circumferential imaging plane of the transducer. Estimates of longitudinal wave group velocity (LWGV) were obtained using previously described lateral time–of–flight algorithms [3]. Estimates of right–traveling (RT) and left–traveling (LT) circumferential wave group velocities (CWGV) were obtained by converting the displacement data into polar coordinates and fitting a regression line to the angular time–of–flight data. The non–axisymmetric phantom was rotated about the transverse axis such that a heterogeneous section was location at either the two o'clock or the ten o'clock position in order to determine the effect of asymmetry on the propagation velocity of the left– and right–traveling waves. Estimates of arterial wave velocity were then obtained from *ex vivo* porcine aortas mounted in a water tank and *in vivo* in the carotid artery of a healthy volunteer.

Results: Results indicate that ARFI–induced elastic waves can be tracked successfully in the longitudinal and circumferential directions using a single transducer that both excites and tracks the propagating wave. Over the physiological pressure range (80–120mmHg), LGWVs were found to vary from 3.2±0.5 and 6.4±0.9mm/ms, with faster group wave velocities associated with stiffer phantom moduli. For *ex vivo* data (n=3 excised porcine aortas), LWGVs were found to vary from 5.1±0.9 and 6.8±1.8mm/ms over the physiological pressure range. In the axisymmetric phantom, CWGVs were found to be 61±9deg/ms and 68±11deg/ms for the LT and RT waves. In the non–axisymmetric phantom, CWGVs were determined to be 28±5deg/ms and 63±9deg/ms for the LT and RT waves with the heterogeneous section oriented at the ten o'clock position and 72±15deg/ms and 23±9deg/ms with the heterogeneous section oriented at the two o'clock position.

Conclusions: ARFI–induced elastic wave velocimetry was demonstrated in vascular phantoms and in arterial tissue using a single transducer. Circumferential material asymmetry can be determined by tracking the group wave velocity for the left–traveling and right–traveling waves.

Acknowledgments: This work is supported by NIH Grants R21–EB–007741, HL075485 and 5T32EB001040, and the FAS Science Challenge.

References:

[1] Zhang, X. and Greenleaf, J, F., "Measurement of wave velocity in arterial walls with ultrasound transducers", Ultrasound in Med. Biol., Vol 32:11, 1655–1660, Nov 2006.
[2] Dahl, J. J., Dumont, D. M., Allen, J. D, Miller, E. M, and Trahey, G. E., "Acoustic Radiation Force Impulse Imaging for Noninvasive Characterization of Carotid Artery Atherosclerotic Plaques: A Feasibility Study", Ultrasound in Med. Biol., 2009, in press.
[3] Palmeri, M. L., Wang, M. H, Dahl, J. J., Frinkley, K. D. and Nightingale, K. R., "Quantifying Hepatic Shear Modulus In Vivo using Acoustic Radiation Force", Ultrasound in Med. Biol., Vol 34:4, 546–558, April 2008.

* *indicates Presenter*

049 **PARAMETRIC ANALYSIS OF MYOCARDIAL STIFFNESS CHANGES WITHIN THE CARDIAC CYCLE WITH ACOUSTIC RADIATION FORCE IMPULSE IMAGING.**

Stephen J. Hsu[1], Patrick D. Wolf[1] and Gregg E. Trahey[1].*
[1]Duke University, 136 Hudson Hall, Durham, NC, USA.

Background: Current clinically accepted methods for determining left ventricular (LV) function measure a value known as elastance, which is a corollary metric to stiffness and derived from parametric analysis of the pressure–volume (PV) relation within the left ventricle [1]. However, elastances are typically measured at end–systole and end–diastole only. Acoustic radiation force impulse (ARFI) imaging has been demonstrated to be capable of visualizing changes in myocardial stiffness through the entire cardiac cycle [2]. A combined ARFI imaging and PV analysis could provide additional insight into LV performance and function.

Aims: To correlate changes in myocardial stiffness with the four phases of the cardiac cycle.

Methods: An atrially paced *ovine* heart was imaged *in vivo* under an open chest preparation. A left thoracotomy was performed, and the pericardium was cut away. The transducer was inserted into a vacuum apparatus and placed directly onto the LV free wall along the long axis of the heart. A Millar Instruments (Houston, TX, USA) pressure catheter was inserted directly into the left ventricle via a trochar puncture at the apex. Co–registered B–mode and ARFI images were acquired across nine heartbeats while simultaneously recording left ventricular pressures, pacing source voltages and the global ECG. LV volumes were extrapolated from LV cross–sectional area estimates made from the B–mode images. These waveforms were temporally registered and compared through the entire cardiac cycle.

Results:

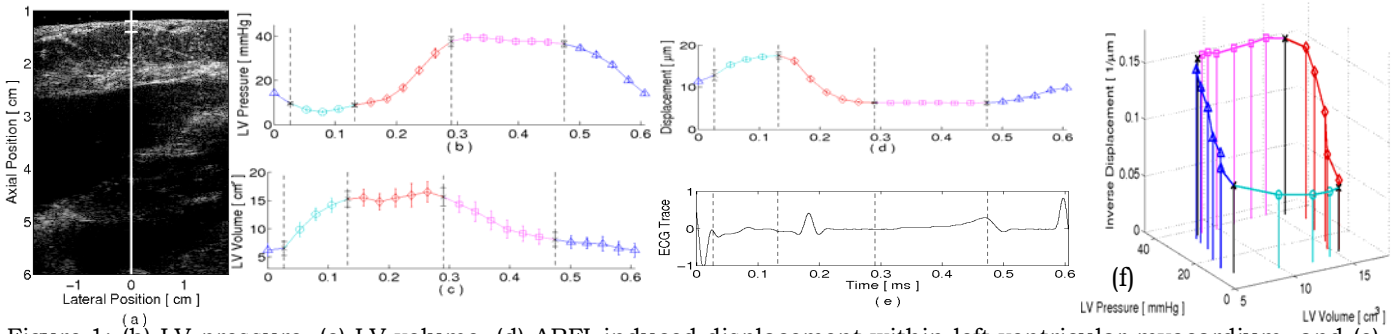

Figure 1: (b) LV pressure, (c) LV volume, (d) ARFI–induced displacement within left ventricular myocardium, and (e) global ECG plots through a single cardiac cycle. The lateral position and regions of interest of the ARFI–induced displacement plot are marked within (a) the matched B–mode image taken at t=0 and from the first recorded heartbeat. The four phases of the cardiac cycle, isovolumic contraction (diamonds), ejection (squares), isovolumic relaxation (triangles), filling (circles), and their transition points (xs) were identified from PV analysis and labeled accordingly in each plot. (f) A three–dimensional parametric plot, using inverse ARFI-induced displacements, provides an indication into the changes in myocardial elasticity through the cardiac cycle.

Conclusions: A parametric analysis of left ventricular pressure, volume and ARFI imaging–based stiffness revealed that myocardial stiffening occurred during isovolumic contraction while myocardial relaxation occurred during both isovolumic relaxation and filling. These plots also indicated that the steady–state ARFI–induced displacement during ejection was reached before the end of isovolumic contraction, while LV pressures continued to climb.

Acknowledgements: This research was funded by NIH Grants #R01–HL–075485, R01–CA–114093 and R21–EB–007741. We would like to thank Siemens Medical Solutions USA, Inc. for their hardware and system support.

References:

[1] D Burkhoff, I Mirsky, and H Suga, Assessment of systolic and diastolic ventricular properties via pressure–volume analysis: a guide for clinical, translational, and basic researchers, Am J Physiol Heart Circ Physiol,, 289(2) 501–512, Aug 2005.
[2] S Hsu, R Bouchard, D Dumont, P Wolf, and G Trahey, *In vivo* assessment of myocardial stiffness with acoustic radiation force impulse imaging, Ultrasound Med Biol, 33(11) 1706–1719, Nov 2007.

* *indicates Presenter*

057 **REAL–TIME ELASTOGRAPHY OF THE BRAIN.**

C Uff[1], L Garcia[1], J Fromageau[1], N Dorward[2], JC Bamber[1].*
[1]Institute of Cancer Research, Sutton, Surrey, England, UK; [2]Royal Free Hospital, London, England, UK.

Background: A recent study by this group [1] demonstrated the safety and feasibility of ultrasound elastography in the human brain with the aim of utilizing it intra–operatively during tumor resection surgery to guide surgical procedure and ensure that the full extent of the lesion had been removed.

Aims: This study aims to continue the work of the previously described study in addition to demonstrating the intra–operative use of a recently developed 3D ultrasound elastography system [2].

Methods: During neurosurgical procedures for brain tumors, data were acquired prior to tumor removal. Two scanning systems were used: Z.One (Zonare Medical Systems Inc., USA) with a 12MHz 2D transducer and Diasus (Dynamic Imaging Ltd, UK) with 5–10MHz 2D transducer and 6–12MHz 3D transducer in conjunction with Stradwin 3.7 (Cambridge University, UK) ultrasound elastography acquisition software. The 5x5cm 3D probe face prevented its use in those cases where the craniotomy area was too small. The Z.One transducer was used to explore the resection cavity for residual tumor in select cases. Different methods were used to generate tissue strain: standard free–hand compression and internal vascular pulsatile forces whilst maintaining constant applied pressure with the transducer. Acquired RF data from the Diasus were also processed offline using standard 2D cross–correlation based displacement tracking methods to provide images of correlation and axial shear strain.

Results: Intra–operative data from brain tumor resection surgery are presented in Figures 1 and 2.

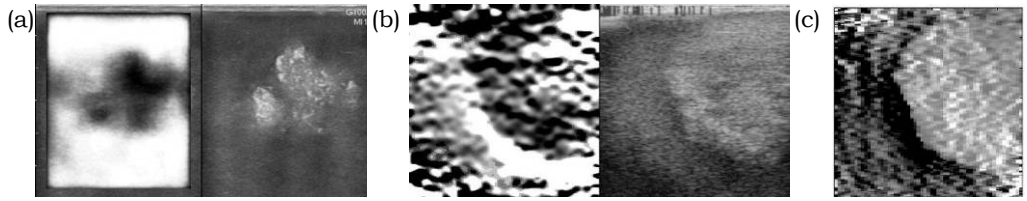

Figure 1: Extrinsic brain tumor showing well defined cleavage plane: (a) Zonare axial strain and B–mode, (b) Stradwin axial strain and B–mode and (c) axial shear strain generated in house.

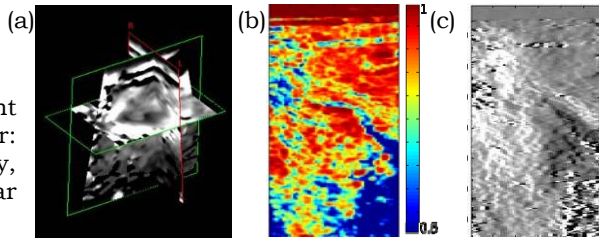

Figure 2: Intrinsic brain tumor with adherent boundary between brain and tumor: (a) Stradwin axial strain 3D display, and (b) correlation and (c) axial shear strain generated in–house as above.

Conclusions: The results indicate that real time 2D and 3D ultrasound axial strain imaging not only viable, but also clinically useful in the human brain. Axial strain images, augmented by axial shear strain images, were useful to the surgeon in identifying and characterizing the tissue–tumor interface (Figure 1b and c). High shear strain (Figure 2c) and areas of decorrelation (Figure 2b) may be used to identify such cleavage planes.

Acknowledgements: This work was funded by the Engineering and Physical Sciences Research Council, UK.

References:

[1] Chakraborty A, Bamber J, Berry G, Bush N, Dorward N, Intra–operative ultrasound elastography and registered MRI of brain tumours; a feasibility study, Proc. 3rd Int Conf on the Ultrasonic Measurement and Imaging of Tissue Elasticity, p.57, 2004.
[2] Treece G, Lindop J, et al., Freehand ultrasound elastography with a 3D probe, UMB 34:463–474, 2008.

* *indicates Presenter*

062 **MEASURING MECHANICAL PROPERTIES OF GRAY AND WHITE MATTER *IN VIVO* USING MAGNETIC RESONANCE ELASTOGRAPHY.**

Adam J. Pattison[1], S. Scott Lollis[2], Phillip R. Perrinez[1], Irina M. Perreard[3], Matthew D.J. McGarry[1], John B. Weaver[1,3], Keith D. Paulsen[1,4].*

[1]Thayer School of Engineering, Dartmouth College, Hanover, NH 03755, USA; [2]Neurosurgery Department, [3]Radiology Department, Dartmouth–Hitchcock Medical Center, Lebanon, NH 03756, USA; [4]Norris Cotton Cancer Center, Lebanon, NH 03756, USA.

Background: Understanding brain tissue biomechanics provides key information into both brain disease and injury. Steady–state time–harmonic magnetic resonance elastography (MRE) provides the ability to estimate different mechanical properties of *in vivo* tissue using gentle vibration. While MRE of brain tissue has become more prevalent in recent years, there is a wide array of shear modulus estimates, promoting the need for further study [1,2]. The ability to decipher average stiffness values for brain tissue and, more specifically, gray matter (consisting of neuronal cell bodies) and white matter (consisting of myelinated axonal tracts) is important for elastographic imaging of brain tissue.

Aims: The aim of this work is to measure *in vivo* elastic properties of feline brain tissue (a common model of brain disease, such as hydrocephalus [3]). Specifically, we investigate the difference in the shear modulus values of gray and white matter of healthy animals to serve as a baseline for comparison with values from diseased tissue.

Methods: A pneumatic actuator was placed below the jaw and actuated at 85Hz. The resulting tissue deformation was measured with a phase–sensitive 2D spin–echo MR sequence. Mechanical properties were fit to Navier's equations of motion using a subzone based inversion algorithm, explained in other publications [4]. Manual segmentation of gray and white matter using T2–weighed MR images.

Results: Figure 1 shows a T2–weighted anatomical MR image and the resulting elastogram for the same geometry. Ten cats were successfully compared with anatomical images and values are plotted. Inter–subject average of white matter was found to be 8.32 +/-3.67kPa, whereas gray matter was found to be lower at 7.09 +/-2.78kPa. While there is large variation between subjects, white matter was consistently found to be stiffer than gray matter (9 out of 10 cases).

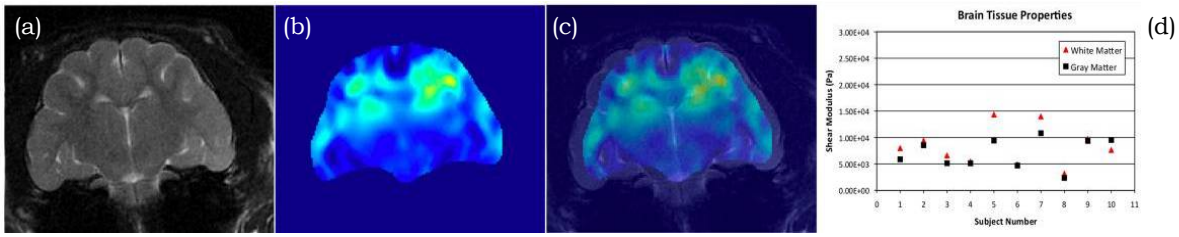

Figure 1: A T2–weighted anatomical image is shown (a) to locate areas of gray and white matter. An example reconstructed shear modulus elastogram (b) is then overlaid on this anatomical image (c). A scatter plot of gray and white matter values for 10 subjects is also shown (d) to illustrate the consistent differences in between the two tissue types.

Conclusions: Shear modulus values were successfully estimated in 10 healthy feline subjects. White matter was consistently found to be stiffer than gray matter. Average shear modulus values for both tissue types were within the range of the existing literature [1,2]. However, large variations in the reconstructed values suggest further investigation into healthy and diseased brain tissue, where values can be compared to find possible differences.

Acknowledgements: This work was supported by NIH Grant 5 P01 CA080139–08.

References:

[1] Green, M., Bilston, L., and Sinkus, R., "*In vivo* brain viscoelastic properties measured by magnetic resonance elastography," NMR Biomedicine, 21(7), 755-764, 2008.

[2] Sack, I., Beierbach, B., Hamhaber, U., Klatt, D., and Braun, J., "Non–invasive measurement of brain viscoelasticity using magnetic resonance elastography," NMR Biomedicine, 3, 265–271, 2008.

[3] Pattison, A., Lollis, S., Perrinez, P., Weaver, J., and Paulsen, K., "MR elastography of hydrocephalus," Proc. SPIE 7262, 2009.

[4] Van Houten, E. E., Miga, M. I., Weaver, J. B., Kennedy, F. E., and Paulsen, K. D., "Three–dimensional subzone–based reconstruction algorithm for MR elastography", Magn Reson Med, 45, 827–837, 2001.

081 **AUTOMATIC PROSTATE SEGMENTATION FROM TRANSRECTAL ULTRASOUND ELASTOGRAPHY IMAGES USING GEOMETRIC ACTIVE CONTOURS.**

O Goksel[1], S.E. Salcudean[1].*
[1]University of British Columbia, Vancouver, BC, CANADA.

Background: Prostate segmentation is an essential step in radiation–treatment planning for prostate cancer. Currently, this segmentation is performed on transverse transrectal ultrasound (TRUS) B–mode images that are collected during a pre–operative volume study. The segmentation takes 5–10 minutes of the clinician's time, and it greatly depends on the B–mode image quality and on the clinician performing the study. Consequently, (semi–)automatic methods for prostate segmentation from B–mode images have been proposed in the literature [1]. Nevertheless, a reliable fully–automatic method has not yet been developed. Recent advances in elastography imaging, making it widely available, allow for its utilization in applications where B–mode images alone may not be suitable for robust image processing algorithms.

Aims: To show that TRUS elastography can be used for automatic prostate segmentation.

Methods: Time sequences of TRUS RF frames are collected through several cross–sections of the prostate, while motion for elastography is induced by displacing the TRUS probe in the axial direction of the ultrasound beam [2]. Using the strain images computed from the RF data, the prostate is segmented in 2D on each slice employing an active contour method [3]. The method employs a region–based constraint, the variance of image pixel intensities inside/outside the contour, within a variational approach with level–set formulation. It is stable and robust for a large range of initializations. Once a slice is segmented, the resulting contour is used to initialize the next neighboring slice. When all slices are segmented, a 3D model is generated using a disc–guided shape–based interpolation technique [4].

Results: In this study, sagittal TRUS data collected prior to the procedure using the setup in [2] at 5° increments from a prostate brachytherapy patient is used. Axial strain images were generated from the displacements computed using a time–domain cross–correlation method. The active contours method was automatically initialized in the central sagittal slice (at 0°) as a rectangle using a simple thresholding on 1D intensity curves averaged through the entire image in both the axial and lateral directions. The active contours algorithm, implemented in Matlab, converges in a few seconds as seen in Figure1 (a–c). Using this segmentation as initialization, the slices at ±5° are segmented next as in Figure1 (d, e). Each subsequent slice acquired at a 5° greater angle is then initialized for contouring using the resulting contour of the previous image (see Figure1 (f–i)). The resulting 3D surface model and contours are presented in Figure1 (j, k).

Conclusions: An automatic segmentation of prostate from elastography images has been presented. This method will facilitate and accelerate the segmentation of pre–operative images for treatment planning. Such fast automatic methods can further enable on–the–fly prostate segmentation intra–operatively.

Acknowledgements: Xu Wen contributed to data collection. Support for this work was provided by NSERC and NIH (R21 CA120232–01).

References: [1] JA Noble, D Boukerroui, "Ultrasound image segmentation: a survey", IEEE TMI, 25:987–1010, 2006.
[2] SE Salcudean, D French, S Bachmann, R Zahiri–Azar, X Wen, WJ Morris, "Viscoelasticity Modeling of the Prostate Region Using Vibro–elastography", MICCAI 2006.
[3] T Chan and L Vese, "Active contours without edges", IEEE Trans Imag Proc,10:266–277, 2001.
[4] GM Treece, RW Prager, AH Gee, L Berman, "Surface interpolation from sparse cross-sections using region correspondence", IEEE Trans Med Imaging,19:1106–14, 2000.

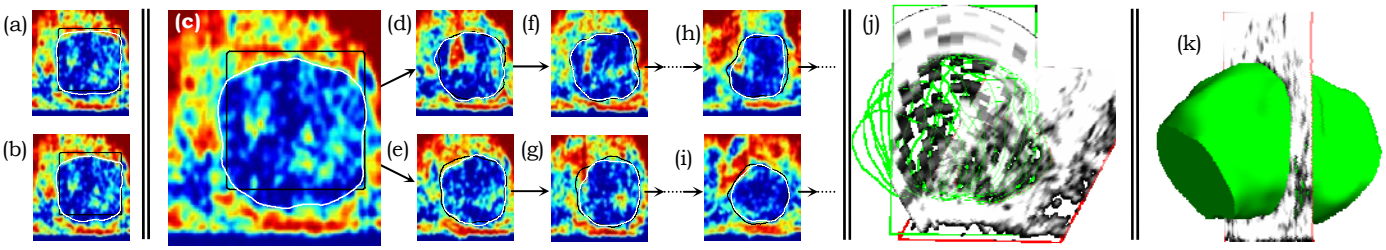

Figure 1: The advance of active contours at two sample iterations (a, b) prior to convergence on the central (0°) sagittal slice; segmentation of 0°(c), +5°(d), -5°(e), +10°(f), -10°(g), +25°(h), and -25°(i) strain images, where black and white curves are initial and converged contours, respectively; contour segmentations in their relative 3D orientations (j); and the final 3D model (k).

* *indicates Presenter*

003 **DEVELOPMENT OF A WEIGHTING SCHEME FOR STRAIN ESTIMATION.**

Lujie Chen[1], R. James Housden[1], Graham M. Treece[1], Andrew H. Gee[1], Richard W. Prager[1].*
[1]University of Cambridge, Cambridge, England, UK.

Background: In freehand, quasistatic strain imaging, a two–step data processing strategy, displacement estimation followed by strain estimation, is commonly adopted. While displacement estimation is responsible for the accuracy of the whole process, strain estimation has a large bearing on the appearance of the resultant image. Apart from taking the gradient of the axial displacement field, strain estimation may include several other sub–procedures, such as normalizing, smoothing and persisting the strain field. In each of these procedures, strain data are often associated with weights to reflect their relative precisions. Hence, the output "pseudo–strain" image is strongly affected by the weighting scheme used.

Aims: To develop an effective weighting scheme for the strain estimation process.

Methods: Data weighting descriptors can be drawn from intra– or inter–window statistics, where a window refers to a block of data used for matching. A typical intra–window weighting descriptor is $Q = C/(1-C)$ [1], where C is the correlation coefficient. An inter–window weighting descriptor is $SNR_e = m_s/\sigma_s$ [2], where m_s and σ_s are respectively the mean and standard deviation of a region of supposedly uniform strain. We propose a combined weighting scheme that uses SNR_e when normalizing a strain field and $Q^{1/2}/\sigma_s$ when smoothing and persisting the strain data.

Results: Four weighting schemes were compared: no weight, weighting by Q, weighting by SNR_e and the combined weighting scheme. Figure 1 shows (a) a thyroid scan and (b) its axial displacement field, which was used to generate strain images with the various weighting schemes. After the normalizing and smoothing processes, the SNR_e–based and the combined weighting schemes produce more plausible strain images than the other two (see Figure 2: Smoothing row). After persistence, the combined weighting scheme suppresses slightly more artefacts than the SNR_e–based scheme. A cyst in a uniform background was simulated and different levels of noise were added to the RF data. Average point–wise absolute differences, excluding the cyst region, between the ground truth elasticity and the pseudo–strain images are shown in Figure 3 (ground truth and pseudo–strain were both normalized to the same value of 1). The combined weighting scheme generates a pseudo–strain distribution that most closely resembles the uniform background, irrespective of the noise level. Similar results were obtained with various other data sets.

Conclusions: The choice of weighting scheme has a considerable effect on strain estimation. It was found that different weighting descriptors are best at different processing steps; hence, a combination of intra– and inter–window statistics can provide better results than using a single descriptor alone.

Acknowledgements: This work was funded by Translation Award 081511/Z/06/Z from the Wellcome Trust.

References:

[1] I. Cespedes, J. Ophir, and S. K. Alam, The combined effect of signal decorrelation and random noise on the variance of time delay estimation. 44, 220–225, 1997.
[2] I. Cespedes and J. Ophir, Reduction of image noise in elastography. 15, 89–102, 1993.

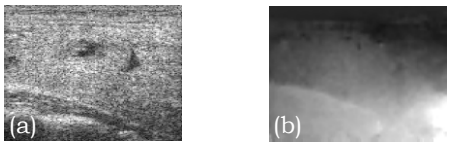

(a) B–mode image (b) axial displacement field.
Figure 1: Thyroid nodule

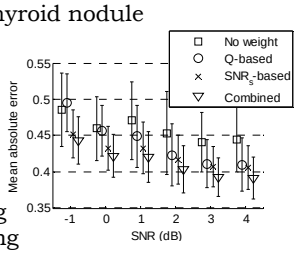

Figure 3: Error in pseudo–strain using the various weighting schemes. The ±1 standard deviation error bars are based on 100 repetitions.

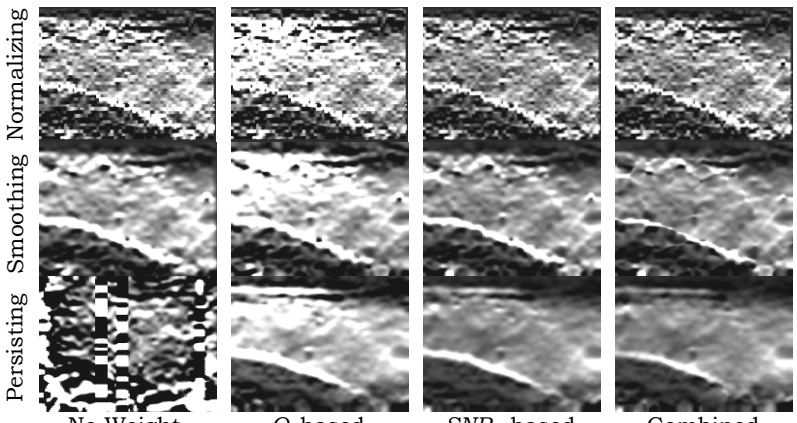

Figure 2: Each column shows strain images obtained using a particular weighting scheme at three processing stages. Persisting is achieved with 30 consecutive strain images.

022 **BLOOD VESSEL STRAIN IMAGING USING LINEAR ARRAY TRANSDUCER WITH STEERING.**

Dong–Ki Ahn[1], Mok–Kun Jeong[1], Sung–Jae Kwon[1], Moo–Ho Bae[2].*
[1]Electronic and Communication Engineering Departments, Daejin University, Pocheon, Gyeonggi, 487-711, KOREA; [2]Electronic Engineering Department, Hallym University, Chuncheon, Gangweon, KOREA.

Background: Brain stroke is one of the major causes of death, so an effective screening method is in urgent need of development. Recently, intravascular ultrasound (IVUS) imaging has been used to diagnose vascular diseases. The IVUS imaging method can estimate the strain of blood vessel walls from their movement due to change in blood pressure because they are perpendicular to the scan line. The potential risk and inconvenience of the invasive IVUS catheter diagnostic method have been an obstacle to its widespread use. To overcome this problem, we present a new method for measuring the strain of a carotid artery wall using a linear array transducer.

Methods: In transmission and reception, ultrasound beams from a linear array transducer oriented to scan the cross–section of a blood vessel are steered so that they are perpendicular to the vessel wall, as is the case with an IVUS probe, and pass through its center. Data acquisition proceeds as follows. First, we locate the center of a blood vessel in a region to be diagnosed from its B–mode image. When we steer scan lines toward the center point, they will form a sector shape around it. In order to interrogate one half of the circumference of the entire vessel, scan lines are steered in steps of one degree within +/- 40° to acquire a total of 81 scan line data that cover one half of the anterior and posterior walls. The strain of a vessel can be estimated by comparing the displacement before and after its expansion.

In order to verify the utility of our algorithm, we fabricated a blood vessel mimicking hexahedron–shaped phantom containing a hollow cylinder with an inner radius of 6 mm and an outer radius of 8 mm. One half of the cylindrical shell covering an angle of 180° was made of soft material, and the other half was made of hard material, which was also used in the background. Using a clinical ultrasound scanner (Medison, Seoul, Korea), RF data were acquired by steering scan lines in steps of 1° over an angle range of -40° to 40° so that they are perpendicular to the vessel wall and pass through the center of the vessel. To emulate the movement of blood vessel, we filled the inside of the vessel phantom with water and applied pressure to expand it. The strain was estimated by using a correlation–based displacement estimator.

Results: We were able to identify soft regions in the blood vessel mimicking phantom by steering scan lines at right angles to the vessel wall. The Figure 1(a) shows a B–mode image of the phantom, where the soft region is delineated by dashed lines. The Figure 1(b) shows its strain image in which the soft region appears bright.

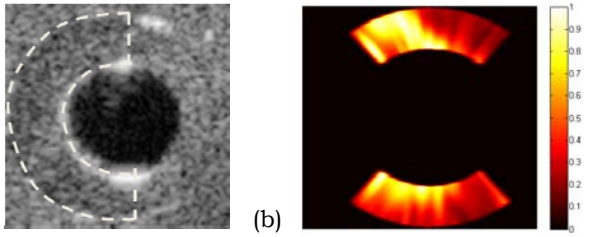

Figure 1: (a) (b)

Conclusions: This new method of estimating strain based on the data of scan lines steered with a linear array transducer is considered to help diagnose vascular diseases by providing ease of diagnosis and removing potential risk associated with IVUS examination.

Acknowledgements: This work was supported by Medison, Korea.

** indicates Presenter*

026 **COMPARISON OF ALTERNATE PHYSIOLOGICAL MOTION FILTERS FOR *IN VIVO* CARDIAC ARFI.**

DM Giannantonio[1], BC Byram[1], GE Trahey[1].*
[1]Duke University, Durham, NC, USA.

Background: Filtering physiological motion is one of the biggest challenges in cardiac ARFI imaging [1]. Currently, the most accurate filtering technique is a temporal polynomial interpolation method which fits a quadratic polynomial to points immediately before the ARFI push and to points after full tissue recovery [2]. This method, while effective, has several problems. First, it is impossible to determine precisely when the shear wave has entirely cleared out of the tissue, and, thus, it may influence the post–track time points used in the interpolation [3]. Second, because this technique requires data over a relatively long period of time, it is susceptible to out of plane motion. Third, data must be collected until full tissue recovery is obtained, decreasing the speed of acquisition.

Aims: This work explored alternate filtering methods to determine whether they may be both more accurate and able to increase the ARFI frame rate. Three methods were investigated: a temporal extrapolation filter, a spatial interpolation filter and a combination of the first two. All three methods aim to minimize the problems of out of plane motion and failure of the shear wave to clear out of the tissue because they do not rely on displacements at time points after full tissue recovery.

Methods: The temporal extrapolation filter fits a quadratic motion only to tracking points acquired before the ARFI push. The spatial interpolation filter functions by acquiring physiological displacements at adjacent lateral locations to the ARFI push (in parallel) and then using the motion at adjacent spatial locations to predict cardiac motion along the ARFI push beam. The combined method aims to fit a polynomial with both temporal and spatial arguments. The methods were compared by acquiring no push cardiac ARFI data and then determining how well the different methods predict the physiological motion of the heart.

Results: Initial comparisons of the traditional temporal interpolation method against the proposed temporal extrapolation method on both transthoracic and epicardial canine data indicate that at times up to 0.5ms after an ARFI push the two methods perform comparably during diastole, but extrapolation significantly outperforms interpolation during systole. During systole for the epicardial data of the left ventricle free wall 0.2ms after the ARFI push (a time near peak displacement in cardiac ARFI), the extrapolation method's mean absolute error for physiological motion removal is 68% less than the traditional interpolation method's mean absolute error. Performing the same analysis but at 0.3ms after the ARFI push, extrapolation's mean absolute error is 18% less than the interpolation method's error. As the time after the ARFI push increases to 0.5ms, the performance of the two methods converges. Extrapolation filtering as a function of the number of tracks before the ARFI push has also been explored. The results for the proposed spatial interpolation method and the combined method are not yet conclusively better than the traditional temporal interpolation based filter.

Conclusions: The early results of this work indicate that the temporal extrapolation method is a better filtering technique than the currently used temporal interpolation method for cardiac data because it both provides a better fit of the physiological motion during systole up to 0.5ms after the ARFI push and increases the ARFI frame rate by not requiring the use of displacements at time points after full tissue recovery. Thus far, the results of the spatial interpolation method and combined method are inconclusive.

Acknowledgements: This research was possible thanks to NIH Grants 5T32EB001040 and 1R01HL096023–01 and the Duke University Pratt Fellows Program.

References:

[1] BJ Fahey, ML Palmeri, and GE Trahey, "The Impact of Physiological Motion on Tissue Tracking During Radiation Force Imaging," Ultrasound Med. Biol., vol. 33, no. 7, pp. 1149–1166, July 2007.
[2] SJ Hsu, RB Bouchard, DM Dumont, PD Wolf, and GE Trahey, "*In Vivo* Acoustic Radiation Force Impulse Imaging of the Cardiac Cycle," Ultrasound Med. Biol., vol. 33, no. 11, pp 1706–1719, Nov. 2007.
[3] BJ Fahey, SJ Hsu, and GE Trahey, "A Novel Motion Compensation Algorithm for Acoustic Radiation Force Elastography," IEEE Transactions on Ultrasonics, Ferroelectrics, and Frequency Control, vol. 55, no. 5, May 2008.

033 **DIAGNOSTIC PERFORMANCE OF FREEHAND ELASTOGRAPHY WITH STRAIN RATIO MEASUREMENT IN THE CHARACTERIZATION OF BREAST LESIONS REFERRED FOR ULTRASOUND GUIDED BIOPSY: INITIAL CLINICAL RESULTS AT A SINGLE CANCER REFERRAL CENTER.**

Todd R. Kumm[1], Alec Chau[1], Margaret Szabunio[1].*
[1]H. Lee Moffitt Cancer Center & Research Institute, 12902 Magnolia Dr., Tampa, FL, 33612 USA.

Background: While patients referred for biopsy of breast lesions represent a small percentage of the screening population, the resources consumed by this patient segment are disproportionately high [1]. Lesions biopsied yield a benign result in more than 75% of cases, therefore, a reliable, non–invasive method to characterize suspicious lesions would be valuable [1,2]. Elastography has been proposed as a potential tool for differentiation of benign from malignant lesions in the breast [2,3]. Our study included the use of strain ratio measurement in addition to elastography scoring of lesions.

Aims: To determine the diagnostic performance of elastography (ES) and strain ratio (SR) measurement for breast lesions referred for biopsy.

Methods: Patients referred for ultrasound guided biopsy of a suspicious breast lesion were included in this study after informed consent was given. Using the Hitachi Hi Vision 900 Ultrasound with integrated Sonoelastography software, elastography score (ES) images and strain ratio (SR) measurements were obtained for each lesion. Elastography system operators and elastogram readers were considered newcomers to the technique, but received specialized training from the equipment manufacturer prior to study initiation. Subjects were evaluated immediately prior to biopsy on the same date. Lesions were assigned an ES using the five–point visual scoring system (Figure 1) proposed by Itoh, et. al. [3]. The lesion was considered ES test negative if scored 0, 1 or 2; while a score of 3, 4 or 5 was considered ES test positive. Calculation of the SR value (Figure 2) was based upon the average strain measured in the lesion as compared to adjacent adipose tissue in the breast. Using proprietary software, the average strain of the lesion was determined by selecting a representative region of interest from the center of the lesion, and was expressed as "ST–ave LESION". A corresponding ROI of adjacent adipose tissue was then selected, and was expressed as "ST–ave FAT". The resultant SR value was expressed as a ratio according to the equation: ST–ave Fat /ST–ave Lesion = SR. A lesion was considered SR test negative if the ratio was <4.5; while a ratio of ≥4.5 was considered SR test positive, according to criteria provided by the manufacturer. Sensitivity, specificity, negative and positive predictive values and test accuracy were calculated using core needle or excisional biopsy result as the standard.

Results: A total of 100 lesions from 85 patients were evaluated (Table 1). Combined ES and SR scoring counted the test as positive if either ES or SR score met the criteria for the positive test.

	Sensitivity	Specificity	PPV	NPV	Accuracy	True Positive	True Negative	False Positive	False Negative
ES	0.79	0.75	0.50	0.92	0.78	19	57	19	5
SR	0.79	0.78	0.53	0.92	0.78	19	59	17	5
ES & SR	0.83	0.76	0.53	0.94	0.78	20	58	18	4

Table1:

Conclusions: Using strain ratio assessment provides additional information about a lesion's strain characteristics and may serve to complement elastography scoring using a visual scale. Combining SR assessment with ES improved sensitivity compared to either scoring system alone. Although combined scoring slightly decreased specificity, a single false negative result was excluded using this technique. Study limitations include a small sample size, operator experience and potential selection bias as our site is a cancer referral center. Ongoing study of these techniques may help to further clarify the value of combining these measurements and determine if the use of ES and SR scoring can help identify patients in which biopsy might be avoided in lieu of clinical follow up.

Acknowledgements: Hitachi Corporation provided the equipment used in this study.

References:

[1] Poplack SP, Carney PA, Weiss JE, Titus–Ernstoff L, Goodrich ME, Tosteson AN, Screening mammography: costs and use of screening–related services. Radiology, 234:79–85, 2005.
[2] Burnside ES, Hall TJ, Sommer AM, et al., Differentiating Benign from Malignant Solid Breast Masses with US Strain Imaging. Radiology, 245:401–410, 2007.
[3] Itoh A, Ueno E, Tohno E, et al., Breast disease: clinical application of US elastography for diagnosis. Radiology, 239:341–350, 2006.

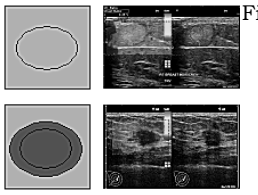

Figure 1: Visual Elastography Scoring (ES) System. Color elastography images are scored according to the scale described by Ueno; the higher the score, the more likely for invasive breast carcinoma [3].
(a) Score = 1: High Strain
(b) Score = 5: No Strain

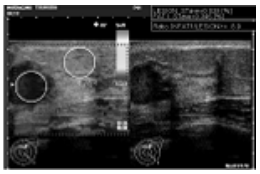

Figure 2: Strain Ratio (SR) Measurement. A region of interest (ROI) selected centrally in the lesion, compared to a corresponding ROI of adjacent fat tissue.
SR = ST – ave FAT/ ST – ave LESION.

* *indicates Presenter*

035 **SOME OF THE FACTORS INFLUENCING THE HEEL PAD COMPRESSIBILITY INDEX (HPCI): A LITERATURE SEARCH.**

Sara Matteoli[1], Jens E. Wilhjelm[1], Søren Torp–Pedersen[2].*
[1]DTU Elektro, Biomedical Engineering, Technical University of Denmark, Ørsteds Plads, Bldg.348, DK–2800, Kgs. Lyngby, DENMARK; [2]The Parker Institute, Frederiksberg Hospital, University of Copenhagen, Nordre Fasanvej 57, DK–2000 Frederiksberg, DENMARK.

Background: The human heel pad is a complex structure that features non–linear visco–elastic characteristics. It acts as an efficient shock absorber reducing the impact forces during gait. Trauma and/or diseases to the heel pad may cause the "destruction" of its intricate septation with resulting permanent damage of its shock absorbency capability. When measuring a mechanical parameter of the heel pad for the purpose of diagnosis, the normal range of this parameter must be known as well as the variation with factors such as age, weight, gender, height, etc.

Aims: The present study concentrates on the variation of one such parameter: the heel pad compressibility index (HPCI). The aim is to combine the results of all known studies, and to investigate whether consistent conclusions may be drawn also taking into consideration that the methodologies of the studies might be different.

Methods: Literature searches have been carried out in the bibliographic databases Inspec, EMBASE via Ovid, Medline via Pubmed and Web of Science ultimo April 2009. Keywords: Heel pad compressibility, heel pad–elderly/diabetes/heel pain. Out of 39 papers identified from these searches, ten papers were in the scope of the present work.

Results: In healthy adults, four studies showed that HPCI increases with age ([1–4], 1505 heels, $p<0.05$). In adults with heel pain, one study showed that HPCI increases with age ([5], 67 heels, $p<0.05$). In healthy adults, two studies showed that HPCI increases with weight ([3,4], 1040 subjects, $p<0.001$), while another study showed it to be unchanged ([6], 220 heels, $p>0.05$). In adults with heel pain, one study found the HPCI increases with weight ([5], 67 heels, $p<0.05$). In patients with diabetes compared to healthy subjects, one study showed that the HPCI is increased ([7], 30 heels, $p<0.001$), while another showed it to be unchanged ([8], 96 heels, $p=0.657$). In patients with heel pain compared to healthy subjects, two studies showed that HPCI is increased ([2,7], 500 heels, $p<0.001$) while three other studies showed it to be unchanged ([4,9,10], 570 heels, $p>0.05$). Six studies ([1,3,4,6–8]) attempts to some degree to control the age/weight factor during their investigation.

Conclusions: As there is an increase in HPCI with age, and there also might be an increase with weight when analyzing both normal subjects and heel pain patients, age and weight can act as confounding factors when investigating the effect of trauma or consequences of diseases such as diabetes. Thus, it is important to match age and weight within control and patient group. When the pool of subjects/patients is limited, such match may be difficult. Considering the influence of age, theoretically, prior knowledge about the relationship between HPCI and age might be used to match the results of control and patient groups in terms of age. This would require, though, that several new studies using the same methods and controlling all other relevant factors (weight, gender, race, etc.) yield the same results.

References:

[1] Hsu, T. C., et al., Comparison of the mechanical properties of the heel pad between young and elderly adults, Archives of Physical Medicine and Rehabilitation, 79(9), 1101–1104, 1998.
[2] Prichasuk, S., The heel pad in plantar heel pain, J. Bone Joint Surg.–British Volume, 76B (1), 140–142, 1994.
[3] Prichasuk, S., et al. The heel–pad compressibility, Clin. Orth. and Rel. Research, (300), 197–200, 1994.
[4] Turgut, A., et al., The relationship of heel pad elasticity and plantar heel pain, Clinical Orthopaedics and Related Research, (360), 191–196, 1999.
[5] Ozdemir, H., Soyuncu, Y., Ozgorgen, M., & Dabak, K., Effects of changes in heel fat pad thickness and elasticity on heel pain, Journal of the American Podiatric Medical Association, 94(1), 47–52, 2004.
[6] Uzel, M., Cetinus, E., Ekerbicer, H. C., & Karaoguz, A., Heel pad thickness and athletic activity in healthy young adults: A sonographic study, Journal of Clinical Ultrasound; 34(5) 231–236, 2006.
[7] Tong, J., Lim, C. S., Goh, O. L., Technique to study the biomechanical properties of the human calcaneal heel pad, The Foot, 13, 83–91, 2003.
[8] Hsu, T. C., Wang, C. L., Shau, Y. W., Tang, F. T., Li, K. L., & Chen, C. Y., Altered heel–pad mechanical properties in patients with type 2 diabetes mellitus, Diabetic Medicine, 17(12), 854–859, 2000.
[9] Kanatli, U., Yetkin, H., Simsek, A., Besli, K., & Ozturk, A., The relationship of the heel pad compressibility and plantar pressure distribution, Foot & Ankle International, 22(8), 662–665, 2001.
[10] Tsai, W. C., Wang, C. L., Hsu, T. C., Hsieh, F. J., & Tang, F. T., The mechanical properties of the heel pad in unilateral plantar heel pain syndrome, Foot & Ankle International, 20(10), 663–668, 1999.

052 **GEOMETRIC MEASURE OF DEFORMATION–A MEASURE OF TISSUE ELASTIC PROPERTIES.**

Kishore Kumar[1], Maneesha E.Andrews[2], V. Jayashankar[1], Ashok K. Mishra[2], S. Suresh[3].*
[1]Electrical Engineering Department, [2]Chemistry Department, Indian Institute of Technology Madras, Chennai, Tamilnadu, INDIA; [3]Mediscan Systems, Chennai, Tamilnadu, INDIA.

Background: The mechanics of hard tissues such as bones, teeth and horns can be analyzed using linear theory of elasticity [1], in which deformation is assumed to be small. Under this condition, the distinction between the geometries of the undeformed and deformed body can be ignored. Soft tissues in contrast, often undergo large or finite deformation. In this case, there will be difference in the geometries of the deformed and undeformed body. Ultrasonic techniques for the measurement and imaging of soft tissue elasticity and motion have been discussed in the literature [2]. Internal mechanical excitation (such as motion of the cardiac muscle and arterial pulsation) or external sources of motion are used to produce displacement of the tissue under investigation.

Aims: To measure geometrical parameters from the high resolution ultrasound B–mode images acquired before and after the compression. If there is significant change in geometrical parameters between compressed and uncompressed lesion, these parameters can be used in clinical diagnosis. Existing ultrasound B–mode equipment can be modified into a system that can measure these geometrical changes as a measure of elastic properties of the tissues.

Methods: Geometric measures considered are stretch, change in angle between two points (Figure 1), change in area, change in volume [3] and change in symmetry. These parameters are measured from the high resolution ultrasound B–mode images acquired before and after the compression by considering the undeformed lesion as the reference. Measurements are performed on polyacrylamide based tissue–mimicking phantoms designed with embedded inclusions of varying stiffness [4].

Results: Preliminary results obtained from tissue–mimicking phantoms indicate that these parameters have clinical potential. Changes in stretch, angle between two points, area and volume are very small for a stiffer lesion as compared to a soft lesion.

Conclusions: Changes in geometrical parameters are measured from the image of the deformed lesion by considering the image of the undeformed lesion as the reference. These measurements are done in tissue–mimicking phantoms with suitable marker points placed on the lesion for tracking. After checking suitability of this method in phantoms, the method can be extended to clinical trials, so that existing B–mode equipment can be modified to measure these parameters as a measure of elastic properties.

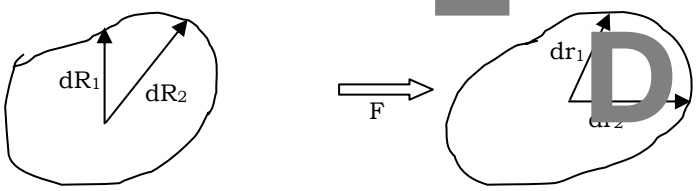

(a) Before deformation (b) After deformation

Figure 1: dR_1 and dR_2 are the lengths of line segments before deformation (a) and dr_1 and dr_2 are the lengths of line segments after deformation (b) due to applied force F. Change in lengths of these segments, change in angle between segments, change in area can be measured.

References:
[1] L. A. Taber, "Nonlinear theory of elasticity applications in Biomechanics", World Scientific, 2004.
[2] I. Cespedes, J. Ophir, et al. "Elastography: elasticity using ultrasound with application to muscle and breast *in vivo*", Ultrasonic Imaging, vol. 15, pp. 73–88, 1993.
[3] T. Varghese, U.Techavipoo, et al., "Elastographic measurement of the area and volume of thermal lesions resulting from radiofrequency ablation: Pathologic correlation", American Journal of Radiology, vol. 181, pp. 701–707, 2003.
[4] Kishore Kumar, M.E.Andrews, et al. "Viscoelastic properties of tissue mimicking phantoms for ultrasound elastography applications", Proceedings IEEE I2MTC '09, pp:1510–1513, May 5–7, 2009.

* *indicates Presenter*

054 **SEGMENTATION OF COLOR ELASTOGRAM FOR BETTER LESION DELINEATION AND DIAGNOSIS.**

K. Kumar[1], V. Jayashankar[1], S. Suresh[2].*
[1]Electrical Engineering Department, Indian Institute of Technology Madras, Chennai, Tamilnadu, INDIA; [2]Mediscan Systems, Chennai, Tamilnadu, INDIA.

Background: Several studies have demonstrated that B–mode ultrasonic imaging tends to underestimate the size of a tumor compared to the measurement of lesion in pathological specimen [1]. The tumor size in elasticity images is a more accurate representation of that measured at pathology [1,2]. Automated diagnosis of tumor margin in breast elastography is essential for better lesion delineation and diagnosis. Early work on semiautomated [3] and automated [1] segmentation of gray elastogram improved the lesion delineation and measurement accuracy of area and volume of the lesion.

Aims: To segment a breast tumor from the surrounding tissue in a color elastogram for locating and distinguishing benign and malignant breast tumors by extracting parameters from segmented region. Once the tumor region and background are defined quantitative measures such as width, depth, area and volume of the lesion and strain contrast can be estimated. Other features like mean and variance of RGB color components and mean hue value can also be measured from the segmented region.

Methods: Segmentation of a color image is performed using two different methods. The first method is a semiautomatic segmentation performed directly in RGB vector space. Given a set of sample color points representative of a color of interest, an estimate of the average color to be segmented is estimated. Now the objective of segmentation is to classify each RGB pixel in an image as having a color in the specified range or not. This is achieved by similarity measure using two methods – Euclidean distance and Mahalanobis distance. In the second method, a color image is transferred into an intensity image where the intensity at a pixel shows the color distance of that pixel to the background. Intensities in the image obtained in this manner are transformed according to a stretching function, to suppress details in the background and the lesion while enhancing details across the lesion boundaries. Finally, images are segmented based on multiple thresholding and expanding or shrinking of initial contour.

Results: Figure 1 shows the results of semiautomatic segmentation of an elastogram of a cyst embedded in polyacrylamide phantom. Segmentation using Mahalanobis distance measure gave better results. Color elastogram segmentation using the second method is better than first as it is fully automatic. Contour obtained using segmentation was compared with contour traced by an expert sonologist.

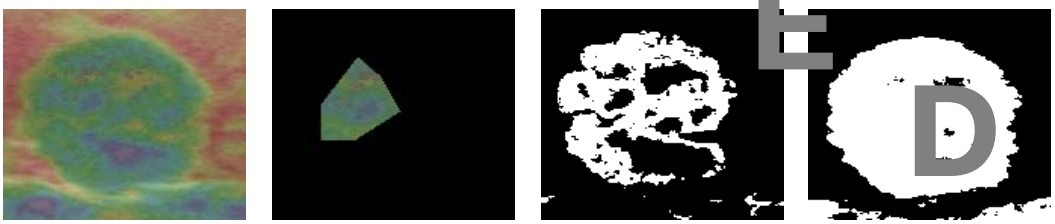

Figure 1:
(a) Elastogram of a cystic lesion
(b) User selected sample color points.
Segmentation using
(c) Euclidean and
(d) Mahalanobis Distance measure

Conclusions: In semiautomated segmentation, user interaction was limited to the selection of a polygonal region with sample color points within the lesion. The automatic method depends on color distance between the lesion pixel and background pixel. Results of segmentation are compared to those obtained using manual segmentation by an expert sonologist. In the future, these methods will be extended to clinical elastography images.

References:

[1] Wu Liu, J.A. Zagzebski, et al. "Segmentation of elastographic images using a coarse–to–fine active contour model", Ultrasound in Medicine and Biology, vol. 32, no. 3, pp. 397–408, 2006.
[2] T. Varghese, U. Techavipoo et al. "Elastographic measurement of the area and volume of thermal lesions resulting from radiofrequency ablation: Pathologic correlation" AJR, vol. 181, pp. 701–707, 2003.
[3] U. Techavipoo, T. Varghese et al. "Semiautomated thermal lesion segmentation for three dimensional elastographic imaging", Ultrasound in Medicine and Biology, vol. 30, no. 5, pp. 655–664, 2004.

063 **TEMPORAL AND SPATIAL STABILITY OF ACOUSTIC RADIATION FORCE-DRIVEN SHEAR WAVE VELOCIMETRY IN MYOCARDIAL TISSUE *IN VIVO*.**

Richard Bouchard[1], Stephen J Hsu[1], Vivek Subramanian[1], Patrick D Wolf[1], Gregg E Trahey[1].*
[1]Duke University, Durham, NC, USA.

Background: Shear wave elasticity imaging (SWEI) [1] has proven useful in non–invasively gleaning mechanical properties of soft tissue. SWEI research was originally focused on fairly isotropic and static organs (e.g. liver and breast). More recently, SWEI, or acoustic radiation force (ARF)–driven shear wave velocimetry, has been implemented in an *in vivo* cardiac environment [2] which is known to be highly anisotropic and dynamic. Given the kernel size (millimeters by tenths of millimeters) and sampling time (tens of milliseconds) currently required for our velocimetry technique (i.e. the lateral time–to–peak (TTP) algorithm) [3] establishing the temporal and spatial stability of velocity estimates in myocardial tissue *in vivo* is crucial in investigating the potential clinical viability of this application.

Aims: To quantify the temporal/spatial stability of SWEI in the mid–myocardium of a beating heart.

Methods: Using a commercially available ultrasound scanner, ARF–driven shear wave velocimetry was achieved in an open–chest preparation canine study. Shear waves were generated and tracked in the mid–myocardium of the left ventricular free wall (LVFW). The ultrasound transducer (5.71MHz; 1.75cm focus) was attached to the LVFW's epicardial surface with a vacuum–coupling device; acquisition was ECG–gated to coincide with the same period of end–diastole (i.e. a period of reduced physiological motion) in all cases. For the temporal stability assessment, shear wave velocimetry was achieved at the same spatial location (1.7mm), but across multiple heartbeats (≈90bpm). For the spatial stability assessment, velocimetry was ECG–gated across multiple heartbeats and was performed at successively offset lateral locations. All velocity estimate means were obtained from an average (N=4) of independent, 0.6mm (in depth) kernels about the transmit focus. For lateral TTP shear wave velocity estimation, a lateral kernel width of 2.2mm was utilized. In the spatial stability study, adjacent acquisitions (e.g. –2.5 to –1.3mm) bore 17–45% kernel overlap. R–squared values were calculated to indicate the degree of linearity of lateral TTP linear interpolation fits; mean(±SD) r-squared values for all fits used in each study are given.

Results:

Table 1: Temporal Stability Experiment

Beat [#]	Velocity [m/s]
1	1.10±0.03
2	0.87±0.04
3	1.12±0.02
4	1.11±0.05
5	1.10±0.05
6	1.06±0.02
7	1.17±0.02

Table 2: Spatial Stability Experiment

Loc. [mm]	Velocity [m/s]
-2.5*	1.70±0.07
-1.3	1.83±0.10
0.5	1.12±0.08
1.7	1.18±0.08
3.5	1.07±0.04
4.6	1.75±0.12
-2.5*	1.86±0.05

Temporal stability (Table 1) and spatial stability (Table 2) of mean (±SD) shear wave velocity estimates across multiple heartbeats. Mean temporal stability velocity estimates (R^2=0.95±0.03) present a standard error of 0.10m/s and vary by at most 29% across all seven heartbeats. If beat #2 (>2 SDs from mean) is removed, these metrics drop to 0.04m/s and 10%, respectively. Spatial stability velocity estimates (R^2=0.88±0.05) were obtained at six locations (kernel center relative to transducer given); beat numbers also apply to spatial data. Spatially alternating (i.e. independent) mean estimates vary by 5–43% across 3mm (e.g. 0.5–3.5mm); adjacent mean estimates (e.g. 0.5–1.7mm), by 5–48% across 1.2mm. The original/final estimates (*) correspond to the same location; these mean estimates vary by 9%, which indicates the measurement drift.

Conclusions: Shear wave velocimetry estimates acquired from the same location can be relatively stable across multiple heartbeats when ECG gating and a coupling device is used. Spatial variation of velocimetry estimates, however, can be significant in just a 1.2mm lateral span. This finding suggests that a 2.2mm lateral kernel might be too large for some regions of mid–myocardium; this notion is further supported by reduced r–squared values in some cases. To gain a better understanding of the inherent spatial stability of shear wave estimates in LVFW mid–myocardium, spatial stability measurements must be repeated in a static *in vitro* environment. Note: Shear wave velocity estimates were lower in this study than in our past study, where velocity estimates were often closer to 2m/s [2].

Acknowledgements: This research was funded by NIH Grants R01–HL–075485 and R21–EB–007741 and by an NSF Graduate Research Fellowship. We would like to thank Siemens Medical Solutions USA, Inc. for in-kind support.

References:

[1] Sarvazyan AP, Rudenko OV, Swanson SD, Fowlkes JB, and Emelianov SY, "Shear wave elasticity imaging: a new ultrasonic technology of medical diagnostics," Ultrasound Med. Biol. 24(9): 1419–1435, 1998.
[2] Bouchard RR, Wolf PD, Hsu SJ, Dumont DM, Trahey GE, "Acoustic Radiation Force–Induced Shear Wave Propagation in Cardiac Tissue," Proceedings of SPIE: 726512–1–8, 2009.
[3] Palmeri ML, Wang MH, Dahl JJ, Frinkley KD, Nightingale KR, "Quantifying Hepatic Shear Modulus *In Vivo* Using Acoustic Radiation Force," Ultrasound Med. Biol. 34(4): 546–558, 2008.

* *indicates Presenter*

077 **TWO–STEP DETECTION OF DISPLACEMENT FOR ELASTOGRAPHY USING GRAPH CUT.**

Naoto Akazawa[1], Satoshi Ozawa[1], Kan Okubo[1], Norio Tagawa[1].*
[1]Tokyo Metropolitan University, 6–6 Asahigaoka, Hino, Tokyo, JAPAN.

Background: A graph cut algorithm can effectively perform global minimization of an energy function and has attracted a lot of researchers as a useful tool for computer vision and image processing problems [1,2]. Especially, it can be used successfully for a stereo matching problem [2]. On the other hand, elastography has been examined as an important medical diagnostic imaging tool [3,4]. Displacement detection between echo signals measured before and after static compression of biological tissue in elastography coincides with a stereo matching problem from the viewpoint of signal processing.

Aims: In this study, we try to apply a graph cut algorithm to elastography in order to solve a trade–off problem stably, which consists of data consistency and smoothness constraint for displacement, with low computational cost. In consideration of high S/N imaging, our algorithm is based on an FM chirp pulse compression method.

Methods: Usual displacement detection in elastography uses RF echo signals for processing, but in this case, an alias problem arises if the displacement is larger than the wave length of a carrier. To solve this problem, a two–step detection strategy is introduced as in [5], in which the registration using an envelope waveform is first performed to detect large displacement, and subsequently the registration using carrier waveform and prior information propagated from the first step is done to detect precise one. For both registrations, the graph cut algorithm is adopted. The energy function to be minimized by the graph cut is defined as the sum of a data term and a smoothing term. The smoothing term means that neighboring sampling points in echo signals are apt to take the same displacement value. The data term means that the ultrasonic amplitude at the certain point should be similar to that at the corresponding point. To control the balance of the two terms, we can adjust the weight parameter's value. Registration needs multi–label assignments. Hence, we use alpha–expansion algorithm to apply the simple graph cut for the on–off problem. As a first attempt of the graph cut application for elastography, we examine the effectiveness of the proposed algorithm through simulations using PZFlex, which is a standard EFEM code. We generate a tissue model with three layers having different elasticity. The transmitted FM chirp has a center frequency of 20 MHz and bandwidth of 4 MHz. By varying the weight parameter's value, the obtained displacements are examined in comparison with those by a simple matching.

Results: As a natural result, the proposed method takes small computational cost as compared with the various optimization methods, for example simulated annealing. From this, we confirm that the graph cut is suitable for two–step detection. It is hard to apply simulated annealing based methods to two–step detection, because of their computational cost. The stability of the proposed method can be controlled by adjusting the weight parameter. When the data term is emphasized, the results coincide with those by simple matching.

Conclusions: We can understand the effectiveness of the graph cut algorithm for displacement detection in elastography through numerical simulations. It is desirable that the weight parameter's value can be automatically determined according to measured echo signals and related conditions. Additionally, experimental evaluations using a phantom are necessary to confirm the actual performance of it. In the future, we intend to study elastography using harmonic components and the graph cut algorithm for high–resolution elasticity imaging.

Acknowledgements: This work was supported by the research funds from Konica Minolta Medical & Graphic, Inc.

References:

[1] S. Fleck, et al., "Graph cut based panoramic 3D modeling and ground truth comparison with a mobile platform – The Wagele," Image and Vision Computing, vol.27, pp.141–152, 2009.
[2] M. Bleyer and M. Gelautz, "Graph–cut–based stereo matching using image segmentation with symmetrical treatment of occlusions," Image Communication, vol.22, pp.127–143, 2007.
[3] J. Ophir, et al., "Elastography: a quantitative method for imaging the elasticity of biological tissues," Ultrasonic Imaging, vol.13, pp.111–134, 1991.
[4] J.E. Lindop, et al., "Estimation of displacement location for enhanced strain imaging," IEEE Trans. UFFC, vol.54, no.9, pp.1751–1771, 2007.
[5] T. Shiina, M.M. Doyley, J.C. Bamber, "Strain imaging using combined RF and envelope autocorrelation processing," IEEE Ultrasonics Symposium, pp.1331–1336, 1996.

092 **A COARSE–TO–FINE APPROACH FOR ELASTICITY IMAGING AND ITS REAL–TIME IMPLEMENTATION IN A LOW COST ULTRASOUND SCANNER.**

Yongjin Zhou[1,2], Yongping Zheng[1,2], Zheng–Ming Huang[1].*
[1]Health Technology and Informatics Department, [2]Research Institute of Innovative Products and Technologies, The Hong Kong Polytechnic University, Hong Kong, CHINA.

Background: In conventional ultrasound elastography, phantoms or tissues are compressed slightly, normally <1% deformation is recommended. Various displacement and strain estimation methods have been proposed using radio frequency (RF) ultrasound data pre– and post–compression, aiming to improve the smoothness of strain field, speed up the calculation, increase the strain image contrast and/or achieve robustness against decorrelation during compression. However, only very few methods have been implemented in commercialized ultrasound machines for real–time elasticity imaging. So far, elastography function can only be provided by some high–end ultrasound scanners but not in relatively low–cost scanners. This greatly affects the promotion of extensive applications of elastography, particularly in those regions where high-end ultrasound scanners are not affordable.

Aims: In this study, we aim to develop a fast, while robust, approach for real–time elasticity imaging and to implement it in a relatively low–cost ultrasound scanner, which may not have the high quality RF data as those provided by high–end ultrasound scanners.

Methods: The proposed method is comprised of three steps of image processing based on RF data. First, we computed a 2D coarse motion field between two consecutive frames, and then we warped the first frame towards the second one according to the results of coarse motion estimation. Finally, the warped frame, paired with the original second frame, was used to compute the finer part of the motion field. Though many methods could be used, in this coarse–to–fine motion estimation, we employed the exhaustive–searching block matching method to secure the robustness to the potential decorrelation in the coarse step. Lucas–Kanade optical flow method [1,2] was used in the fine step to tune the motion field. The 2D displacement fields obtained in the two steps were combined to construct the overall displacements. The fine step was reiterated until certain convergence criteria were met. The strain image was calculated from the axial displacements.

Results: The proposed method was coded in Visual C++ 6.0 and was successfully implemented in a commercialized ultrasound scanner (CTS–8800, Shantou Institute of Ultrasonic Instruments Co., Ltd. Shantou, China), which includes a PC with Windows XP, Intel Core Duo 2.79GHz CPU and 2G memory. The interface of the scanner with elasticity function is shown in Figure 1b. The elastogram on a breast phantom (Model 047, CIRS, Inc., Norfolk, VA, USA) is shown in Figure 1a. The firmware of the scanner was modified so that RF data of a selected region can be transferred to a PC after generating a B–mode image. With a region of interest of 18*30mm^2 for elastography, we achieved images with 10 frames/s.

Conclusions: The proposed 2D coarse–to–fine approach overcomes several common challenges in elasticity imaging, including lateral motion, decorrelation caused by strains larger than 1% and real–time requirement. The scanner is now in clinical trials.

Acknowledgements: The project was supported by The Hong Kong Polytechnic University (J–BB69).

References:

[1] Lucas BD, and Kanade T, An iterative image registration technique with an application to stereo vision, Proc. Imaging Understanding Workshop, 121–130, 1981.
[2] Zhou YJ, Zheng YP, Development of a strain imaging method using Lucas–Kanade optical flow method in conjunction with expectation–maximization algorithm, Proc. 6th International Conference on the Ultrasonic Measurement and Imaging of Tissue Elasticity, p58, 2007.

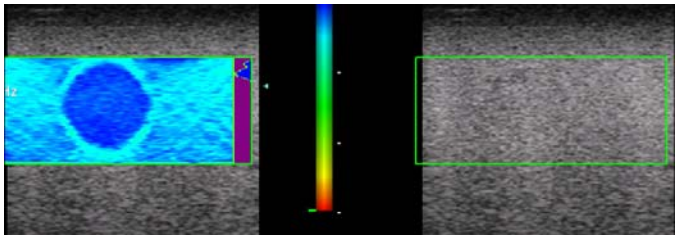

Figure 1: The software interface showing a typical result of B–mode (b) and elasticity imaging (a) obtained from a breast phantom with hard inclusion using the proposed coarse–to–fine approach in CTS–8800. The elastogram is coded with pseudo color.

* *indicates Presenter*

104 **SPECKLE TRACKING UNDER CONDITIONS OF SMALL KERNEL TO SPECKLE SIZE RATIO.**

Florence Kremer[1], Matilda Larsson[1,2], Hon Fai Choi[1], Piet Claus[1], Jan D'hooge[1].*
[1]Katholieke Universiteit Leuven, UZ Gasthuisberg, Herestraat 49, Leuven, BELGIUM; [2]Technology and Health School, Stockholm, SWEDEN.

Background and Aims: Echocardiography remains an important modality for the assessment of the morphology and function of the murine heart. Often, clinical cardiac scanners equipped with vascular transducers (imaging at 13–15MHz) are used for this purpose. Quantification of myocardial deformation properties could add valuable data to the conventional diagnostic information. To this aim, speckle tracking has received renewed attention. However, estimating strain in the lateral direction using this methodology remains challenging given the lack of phase information. This appears to be even more the case in the murine setting given that the kernel width has to be small in order to obtain multiple motion estimation across the wall as required for strain estimation. As such, for these clinical devices, the kernel width can become smaller than the lateral speckle size which results in more difficult pattern matching. In this study, a tissue–mimicking phantom deforming at velocities realistic for the murine heart was simulated in order to optimize block matching under these conditions.

Methods: A cylindrical tissue–mimicking phantom (2mm length, 1.37mm radius and 0.45mm wall thickness) was filled with randomly positioned scatterers. Their position was subsequently changed based on realistic radial and longitudinal deformation rate properties. Long axis RF images (FOV 4.5mm x 4mm) were obtained at a frame rate of 300Hz according to a previously described methodology [1] using a linear array transducer transmitting at 15MHz; bandwidth 60% and lateral pulse width of 0.5mm. This procedure was repeated 5 times in order to obtain 10 wall measurements. For displacement estimation, normalized cross–correlation was applied using a kernel size of 2x5λ and spline interpolation. Two–dimensional linear interpolation was then used to get a motion estimate in every pixel. Next, inter–frame displacement maps were summed over the whole cardiac cycle to obtain the cumulative displacements from which the (cumulative) strain was computed by linear regression. This strain estimation procedure was repeated for different amounts of axial (40, 60, 80%) and lateral (0, 20, 40, 60, 80%) window overlap. As an error measure, the square root of the sum of squared differences between the estimated strain and the ground truth was subsequently calculated. Differences between estimates were statistically tested using a one–way ANOVA.

Results: Lateral and axial strain error as a function of window overlap are shown in Figure 1. Although there was a tendency for smaller lateral strain error with decreasing lateral window overlap (independent of the axial overlap), this showed to be only statistically significant between 0 and 80% overlap (with axial overlap of 40%). Axial estimates remained of similar quality for all lateral overlap conditions although large window overlap in both directions tends to increase the error.

Conclusions: Under the challenging conditions where kernel size is small relative to the typical speckle size, this study shows that less overlap between kernels can improve strain estimation.

References:

[1] Gao H., Choi H.F., et al., "A Fast Convolution–based Methodology to Simulate 2D/3D Cardiac Ultrasound Images", IEEE Trans UFFC, 56(2):404–409, 2009.

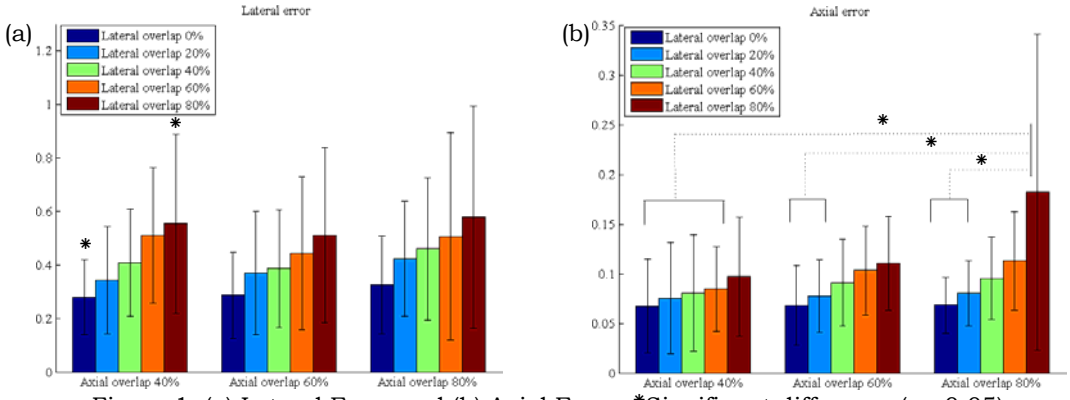

Figure 1: (a) Lateral Error and (b) Axial Error. *Significant difference ($p < 0.05$).

106 **REAL–TIME ULTRASOUND BREAST ELASTOGRAPHY: CLINICAL EXPERIENCE WITH DIFFERENT ULTRASOUND MANUFACTURERS' EQUIPMENT, WORK IN PROGRESS.**

William E Svensson[1], Ruth Williamson[1], Neelofer Zaman[1], Leslie North[1], Ortansia Doryforou[1], Smitha Putturaya[1].*

[1]Breast Imaging and Radiology Department, Imperial College Healthcare NHS Trust, Charing Cross Hospital, London, England, UK.

Background: Real–time elastography in the breast using freehand compression is a comparative displacement elastography method and currently cannot be used to measure absolute stiffness. Current techniques use kernel tracking (block matching) on the RF data line, phase shift or a combination of the two to measure deformation of tissues. Real–time shear velocity elastography with ultrafast imaging, which is not comparative, provides information which may, under some conditions, possibly be more accurate in providing absolute measurement of tissue stiffness with a reduction in effects from boundary conditions. All these techniques demonstrate focal areas of increased tissue stiffness which correlate with focal pathology.

Aims: We report our growing experience with the four different manufacturers' ultrasound elastography equipment in regular use for breast ultrasound. This presentation will describe the similarities and differences among four different manufacturers of elastography imaging equipment. The authors' understanding of the methods by which elastograms are obtained are based on a mixture of information provided by manufacturers and observation of the way in which variations in elastographic information help to possibly explain the methodology of the elastographic techniques

Results: The variation in elastographic appearances with strain and shear velocity techniques, which is partly due to the algorithms and approaches by individual manufacturers, also provides more information about the true variations of stiffness within and around different lesions. Information on factors which explain differences between cancers and benign lesions using the different equipment can increase our understanding of the complexities of elastography.

Discussion:

- With minimal movement pre–compression, boundary effects (Figures 1a & 2a) may be more significant resulting in potential loss of information from within focal abnormalities but may provide alternative information based on those same boundary effects and the degree of bonding.
- Increased movement and amounts of compression can provide information related to nonlinearity in the tissues being deformed (Figure 3b).
- Absolute measurement of tissue stiffness may be important in defining normality as well as the potential of serial measurement when changes are occurring in tissues (Figures 1b & 2b).
- Varying elastographic appearances provide more information about differences in internal characteristics of so called simple cysts as well as more complex cysts (Figures 2a & b).

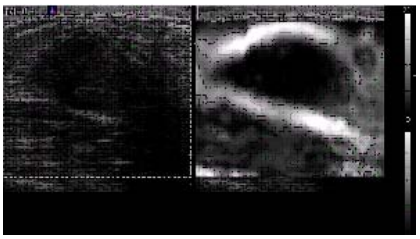

(a) freehand compression (black =stiff)

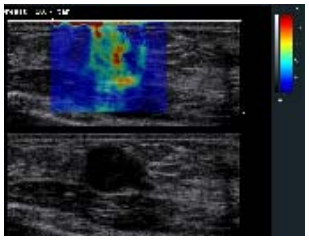

(b) shearwave ultrafast imaging (red=stiff)

Figure 1: Grade 2 intraductal carcinoma, very stiff

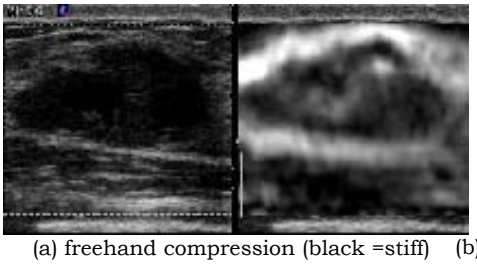

(a) freehand compression (black =stiff)

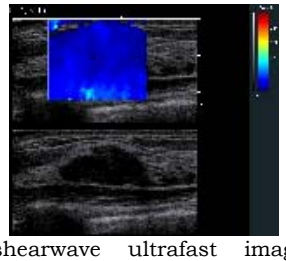

(b) shearwave ultrafast imaging (red=stiff) [black spot in its centre due to non-transmission of shearwave]

Figure 2: Fibroadenoma, mildly stiff with small cystic area

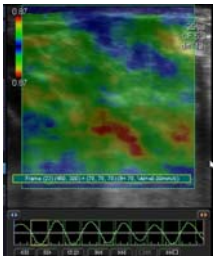

(a) Strain color overlay (blue=stiff)

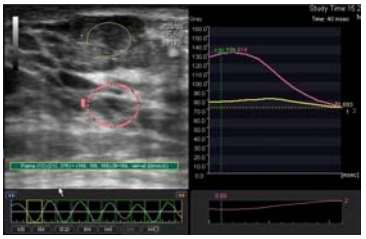

(b) Minimal change in stiffness during compression of lesion (yellow) and non linearity normal mixed fatty parenchyma (purple)

Figure 3: Fibroadenoma – Freehand compression

* *indicates Presenter*

108 **ELASTOGRAPHY ON GENERAL PURPOSE GRAPHICS PROCESSING UNIT (GPGPU) FOR REAL–TIME APPLICATIONS.**

Xu Yang[1], Sthiti Deka[1], Raffaella Righetti[1].*
[1]Electrical and Computer Engineering Department, Texas A&M University, College Station, TX, USA.

Background: Conventional strain estimators in elastography use time domain cross–correlation techniques to estimate local tissue displacements. Cross–correlation techniques are computationally intense, and, therefore, usually not suitable for real–time clinical applications. While several real–time elastography algorithms have been proposed in the recent years, improvements in computational speed to achieve real–time are often accompanied with losses in image quality of the resulting elastograms. In the recent past, the use of massively parallel General Purpose Graphics Processing Unit (GPGPU) for accelerating biomedical applications has received great interest [1,2]. A GPGPU is a parallel multithreaded multi–core processor which provides increased computational power with higher memory bandwidth in comparison with a standard CPU.

Aims: In this presentation, we investigate the use of GPGPU for real–time elastography applications. Implementation of conventional strain estimators on GPGPU cards could allow generation of real–time elastograms with no deterioration in elastographic image quality.

Methods: A conventional cross–correlation elastography algorithm was first implemented on standard CPU in C language. The algorithm was then analyzed in terms of computational efficiency and divided into three parts. The performance bottleneck was then identified and selected for execution on GPGPU's supporting CUDA [3] architecture. The remaining parts of the algorithm were modified for multi–thread processing, which allows CPU and GPU executing different parts of the algorithm at the same time. Both CPU and GPU codes were tested on an Intel Core Duo E4500 at 2.2GHz and a GeForce 8800 GTX graphics card, which has a G80 core equipped by 128 Streaming Processors at 1.35GHz and memory bandwidth of 86.4GB/s. Standard image quality analysis was carried out to evaluate the existence of any significant changes in elastographic signal–to–noise ratio (SNR), contrast–to–noise ratio (CNR) and resolution with respect to the conventional CPU elastography algorithm.

Results: The first native implementation of the elastography algorithm on GPGPU produced one frame per 3.59s, compared to 6.55s for the CPU algorithm for a typical elastogram corresponding to a 40x38mm^2 tissue area (RF data were collected at 6.6MHz, 40MHz sampling frequency and 128 channels processed using ~2mm window length and 80% overlap). With further optimization of memory bandwidth and program structure, our latest software version is now capable of producing 8.3 frames/s. Thus, our GPGPU accelerated implementation runs 54.3 times faster than the CPU–based code. The results of our statistical analysis indicate that there is no statistically significant difference in image quality of GPGPU vs. conventional CPU elastograms in all analyzed cases.

Conclusions: The use of GPGPU may provide a valid tool for obtaining real–time elastograms with no loss in resulting image quality with respect to conventional CPU elastograms. Further studies are required to assess the performance of GPGPU–based real–time elastography techniques on data *in vivo*.

Acknowledgements: This work is supported by funds from TEES and TAMU. We thank Dr. Riccardo Bettati, Professor in the Department of Computer Science and Engineering at Texas A&M University for his helpful suggestions on the use of GPGPU. We also thank Raghavendra Desai for his help in the implementation of the elastography algorithms.

References:

[1] Xu F, Muller K, Accelerating popular tomographic reconstruction algorithms on commodity PC graphics hardware, IEEE Trans. Nuclear Science, vol. 52(3): 654–663, 2005.
[2] Lim S, Kwon K, Shin BS, GPU–based interactive visualization framework for ultrasound datasets, Comp. Anim. Virtual Worlds, vol. 20:11–23, 2009.
[3] NVIDIA Corporation, CUDA Programming Guide Version 2.0, www.nvidia.com.

109 **PERFORMANCE ANALYSIS OF NEW LSE–BASED TIME CONSTANT ESTIMATORS FOR POROELASTOGRAPHY APPLICATIONS.**

Sanjay Nair[1], Thomas A. Krouskop[2], Raffaella Righetti[1].*
[1]Electrical and Computer Engineering Department, Texas A&M University, College Station, TX, USA; 2National Center for Human Performance, Texas Medical Center, Houston, TX, USA.

Background: In recent years, new elastography techniques for imaging the temporal behavior of tissues have been proposed [1,2]. Among these, viscoelasticity imaging and novel poroelastography techniques have shown the potential to be important clinical tools [3,4]. Some of these novel techniques aim at imaging the time constant (TC) of one or more elastographic parameters of interest. The TC is usually estimated by applying curve–fitting models to a temporal series of elastograms. Key issues to obtain accurate estimates of the TC values of the elastographic parameter(s) of interest are the employed curve fitting method and the related root–finding algorithms.

Aims: This work investigates the performance of two TC estimators for poroelastography applications, which are based on the least–square error (LSE) with minimization. More specifically, we aim to discuss the performance of LSE–based estimators executed by the use of the Levenberg–Marquardt (LM) and the bisection method.

Methods: This study consists of two parts: a simulation–based study for the statistical analysis of the performance of both LSE estimators and an experimental study to demonstrate the technical applicability of the two TC estimators on experimental elastographic data. Simulations are carried out on 1D TC curves with different degrees of additive zero mean Gaussian noise at constant SNR for all strains. The performance of the two LSE–based estimators is studied in terms of estimators' sensitivity, accuracy, precision and runtime. For comparison, the estimators' results are benchmarked against MATLAB's built–in curve fitting function. Preliminary experiments are performed on blocks of tofu, a poroelastic material that has been found to be a suitable phantom for ultrasound experiments [2]. For the purpose of the present study, the two TC estimators are used to generate axial strain TC elastograms from temporal series of axial strain elastograms obtained from the tofu samples under creep compression. It should be noted, however, that the proposed estimators can be similarly applied for the TC imaging of other elastographic parameters such as the effective Poisson's ratio [3].

Results: The results obtained from the simulation study demonstrate that overall the Levenberg–Marquardt estimator outperforms both the bisection search and the benchmark MATLAB function. Furthermore, this estimator can provide estimates of multiple elastographic parameters with high accuracy and sensitivity <1%. The bisection search estimator is found to be the most computationally efficient among the three analyzed in this study, but it provides accurate TC estimates only for acquisition intervals significantly longer than the true TC value. The preliminary experimental results show that it is technically feasible to generate experimental axial strain TC elastograms using both estimators. The experimental results are found to be in good agreement with previously published values obtained for similar tofu experiments [2].

Conclusions: The two new LSE–based estimators presented here have the potential to become effective tools for novel TC elastography applications. Additional experiments are required to assess the performance of these estimators in different experimental conditions of practical interest.

Acknowledgements: This work is supported by funds from TEES and TAMU.

References:

[1] Konofagou, EE, Harrigan, TP, Ophir, J, Krouskop, TA, Poroelastography: imaging the poroelastic properties of tissues, Ultras. Med. Biol., vol. 27: 1387–1397, 2001.
[2] Righetti, R, Ophir, J, Krouskop, TA, A method for generating permeability elastograms and Poisson's ratio time constant elastograms, Ultras. Med. Biol., vol. 31:6: 803–816, 2005.
[3] Qiu, Y, et. al., Ultrasonic viscoelasticity imaging of nonpalpable breast tumors: preliminary results, Academic Radiology, vol. 15: 1526–1533, 2008.
[4] Righetti, R, et. al., The feasibility of using poroelastographic techniques for distinguishing between normal and lymphedematous tissues *in vivo*, Phys. Med. Biol., vol. 52(21): 6525–41, 2007.

* *indicates Presenter*

110 **THE FEASIBILITY OF USING ULTRASOUND ELASTOGRAPHY TECHNIQUES TO IMPROVE VISUALIZATION OF BONE STRUCTURE.**

Biren Parmar[1], Raffaella Righetti[1], Ennio Tasciotti[2], Mauro Ferrari[2].*
[1]Electrical and Computer Engineering Department, Texas A&M University, College Station, TX, USA; [2]Nanomedicine and Biomedical Engineering Department, The University of Texas Health Science Center at Houston, Houston, TX, USA.

Background: Recently, ultrasound techniques have been gaining popularity as an alternative modality to characterize bone properties and image bone defects. Most of the work in the literature has focused on ultrasound characterization of bone surfaces based on the high reflectivity of sound at the soft tissue/bone interface [1]. However, additional information about soft tissue/bone mechanical properties may be obtained through strain imaging techniques.

Aims: This study aims at demonstrating the feasibility of using elastography techniques for bone imaging applications to augment the diagnostic information obtainable using standard B–mode imaging.

Methods: Preliminary *in vitro* experiments were performed on 35 bone samples obtained both from mammalian and non–mammalian animals. Elastography experiments were carried out both on intact animal samples and on bones embedded in gelatin phantoms. Additionally, controlled fractural defects were induced in a sub–set of animal bones to analyze changes in the distribution of elastographic parameters in intact vs. fractured bones. For elastographic data collection, the samples were subjected to sustained axial strain compression. Different types of strain elastograms were computed from pre– and post–compression RF data using C–based signal processing algorithms developed in our laboratory.

Results: Figure 1 shows preliminary results obtained from an intact bone sample (top row) and a bone sample with a non–union fracture (bottom row). For each sample, B–mode, axial strain elastogram and axial shear strain elastogram are shown (pixels corresponding to cross–correlation values below 0.9 are masked in the elastograms). In Figure 1 (top row), in the correspondence of the bone tissue (arrows), the axial strain elastogram shows a low strain area embedded between two higher strain areas, presumably representing the two soft tissue/bone interfaces. At corresponding locations, the axial shear strain elastogram shows a change in the directionality of the axial shear strain distribution. Analysis of the preliminary *in vitro* results obtained from intact vs. fractured bones indicates that the distribution of all elastographic parameters is significantly affected by the presence of bone fractures (indicated by the arrows in Figure 1 (bottom row)).

Conclusions: These preliminary results suggest that elastography techniques may provide complementary information to standard B–mode imaging for the visualization of soft tissue/bone structure. Additional experiments and independent validation methods are currently undergoing to confirm these findings.

Acknowledgements: This work is partially supported by funds from TEES and TAMU and by funds from DARPA to UTHSC, Department of Nanomedicine and Biomedical Engineering.

References:

[1] Xu W, Salcudean SE, Enhancement of Bone Surface Visualization Using Ultrasound Radio–Frequency Signals. IEEE Ultrasonics Symposium, 2535–2538, 2007.

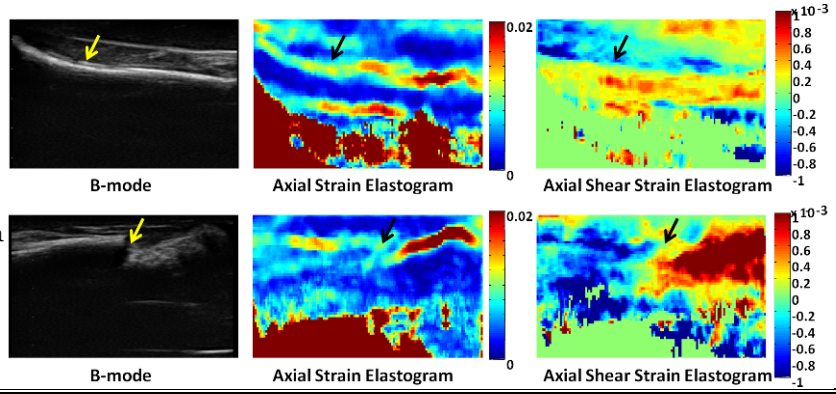

Figure 1:

114 **AXIAL–SHEAR STRAIN DISTRIBUTIONS IN BEEF MUSCLE SAMPLES UNDER LOAD: AN *IN VITRO* STUDY.**

A Thitai Kumar[1], B Galaz[1], R Miller[2] and J Ophir[1].*
[1]The University of Texas Health Science Center at Houston, Houston, TX, USA; [2]Texas A&M University, College Station, TX, USA.

Background: The thickness and bonding of the perimysium between fiber bundles (fascicles) have been shown to vary and to be associated with meat tenderness (see Figure 1 [1]). Higher use muscles have higher amounts of perimysial connective tissue that binds fascicles together tightly. When these muscles contract, slippage between muscle bundles is more controlled due to tighter connections or network than in muscles with less connective tissue [1]. The aim of the work reported here is to demonstrate the feasibility of visualizing the perimysial connective tissue and its behavior under load, using Axial–Shear Strain Elastography (ASSE).

Methods: Experiments were performed on isolated beef muscle samples (n=8) *in vitro*. Beef Longissimus muscles were removed 12.7cm anterior from the 12–13th rib inter–phase at 3 days post–harvest. Samples were 7.6x5.0x7.6cm (l x w x h) rectangles so that the muscle fiber orientation ran diagonally from the top to the bottom of the muscle. During imaging, each sample block was placed in a container and immersed in water at room temperature. Ultrasonic data were acquired using a Sonix 500RP ultrasound machine (Ultrasonix Medical Corporation, BC, Canada) with a linear array transducer operating at 10MHz center frequency. Pre– and post–compression RF data sets were acquired from each sample at 5 different planes along the elevational direction and processed to obtain ASSEs. The location of the imaging planes relative to one of the end-planes was measured. After imaging, the sample was taken out of the container and cut along the imaging plane that was closest to center of the sample. This cut plane was then photographed using a high resolution digital camera.

Results: We consistently observed a visual correspondence among diagonal striations appearing in the muscle samples, hyper–echoic pattern in the sonogram and high–intensity axial–shear strain zones in ASSE. An example set of images from one sample is shown in Figure 2. Notice that the sonogram, ASSE and axial strain elastogram have the same overall dimensions. However, because of lack of exact registration landmarks, we are unable to rigorously register these images to the corresponding photograph of the beef muscle sample. Nevertheless, it is interesting to note that structural details of the fascicles are visualized in the ASSE with high contrast at an acceptable image quality.

Conclusions: These initial experiments demonstrated the feasibility of visualizing the morphology and the shearing behavior under load in beef muscle sample using ASSE. Specifically, ASSE may become a useful technique to image the perimysial connective tissue and state of bonding at the various fascicles in muscle. The morphology and state of bonding between adjacent fascicles is thought to be related to the commercially important tenderness attribute of beef [1].

Acknowledgements: This work was supported in part by NIH grant R21–CA135580–01 and by the John S. Dunn foundation. The *in–vitro meat* samples were provided by Dr. Rhonda Miller.

References:

[1] Purslow, P., Physiology and biochemistry of connective tissue within meat, Recip. Meat Conf. 57, University of Kentucky, Lexington, 2004.

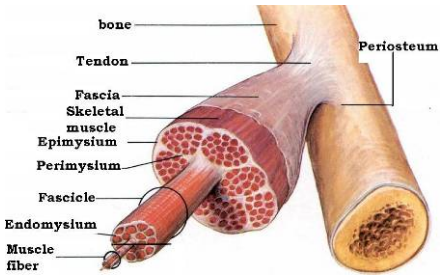

Figure 1: Sketch of skeletal muscle structure [1].

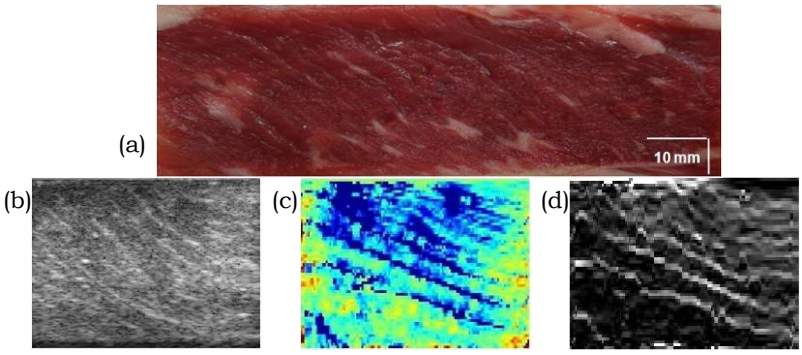

Figure 2: Visual comparison of different images from beef muscle sample experiment (a) photograph (b) sonogram (c) ASSE (d) axial strain elastogram.

* *indicates Presenter*

040 **IMPROVEMENT OF STRAIN UNIFORMITIES IN ELASTOGRAPHY BY INSERTION OF DAMPER.**

T. Sato[1], S. Sato[1], Y. Watanabe[1], S. Goka[1] and H. Sekimoto[1].*
[1]Faculty of Engineering, Tokyo Metropolitan University, 1–1 Minami Osawa, Hachioji, Tokyo, 192–0397, JAPAN.

Background: Using the Transmit/Receive face of a transducer as a compression board is regarded as a practical means in elastography because of its convenience. It is necessary to be careful with the specific distribution of strain produced by the shape of the T/R face [1]. In general, this strain is transferred radially, even inside multi–layered tissue. In this case, the non–uniformity of the strain is clearly observed at the tissue surface by the "edge effect" and is transferred to the deeper layers. This non–uniform strain causes inappropriate estimation or imaging of elastic moduli. We propose the insertion of a damper between the transducer and the tissue as a technique for softening non–uniformity.

Aims: This study aims to develop an optimization tool for applying strain and to investigate the effectiveness of inserting a damper.

Methods: The simulation tool developed in this study consists of 2–D structural analyses based on the finite element method and 2–D sonic analyses based on the finite difference time domain method. The tool is used to calculate the deformation of compressed tissue from a given (assumed) model of elasticity distribution and perform sonic analyses to obtain pre– and post–compression echoes. A strain image is obtained from these echoes via a cross–correlation process between them. Using this tool, the strain distributions with and without the damper are estimated, and the uniformities of the strain are assessed. An assessment model is illustrated in Figure 1. The tissue consisted of three layers of 50kPa, 100kPa and 50kPa in Young's modulus, and the damper was 50kPa and 0.4mm in thickness. The transducer was 60% of the width of the tissue model. Flatness, which is a ratio of the strain directly under the edge of the transducer to the strain directly under the center of the transducer in the same depth, is referred to as an assessment index.

Results: Figure 2 (a) and (b) shows the results of the strain distributions of the structural analysis without and with the damper, respectively. An edge effect can be seen in each case. However, only Figure 2 (b) clearly shows the non–uniformity in the middle layer. The results shown in Figure 3 demonstrate the flatness in the depth direction. The flatness at the tissue surface is markedly improved. These results are reflected in the simulation tool, then, the sonic analyses with a 10MHz transducer consisted of 240 point sound sources are executed in the tool. Figure 4 (a) and (b) demonstrates the results of the strain distribution obtained from the sonic analyses. A reasonable strain distribution is can be seen in Figure 4 (b) with the damper.

Conclusions: We presented possible improvement in elastography by the insertion of a damper. Future work will be the automatic optimization of the damper design.

References:

[1] E. Konofagou, P. Dutta, J. Ophir, et al: Reduction of stress non–uniformities by apodization of compressor displacement in elastography. Ultrasound in Med & Biol., No.9, 1229–1336, 1996.

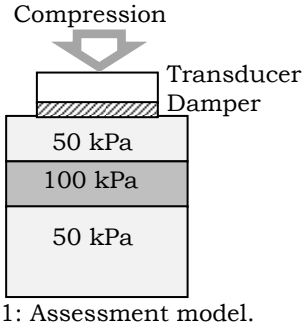

Figure 1: Assessment model.

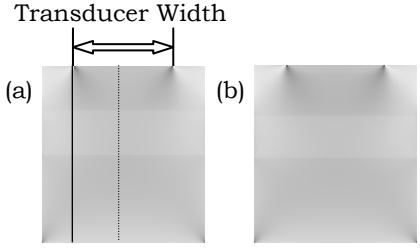

Figure 2: Calculated strain distributions. (a) without damper, (b) with damper.

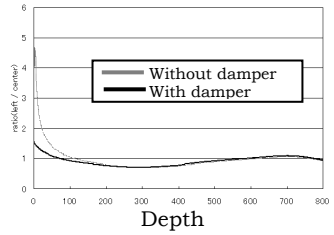

Figure 3: Flatness in depth direction.

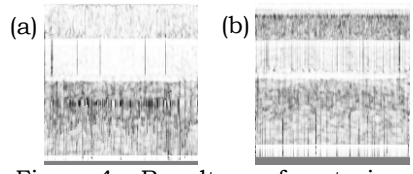

Figure 4: Results of strain distribution obtained from sonic analyses. (a) without damper, (b) with damper.

087 **2ND REPORT ON PROPER POINT SPREAD FUNCTION FOR LATERAL MODULATION.**

C. Sumi[1], K. Shimizu[1], Y. Takanashi[1], Y. Tadokoro[1], Y. Nozaki[1].*
[1]Sophia University, 7–1, Kioicho, Chiyodaku, Tokyo 102–8554, JAPAN.

Background: We have realized the beamformings [1,2], by using steering of the multiple beams and apodization, for accurately measuring tissue or blood displacement vectors or strain tensors using the multidimensional cross–spectrum phase gradient method (MCSPGM), and autocorrelation and Doppler methods (MAM and MDM). In [1,2], we reported lateral cosine modulation methods (LCMMs) that use several apodization functions in addition to the multidirectional synthetic aperture method (MDSAM) and the multiple transmitting methods (MTM). These modulations can also be used for B–mode imaging simultaneously. For these beamformings, in [3,4], we also reported more proper apodization functions than that expressed using Gaussian functions that we proposed previously, e.g., that using parabolic functions. Echo data having wider lateral bandwidths and higher signal–to–noise ratios (SNRs) can be obtained. Such echo data can also be obtained by realizing a proper point spread function (PSF) of which envelope has a wide FWHM and short feet such as a parabolic function (PA) rather than a Gaussian function (GA) and Hanning window (HA). In order to obtain a better approximation of such a PSF than that obtained by Fraunhofer approximation, we also developed optimization methods [3,4] for yielding the best apodization function in a linear least squares sense and a nonlinear manner (i.e., truncation of the feet of the apodization function).

Aims: In this study, the better envelope shape of the PSF than PA is searched for on the basis of the knowledge about the ideal shape obtained previously [3], i.e., having a wide FWHM and short feet. The properness is examined by evaluating the spectra for the LCM imaging and the accuracy for a displacement vector measurement.

Methods: The candidates of the proper envelope are selected from representative 15 analytic windows/functions (i.e., Akaike, Bartlett, Bartlett–Hann, Blackman, Blakman–Harris, Blackman–Nutall, Parazen, Nutall, Flap top, Kaiser, Chebychef, power function (power order, n>2), parabolic (PA), Turkey, rectangular) by drawing the windows having the same energy. On the basis of power function and Turkey window, a new function is also designed. For the candidates, independent laterally modulated echo data are simulated using white data, of which spectra are compared. In addition, the accuracies of the 2D displacement vector measurements are also compared using the above–mentioned displacement vector measurement methods. Only axial strains (0.1–2%) are simulated (ultrasound frequency = lateral modulation frequency, fy, 1–5 MHz; axial and lateral SDs for GA, 0.4–1.2 mm; echo SNR, 10–30 dB).

Results: By the drawing of the 15 envelopes, for better envelopes than PA, power functions (n > 2), rectangular window and Akaike window were obtained. n was changed up to 20. Moreover, a new analytic window was also obtained by changing Hanning windows by power functions in Turkey window (r, a relative length of direct current with respect to a total length). For SDs of 0.4 mm and frequencies of 3.5MHz for 16 candidates, the order of the measurement accuracy of axial displacement was, new function (e.g., Figure 1 when n=2 and SNR=10dB, r from 0.35 to 0.4) > rectangular window > power function (n>2) > PA > Akaike.

Conclusions: In simulations, using proper PSFs obtained, the accuracy of a displacement vector measurement was improved along with image quality (i.e., rather than PA). For human *in vivo* tissues (liver, blood etc), a real–time, freehand displacement vector measurement using new 2D and 3D measurement systems will also be reported together with a shear modulus reconstruction. For the better PSF, an analogue design or a dynamic programming will be performed.

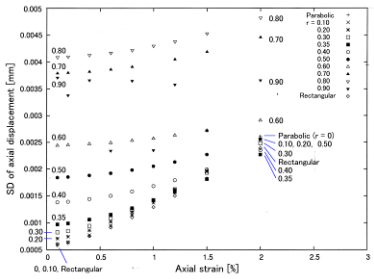

Figure 1: Simulations (10dB echo SNR).

References:
[1] C. Sumi et al., Jpn J Appl Phys, vol. 47(5B), pp. 4137, 2008.
[2] C. Sumi et al., IEEE Trans UFFC, vol. 55, pp. 2607, 2008.
[3] C. Sumi et al., "Proper point spread function for lateral modulation", Proc 7th ITEC, full paper version, 2008.
[4] C. Sumi et al., Jpn J Appl Phys, vol. 48(7B), 2008 (in press).

* *indicates Presenter*

105 **IS REAL–TIME ELASTOGRAPHY TARGETED BIOPSY ABLE TO ENHANCE PROSTATE CANCER DETECTION? ANALYSIS OF DETECTION RATE BASED ON AN ELASTICITY SCORING SYSTEM.**

Leo Pallwein[1], Fritz Aigner[1], Ralph Faschingbauer[1], Eva Pallwein[1], Germar Pinggera[2], Georg Bartsch[2], Georg Schaefer[3], Peter Struve[1], Florian Pedross[4], Werner Jaschke[1], Ferdinand Frauscher[1].*

[1]Radiology, [2]Urology, [3]Pathology, [4]Medical Statistics, Information and Health Economics Departments, Medical University Innsbruck, AUSTRIA.

Objective: This prospective study was performed to evaluate real–time elastography (RTE) by using an elasticity score for targeted prostate biopsy compared with systematic biopsy in a PSA first line screening population.

Material and Methods: 383 patients were included with elevated PSA (mean: 7.0± 13.8) and scheduled for systematic biopsy. Prior to a 10 core systematic approach, a targeted biopsy with a limited number of cores (maximum 5) was performed. Targeted biopsy was based on findings in RTE. Stiff lesions were considered malignant. Appearance of elasticity of outer gland areas was divided into: Score 1: normal (regular stiffness), Score 2: indeterminate (inhomogeneously increased stiffness) and Score 3: suspicious (homogeneously increased stiffness). PCa detection rate of each elasticity score was compared with findings of the systematic biopsy.

Results: Sensitivity for PCa detection (134 of 383 patients; 35%) was 88.8% (119/134) for the RTE targeted biopsy and 76.9% (103/134) for the systematic biopsy.

Score 1: elasticity pattern was found in 143 patients, 17 of which (11.9%) showing cancer;
Score 2: elasticity was assessed in 140 patients, 37 of which (26.4%) showing cancer
and Score 3: elasticity appeared in 100 patients, 68 of which (68.0%) showing cancer.

The difference of detection rate between Score 1 to Score 3 groups was significant ($p<0.001$). We found significant differences ($p<0.001$) of Gleason scores, PSA values and prostate volumes between different elasticity score groups.

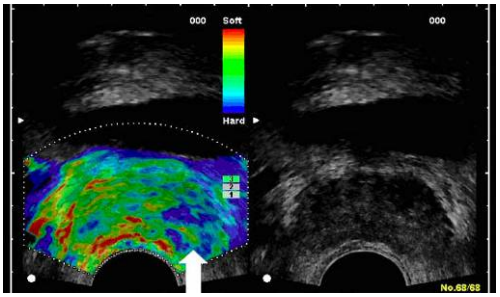

Figure 1: Typical appearance of a Score 2 elasticity pattern (arrow) fulfilling all criteria: inhomogeneous distribution of stiffness (i.e. alternating blue and green areas), diameter of each blue area of less than 5mm and reproducible after tilting the US probe.

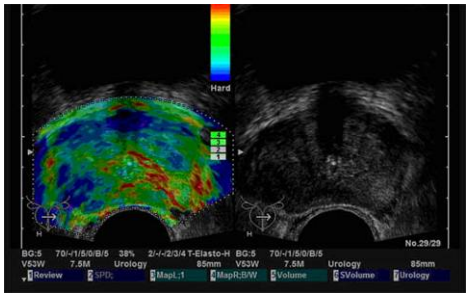

Figure 2: Typical appearance of a Score 3 elasticity pattern fulfilling all criteria: nearly homogeneous localized increase of stiffness (blue areas), diameter of at least 5mm and reproducible after tilting the US probe. Please notice the Score 2 stiffness pattern in the inner gland.

Conclusion: RTE by using the elasticity score improves PCa detection when compared with systematic biopsy.

References:

[1] Krouskop TA, Wheeler TM, Kallel F, Garra BS, Hall T, Elastic moduli of breast and prostate tissues under compression, Ultrason Imaging, 20(4):260–74, Oct 1998.

[2] Pallwein L, Mitterberger M, Struve P, Horninger W, Aigner F, Bartsch G, Gradl J, Schurich M, Pedross F, Frauscher F, Comparison of sonoelastography guided biopsy with systematic biopsy: impact on prostate cancer detection, Eur Radiol., 17(9):2278–85, Sep 2007.

[3] Frey H, Realtime elastography. A new ultrasound procedure for the reconstruction of tissue elasticity, Radiologe, 43: 850–855, 2003.

[4] Shiina TD, Doyley MM, Bamber JC, Strain imaging using combined RF and envelope autocorrelation processing, Proc of 1996 IEEE Ultrasonics Symp., 4:1331–1336, 1996.

[5] Sumura M, Shigeno K, Hyuga T, Yoneda T, Shiina H, Igawa M, Initial evaluation of prostate cancer with real–time elastography based on step–section pathologic analysis after radical prostatectomy: A preliminary study, Int J Urol., 14(9):811–6, Sep 2007.

085 **VIBRO–ELASTOGRAPHY IMAGING OF THE PROSTATE.**

S. E. Salcudean[1], X. Wen, S. S. Mahdavi[1], W. J. Morris [2], I. Spadinger[2].*
[1]Electrical and Computer Engineering Department, University of British Columbia, Vancouver, BC, CANADA; [2]Vancouver Cancer Centre, BC Cancer Agency, Vancouver, BC, CANADA.

Background: Radiation treatment of the prostate requires accurate segmentation of the prostate in ultrasound B–mode images, which has been shown to be unreliable. In our prior work [1], we have introduced ultrasound vibro–elastography imaging of the prostate, showing its feasibility in phantoms and limited patient studies.

Aims: To show that vibro–elastography images of the prostate can be carried out in a reliable manner using minor modifications to brachytherapy and ultrasound equipment.

Methods: We modified a brachytherapy stepper (EXII, CIVCO Medical Solutions) to acquire 3D dynamic elastography images by employing a cam–driven shaker and motorizing the probe rotation (Figure 1). A time–varying compression of up to 3mm amplitude can be programmed as a harmonic motion or band–pass filtered white noise in the 0–20Hz range. RF data are acquired while the transducer is in motion using the sagittal array of a bi–plane linear/micro–convex broadband 5–9MHz endorectal transducer of a Sonix RP ultrasound machine (Ultrasonix Medical Corp.). The RF data are processed to compute transfer function images as described in [2]. Vibro–elastography images are generated by computing the L_2 difference between transfer functions, applying 2D median filtering, histogram equalization and thresholding.

Prostate sector volume images were acquired from patients during the volume study (9 patients) and in the OR prior to brachytherapy (11 patients), with excitation amplitude of 0.5mm, and frequency of excitation from 0.5–4.5Hz (volume study) and 2–10Hz (OR). Preoperative MRI was also carried out in 4 of the patients imaged pre–operatively.

Results: The acquired images show average correlation values above 92% and coherence functions, computed with respect to the motion of the tissue in the focal area of the transducer, above 80%. The volumes of the errors between rigidly–registered segmented prostates from MRI and vibro–elastography images were found to be less that 5%. Images of the prostate, as shown in Figure 2, show excellent delineation of the gland.

Conclusions: Vibro–elastography produces consistently good images of the prostate. These may be useful for prostate segmentation for radiation treatment planning.

References:

[1] Salcudean, S.E., French, D., Bachmann, S., Zahiri–Azar, R., Wen, X., Morris, W.J., Viscoelasticity modeling of the prostate region using vibro–elastography. MICCAI, pp. 389–396, 2006.
[2] Turgay, E., S.E. Salcudean and R. Rohling, Identification of mechanical properties of tissue by ultrasound, Ultrasound Med. Biol., 32, 221–235, 2006.

Figure 1: Modified stepper with shaker and probe.

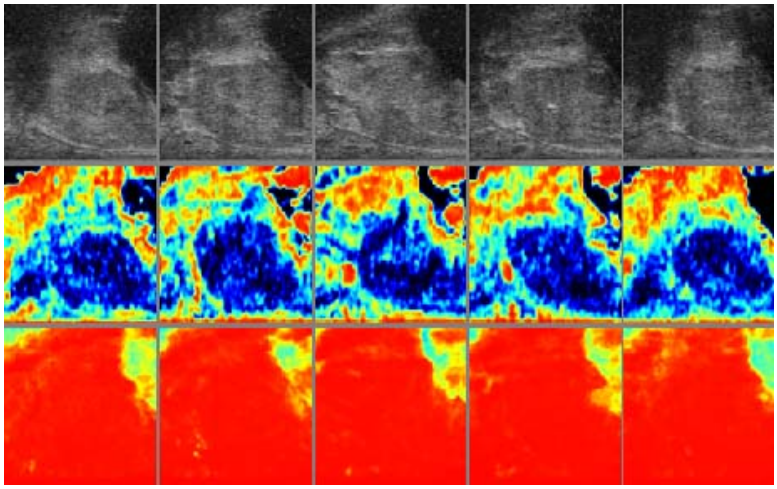

Figure 2: B–mode (top row), transfer function (middle row, red/dark is stiff) and average normalized correlation (NC) maps (bottom row, red/dark shows NC=1).

* *indicates Presenter*

031 **CLINICAL APPLICATIONS OF ELASTOGRAPHY IN ROUTINE SYMPTOMATIC BREAST ULTRASOUND.**

S Putturaya[1], WE Svensson[1], V Stewart[1], K Satchithananda[1], R Williamson[1], N Zaman[1], N Barrett[1], S Comitis[1], A Gupta[1].*

[1]Charing Cross Hospital, Fulham Palace Road, London, England, UK.

Background: We have been using real time elastography as an adjunct to routine breast ultrasound for the past 7 years. We have audited our practice and studied the clinical utility of elastography.

Aims: To highlight the clinical applications of real time elastography in routine symptomatic breast ultrasound.

Methods: Patients attending the one–stop clinic with palpable breast abnormalities had elastography as an addition to routine breast ultrasound. The combined results were correlated with final histology or follow–up. The strain imaging was done on a Siemens Elegra ultrasound machine as a part of research for the first 3 years. For the last 4 years, it has been done on a Siemens Antares machine as a part of routine work–up.

Results: 1058 cases have been analysed to date (research 334, audit 724).These include 257 cancers, 45 intermediate grade lesions and 758 benign pathologies.

Elasticity imaging alone, using an elasticity/B–mode lesion size ratio >0.75 [1] as an indicator for cancers and intermediate lesions, had sensitivity 96%, specificity of 52%. Elasticity combined with B–mode and colour Doppler had sensitivity 99% (for invasive cancers, dropping to 98% if intermediate lesions are included), specificity 47% (72% including cases with no B–mode abnormality). In 45% of cases, strain imaging increased diagnostic confidence. In 2% of cases, strain imaging affected management. 90% of cancers are stiff and appear larger on strain imaging with better demonstration of tumour extent. 40% of benign lesions appear significantly smaller, and many cysts have a variety of identifiable patterns on strain imaging [2]. No stiffness is seen in normal parenchyma, fat islands and gynaecomastia.

False negatives included 2 ADH and 2 DCIS, one radial scar, one invasive ductal carcinoma and one grade 2 invasive lobular carcinoma with LCIS. 7 phylloides, 6 mucinous cancers, 11 intraductal papilloma, and 8 pure DCIS were true positives.

Conclusions: We have found elasticity imaging to be a useful adjunct to routine breast ultrasound with a potential to safely decrease biopsies for benign lesions and map tumours more accurately. Increasing skill and experience provides greater accuracy in diagnosis. Correlation with B–mode, colour Doppler, subsequent histology and follow–up is crucial. Cysts with echogenic contents and isoechoic fibroadenomas were identified more easily, ensuring appropriate management. Eyeballing of the lesion size is as reliable as measurement in most cases for experienced operators.

Acknowledgements: Christina Vajdi for helping with data collection, Siemens Medical Solutions Ultrasound Division, Mountain View, CA USA for equipment loan and financial support.

References:

[1] Svensson WE, et al., Elasticity imaging of 67 cancers and 167 benign breast lesions shows that it could halve biopsy rates of benign lesions, Proc 4th International Conference on the Ultrasonic measurement and Imaging of Tissue Elasticity©, p 87, 2005.

[2] Brian S. Garra, et al., Elastography of breast lesions: Initial Clinical Results, Radiology, 202:79–86, 1997.

012 **USE OF SONOGRAPHIC ELASTOGRAPHY IN SUPERFICIAL SOFT TISSUE INFECTION.**

RJ Gaspari[1], D Blehar[1], M Mendoza[1], C Moon[1], D Polan[1].*
[1]University of Massachusetts, Worcester, MA, USA.

Background: Elastography is a new adjunct to real–time ultrasound imaging that overlays traditional B–mode imaging with a colored graphical representation of tissue elasticity. Soft tissue infections represent a common presenting condition to the emergency department and the differentiation of superficial cellulitis from soft tissue abscess can be challenging but relies mostly on physical exam with additional imaging by CAT scan or ultrasound [1,2]. Sonographic elastography has the potential to help in diagnosis and treatment of evolving soft tissue infections as they progress from induration to fluctuant abscess.

Aim: Describe the elastographic imaging characteristics of superficial soft tissue infections.

Methods: This was a prospective case series of patients with a suspected skin abscess requiring surgical drainage in the emergency department of an urban tertiary care center. Patients under the age of 18 or pregnant patients were excluded from the study. Patients with symptoms isolated to the genitalia or rectal area were also excluded. Ultrasounds were performed at presentation using an Ultrasonix Ultrasound Machine (Richmond, BC, Canada). Standard images were obtained of suspected soft tissue abscess collections including long and transverse B–mode images of the abscess, long and transverse images of abscess with elastography and B–mode images of a contralateral site for comparison. Ultrasound images were analyzed for the image characteristics of the elastographic images. Review of the ultrasound images was done in a blinded fashion with the reviewer unaware of any patient characteristics. Data analysis included descriptive statistics (mean +/- SEM).

Results: A total of 50 patients were enrolled in the study with a documented abscess by ultrasound and purulent material from incision and drainage. Most of the abscess cavities were visualized with B–mode imaging but only 58% (n=50) of the abscess cavities were visualized with elastography. Interestingly, some isoechoic abscesses that were difficult to identify by B–mode imaging were visible with elastography (Figure 1). Due to the heterogeneous nature of soft tissue abscesses, elastography ranged from confluent bands of color (27.6%), to large spotted signaling (38%) to small specked signaling (34.4%) (n=29) Although the surrounding tissue induration was not easily identifiable in B–mode imaging, the limits of the induration were identifiable using elastography in 98% (n=47) of the patients in this study (Figure 2). Imaging with elastography provided information unavailable through traditional B–mode imaging which may be useful for the diagnosis and treatment of soft tissue infections. In summary, elastography was useful in identifying isoechoic abscess cavities and accurately differentiated the induration surrounding the abscess from the surrounding healthy tissue.

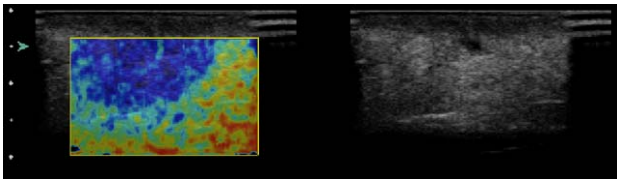

Figure 1: Hard indurated tissue is visualized with elastography as regions of stiff (blue) surrounding the abscess cavity, even if the cavity is not visualized on ultrasound.

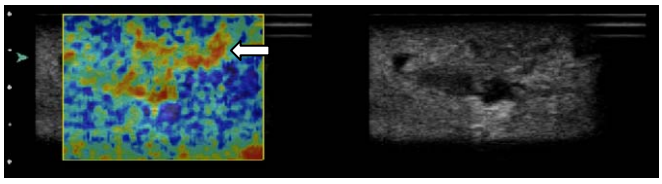

Figure 2: An abscess with mixed isoechoic and hypoechoic echoes shows additional extensions of the abscess cavity (white arrow) on elastography (red on yellow) that is not visible on grey scale B–mode.

Conclusions: Sonographic elastography accurately differentiates the induration surrounding an abscess from both the abscess cavity and the surrounding healthy tissue. Elastography has the potential to assist in the diagnosis and management of superficial soft tissue infections, but verification in larger clinical studies is necessary.

Acknowledgements: We would like to acknowledge the generous support of Ultrasonix Corporation who donated the equipment used in this study.

References:

[1] Squire, BT, JC Fox, and C Anderson, ABSCESS: applied bedside sonography for convenient evaluation of superficial soft tissue infections, Acad Emerg Med,12, 7: p. 601–606, 2005.
[2] Struk, DW, PL Munk, MJ Lee, SG Ho, and DF Worsley, Imaging of soft tissue infections, Radiol Clin North Am, 39, 2: p. 277–303, 2001.

* *indicates Presenter*

025 **MAGNETIC RESONANCE ELASTOGRAPHY (MRE) OF THE KIDNEY IN HEALTHY VOLUNTEERS.**

Rémi Souchon[1], Mustapha Bouhrara[1], Gaële Pagnoux[2], Jean–Michel Ménager[3], Richard L. Ehman[4], Olivier Rouvière[1,2].*

[1]INSERM U556, Lyon, FRANCE; [2]Hôpital E. Herriot, Lyon, FRANCE; [3]IRM du Tonkin, Villeurbanne, FRANCE; [4]Mayo Clinic, Rochester, MN, USA.

Background: Interstitial fibrosis is a pathological process associated with renal failure. Staging fibrosis is currently performed by biopsies. This process is prone to sampling errors and to eventual complications. We hypothesize that fibrosis stiffens the renal cortex, making it detectable and quantifiable by MRE [1].

Aims: The aim of this preliminary study was to assess the feasibility of the technique, its reproducibility and to provide initial stiffness values in the normal kidney.

Methods: Seven healthy volunteers were enrolled in the study. MRE was performed on a 1.5T scanner with a system similar to that used for liver (2]. A passive driver was placed against the posterior abdominal wall. A continuous vibration was applied using a loudspeaker. All three components of the displacements field were acquired in three contiguous imaging planes, with eight frames per vibration cycle. The curl operator was applied to the displacement field to remove the contribution of the longitudinal wave [3]. The resulting images were processed by directional filtering and local frequency estimator [4] to estimate the shear modulus. This process provided three stiffness images (one for each component of the curl vector) in each imaging plane. MRE was successively performed at two frequencies (45 and 76Hz). The total acquisition time was approximately 1 hour.

Results: The average shear modulus in the kidney was 5 ± 0.8 (3.4–6.5) kPa at 45Hz, and 8.7 ± 1.4 (7–11.5) kPa at 76Hz (results reported as mean ± standard deviation (minimum–maximum)). MRE was feasible in all volunteers. Individual results are reported Figure 1.

Conclusions: The study showed that MRE of the kidney was feasible. It also provided initial stiffness values for normal kidney. Further work is now needed to assess the correlation between stiffness and fibrosis.

Acknowledgements: The authors gratefully acknowledge Roger Grimm (Mayo Clinic) for support with the MRE sequence and software, Jean–Christophe Béra and Bruno Gilles (INSERM) for their help with the design of the driver, the staff at IRM du Tonkin and the volunteers.

References:

[1] Muthupillai R, et al., Magnetic resonance elastography by direct visualization of propagating acoustic strain waves, Science, 269(5232), 1854–1857, 1995.
[2] Rouvière O, et al., MR elastography of the liver: preliminary results, Radiology, 240(2), 440-448, 2006.
[3] Sinkus R, et al., Viscoelastic shear properties of *in vivo* breast lesions measured by MR elastography, Magn Reson Imaging, 23(2), 159–165, 2005.
[4] Manduca A, et al., Spatio–temporal directional filtering for improved inversion of MR elastography images, Medical Image Analysis, 7(4), 465–473, 2003.

Figure 1: Average shear modulus (kPa)
Each volunteer represented by a unique color.

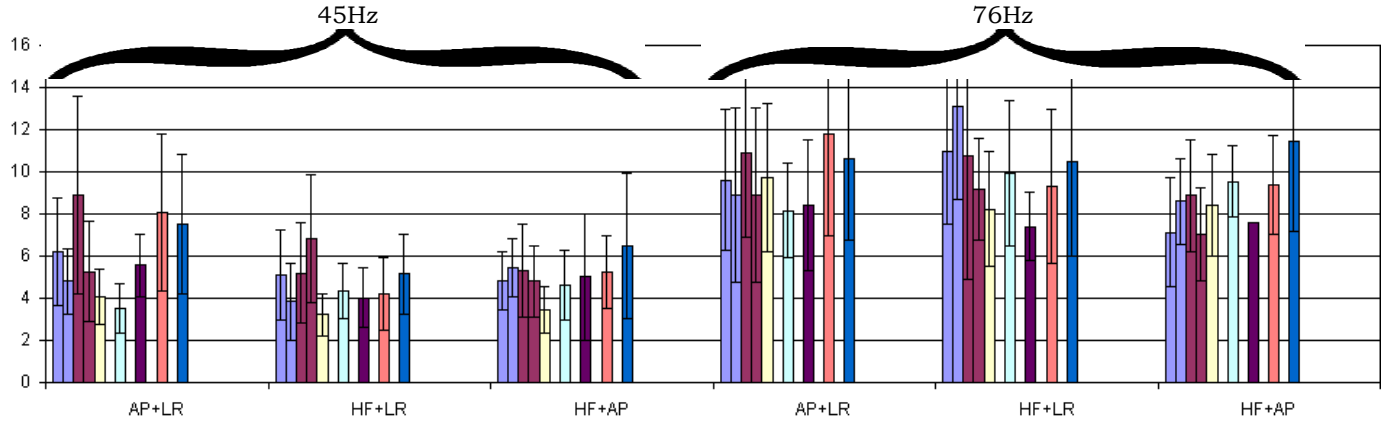

020 **FIBROSCAN® IN HEPATOLOGY: A REVIEW.**

Laurent Sandrin[1], Céline Fournier[1], Michel Beaugrand[2], Véronique Miette[1].*
[1]Echosens, 153 avenue d'Italie, Paris, FRANCE; [2]Service d'Hépatogastroentérologie, Hopital Jean Verdier, Bondy, FRANCE.

Background: Chronic liver diseases result in the accumulation of fibrosis inside the liver parenchyma which may eventually lead to cirrhosis. Cirrhotic liver is known to be stiffer than normal liver. Liver biopsy used to be the only gold standard for the assessment of liver fibrosis. At present, vibration–controlled transient elastography (VCTE) is used more and more for the staging of liver fibrosis.

Aims: In this presentation, the characteristics and performances of vibration–controlled transient elastography (VCTE) for the staging of liver fibrosis are presented.

Methods: VCTE (Fibroscan, Echosens, Paris, France) is used in clinical practice to quantify liver stiffness non–invasively and rapidly. Liver stiffness is compared to the fibrosis stage obtained by liver biopsy. Diagnostic performance of liver stiffness measurement (LSM) is evaluated using the area under the receiver operating curve statistical approach by comparison with fibrosis staging by liver biopsy published in literature databases [1] in multiple liver diseases. Tests were performed in the general population [2] in 1358 subjects. 28 subjects with LSM over 8kPa underwent liver biopsy (LB).

Results: Strong correlation between the liver biopsy fibrosis stage and liver stiffness are reported. AUROC for the diagnosis of significant fibrosis and cirrhosis are 0.84 and 0.94, respectively. In the general population, cirrhosis was diagnosed in all patients with LSM above 14.6kPa and liver fibrosis was observed in all biopsies performed in 20 patients with LSM between 8kPa and 14.6kPa.

Conclusions: Diagnostic accuracy of LSM by VCTE is very good for significant fibrosis and excellent for cirrhosis in a number of liver diseases: hepatitis B and/or C, HIV, co–infection, alcoholism, etc. Moreover, LSM was applied successfully in the general population as a screening tool for liver fibrosis with very high positive predictive value. However, liver stiffness is influenced by other hepatic conditions such as venous pressure [3] and acute hepatitis [4] that tend to increase stiffness values as biological tissues exhibit strongly nonlinear stress–strain relationships.

References:

[1] Friedrich–Rust, et al., Performance of Transient Elastography for the Staging of Liver Fibrosis: A Meta–Analysis, Gastroenetrology, 134,960–974, 2008.
[2] Roulot, et al., Liver Stiffness Measurement: an Appropriate Screening Method to Detect Liver Fibrosis in the General Population, EASL meeting, Copenhagen, 2009.
[3] Millonig, et al., Venous pressure increases liver stiffness (Fibroscan®) independent of liver fibrosis, EASL meeting, Copenhagen, 2009.
[4] Arena, et al., Acute Viral Hepatitis Increases Liver Stiffness Values Measured by Transient Elastography, Hepatology, 380–384, 2008.

006 **HAND–HELD ELASTOGRAPHY FOR GUIDING LIVER ABLATIONS PRODUCED USING A TOROIDAL HIFU TRANSDUCER.**

Jérémy Chenot[12], David Melodelima[12], Rémi Souchon[12], Jean–Yves Chapelon[12]*
[1]Inserm, U556, Lyon, F–69003, FRANCE; [2]University of Lyon, Lyon, F–69003, FRANCE.

Background: Imaging elastic properties of tissue for diagnosis of disease or for thermal treatment guidance is gaining attention since it is non–invasive and can provide new information regarding tissue.

Aims: The use of real–time elastography for imaging HIFU ablation during surgery in porcine liver by a toroidal HIFU transducer was investigated.

Methods: A conventional linear 12MHz real–time ultrasound imaging probe was used to obtain radiofrequency signals from a modified B–K ultrasound scanner. Strain images were calculated and displayed in real–time at 60 frames/s using a correlation–based method. Ablations produced in pigs during *in vivo* treatments were imaged. The quality of the elastograms corresponding to the elastically inhomogeneous liver (normal and ablated tissues) was assessed by computing the contrast–to–noise ratio (CNRe) and the signal–to–noise ratio (SNRe). In addition, the ablation dimensions measured on sonograms and elastograms were compared to gross pathology. The contrast observed between sonograms and elastograms was also compared.

Results: Sonograms and elastograms allowed observation of ablations with dimensions corresponding well to dimensions measured on gross pathology (r=0.82 and 0.94 respectively). The average CNRe and SNRe were 4.7 ± 5.1 (0.1 – 24.7) and 2.7 ± 1.3 (1.1 – 7.5) for elastograms and sonograms respectively. The contrast between ablated and non–ablated tissue was higher on elastograms (-15.6 dB) when compared with sonograms (-9.5 dB). In two specific cases, elastograms allowed a better evaluation of the ablation extent than sonograms (see Figures).

Conclusions: Hand–held sonography/elastography is straightforward and allows combining the advantages of both modalities used in a highly complementary manner for guidance of ablations produced in the liver during surgical HIFU therapy.

Acknowledgements: The authors wish to thank the staff of the laboratory for experimental surgery for their aid in the animal study. This work was supported by funding from EDAP TMS (N° EDAP 88513 B45) and by NIH/NIBIB Program Project Grant P01–EB–02105 to the University of Texas Health Science Center at Houston.

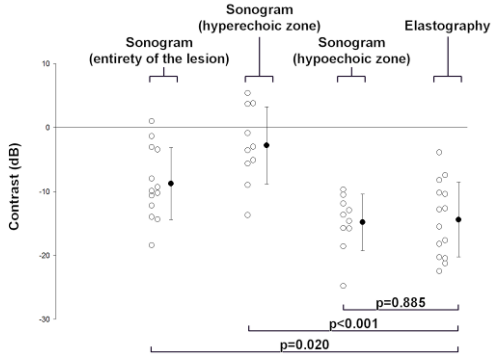

Figure 1: Comparison using Student's t–tests of the contrasts measured on sonograms and elastograms. Raw data (○) and mean ± SD are shown. The contrast of the entire lesion observed on elastograms was significantly higher when compared to the contrast of the entire lesion observed on sonograms ($p<0.05$) or when only the hyperechoic zone observed on sonograms was taken into account ($p<0.05$). The contrast of only the hypoechoic zone observed on sonograms was not significantly different ($p=0.885$) when compared to the contrast of the entire lesion observed on elastograms.

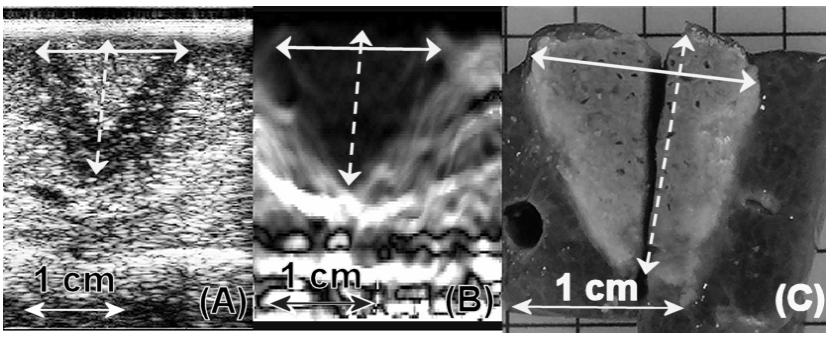

Figure 2: Single ablation produced in 40 seconds using the toroidal HIFU device.
(A) Sonogram: full arrow = 15mm, doted arrow = 17mm, contrast = -5.62 dB;
(B) Elastogram: full arrow = 15mm, doted arrow = 18mm, contrast = -22.53 dB, CNRe = 9.31, SNRe = 2.09;
(C) Pathology: full arrow = 16mm, doted arrow = 18mm.

098 **INTRAOPERATIVE CHARACTERIZATION OF THE MECHANICAL BEHAVIOR OF HUMAN LIVER.**

Marc Hollenstein[1], Mahmood Jabareen[1,2], Stefan Breitenstein[3], Marc–Oliver Riener[3], Pierre–Alain Clavien[3], Michael Bajka[3], Edoardo Mazza[1].*

[1]Swiss Federal Institute of Technology, 8092 Zurich, SWITZERLAND; [2]Technion – Israel Institute of Technology, Haifa 32000, ISRAEL; [3]University Hospital Zurich, 8091 Zurich, SWITZERLAND.

Aims: Aspiration experiments are carried out in order to determine the mechanical properties of human liver and their dependence on the histopathologic state. We will present the results of the clinical study currently ongoing at the University Hospital in Zurich.

Background: Measurements were carried out on 30 patients over the last 12 months. Human livers were tested during open surgery under sterile conditions using the aspiration device. Excision biopsies were taken from each measuring site for histology and microscopic assessment. Mechanical parameters were determined from the inverse analysis of the aspiration experiment.

Methods: The aspiration device has been used for the intra–operative mechanical measurements, Figure 1. Mechanical parameters for a non–linear visco–elastic constitutive model were determined through an inverse finite element analysis. The measurement was performed on the fully perfused organ during standard hepatectomy after opening of the abdomen and mobilization of the liver for resection. The surgeon applied the probe perpendicular to the tissue surface with a small contact force and tracked any relative motion of the liver due to respiration of the patient to avoid changes in the contact conditions. Measuring sites were defined on normal liver tissue and, on the tumor, on the portion of the organ that was to be resected. Each measuring cycle lasts 25 seconds, leading to a prolongation of the operation of not more than five minutes. After the resection, the measurements were repeated *ex–vivo* on a back table in the operating room; this enables comparison of *in–vivo* (fully perfused organ) versus *ex–vivo* properties. All of the measurements were performed by one single surgeon in order to avoid inter–tester variability.

Results: Analysis of the mechanical and histological data from all measurements is currently being carried out, and the results will be presented at the Conference. Preliminary results indicate that the small strain shear modulus of normal parenchyma is about 1.5kPa. The displacement (of point P, Figure 1) observed in the aspiration experiments for liver with tumor (metastasis carcinoma) is about 15% lower than the one of normal tissue, Figure 2. The corresponding inverse problem solution delivered a 40% higher initial stiffness for the tumor tissue. The corresponding histology revealed for the latter >40% fibrosis.

Conclusions: A reliable procedure for measurement, mechanical and histological data acquisition and analysis has been defined. Quantitative correlation between mechanical response and histopathological state can be determined from the results of this study. Preliminary assessments indicate a difference of about 40% in the initial stiffness between peri–tumor–normal liver tissue and liver tumor.

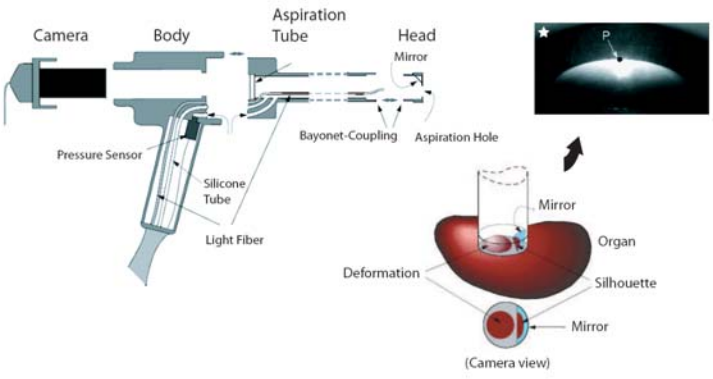

Figure 1: Aspiration experiment, main components

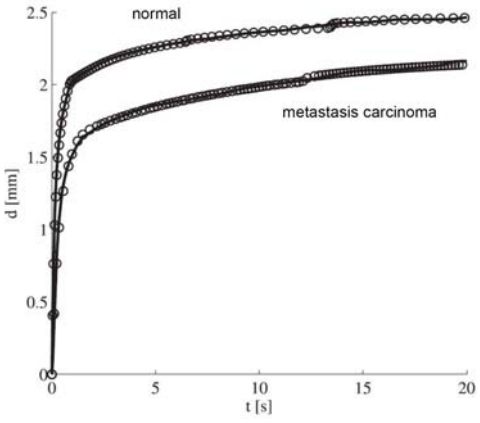

Figure 2: Comparison of apex displacement

* *indicates Presenter*

065 **MODEL–BASED ESTIMATION OF WAVE SPEED FOR THE SCALAR WAVE EQUATION.**

Jérome Fehrenbach[1], Véronique Miette[2], Laurent Sandrin[2].*
[1]Institut de Mathematiques de Toulouse, Toulouse, FRANCE; [2]Echosens, Paris, FRANCE.

Background: Transient elastography is a modality that allows the imaging of shear waves travelling in an elastic medium [1]. The reconstruction of shear velocity provides information on the shear modulus of the medium. Several algorithms have been proposed to recover the wave speed from the observation of the displacements [1,2,3].

Aims: The present study proposes an alternative method to reconstruct the wave speed from the displacement data. In this work, we do not differentiate the data. We use the wave equation directly and data assimilation techniques [4] to reconstruct the wave speed distribution.

Methods: The model used here is the scalar wave equation in an infinite domain. The solution depends on the initial condition and on the wave speed. The data are the values of the displacement at some points in the domain and at some instants. The unknowns are the initial value and the wave speed.

From the theoretical point of view, a cost function is defined that measures the L2 difference between the observations and the predictions of the model. The gradient of this cost function is estimated using the resolution of an adjoint wave problem. See [5,6,7] for the static case.

From the numerical point of view, direct simulations are performed in 1D and 2D. The computational domain is surrounded by an absorbing layer in order to mimic infinite space [8]. The wave equation is solved in the time domain with a Crank–Nicholson scheme.

The inverse problem of estimating the parameters (initial value and wave speed) amounts to minimizing the cost–function. The direct and adjoint derivative of the cost–function are estimated using direct and adjoint differentiation techniques, and the minimization of the cost–function is implemented with a zero–memory Gauss–Newton method [7].

Results: One–dimensional (1D) results are presented in Figure 1 at a noise level of 5%, and two-dimensional (2D) results for a plane wave in a unit square are presented in Figure 2 at a noise level of 2%.

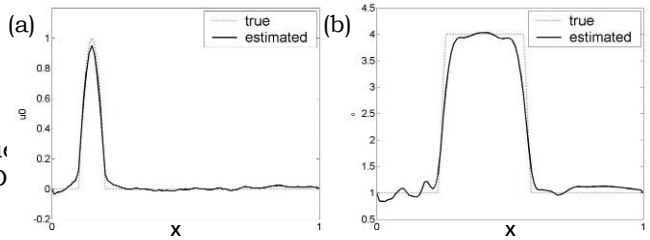

Figure 1: Reconstruction of the initial valu (a) and wave speed (b) in 1D 5% noise added to the data.

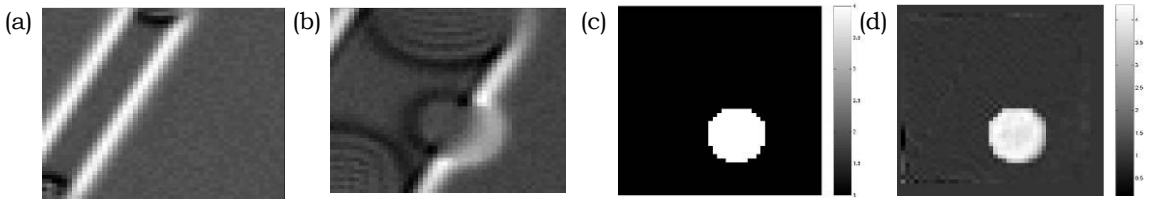

Figure 2: (a) the wave observed at t=0.13 and t=0.4; (b) true wave speed; (c) reconstructed wave speed, (d) 2% noise added to the data.

Conclusions: The model–based inversion of the wave equation proposed here shows a good potential to estimate wave speed, even in presence of noise.

References:

[1] L Sandrin et al., IEEE UFFC, Vol. 49, pp. 426–435, 2002.
[2] J McLaughlin and D Renzi, Inverse Problems, Vol. 22, pp. 681–706, 2006.
[3] R Sinkus et al., MRI, Vol. 23, pp. 159–165, 2005.
[4] FX Le Dimet, O Talagrand, Tellus A, Vol. 38, p.97, 1986.
[5] F Kallel and M Bertrand, IEEE TMI, Vol. 15, pp. 299–313, 1996.
[6] A Oberai et al., Inverse Problems, Vol. 19, pp. 297–313, 2003.
[7] J Fehrenbach et al., Inverse Problems, Vol. 22, pp. 1055–1069, 2006.
[8] J–P Bérenger, J. Comput. Phys., Vol. 114, pp. 185–200, 1994.

010 **VARIATIONAL MESH ADAPTION IN ELASTICITY IMAGING OF SOFT TISSUE.**

A Arnold[1], OT Bruhns[1], J Mosler[2].*
[1]Institute of Mechanics, Ruhr–University Bochum, Bochum, GERMANY; [2]Institute of Materials Research, Materials Mechanics, GKSS Research Centre Geesthacht, Geesthacht, GERMANY.

Background: It is well known that many different pathologies affect the stiffness of soft tissue. This is evident in breast and prostate cancer and in other tumors being recognised as hard lumps. Ultrasound elasticity imaging, or elastography, is an emerging medical imaging technique in which images of the spatial distribution of the stiffness of soft tissue are visualised. In this regard, ultrasound echo signals are measured before and after a defined compression. A displacement field can be calculated with these signals and subsequently, the stiffness distribution can be determined using quantitative elastography, cf. [1].

Aims: In order to reduce the numerical cost of reconstructing the stiffness distribution in quantitative elastography and to improve the accuracy of the results, a variational h–refinement is applied. In this way, the discretization can be adapted in two steps, i.e., the *a priori* unknown areas exhibiting a high stiffness distribution gradient are first localized and, subsequently, discretized with a higher resolution. In so doing, the displacement field can be better approximated. The same holds for the interfaces between different materials (healthy and cancerous tissue). The efficiency of the algorithm is further increased by applying a clustering technique similar to that known in image compression.

Methods: The unknown shear modulus distribution is computed by applying a relaxed minimization problem of Tikhonov–type. Using h–refinement of the underlying finite element triangulation, the resolution of the shear modulus distribution is increased, and, thus, the approximation of the numerical solution is improved. To identify the elements whose refinement improves the result significantly, an error indicator is calculated for each element. The applied error indicator was recently proposed in [2]. It is based on local sub–problems which shows a linear complexity and, thus, it is numerically very efficient. In order to reduce the number of degrees of freedom resulting from h–refinement further, elements are grouped according to their shear moduli. More precisely, a clustering technique known from digital image compression is employed.

Results: The performance of the variational h–refinement and the proposed clustering technique is demonstrated by means of a shear modulus reconstruction. The displacement field is generated by solving the forward problem. The analyzed prototype consists of one big and one small inclusion and the surrounding material. The ratio of the shear modulus is set to $\mu_1/\mu_2/\mu_{mat}=5/3/1$ (the first inclusion is the large one). The mesh adaption and the resulting shear modulus are shown in Figure 1.

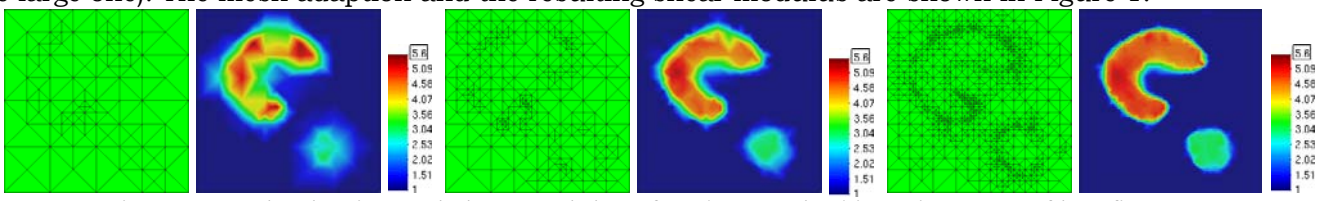

Figure 1: Mesh adaption and shear modulus after 5, 10 and 15 iteration steps of h–refinement

Conclusions: The proposed h–refinement leads to a better approximation of the measured displacement field and to a better representation of the shear modulus distribution by requiring only a relatively small number of degrees of freedom. By combining the method with a clustering technique, the numerical cost can be further reduced.

Acknowledgements: The financial support of the DFG (German Research Foundation) within the project BR 580/32–1 is gratefully acknowledged.

References:

[1] Oberai AA, Gokhale NH, Doyley MM and Bamber JC, Evaluation of the adjoint equation based algorithm for elasticity imaging, Physics in Medicine and Biology, 49, pp 2955–2974, 2004.
[2] Mosler J and Ortiz M, Variational h–adaption in finite deformation elasticity and plasticity, International Journal for Numerical Methods in Engineering, 72, pp 505–523, 2007.

* *indicates Presenter*

061 **THE EFFECTS OF THE BOUNDARY CONDITIONS AND SHAPE OF EXCITATION ON THE PHASE SPEED AND INVERSE PROBLEM SOLUTION.**

A Baghani[1], SE Salcudean[1], R Rohling[1].*
[1]University of British Columbia, Vancouver, BC, CANADA.

Background: Many of the inverse problem techniques used in dynamic elastography estimate the phase speed of the mechanical waves in the tissue [1–3]. These techniques typically assume a fixed relation between the phase speed and the tissue mechanical properties. For instance, the phase speed of the waves is related to the shear modulus of elasticity by $c = \sqrt{\mu/\rho}$.

Aims: This research was an analysis on the use of the phase speed for the estimation of mechanical properties. The question to be answered was whether the shape and condition of the boundaries and the shape of the excitation has an effect on the phase speed of the mechanical waves.

Methods: The solution to the wave equation with cylindrical symmetry was studied in the cylindrical coordinate system. The analytical solutions were found in terms of Bessel functions. In particular the displacements were assumed to have the following form:

$$u_r = U(r)\exp(i(k_z z+\omega t))$$
$$u_z = V(r)\exp(i(k_z z+\omega t))$$

This waveform represents a beam which travels in the z–direction. The beam form does not depend on z, and, therefore, the beam does not spread as the wave travels. The wave has a phase speed given by, $c = \omega/k_z$.

Results: It is shown that in an infinite medium, based on the beam form, the phase speed can take any value in the range $\sqrt{\mu/\rho} \le c < \sqrt{(\lambda+2\mu)/\rho}$, while the wave is purely of shear nature. λ and μ are the Lamé constants. In other words, for each chosen value of c in this range, a solution to the wave equation exists with that phase speed. For waves which involve both shear and irrotational components, the phase speed can take any value, $\sqrt{(\lambda+2\mu)/\rho} \le c$. In an infinitely long cylinder with stress free boundaries, for very low frequencies, the phase speed is given by $c = \sqrt{E/\rho}$, where E is the Young's modulus. For higher frequencies, multiple phase speeds could coexist at a single frequency, and the phase speed estimation might be meaningless in this case. Figure 1 shows the different phase speeds present in an infinitely long cylinder of r=5cm and μ = 10kPa for the waves travelling in the direction of the cylinder's axis. As can be seen for a typical frequency of 100 Hz, multiple phase speeds can coexist. Figure 2 shows *U(r)* and *V(r)* for mode 1.

Conclusions: Although the phase speed has been proven to provide useful information about tissue elasticity, care should be taken when interpreting the elasticity information extracted from it. In particular the boundary conditions and the shape of the exciter affect the relation between the phase speed and the tissue elasticity parameters.

Acknowledgements: This research was supported by NSERC.

References:

[1] L. Sandrin, M. Tanter, S. Catheline, and M. Fink, "Shear modulus imaging with 2–D transient elastography", IEEE Trans. Ultrason. Ferroelect. Freq. Contr. 49, 426–435, 2002.
[2] A. Manduca, T. Oliphant, M. Dresner, J. Mahowald, S. Kruse, E. Amromin, J. Felmlee, J. Greenleaf, and R. Ehman, "Magnetic resonance elastography: Non–invasive mapping of tissue elasticity", Medical Image Analysis 5, 237–2540, 2001.
[3] A. Romano, J. Bucaro, P. Abraham, and S. Dey, "Inversion methods for the detection and localization of inclusions in structures utilizing dynamic surface displacements", in Proceedings of SPIE Vol. 5503, volume 5503, 367–374, 2004.

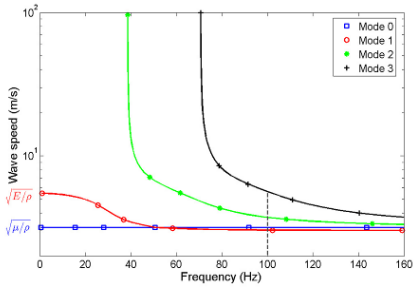

Figure 1: The first four modes of an infinitely long cylinder.

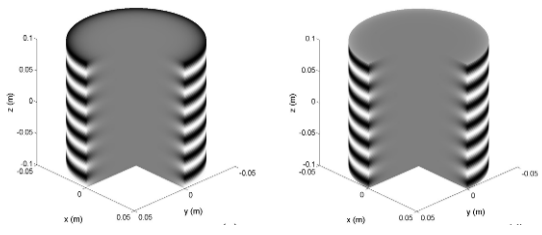

Figure 2: $U(r)$ and $V(r)$ for mode 1.

030 **LINEAR ELASTIC MATERIAL RECONSTRUCTIONS OF NON–LINEARLY ELASTIC MRE PHANTOMS.**

Irina M. Perreard[1], Adam J. Pattison[2], Matthew D. J. McGarry[2], Phillip R. Perrinez[2], Zohreh Barani[3], Elijah E.W. Van Houten[3], John B. Weaver[1] and Keith D. Paulsen[2].*

[1]Radiology Department, Dartmouth–Hitchcock Medical Center, One Medical Center Drive, Lebanon, NH 03756, USA; [2]Thayer School of Engineering, Dartmouth College, 8000 Cummings Hall, Hanover, NH 03755, USA; [3]Mechanical Engineering Department, University of Canterbury, Private Bag 4800, Christchurch, NEW ZEALAND.

Background: To date the most widely used MRE reconstruction procedures are based on linear elasticity, although the material behavior of soft tissue is better characterized by viscoelastic, anisotropic or poroelastic models [1,2,3].

Aims: This work aims to characterize the effects of reconstructing the shear stiffness of materials which do not behave in a linear elastic manner, using a linear elastic model. Linear elasticity assumption requires taking the real component of complex motions which becomes less valid with increasing damping levels; therefore the effect of introducing a phase shift (by adding $\pi/4$, $\pi/2$, $3\pi/4$) in the measured motion is investigated, as well as the frequency dependence of material non–linearities. The quantitative influence of the physical composition of the phantoms (volume fractions of inclusion(s) and background) on the reconstructed shear stiffness is examined.

Methods: Gelatin based phantoms were manufactured, and MRE data was collected. An elastic phantom (gelatin background and inclusion) served as baseline. Several viscoelastic phantoms (gelatin and glycerol), an anisotropic phantom (gelatin and pineapple) and a poroelastic phantom (gelatin and tofu) were tested. The iterative inverse algorithm employed to obtain the reconstructed material properties is described in [4]. Elastic reconstructions of the shear stiffness were compared with the baseline results. For comparison, experimental measurements of material properties were conducted with a dynamic mechanical analyzer.

Results:

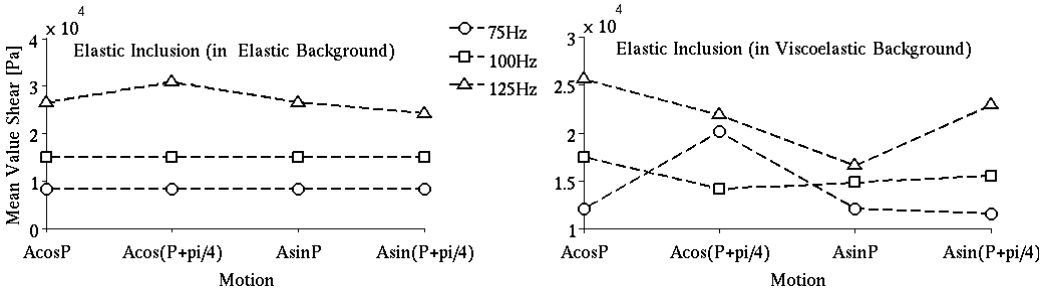

Figure 1: Reconstructed shear stiffness for (a) the elastic inclusion (15% w/w gelatin) in elastic background (5% w/w gelatin) and (b) elastic inclusion in viscoelastic background (7.8% gelatin and 12% glycerol). The influence of a phase shift is minimal in the baseline phantom as the linear elasticity model predicts, whereas in the nonlinear elastic phantom the results show up to 60% variation in the reconstructed shear stiffness.

Conclusions: Elastic reconstructions of non–linear MRE data produce quantitatively questionable values although they are spatially correct. The same material will show different reconstructed stiffness depending on its volume fraction and the composition of the phantom. Linear elastic phantoms do not show a lot of variation with assumed motion phase shift, whereas non–linear phantoms do due to the greater degree of spatial variation in phase of the harmonic motions.

Acknowledgements: This work was supported by NIH Grant 5 P01 CA080139–08.

References:

[1] Sinkus, R., Tanter, M., Catheline, S., Lorenzen, J., Kuhl, C., Sondermann, E., and Fink, M., "Imaging anisotropic and viscous properties of breast tissue by magnetic resonance-elastography", Magn Reson Med, 53, pp. 372–387, 2005.

[2] Perriñez, P. R., Kennedy, F. E., Van Houten, E. W., Weaver, J. B., and Paulsen, K. D., "Modeling of Soft Poroelastic Tissue in Time–Harmonic MR Elastography", TBME, in press, 2009.

[3] Van Houten, E. E., McGarry M. D. J., Weaver, J. B., and Paulsen, K. D., "First Results in the Measurement of Rayleigh Elasticity Parameters in Phantoms and *In–Vivo* Breast Tissue", Proc. 7th Intl. Conf. Ultrasonic. Meas. and Imag. of Tissue Elasticity, pp. 42, 2008.

[4] Van Houten, E. E., Miga, M. I., Weaver, J. B., Kennedy, F. E., and Paulsen, K. D., "Three–dimensional subzone–based reconstruction algorithm for MR elastography", Magn Reson Med, 45, pp. 827–837, 2001.

* *indicates Presenter*

017 **ACCURACY OF ENDOSCOPIC ULTRASOUND ELASTOGRAPHY USED FOR THE DIFFERENTIAL DIAGNOSIS OF CHRONIC PANCREATITIS AND PANCREATIC CANCER: A MULTICENTRIC STUDY.**

Adrian Săftoiu[1], Peter Vilmann[3], Florin Gorunescu[2], Uwe Will[4], Marc Giovannini[5], Jan Janssen[6], Julio Iglesias–Garcia[7], Paolo Arcidiacono[8], Michael Hocke[9], Collin McKay[10], Dan Ionuț Gheonea[1].*

[1]Gastroenterology Department, [2]Biostatistics and Computer Science Department, University of Medicine and Pharmacy Craiova, Dolj, ROMÂNIA; [3]Surgical Gastroenterology Department, Gentofte University Hospital, Hellerup, DENMARK; [4]Gastroenterology Department, SRH Wald–Klinikum Gera, GERMANY; [5]Endoscopic Unit, Paoli–Calmettes Institut, Marseilles, FRANCE; [6]HELIOS Klinikum, Wuppertal, GERMANY; [7]Gastroenterology Department, University Hospital Santiago de Compostela, SPAIN; [8]Division of Gastroenterology & Gastrointestinal Endoscopy, University Vita–Salute San Raffaele, Milan, ITALY; [9]Internal Medicine II Department, Friedrich–Schiller University, Jena, GERMANY; [10]Hepatobiliary Surgery Department, Glasgow Royal Infirmary, Glasgow, Scotland, UK.

Background: Endoscopic ultrasound (EUS) elastography represents a new imaging procedure that might characterize the differences of hardness and strain between diseased tissue and normal tissue. The method has been used for the differential diagnosis of focal pancreatic masses (pancreatic cancer and chronic pancreatitis) with variable accuracy and contradictory results [1].

Aim: The aim of the study was to assess elastography during EUS examinations of focal pancreatic masses, and to consequently differentiate benign vs. malignant pancreatic masses in a prospective, blinded and multi–center design.

Method: A post–processing software analysis (based on the ImageJ software, NIH, Bethesda, MD, USA) was used to examine the EUS elastography movies by calculating average hue histograms from individual elastography images. The data was further subjected to an extended collaborative neural networks (NNs) computing analysis in order to differentiate benign versus malignant patterns. The study group comprised 125 patients with focal pancreatic masses which were included prospectively in 9 reference centers. For each patient, three separate individual movies of 10 seconds were recorded digitally and uploaded in an on–line database system (Figure 1). Final diagnosis was based on positive cytology results obtained through EUS–guided FNA, final pathology results obtained after surgery, as well as typical imaging findings associated with minimum 6 months of follow–up.

Results: The effectiveness of a collaborative computing system, based on a NN approach was assessed in order to provide a real–time decision support for the medical diagnosis. A thorough statistical benchmarking process and a weighted voting system were employed to identify the best NN models as reliable classifiers and to obtain the overall automatic diagnosis. Multi–layer perceptron (MLP) neural networks with both one and two hidden layers of neurons (three–layer perceptron and four–layer perceptron) were trained to learn how to classify focal masses as benign or malignant and yielded an excellent testing performance, together with a high training performance. Consequently, the accuracy of both MLP models was higher than 90%, in accordance with previously published data. However, the NNs approach might provide a very fast and accurate diagnosis supporting and improving the human decision making, especially in difficult cases.

Conclusions: EUS elastography is a promising method that allows characterization and differentiation of pancreatic cancer and chronic pancreatitis, especially if the standard methods of diagnosis fail to indicate precisely the benign or malignant nature. A robust methodology based on artificial NNs processing of the digital EUS elastography movies, enabled an optimal prediction of the type of pancreatic lesions. The final results of the study will be analyzed and confirmed as soon as the patient inclusion period ends.

Acknowledgements: This presentation was partially financed through the research grant PNCDI II (Ideas) no. 239/2007.

References:

[1] Săftoiu A, et al., Neural network analysis of dynamic sequences of EUS elastography used for the differential diagnosis of chronic pancreatitis and pancreatic cancer, Gastrointest Endosc., 68:1086–1094, 2008.

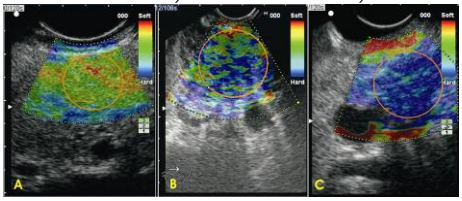

Figure 1: Comparative EUS elastography aspects of (A) normal pancreas, (B) chronic pancreatitis and (C) pancreatic cancer

002 **A HYBRID DISPLACEMENT ESTIMATION METHOD FOR STRAIN IMAGING.**

Lujie Chen[1], R. James Housden[1], Graham M. Treece[1], Andrew H. Gee[1], Richard W. Prager[1].*
[1]University of Cambridge, Cambridge, England, UK.

Background: Axial displacement estimation is fundamental to many quasistatic, ultrasonic strain imaging systems. An efficient way to track axial displacements is to use a phase–based metric [1,2]. However, phase–zero tracking is a one–dimensional, axial process and lateral motion must be determined by some other means. Multi–level correlation strategies [3] estimate both axial and lateral displacements but are subject to the processing overhead of the higher level searches. Both single–level tracking and multi–level strategies suffer from certain types of error propagation. Errors can propagate from one window to its neighbours (single–level tracking) or from one level to the next level (multi–level).

Aims: To develop a novel estimation method that combines elements of multi–level correlation and phase–zero search, improving on the noise tolerance of both approaches.

Methods: There are three levels of processing that we shall refer to as L1, L2 and L3. Successive levels are seeded by their immediate predecessors and recover an increasingly fine–scale grid of displacement estimates by matching windows between pre– and post–deformation frames. There are only nine L1 windows, whose centres coincide with a subset of the L2 windows. Likewise, the L2 window centres coincide with a subset of the L3 windows. In this way, displacement estimates can be passed from one level to the next using quality–guided tracking [2] with no need for interpolation. L1 and L2 operate on RF magnitude data. Each L1 window is searched independently within predetermined axial and lateral bounds, while L2 employs quality–guided axial–lateral displacement tracking. L3 operates on baseband analytic data and performs fine scale axial displacement estimation using a phase–based algorithm, again with quality–guided tracking. Lateral displacement estimates are not refined at L3.

Results: Three algorithms, a single–level [1], a multi–level [3] and the hybrid method were compared based on *in vivo* and simulated data sets. Figure 1 shows a human testis scan. Visual inspection reveals that the hybrid method is more capable of reducing peak hopping errors than the other two algorithms. A hard inclusion in a uniform background was simulated using Abaqus FEA software with an applied deformation of about 1% in the axial direction. The experimental protocol involved corrupting the simulated RF echo data with additive noise at six signal–to–noise ratios (SNR) in the range 4dB to -1dB. Each method was evaluated 200 times (with different random noise) at each SNR level. The estimated axial displacement field was compared with the known ground truth, and the average absolute point–wise difference was recorded. Figure 2 shows that the hybrid method produces the smallest errors. One of the key advantages of the hybrid method is that the lateral estimates provided by the L1 and L2 search are relatively insensitive to noise due to their low resolution and are sufficiently accurate to compensate for lateral motion. There is no error–prone lateral search at the finest resolution, which significantly improves the robustness to noise.

Conclusions: Owing to its carefully designed algorithmic structure, the hybrid method has superior accuracy to both the single–level tracking and the multi–level approaches.

Acknowledgements: This work was funded by Translation Award 081511/Z/06/Z from the Wellcome Trust.

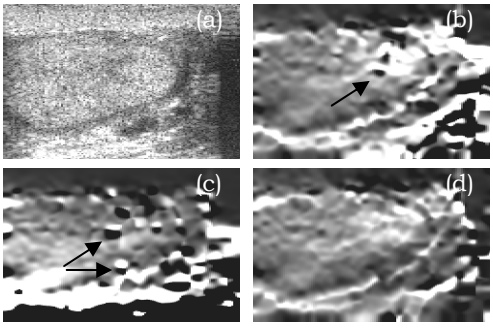

Figure 1: Testis scan. (a) B–mode image. Axial strain images obtained by (b) the single–level, (c) the multi–level and (d) the hybrid method. Arrows indicate peak hopping errors.

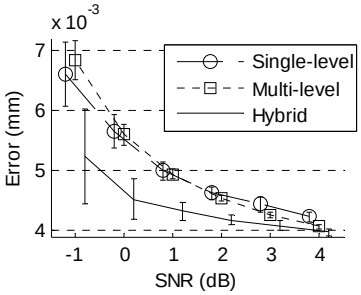

Figure 2: Difference between the ground truth axial displacement field and those obtained by the various methods.

References:

[1] G. M. Treece, J. E. Lindop, A. H. Gee, and R. W. Prager, Freehand ultrasound elastography with a 3–D probe, Ultrasound in Medicine and Biology, 34, 463–474, 2008.
[2] L. Chen, G. M. Treece, J. E. Lindop, A. H. Gee, and R. W. Prager, A quality–guided displacement tracking algorithm for ultrasonic elasticity imaging, Medical Image Analysis, 13, 286–296, 2009.
[3] H. Shi and T. Varghese, Two–dimensional multi–level strain estimation for discontinuous tissue, Physics in Medicine and Biology, 52, 389–401, 2007.

* *indicates Presenter*

013 **ELASTICITY MAP RECONSTRUCTION OF ATHEROSCLEROTIC PLAQUES BASED ON A SEGMENTATION–DRIVEN OPTIMIZATION PROCEDURE USING STRAIN MEASUREMENTS.**

Jacques Ohayon[1,3], Simon Le Floc'h[1], Philippe Tracqui[1], Gérard Finet[2], Ahmed M. Gharib[3], Roch L. Maurice[4], Guy Cloutier[4], Roderic I. Pettigrew[3].*

[1]Laboratory TIMC–IMAG UJF, DynaCell, CNRS UMR 5525, Grenoble, FRANCE; [2]Hemodynamics and Interventional Cardiology Department, INSERM Unit 886, Lyon, FRANCE; [3]Laboratory of Integrative Cardiovascular Imaging Science, NIDDK, NIH, Bethesda, MD, USA; [4]Laboratory LBUM, CRCHUM, Montréal, Québec, CANADA.

Background: The challenge in arterial wall imaging methods is that prediction of the coronary plaque rupture requires not only an accurate quantification of fibrous cap thickness and necrotic core morphology but also a precise knowledge of the mechanical properties of the arterial wall and plaque components at any given stage of the plaque growth and remodeling. Such knowledge can allow a precise evaluation of the thin–cap fibro–atheroma peak stress amplitude which appears to be a good biomechanical predictor of plaque rupture. Several groups developed robust optimization algorithms for extracting elastic moduli of plaque components, assuming a known plaque morphology. However, we believe that the main issue for improving such methods does not rely mostly on the improvement of the optimization algorithm itself, but rather on the pre–conditioning of the algorithm based on the best estimation of the plaque components' contours. The latter is the main goal of the current study [1].

Aims: The present theoretical study was, therefore, designed to develop: 1) an original pre–conditioning method which allows extracting the plaque morphology in order to initiate the optimization process for the elasticity reconstruction, and 2) a novel approach of combining a dynamic segmentation method with an optimization procedure to highlight the elasticity map of the atherosclerotic plaque.

Methods: Assuming that the mechanical plaque properties vary continuously in space [2] and by writing the local equilibrium equation for isotropic incompressible media solicited under plane strain condition, we derived a strain–dependent term which was very sensitive to the Young modulus gradient. This new mathematical criterion was used in the pre–conditioning model to extract the plaque morphology in order to initiate the optimization process. The modulogram of complex atherosclerotic plaques was then obtained by coupling this original pre–conditioning step with an approach combining a dynamic watershed segmentation method with the optimization procedure to extract the morphology and Young's modulus of each plaque component [3].

Results: This combined approach, based on the continuum mechanics theory prescribing the strain field, was successfully applied to several plaque morphologies from patients imaged *in vivo* with IVUS. The reconstructed cap thickness, necrotic core area, calcium area and the Young's moduli of the calcium, necrotic core and fibrosis were obtained with mean relative errors of 12%, 4% and 1%, 43%, 32% and 2%, respectively. Figure 1 illustrates the reconstruction steps of a plaque containing two soft neighboring necrotic cores. Figure 1e indicates the results found by the algorithm with the exact values in parentheses.

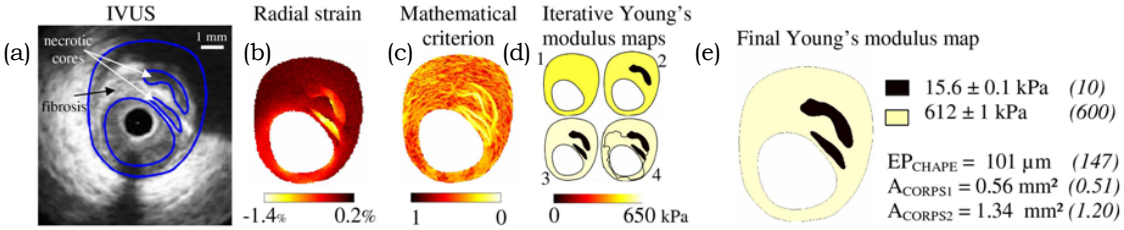

Conclusions: This study showed the robustness and performance of the proposed elasticity reconstruction method with regard to various factors which may affect prediction of plaque vulnerability. Many studies of structural variations of the fibrous cap and necrotic core have shown how very slight structural changes can tilt a vulnerable plaque from stability to instability or vice versa. Such small changes may either "precipitate" rupture or, conversely, "stabilize" a vulnerable plaque. Swings of this sort could only be observed in clinical setting with such modulography methods.

References:

[1] R. A. Baldewsing, et al., Ultrasound Med Biol, vol. 31, pp. 1631–45, 2005.
[2] C. Sumi, et al., IEEE Transactions Medical Imaging, vol. 17, pp. 419–28, 1998.
[3] Le Floc'h, et al., IEEE Transactions Medical Imaging, 2009 (in press).

014 **SIGNATURES OF MULTIPLE SHEAR WAVE SCATTERING IN BRAIN MRE WAVE IMAGES.**

Sebastian Papazoglou[1], Dieter Klatt[1], Jürgen Braun[2], Ingolf Sack[1]*
[1]Radiology Department, [2]Institute of Medical Informatics, Charité Berlin, Berlin, GERMANY.

Introduction: In traditional Magnetic Resonance Elastography (MRE), images of propagating shear waves inside *in vivo* human soft tissue are used to determine its shear elasticity through wave inversion. In contrast, recent developments have aimed at identifying tissue regions of different shear elasticity by analyzing wave scattering [1]. In the present study, wave scattering is quantified by means of the distribution function of wave intensity in order to deduce structure–related parameters of heterogeneous media. Simulations, phantom experiments and *in vivo* brain MRE experiments are presented.

Theory: The propagation of waves through heterogeneous disordered media is accompanied by scattering. Depending on the amount of heterogeneity and the change in elasticity, random intensity fluctuations in the wave image occur. The fluctuations are described by the distribution function $P(I)$, where I is the absolute square of the displacement amplitude normalized with respect to its mean. At low intensities, $P(I)$ is a Rayleigh–distribution which is a negative exponential. If the amount of disorder is large, $P(I)$ deviates from Rayleigh–statistics [2]. Instead, the distribution can be fit to a stretched exponential:

$$P(I) \approx \exp(-2\sqrt{gI}) \qquad \text{Equation (1),}$$

where g is the fit parameter. The deviation from Rayleigh–statistics is due to constructive interferences of scattered waves yielding higher probabilities for large intensities.

Methods: Simulations of multiple scattering were performed at a scatterer volume fraction of 40%. Shear elasticity was 1.8kPa for the matrix material and 0.18kPa for the inclusions. A standard MRE experiment on a homogenous gel phantom was performed and compared to a simple plane wave model with Gaussian noise. MRE experiments on brain were performed as described in [3] and were fit to Equation (1).

Results: The results shown in Figure 1 clearly demonstrate that multiple scattering of shear waves has occurred in brain MRE while multiple scattering has not occurred in the phantom.

Discussion and Conclusions: The distribution of intensity in brain MRE wave images shows signatures of multiple scattering. While viscous damping and noise cause pure exponential distributions of wave intensities, the deviation from Rayleigh–statistics reveals structural information. The dimensionless parameter, g, provides a measure for the efficiency of shear wave scattering and is, thus, a potential measure for the heterogeneity of the brain.

References:

[1] Papazoglou S., et al., Scatter–based magnetic resonance elastography, Phys. Med Biol. 54, 2229–2241, 2009.
[2] Nieuwenhuizen Th.M. and Van Rossum M.C.W., Intensity distributions of waves transmitted through a multiple scattering medium, Phys. Rev. Lett. 74, 2674–2677, 1995.
[3] Sack I., et al., The impact of aging and gender on brain viscoelasticity, Neuroimage, 46, 652–657, 2009.

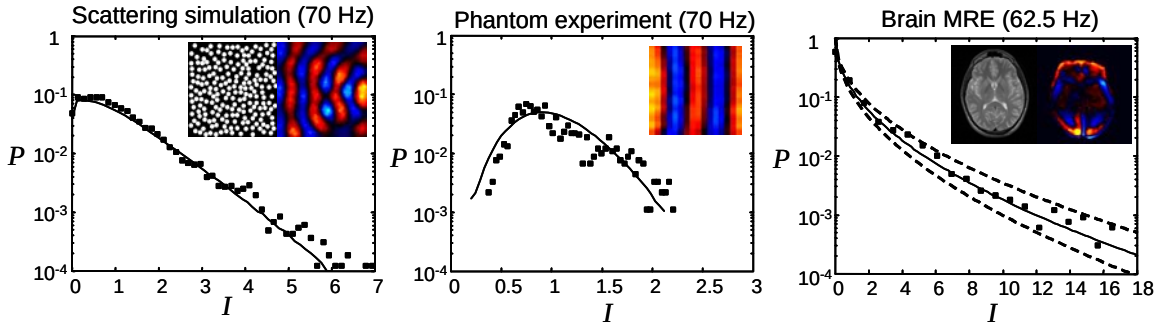

Figure 1: Simulated $P(I)$ is shown for a single disorder configuration (squares) and averaged over 150 configurations (solid line). The insert shows a sample configuration and the corresponding simulated wave image. The phantom experiment yields a much narrower distribution close to a Gaussian (squares), which is reproduced by the plane wave model (solid line). In case of brain MRE, $P(I)$ fits well to a stretched exponential with g=1±0.2 (solid line). The upper and lower thresholds are shown as dashed lines.

* *indicates Presenter*

028 **ESTIMATION OF DISPLACEMENT WAVEFORMS WITH TRANSIENT MR ELASTOGRAPHY.**

Rémi Souchon[1], Rarès Salomir[1], Denis Lyonnet[2], Jean–Yves Chapelon[1], Olivier Rouvière[1,2].*
[1]INSERM U556, Lyon, FRANCE; [2]Hôpital E. Herriot, Lyon, FRANCE.

Background: Transient magnetic resonance elastography (TMRE) was recently proposed [1–3]. This technique uses pulsed shear waves instead of a continuous excitation, so that longitudinal waves and transverse waves can be clearly separated in the time domain. Estimating the displacement waveform from the MR images is a fundamental prerequisite to solving for the viscoelastic properties of tissues. In conventional MRE, there exists a simple linear relationship between the phase of the MR signal and the displacement of the tissues. However, in transient MRE the relationship is more complicated.

Aims: The aim of this study was to develop and test new methods for estimating transient displacement waveforms from TMRE sequences in *in vitro* tissue samples.

Methods: Two methods were developed. The first method uses Wiener deconvolution of the sampled phase shift waveforms (for each pixel). The second method uses a waveform model [4] coupled to an optimization algorithm that minimizes the difference between the phase shift waveform in the model and the experimental measurement. Both methods were tested in experimental data acquired with a TMRE system where excitation pulses were generated using the radiation force of a focused ultrasound beam [3].

Results: Waveforms obtained in three porcine kidney samples by varying the burst duration between 2 and 8ms are shown in Figure 1. The waveforms were normalized by their peak value. The peak displacement in these experiments was 91µm. The waveforms obtained by deconvolution suffered a DC bias because a standard MRE sequence with bipolar MEG was used in the experiments. The waveforms obtained with burst duration 2ms in porcine liver, kidney and muscle are shown in Figure 2. These waveforms were normalized to highlight the strong dependence of their full width at half maximum (FWHM) on the tissue type.

Conclusions: Both methods were able to estimate realistic waveforms. In addition, the study showed that the waveforms are highly dependent on the type of tissues.

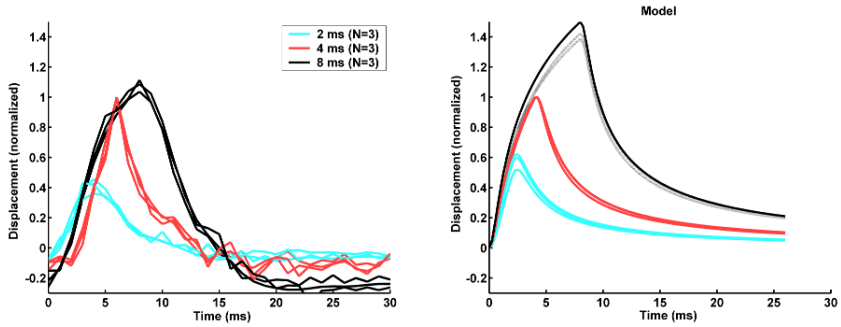

Figure 1: Transient displacement waveforms obtained in three porcine kidney samples by varying the burst duration from 2–8ms (a) deconvolution, (b) model–based

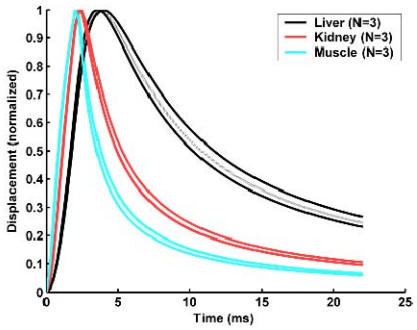

Figure 2: Waveforms (model–based) obtained with 2ms burst duration in porcine liver, kidney and muscle. The waveforms were normalized to highlight the strong tissue–dependence of their FWHM.

References:

[1] Sarvazyan A, et al., Shear wave elasticity imaging: a new ultrasonic technology of medical diagnostics, Ultrasound Med Biol, 24(9), 1419–1435, 1998.
[2] McCracken PJ, et al., Mechanical transient–based magnetic resonance elastography, Magn Reson Med, 53(3), 628–639, 2005.
[3] Souchon R, et al., Transient MR elastography (t–MRE) using ultrasound radiation force: theory, safety, and initial experiments *in vitro*, Magn Reson Med, 60(4), 871–881, 2008.
[4] Andreev VG, et al., Observation of shear waves excited by focused ultrasound in a rubber–like medium, Acoustical Physics, 43(2), 123–128, 1997.

* *indicates Presenter*

032 **NON INVASIVE ASSESSMENT OF COMPARTMENT PRESSURES BY ULTRASOUND: AN *IN VITRO* MODEL.**

Richard M Sellei[1], Simon J Hingmann[1], Matthias Knobe[1], Matias de la Fuente[2], Frauke Schmidt[2], Klaus Radermacher[2], Hans C Pape[1].*

[1]Orthopedics and Trauma Surgery Department, University Hospital RWTH Aachen, Aachen, GERMANY; [2]Helmholtz Institute for Biomedical Engineering, Pauwelsst. 20, 52074 Aachen, GERMANY.

Background: Overlooked compartment syndrome represents a catastrophic complication for orthopedic surgeons. Invasive compartment pressure measurement continues to be the gold standard. However, repeated measurements in uncertain cases can be difficult to achieve. We, therefore, developed a model for a noninvasive technique to assess tissue pressure by ultrasound.

Methods: A perforated plastic tube filled with saline was surrounded by a silicone sealed plastic cover, mimicking the shape of the tibial compartment. A pressure transducer inside the compartment was installed. A second pressure transducer was installed on the ultrasound probe to allow simultaneous monitoring of the pressure inside the compartment and the tissue deformity. For calibration, ultrasound images were generated at 0 and 130mmHg. The plastic cover to tube distance was measured before and after compression (Δd). Subsequently, increments of 5mmHg pressure increases were used to generate a standard curve (0–60mmHg), thus mimicking rising compartment pressures. The intra–observer reliability was tested by using 10 subsequent measurements. A correlation was determined between the skin to bone distance (Δd) and the pressure measurement (p). The Pearson correlation coefficient was calculated, and a regression analysis was performed.

Results: With rising compartmental pressure, a reciprocal proportional relation between Δd and p occurred. The Pearson coefficient was significant at r=-0.960 ($p<0.0001$). Within a pressure ranging from 5–35mmHg there was an almost linear behavior.

Conclusions: Our model reveals that a close correlation between tissue displacement assessed by ultrasound and intra–compartmental pressure changes occurs. Further studies are required to assess whether the good correlation also applies for the clinical scenario. If so, this information may be useful to monitor trends in the compartment pressures.

079 **ELASTIC MODULUS IMAGING (EMI) FOR VISUALIZING THERMAL ABLATION ZONE: INITIAL EXPERIENCE IN A PORCINE MODEL.**

J Jiang[1], C Brace[2,3], A Andreano[2], R DeWall[1,3], N Rubert[1], T Varghese[1,3], F Lee Jr[2] and T Hall[1].*
[1]Medical Physics, [2]Radiology and [3]Biomedical Engineering Departments, University of Wisconsin–Madison, Madison, WI, USA.

Background and Aims: Effective tumor localization and intra–procedural monitoring are critical to treatment success during thermal ablation. Ultrasound–based elasticity imaging methods (e.g. strain imaging, acoustic radiation force impulse (ARFI) imaging and sonoelastography) show great potential in determining the size and shape of the ablated area (protein denaturation and water vaporization increase the tissue elastic modulus). Our aim in this study is to investigate the feasibility of using elastic modulus imaging (EMI), also known as inverse modulus reconstruction, for evaluation of thermal ablation zones.

Methods: A total of 14 radiofrequency (RF) and microwave ablation zones (1–3cm in diameter) were created in vivo in 5 porcine animals with normal livers. Thirteen RF ablation procedures were performed using a 17–guage cooled needle electrode (Valleylab Inc., CO, USA) with a 30mm electrically–active tip, while the single microwave ablation experiment was performed using a 17–gauge triaxial antenna prototype [3]. After open–abdominal ablation, RF ultrasound echo data were acquired under the guidance of a real–time strain imaging system (eSieTouch, Siemens Antares, Siemens Health Care, CA, USA).

A regularized block–matching algorithm [1] was used to obtain displacement data between a pair of pre– and post–deformation (induced by the ablation applicator) ultrasound echo fields. 2D strain (i.e. axial gradients of displacements) and elastic modulus images were then reconstructed from their corresponding displacement data. Compared to strain estimation, the formation of elastic modulus images is a much more involved process. We formulate the EMI as a finite element–based constrained minimization problem, assuming that the tissue being imaged is linearly elastic as a first approximation for small deformations. Specifically, the EMI method iteratively adjusts local modulus values to enforce a FEA–based biomechanical model to produce displacements close to those obtained from ultrasonic speckle tracking [2]. The final elastic modulus distribution of the biomechanical model is used to form an elastic modulus image of the tissue being imaged. Both motion tracking and elastic modulus imaging (EMI) algorithms were implemented using MATLAB (Mathworks Inc., MA, USA) to post–process the RF echo data acquired during the ablation experiments. Ablation areas at gross pathology in the corresponding imaging planes were then compared to imaging results obtained by the EMI and strain imaging methods.

Results: Comparing ablation area measurements, EMI had higher correlation with gross pathology measurements than strain imaging (EMI Pearson coefficient = 0.950, $p<0.0001$; strain Pearson coefficient = 0.853, $p<0.0001$). We also found that EMI more accurately depicts thermal ablation zone size than strain imaging (14.7% versus 22.3% absolute percent error of in area measurements, respectively). Furthermore, the EMI method improved contrast–to–noise ratios by approximately a factor of 2 compared to strain images.

Conclusions: These preliminary results support the hypothesis that EMI may potentially enhance the ability to visualize thermal ablation zones, thereby improving assessment of ablative therapies. Our future work will be directed toward testing the EMI method in tumor–bearing animal models and toward rigorously validate our results with histology in these models.

Acknowledgements: This work was supported in part by the U.S. National Institutes of Health under Grants R01CA100373 and R01CA112192. We want to thank our colleagues, especially Dr. Shyam Bharat and Lisa Sampson at the University of Wisconsin for their help during animal studies.

References:

[1] J. Jiang and T.J. Hall, "A Generalized Speckle Tracking Algorithm for Ultrasonic Strain Imaging Using Dynamic Programming," Ultrasound in Medicine & Biology, in press, 2009.
[2] J. Jiang, T. Varghese, C. Brace, et al., "Young's Modulus Reconstruction for Radio–Frequency Ablation Electrode–Induced Displacement Fields: A Feasibility Study", IEEE Trans Med Imaging, in press, 2009.
[3] C Brace, et al., "Microwave ablation with a single small–gauge triaxial antenna: *in vivo* porcine liver model", Radiology, 242(2): 435–440, February 2007.

037 **PERFORMANCE OF RF–BASED 2D STRAIN IMAGING TECHNIQUES IN DEFORMING STRUCTURES WITH LARGE SHEARING AND ROTATIONAL MOVEMENT.**

RGP Lopata[1], MM Nillesen[1], HHG Hansen[1], JM Thijssen[1], CL de Korte[1].*
[1]Clinical Physics Lab, Radboud University Nijmegen Medical Center, Nijmegen, The NETHERLANDS.

Background: 2D and 3D RF–based strain imaging methods are being used in a variety of applications. In cardiovascular applications, shearing and rotational movement of tissue often occurs. This follow–up study expands the fundamental study on the feasibility of measuring strain when shearing and rotations occur using four different RF–based methods [1].

Aims: To assess the performance of 1D and 2D kernel matching techniques by using data of deforming structures in combination with large shearing or rotation.

Methods: A random block (5cmx5cm) containing 3.5 million scatterers was used as the input for Field II©. The block was subjected to an applied shear strain of 2.0, 4.0 and 6.0% in combination with an applied load equivalent to 0.0, 1.0 and 2.0% vertical strain. Furthermore, simulation experiments with a rotating block were performed over a range of 0.5° to 5.0° and 10°. Again, a vertical load of 0.0, 1.0 and 2.0% strain was applied. RF–data were simulated for a linear array transducer with a center frequency of 8.7MHz and a pitch of 135μm, resulting in images of 5.0cmx3.0cm. Displacements were estimated using a coarse–to–fine strain algorithm with parabolic interpolation and sub–sample aligning and stretching of kernels using 1D and 2D pre–compression kernels (Method I and II, respectively) [2]. A different approach was introduced previously [1], in which the search area was not limited to a box–shaped 2D region: Axial displacements were used to deform the search area in the axial direction freely (Method Ia and IIa). All four methods were applied to the aforementioned simulated data and the displacements, strains, rotations and cross–correlation values were estimated. The root–mean–squared error (RMSE) between applied and measured, unfiltered displacements was calculated. Furthermore, the elastographic SNR (SNRe) was calculated when a vertical load was applied.

Results: The study revealed that Method IIa (free shape 2D kernel matching) outperformed the other three methods, especially when large displacements were present. The shearing experiment showed a significant improvement for higher shear strains for each applied load (up to 33% and 40% lowered axial and lateral RMSE, respectively). The RMSE of the axial strain reduced with 70% when a load of 1.0 or 2.0% was applied. Method IIa yielded an increase in axial SNRe of 10dB and was 18dB (1.0% strain) and 25dB (2.0% strain). The axial SNRe (2.0% load, 6% shear strain) dropped by -15dB for Method II but only -5dB for Method IIa. Rotations could be measured up to 5.0° by all methods. The maximum axial and lateral displacements at 5.0° were ±1.4mm. Method IIa outperformed the other methods, and the axial and lateral RMSE decreased with 47 to 94% and 18 to 36%, respectively. The measured cross–correlation decreased for larger angles (0.5–5.0°) from 0.92 to 0.50 for Method II and from 0.91 to 0.65 for Method IIa. After reconstruction, the mean angles were 0.5, 0.9, 1.9, 2.8, 3.8 and 4.8, with a standard deviation of 15% on average. When a vertical load was applied, the RMSE of the strains increases for increasing rotation angle. The axial and lateral RMSE of the strains of Method IIa were reduced by 95% and 75%, respectively. For increasing rotation, the axial SNRe dropped 14dB for Method IIa (37–22dB), thereby outperforming Method II (large drop of -65dB). The lateral SNRe revealed a negative correlation with rotation angle for all methods (-5dB/degree), although Method IIa outperformed the other methods by +24dB.

Conclusions: Shearing and rotational movement result in displacements that are difficult to assess, which results in a lower precision of the displacement and strain estimates. These effects can be partly overcome by accounting for axial movement (Method IIa). Rotational movement results in an enormous decrease in SNRe. Experimental validation of the method should be performed and the feasibility of torsion measurements will be examined in the future.

Acknowlegdements: The support of the Dutch Technology Foundation (Project 06466) is kindly acknowledged.

References:

[1] Lopata, et al., Free–shape 2D Kernels for Improved Measurement of Rotations & Strains in Shearing Structures, Proceedings 7th International Conference on the Ultrasonic Measurement & Imaging of Tissue Elasticity, Austin, Tx, USA, 2008.
[2] Lopata, et al., Performance Evaluation of Methods for Two–Dimensional Displacement and Strain Estimation using Ultrasound Radio Frequency Data, Ultras Med Biol, 35(5), p.796–812, 2009.

* *indicates Presenter*

001 **QUANTIFYING ACOUSTIC RADIATION FORCE IMPULSE–INDUCED DYNAMICS THROUGH OPTICAL METHODS: EXPERIMENTAL AND SIMULATION RESULTS.**

Richard R. Bouchard[1], Jason E. Streeter[2,3], Mark L. Palmeri[1], Paul A. Dayton[2,3].*
[1]Duke University, Durham, NC, 27708, USA; [2]University of North Carolina at Chapel Hill, [3]North Carolina State University, Chapel Hill, NC, 27599, USA.

Background: Despite their practical utility, ultrasonically–based tissue displacement estimators are hindered by a few fundamental limitations: poor tracking resolution in the lateral dimension, sampling limitations due to interference from previous pulses and a large effective tracking kernel. Optically–based (i.e. visible spectrum) tracking, which is impractical in most clinical applications due to near–field scattering, can overcome some of the aforementioned limitations in an experimental setting that utilizes a translucent phantom. Past research groups have successfully tracked the acoustic radiation force impulse (ARFI)–induced dynamic response in a phantom with optically–based techniques that relied on a laser source [1,2]. These techniques, however, offered either limited spatial/temporal resolution or were restricted to uniaxial tracking. We propose an optically–based technique that utilizes conventional optical microscopy to investigate, with good spatial/temporal displacement resolution, the ARFI–induced response in a translucent, tissue–mimicking phantom.

Aims: To track ARFI–induced dynamics in a tissue–mimicking phantom using optically–based methods.

Methods: Suspended 10µm microspheres were tracked axially and laterally at multiple locations throughout the field of view (FOV) with 0.5µm tracking resolution, in both dimensions, and at frame rates of up to 36kHz. Induced dynamics were successfully captured before, during and after the ARFI excitation at depths of up to 4.8mm from a translucent phantom's proximal boundary. Results are presented for tracked axial and lateral displacements resulting from on–axis and off–axis (i.e. shear wave) acquisitions. These results are compared to matched finite element method (FEM) modeling and independent ultrasonically–based empirical results.

Results:
Optically–tracked (3.3mm depth; 24k fps) axial (Figure 1) and lateral (Figure 2) displacement data resulting from a 400µs ARFI excitation in a phantom. Four FOVs (a–d) are depicted (each with lateral offsets from excitation center); five distinct tracking kernels within each FOV are plotted. In the axial data (Figure 1), displacement peaks occur later in time and with decreasing amplitude as the FOV becomes more offset, which is characteristic of shear wave propagation. In the lateral data (Figure 2), displacement occurs almost immediately after the excitation while times to displacement peaks do not share a direct relationship with FOV offset.

Figure 1

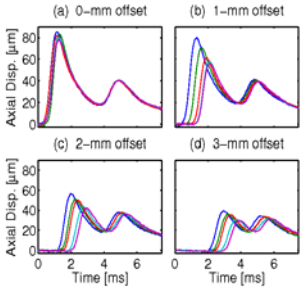

Figure 2

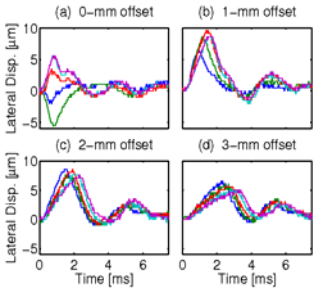

Conclusions: Optical tracking of ARFI–induced dynamics in a translucent tissue–mimicking phantom was successfully achieved at frame rates of up to 36kHz and with sub–micron displacement resolution in the axial and lateral dimensions. These tracking data show good agreement with all basic trends and phenomena observed in matched FEM modeling results early in time (up to 4ms). Excellent agreement is also observed between shear wave velocities derived from the optical technique and those yielded by an independent, ultrasonically–based method. Due to the closeness of the phantom's proximal boundary, an artifact–inducing shear wave reflection was observed in all data sets later in time (around 5ms in most cases). Despite the restricted clinical applicability of this tracking technique, it could assist in gaining a greater understanding of complex, radiation force dynamics in tissue–mimicking phantoms.

Acknowledgements: This work was supported in part by a NSF Graduate Research Fellowship. The authors thank Gijs van Soest and Carl Herickhoff for their insight and Ned Rouze for intensity measurement assistance.

References:

[1] V. G. Andreev, V. N. Dmitriev, Y. A. Pischal'nikov, O. V. Rudenko, O. A. Sapozhnikov, and A. P. Sarvazyan, "Observation of Shear Waves Excited by Focused Ultrasouond in a Rubber-like Medium," Acoust. Phys. 43, 123–128, 1996.
[2] E. Bossy, A. R. Funke, K. Daoudi, A.-C. Boccara, M. Tanter, and M. Fink, "Transient optoelastography in optically diffusive media," Applied Physics Letters 90, 174111, 2007.

038 **3D RADIATION DOSIMETRY: DOSE READ–OUT OF GELS WITH SHEAR WAVE ELASTOGRAPHY.**

Remo A Crescenti[1], Jeffrey C Bamber[1], Nigel L Bush[1], and Steve Webb[1].*
[1]Institute of Cancer Research and Royal Marsden NHS Foundation Trust, Downs Road, Sutton, Surrey, England, UK.

Background: Radiation–sensitive polymer gels may be employed as dosimeters in modern radiotherapy, where 3D dosimetry is needed. Previously we have shown that Young's modulus is dependent on the radiation dose [1] and have determined dose contrast in such gels using pseudo–static ultrasound elastography combined with inverse algorithms [2]. The success has been limited by the influence of friction at the boundaries, noise in the measurement and smoothing introduced by the inverse reconstruction.

Aim: This presentation investigates the potential experimental improvements brought about by shear–wave elastography and compares and discusses the application of pseudo–static and shear–wave elastography on gel dosimetry.

Material and Methods: A block (4x4x12cm^3 along x, y and z–axis, respectively) of radiation–sensitive polymer gel [3] was irradiated to produce a relatively stiff rod–shaped region (1x1cm^2) along the z–axis. For the ultrasonic imaging, the gel was taken out of its container and scanned in a water bath. Ultrasound B–mode and Young's modulus images were acquired in regions of interest of different sizes with the Aixplorer® (Supersonic Imagine, Aix–en–Provence, France).

Results and Discussion: Young's modulus maps are shown in regions of interest in Figure 1. The irradiated area is clearly visible as a hard, bright region (mean of 7.2kPa) in a softer, dark background (mean of 2.4kPa). The shape of the irradiated area was accurately preserved if the small ROI was chosen for Young's modulus estimation, which is an improvement when compared to pseudo–static elastography. Also, no influence of the boundaries was observed. Further advantages include the ease of directly and rapidly obtaining 3D Young's modulus data. The background noise level was similar as in pseudo–static elastography, but dependence on the size of the ROI suggests that some accuracy may be gained by optimizing the shear–wave elastography sequence for the application in gel dosimetry. For example, a denser mesh of radiation force pushes could be applied. Optimization may lead to longer measurement times, but this is fine if the accuracy is improved. While real–time elastography and avoidance of movement artefacts of the object are important in clinical applications, they are not an issue in gel dosimetry. A further optimization could be the use of a lower ultrasonic frequency for the applied radiation force, which will potentially increase the Young's modulus imaging depth.

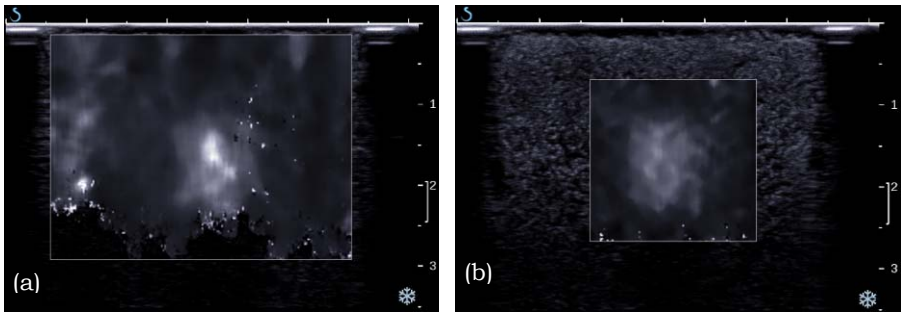

Figure1: The Young's modulus map in a large (a) and small (b) region of interest is overlaid on the B–mode image. The scale at the side and top is in cm.

Acknowledgement: This work was funded by The Institute of Cancer Research. The authors thank Supersonic Imagine and Nicolas Felix, in particular, for providing the opportunity to use the Aixplorer® for this experiment and for their help.

References:

[1] Crescenti, et al., Characterization of dose–dependent Young's modulus for a radiation–sensitive polymer gel, Phys. Med. Biol., 54 (24) 843–857, 2009.
[2] Crescenti, et al., Advances and difficulties in the use of ultrasound elastography and inverse algorithms for gel dosimetry, Proceedings 7th International Conference on the Ultrasonic Measurement & Imaging of Tissue Elasticity, Austin, Tx, USA, 2008.
3] Fong, et al., Polymer gels for magnetic resonance imaging of radiation dose distributions at normal room atmosphere, Phys. Med. Biol., 46 3105–3113, 2001.

* *indicates Presenter*

053 **PHYSICAL BASIS FOR TYPICAL ELASTOGRAPHIC APPEARANCE OF CYSTIC LESIONS – PHANTOM BASED ANALYSIS.**

Kishore Kumar[1], Maneesha E.Andrews[2], V. Jayashankar[1], S. Suresh[3], Ashok K. Mishra[2].*
[1]Electrical Engineering Department, [2]Chemistry Department, Indian Institute of Technology Madras, Chennai, Tamilnadu, INDIA; [3]Mediscan Systems, Chennai, Tamilnadu, INDIA.

Background: Cysts can be classified as either simple or complex. Cysts arising from any organ that meet strict criteria for being simple cysts are benign with almost absolute certainty. Confusion remains in the description and management of complex cystic lesions using sonography. Cysts appear as black regions on ultrasound B–mode images due to their anechoic nature. But in most of the cases, Fine Needle Aspiration (FNA) shows the fluid present in this region is not just water but is made up of many complex viscous fluids such as pus, blood, etc. Diagnosis of cystic lesions using elastography has not been fully explored.

Aims: To evaluate the physical basis for the characteristic elastographic pattern of the cystic lesions for better clinical diagnosis. The common patterns considered are Bull's eye appearance [1], three layered pattern, high variability of strain inside cysts (noise like appearance) [2] and specific patterns for cysts filled with high viscous fluids [3].

Methods: Polyacrylamide based tissue–mimicking phantoms with embedded cysts were developed [3]. Different categories of cysts were prepared. Cysts of varying size were filled with plain fluid like water and fluids with varying viscosities. The second category of cysts consists of known amounts of fluid with varying amounts of scatters in the cysts to mimic complex cysts. The third category consists of cysts filled with milk, a very common finding in breast cysts. The fourth category consists of cysts filled with turbid fluids like cholesterol crystals, egg white, protein particles with particulate matters, etc. Parameters were measured from grey and color elastogram as the characterizing parameters for specific patterns.

Results: Preliminary results showed that cyst elastograms follow a particular pattern depending upon their content, fluid composition, etc. Figure 1 shows the ultrasound B–mode image and elastogram of two cystic lesions filled with water and oil respectively.

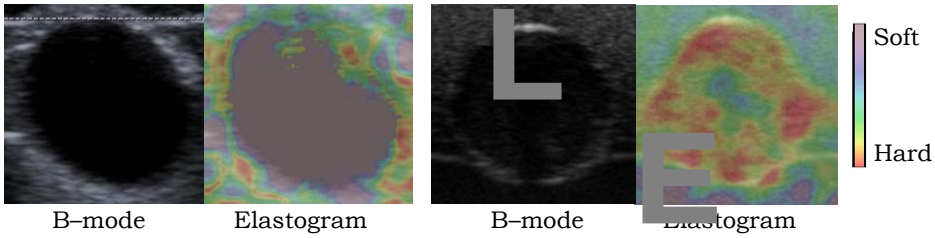

Figure1: Ultrasound B–mode image and elastogram of two cysts filled with water and viscous fluid oil with color scale for elastogram.

Conclusions: Phantoms embedded with cystic lesions were used to evaluate the specific elastographic patterns for different cystic lesions so that elastograms of biological cysts can be better understood. Elastography can not only differentiate simple and complex cysts but can also provide information on complexity of fluid present inside the cysts.

References:

[1] RG Barr, JR Grajo, " Initial results of real–time elasticity imaging in the evaluation of breast lesions", Proc. 6th Intrnl Conf on the Ultrasonic Measurement and Imaging of Tissue Elasticity, New Mexico, USA, p94, Nov, 2007.
[2] B.S. Garra et al. "Elastography of breast lesions: initial clinical results", Radiology, vol. 202, pp. 79–86, 1997.
[3] Kishore Kumar et al. "Design development and characterization of cyst phantoms for ultrasound elastography applications" Proceedings of 30th Annual International Conference of IEEE EMBS, pp. 2972–2975, 2008.

060 **A HIGH FRAME RATE ULTRASOUND SYSTEM FOR THE STUDY OF TISSUE MOTIONS.**

A Baghani[1], SE Salcudean[1], R Rohling[1].*
[1]University of British Columbia, Vancouver, BC, CANADA.

Background: A fundamental limitation of ultrasound based motion tracking is the inherent low frame rate of the ultrasound systems. A low frame rate limits the scope of the motions that can be properly detected by the system. Motions induced inside the tissue to study its mechanical characteristics, as in dynamic elastography, require higher frame rates in many cases. Different techniques have been devised over the years to increase the frame rate of the ultrasound systems for motion estimation [1–3].

Aims: The purpose of this research was to develop an imaging system which can readily be implemented on conventional ultrasound systems and provides higher frame rates for motion tracking without a need for extensive hardware upgrade. In particular, the developed system compensates for the time delays in the acquisition process and yields virtually simultaneous measurements of the tissue displacement. A number of criteria has also been introduced on the excitation for the motion to be detected properly.

Methods: The system uses the concept of image subdivision and re–assembly of the data for increasing the effective frame rate. The region of interest is divided into a number of sectors, each of which can be acquired at a higher frame rate. After the desired number of frames are acquired over one sector, the system moves on to the next sector. The frame rate depends on the number of scan lines in the sector. Since the motion of different points is sampled at different instances in time, a time delay exists. The system compensates for this time delay in the frequency domain in three steps. First, the time delay between different sectors is compensated. Next, the time delay between different scan–lines in each sector is compensated, and, finally, the time delay associated with each scan–line is compensated. At a frequency, f, in the frequency domain, a time delay, t, is compensated for by subtracting the associated phase, $2\pi ft$, from the phase of the displacement phasor. Since the tissue motion is observed over a finite interval, T_{obs}, to make the observations over different intervals of time similar, the excitation should be chosen to contain only integer multiples of $f_{fund} = 1/T_{obs}$.

Results: A sinusoidal longitudinal excitation at 100Hz is used on a cylindrical homogenous phantom. This excitation is applied to the phantom using a speaker. The axial tissue displacement is tracked using a conventional speckle tracking algorithm, and the phasor of displacement at 100Hz is extracted. Figure 1 shows how the system corrects this phase in three steps to compensate for the time delays.

Conclusions: The presented high frame rate system can be used together with the exciters used in elastography techniques, such as mechanical exciters and acoustic radiation force (ARF) exciters, to obtain displacement data of the tissue at different frequencies of excitation. The excitation frequency can go up to a few kHz, and the system can still estimate the displacement data. These data can then be used in the inverse problem solving techniques to recover the tissue elasticity and viscosity.

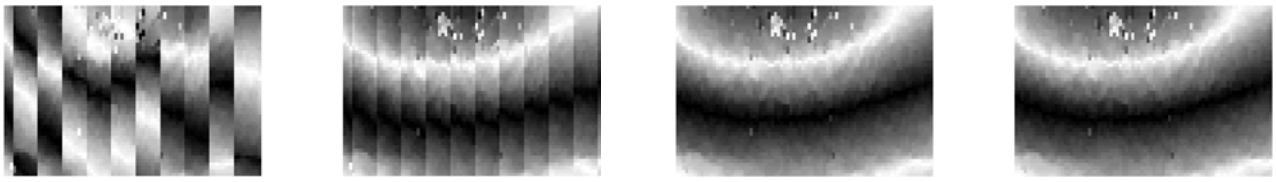

Figure 1: Different steps in the phase correction process of a longitudinal wave: the phase (a) before any compensation (b) after compensation for the delays between the sectors (c) after compensation for the delays between the scan-lines in each sector (d) after compensation for the delays on each scan-line.

Acknowledgements: This research was supported by NSERC.

References:

[1] S. Wang, W.N. Lee, J. Provost, J. Luo, and E. E. Konofagou, "A composite high–frame–rate system for clinical cardiovascular imaging," IEEE Trans. Ultrason., Ferroelect., Freq. Contr., vol. 55, no. 10, pp. 2221–2233, 2008.
[2] S. Brekke, C. B. Ingul., S. A. Aase., and H. G. Torp, "Increasing frame rate in ultrasound imaging by temporal morphing using tissue doppler," in Proc. of IEEE Ultrasonics Symposium, pp. 118–121, 2004.
[3] M. Fink, L. Sandrin, M. Tanter, S. Catheline, S. Chaffai, J. Bercoff, and J. Gennisson, "Ultra high speed imaging of elasticity," in IEEE Ultrasonics Symposium, pp. 1811–1820, 2002.

* *indicates Presenter*

078 **IMPROVED 2D MOTION TRACKING FOR ELASTOGRAPHY USING DUAL TRANSDUCERS.**

Jeffrey M. Abeysekera[1], Robert Rohling[1].*
[1]University of British Columbia, 2329 West Mall, Vancouver, BC, CANADA.

Background: The addition of lateral displacement tracking to the typical axial tracking gives some advantages to several elastography methods [1]. The accuracy of lateral displacement estimates are known to be less accurate because lateral resolution is limited by the beam width, but axial motion sensitivity is related to the ultrasonic sample spacing which is an order of magnitude smaller [2]. The advent of dual plane transducers means it is now feasible to obtain synchronous acquisition from two transducer arrays on commercial ultrasound machines.

Aims: The aims of this study are to demonstrate an experimental apparatus for measuring two–dimensional motion with two linear array transducers within a single coincident scan plane, and to show the axial estimates from two orthogonal transducers is more accurate than using the axial and lateral estimates from a single transducer. The critical issue is alignment of the planes.

Methods: Two ultrasound transducers (L12–5, Ultrasonix Medical Corp., Richmond, BC, Canada) are clamped orthogonally and immersed in a water bath. Linear motion stages are used to translate the transducers in their elevational direction until their scan planes coincide. Alignment is achieved by using a custom cross–wire phantom that produces a symmetric pattern of echoes in each ultrasound image when the transducer is aligned with the central plane of the phantom. The three–dimensional angular misalignment for each plane is calculated based on the geometry of the echoes. Alignment is quantified by calculating the angle between the normals of the two planes. A rectangular PVC phantom, with 3% by mass cellulose, is placed in the water bath and known displacements (±2 μm) are applied in two directions with the motion stage (Figure 1). Axial and lateral estimates are obtained by correlation–based RF tracking [3]. The root mean square (RMS) error between the estimates and the applied motion is computed.

Results: The RMS errors in the axial estimates in both transducers are an order of magnitude smaller than the errors in the lateral direction (Table 1). This demonstrates the advantage of using two transducers to obtain axial estimates in two dimensions.

Conclusions: Ultrasonic signal sample spacing is on the order of tens of microns compared to element–to–element spacing on the order of hundreds of microns for typical linear arrays. As a result, axial motion estimates are inherently more accurate. By using two transducers, high quality axial tracking can be tracked in the axial and lateral directions of motion in real time. Higher quality displacement estimates should improve elasticity reconstruction. This system can be used on areas such as the breast where the two transducers can easily be placed around the tissue. Future work will focus on dual 3D transducers where improved elevational tracking is especially needed.

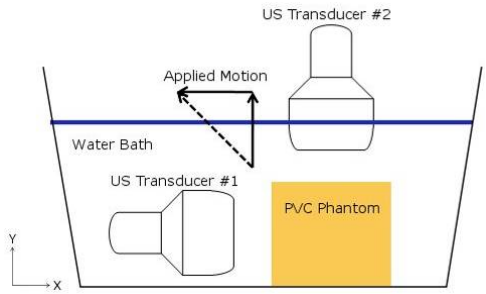

Figure 1: Schematic of motion tracking setup

Applied motion in each axis (μm)	X Axis		Y Axis	
	Axial Transducer #1	Lateral Transducer #2	Axial Transducer #2	Lateral Transducer #1
0	0.02	3.03	0.03	2.97
50	11.89	226.54	10.20	225.52
100	10.28	191.26	12.32	322.60
150	10.35	176.46	15.54	271.19
200	8.27	157.31	5.15	380.08
250	10.95	121.96	9.27	355.84
300	13.77	93.67	16.98	344.28
350	19.74	112.89	25.97	338.79
400	17.96	112.08	18.05	200.64
450	24.79	61.26	32.40	260.50

Table 1: RMS errors calculated over one image [μm]

Acknowledgements: This research is supported by NSERC and CIHR.

References:

[1] Konofagou E, Ophir J. "New elastographic method for estimation and imaging of lateral displacements, lateral strains, corrected axial strains and poisson's ratios in tissues." Ultrasound Med Biol, 24(8):1183–99, 1998.
[2] Righetti R, Srinivasan S, Ophir J. "Lateral resolution in elastography." Ultrasound Med Biol, 29(5):695–704, 2003.
[3] Zahiri–Azar R, Salcudean SE. "Real–time estimation of lateral displacements using time domain cross correlation with prior estimates." IEEE Ultrasonics Symposium, 1209–1212, 2006.

094 **SIMULTANEOUS ULTRASOUND B–MODE IMAGING AND ELASTICITY MEASUREMENT USING VIBRATION BASED ON A CONVENTIONAL ULTRASOUND SCANNER.**

Yong–Ping Zheng[1,2], Zheng–Ming Huang[1], Yong–Jin Zhou[1,2], Jun–Feng He[1], James C.W. Cheung[1].*
[1]Health Technology and Informatics Department, [2]Research Institute of Innovative Products and Technologies, The Hong Kong Polytechnic University, Hong Kong, CHINA.

Background: Recently, elasticity measurement based on transient ultrasound (US) elastography (Fibroscan®) has been successfully used for liver fibrosis assessment [1]. It uses an A–mode US with a very high frame rate to monitor shear wave propagation generated by a vibration source. The wave propagation speed of the shear wave is used to calculate tissue modulus. While it can provide a quantitative measure for the elasticity, the available device cannot provide a real–time B–mode image for localization and guiding during the test. The operator does not know the exact portion of liver being tested. Using imaging systems based on acoustic radiation force, such as supersonic shear imaging [2], B–mode imaging and elasticity measurement can be achieved simultaneously. However, such a system normally requires a complete new design of an US scanner, due to requirement of an ultra high frame rate.

Aims: In this study, we aim to develop a system for simultaneous B–mode imaging and tissue elasticity measurement using vibration, but based on a conventional B–mode US scanner.

Methods: The firmware of a B–mode US scanner (CTS8800, Shantou Institute of Ultrasound Instruments, Guangdong, China) was modified so that it can provide B–mode imaging together with transient M–mode imaging (formed by RF data) with an A–mode repetition rate up to 10,000 frame/s. The scanner first forms a B–mode image, then it switches to the transient M–mode imaging for the selected A–line. When the M–mode imaging is started, a trigger signal is generated by the scanner and used to control a driving circuit for a vibrator. The vibrator was installed inside the case of a probe, which can be a linear or curved array. The propagation of the vibration applied to the tissue via the probe could then be viewed by the transient M–mode image. The disturbance in the M–mode image caused by the shear wave was enhanced using image processing so that the propagation trace can be clearly viewed. The wave propagation speed could then be calculated according to the slope of the inclined trace in the image.

Results: Figure 1 shows the simultaneous display of the B–mode image and enhanced transient M–mode image in the proposed system. The operator can easily view what tissues being tested by the transient M–mode according to the B–mode image and can select different locations for measurement by changing the position of the A–line in the B–mode image. The system has been tested on tissue–mimicking phantoms with different elasticity and porcine livers. The results demonstrated that the proposed method can provide reliable elasticity measurement.

Conclusions: The proposed US system can successfully provide the simultaneous B–mode imaging and elasticity measurement. It was found that simultaneous B–mode image can provide very useful information for the localization of the measurement site. Applications of the system for assessing various soft tissues are being continued.

Acknowledgements: The project was supported by The Hong Kong Polytechnic University (J–BB69).

References:

[1] Sandrin L, et al., Transient elastography: A new noninvasive method for assessment of hepatic fibrosis, Ultrasound in Medicine and Biology, 29: 1705–1713, 2003.
[2] Bercoff J, et al., Supersonic shear imaging: A new technique for soft tissue elasticity mapping, IEEE Transactions on Ultrasonics Ferroelectrics and Frequency Control, 51: 396–409, 2004.

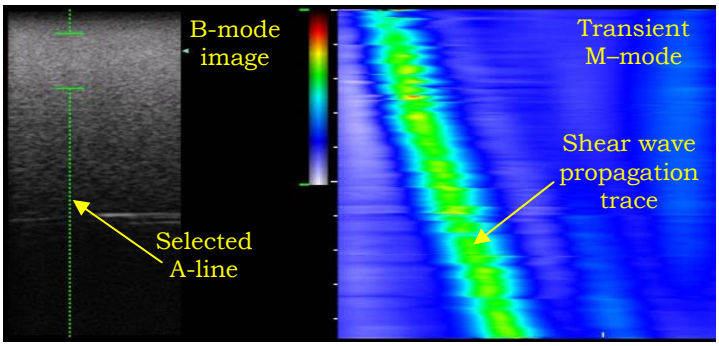

Figure 1: The software interface showing a typical result for simultaneous B–mode imaging (a) and elasticity measurement using transient M–mode image (b) of a tissue–mimicking phantom. The inclined trace in the transient M–mode image indicates the propagation of the shear wave induced by the vibration applied on the array probe. The Young's modulus of tissue can be calculated from the propagation speed.

* *indicates Presenter*

009 **A COMPENSATIVE MODEL FOR THE ANGLE DEPENDENCE OF MOTION ESTIMATES IN NON–INVASIVE VASCULAR ELASTOGRAPHY.**

Elizabeth Mercure[1], Guy Cloutier[1,2,3], Roch L. Maurice[1,2,3].*
[1]Laboratory of Biorheology and Medical Ultrasonics, University of Montréal Hospital Research Center (CRCHUM), Montréal, Québec, CANADA; [2]Institute of Biomedical Engineering, [3]Radiology Department, Radio–Oncology and Nuclear Medicine, University of Montréal, Montréal, Québec, CANADA.

Background: Atherosclerosis of peripheral cerebral arteries can lead to a stroke, either by the formation of a stenosis or by plaque rupture. This pathology is initiated by an alteration of the arterial wall mechanical properties that was shown to be assessable with ultrasound elastography. Recently, Non–Invasive Vascular Elastography (NIVE) was introduced with the purpose of non–invasively imaging mechanical properties of superficial arteries as markers of vulnerable plaques. Nevertheless, NIVE motion estimates are angle–dependent. The optimal scanning angle, represented by the alignment of the tissue motion with the ultrasound beam orientation ($\theta = 0°$), is required for unbiased motion estimations.

Aims: The objective of this study was to evaluate and compensate for the angle–dependence of NIVE axial strain estimates.

Methods: A theoretical formulation that describes the bias on the axial strain parameter as a function of scanning angles is presented. Experiments were performed on vessel–mimicking phantoms. As illustrated in the elastograms below, axial strain estimates could be underestimated with biases increasing with the scanning angle according to a simple trigonometric function. A model that allows compensating for such an angle–dependence is proposed in order to improve NIVE motion estimates. It is based on the four deformation parameters as computed with the Lagrangian Speckle Model Estimator (LSME).

Results: The model was found to reduce biases on axial strain estimates by close to 15% when deviations of nearly 15° from the optimal scanning angle ($\theta = 0°$) were considered. Initial *in vivo* data are also introduced to assess the feasibility of the compensating method.

Conclusions: Theoretical formulations, properly validated with *in vitro* experiments, indicate that angle dependence may be an important factor to consider in NIVE. Since this may distort clinical diagnoses, it is thus important to be able to compensate for its effect. Provided the LSME enables a compensative model for angle dependence of motion estimates, it potentially might be considered as a very interesting and promising clinical tool for NIVE applications.

Acknowledgements: The financial support for this research was provided by the Collaborative Health Research Program and Discovery Program of the Natural Sciences and Engineering Research Council of Canada (grants NSERC #323405–06, NSERC #312136–06, and CIHR CPG–80085). Dr. Cloutier was recipient of the National Scientist award of the Fonds de la Recherche en Santé du Québec (FRSQ, 2004–2009). The salary of Dr. Maurice was partially supported by a research scholarship from FRSQ.

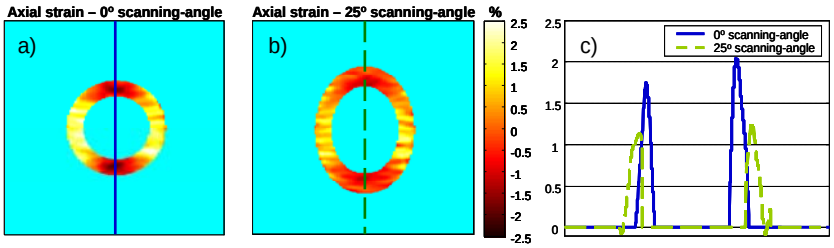

Figure 1: a) Cross–sectional axial strain elastogram for a 0°–scanning angle;
b) cross–sectional axial strain elastogram for a 25°–scanning angle;
c) axial strain estimates are underestimated with respect to the scanning angle.

039 **LOCAL ARTERIAL STIFFNESS MEASUREMENT USING A HIGH FRAME RATE ULTRASOUND SYSTEM.**

Cong–Zhi Wang[1], Yong–Ping Zheng[1,2].*
[1]Health Technology and Informatics Department, [2]Research Institute of Innovative Products and Technologies, Hong Kong Polytechnic University, Hong Kong, CHINA.

Background: Determination of local arterial stiffness is becoming increasingly important in the diagnosis of arteriosclerosis. As an indicator of arterial stiffness, local pulse wave velocity (PWV) can be calculated from the time delay between the distension waveforms acquired by ultrasound at two adjacent sites along the artery. Since the values of PWV in the distal arteries can reach up to 5–10m/s and usually the distance between the two sites for measurement is only 10–30mm, the frame rate of the ultrasound system is desired to be as high as possible to improve the temporal resolution.

Aims: In this study, we aim to develop an ultrasound method with up to 12kHz frame rate to detect PWV and to evaluate its applicability on human subjects for the assessment of local arterial stiffness.

Methods: The system was developed based on Sonix RP system (Ultrasonix Medical Corporation, Canada) and its software developing kits of Visual C++ (Microsoft Corporation, USA). We developed a custom deigned ultrasound sequence by programming individual scan lines. Once the sequence was run, data could be acquired. B–mode images with 256 scan lines were acquired at first to help positioning the transducer on the artery. Then only two scan lines with a predefined distance were reserved to achieve the maximal frame rate. The distension waveforms were determined using the consecutive radio–frequency (RF) ultrasound signals by a cross–correlation method. Second–derivation method was used to select the inflexion points for calculating the time delay. The sample frequency was 40MHz, and the spatial precision could be improved up to 0.2μm by an interpolation technique which was used to find the maximum of a fitted parabola linking the top three points of the peak. The frame rate could be improved up to 12kHz by reducing the scan line duration. Data was collected from the carotid artery of a 32 year old healthy male. A 14MHz linear array transducer was used. Besides the PWV, c, the mean diameter of carotid, D, and the thickness of arterial wall, h, could also be obtained from the RF signals. So the elastic modulus, E, could be calculated using Moen–Korteweg equation: $E = c^2\rho D/h$, where ρ is the density of blood, and its value is about 1050kg/m^3.

Results: Typical distension waveforms obtained by two A–lines with a 28.5mm distance are shown in Figure 1. Ten pulsations were measured and the corresponding PWV values were calculated. The mean and standard deviation of them was 6.37±0.21m/s. The mean diameter of carotid was 7.27mm, and the mean thickness of arterial wall was 0.77mm. The calculated elastic modulus of the carotid was 402kPa.

Conclusions: The estimated value of the elastic modulus of the carotid is in agreement with the ones given in the literature, which are 300–800kPa [1]. This result shows the ultrasound system with high frame rate has a potential to improve the accuracy of the determination of the local arterial stiffness.

References:

[1] Y. Yokota, R. Taniguchi, et al., "Estimation of Carotid Stiffness Using Ultrasonic Dynamic Images for Evaluating the Degree of Arteriosclerosis", 4th European Conference of the International Federation for Medical and Biological Engineering, vol. 22, pp.856–860, 2008.

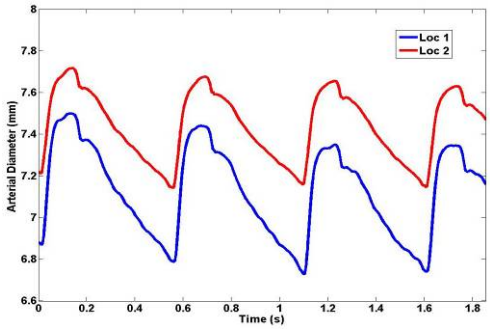

Figure 1: Typical distension waveforms measured by two A–lines in a distance of 28.5mm.

* *indicates Presenter*

041 **3–D, HIGH VOLUME RATE, RAW AND DETECTED *IN VIVO* CARDIAC SPECKLE TRACKING: MOVEMENT TOWARDS OPTIMIZED STRAIN AND STRAIN RATE IMAGING.**

BC Byram[1], G Holley[2], D Need[2], DM Giannantonio[1], GE Trahey[1].*

[1]Duke University, 136 Hudson Hall, Durham, NC, 27708, USA; [2]Siemens Healthcare Sector, Ultrasound Business Unit, 1230 Shorebird Way, Mountain View, CA, 94039, USA.

Background: Elastography techniques require estimates of tissue displacement in order to quantify various mechanical properties. The quality and dimensionality of displacement measurements directly impacts the accuracy and confidence associated with the estimates of mechanical properties [1]. This is true for cardiac strain and strain rate imaging, which rely on motion vectors for their calculation. In order to improve cardiac strain and strain rate imaging, several researchers have demonstrated 3–D speckle tracking [2]. 3–D cardiac speckle tracking has, thus far, used detected data at low volume rates [2–4].

Aims: The effects of kernel size, volume rate, pixel/peak hopping and data type are examined, and first comparisons are made within the stated variables for 3–D speckle tracking.

Methods: Ultrasound volumetric, raw baseband data in an IQ format were acquired using a matrix array attached to a Siemens SC2000 scanner (Siemens Healthcare Sector, Ultrasound Business Unit, Mountain View, CA). Phantom and *in vivo* left ventricular short–axis data were acquired. The *in vivo* cardiac data were used to demonstrate the feasibility of 3–D motion tracking using raw data and a matrix array in dynamic *in vivo* scenarios. Data volumes were acquired at volume rates up to 1000Hz for a 10ºx12º lateral and elevational extent, respectively, and to an axial depth of 14cm. The acquired volumes consisted of 120 receive beams acquired in sections of 30 beams received in parallel. Motion tracking was done using phase–sensitive normalized cross–correlation [5,6]. Subsample refinement of the lateral and elevational dimensions was performed using the grid–slopes algorithm [7]. Kernel sizes of 1.2x.85x.85mm, 2.2x1.7x1.7mm and 4.3x3.5x3.5mm were compared. Volume rates between 50 and 1000Hz were assessed. All comparisons were done for both raw and detected data types.

Results: Data were used to examine volume rate, kernel size and data type, and their effect on 3–D speckle tracking. Volume rate was analyzed by comparing velocity estimates from lower volume rates against velocity estimates derived from 1000Hz volume rate data which were summed appropriately to simulate the lower volume rate estimates. This comparison was made for both raw and detected data. The resulting lateral and elevational tracking performance is similar for both IQ and detected data. The axial tracking performance is best when IQ data is used, but this is primarily due to lower estimation jitter. The performance of tracking axial displacement using detected data is still better than the tracking performance in the lateral or elevational dimensions, which is consistent with the literature. Additionally, the results show little improvement when tracking above 200Hz (although this is kernel dependent). For the largest kernel, there is little perceived benefit for tracking at volume rates above 100Hz. Rates of peak/pixel hopping also show kernel size and volume rate dependencies. Peak/pixel hopping is decreased when raw data is used for the two smallest kernels. The employed tracking method and data shows, qualitatively, good temporal and spatial stability at high volume rates.

Conclusions: Three–dimensional speckle tracking on raw data has been demonstrated in a dynamic *in vivo* scenario. The results should move towards answering standing questions about *in vivo* 3–D speckle tracking and its effect on optimizing cardiac strain and strain rate imaging.

Acknowledgements: This research was possible thanks to NIH grants 5T32EB001040 and 1R01HL096023–01 and the Duke University Pratt Fellows Program.

References:

[1] M Bilgen, "Dynamics of Errors in 3D Motion Estimation and Implications for Strain-Tenser Imaging in Acoustic Elastography," Phys. Med. Biol., vol. 45, pp. 1565–1578, 2000.

[2] J Crosby, BH Amundsen, T Hergum, EW Remme, S Langeland, H Torp, "3–D Speckle Tracking for Assessment of Regional Left Ventricular Function," Ultrason. Med. Biol., vol. 35, pp 458–471, 2009.

[3] MG Linguraru, NV Vasilyev, GR Marx, W Tworetzky, PJ Del Nido, RD Howe, "Fast Block Flow Tracking of Atrial Septal Defects in 4D Echocardiography", Med. Img. Anal., vol. 12, pp. 397–412, 2008.

[4] AA Morsy, OT von Ramm, "3D Ultrasound Tissue Motion Tracking using Correlation Search," Ultrason. Img., vol. 20, pp. 151–159, 1998.

[5] T Shiina, MM Doyley, JC Bamber, "Strain Imaging Using Combined RF and Envelope Autocorrelation Processing," IEEE Ultrason. Symp., pp. 1331–1336, 1996.

[6] NA Cohn, SY Emelianov, MA Lubinski, M O'Donnell, "An Elasticity Microscope. Part I: Methods", IEEE Ultrason., Ferroelec. and Freq. Contr., vol. 44, pp. 1304–1319, 1997.

[7] BJ Geiman, LN Bohs, ME Anderson, SM Breit, GE Trahey, "A Novel Interpolation Strategy for Estimating Subsample Speckle Motion," Phys. Med. Biol., vol. 45, pp. 1541–1552, 2000.

069 **VALIDATION OF PULSE WAVE IMAGING (PWI) AS A QUANTITATIVE METHOD FOR MAPPING ARTERIAL ELASTICITY.**

Jonathan Vappou[1], Jianwen Luo[1] and Elisa E. Konofagou[1].*
[1]Ultrasound and Elasticity Imaging Laboratory, Biomedical Engineering Department, Columbia University, New York, NY, USA.

Background: Abnormal changes in arterial stiffness can serve as good indicator of cardiovascular disease. Pulse Wave Imaging (PWI) is a non–invasive ultrasound–based method for characterization of local mechanical properties of the aortic wall by using the propagation of the intrinsic pulse wave [1]. Its feasibility *in vivo* has been demonstrated in mice and humans, in both healthy and diseased aortas [2,3], but the measurement of the elasticity by this technique has not been validated.

Aims: This phantom study aims at evaluating the quantitative nature of the PWI method through comparison with mechanical testing.

Methods: Three homogeneous aortic phantoms were made of polyacrylamide gels (gel1=20%, gel2=25%, gel3=30%). Pulsatile flow was generated by a peristaltic pump while the wall motion was imaged using a linear array (Ultrasonix RP, 446 frames/s, 20MHz sampling frequency). Axial displacements (Figure 1) were calculated using cross–correlation techniques on the acquired RF signals. The pulse wave velocity was then determined from the spatio–temporal variations of the wall displacement and the Young's modulus was calculated using the Moens–Korteweg equation, under the assumption of a homogeneous, linear elastic medium. These results were compared to those obtained by mechanical testing (quasi–static shear tests) on the same gels on the same day.

Results: Averaged pulse wave velocity values were equal to 0.48m/s, 0.78m/s and 1.1m/s, corresponding to Young's modulus values of E=820Pa, E=2.2kPa and E=4.4kPa for gels 1, 2 and 3, respectively. When compared to the results found by mechanical testing, this represents relative differences of 17%, 37% and 30% and p–values of 0.15, 0.05 and 0.01. This indicates a relatively good agreement when comparing the two different methods for elasticity measurement.

Conclusions: Despite its limitations regarding physical assumptions, this phantom study represents an essential step, since it demonstrates that PWI is a quantitative method for noninvasive determination of regional arterial elasticity. Ongoing research is focused on evaluating the method on significantly heterogeneous arterial wall cases using both phantom and numerical approaches.

Acknowledgements: This study was supported in part by the National Institutes of Health (R01EB006042) and the American Heart Association (SDG0435444T).

References:

[1] Fujikura, et al., A Novel, Non–Invasive Technique for Pulse–Wave Imaging and Characterization of Clinically Significant Vascular Mechanical Properties *in vivo*, Ultrasonic Imaging 29:137–154, 2007.
[2] Luo, et al., Pulse wave imaging of normal and aneurysmal abdominal aortas *in vivo*, IEEE Trans. Med. Imaging 28(4): 477–486, 2009.
[3] Luo, et al., Pulse Wave Imaging of Human Abdominal Aortas *In Vivo*, IEEE International Ultrasonics Symposium Proceedings, 859–862, 2008.

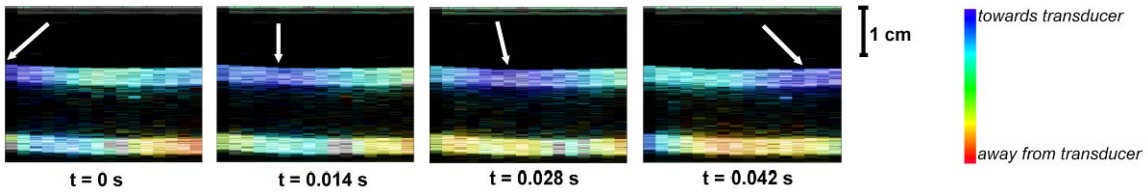

Figure 2: Incremental displacement of the wall overlaid onto the B–mode image, showing the propagation of the pulse wave from left to right.

* *indicates Presenter*

064 ***IN VIVO* DIFFERENTIATION OF MYOCARDIAL ABLATION LESIONS VIA A STIFFNESS RATIO WITH ACOUSTIC RADIATION FORCE IMPULSE IMAGING.**

Stephanie A. Eyerly[1], Stephen J. Hsu[1], Gregg E. Trahey[1], Patrick D. Wolf[1].
[1]Duke University, 136 Hudson Hall, Durham, NC, USA.

Background: Acoustic radiation force impulse (ARFI) imaging has been shown to be capable of visualizing cardiac radiofrequency ablation (RFA) lesions in myocardium based on ARFI–induced displacements [1]. Current lesion segmentation methods successfully threshold normalized ARFI–induced displacements based on user defined parameters to visualize the boundary of the lesion, but these methods may be biased by subjective variability. Stiffer, ablated tissue has been shown to undergo only moderate elasticity changes throughout the cardiac cycle unlike the surrounding, untreated myocardium [2]. This fact suggests that the intrinsic cyclic stiffening of the myocardium could facilitate the formulation of a systolic to diastolic normalization for ARFI–induced displacement data.

Aims: To automatically normalize and detect ablation lesions *in vivo* in ARFI–induced displacement images based on changes, or lack thereof, in myocardial elasticity from systole to diastole.

Methods: A canine heart was imaged epicardially *in vivo* using with an open chest preparation. An ablation lesion was created on the epicardial surface, and a transducer, held in place using a vacuum–coupling device, was positioned directly above the lesion and along the long axis of the heart. While pacing from the ventricular surface, two–line M–mode ARFI images were acquired at 120Hz for multiple cardiac cycles. 1–D speckle tracking was employed to follow specific regions of myocardium through time for each M–mode line, one inside and one outside the ablation lesion. An average diastolic to systolic ARFI–induced displacement ratio for the each line was formulated.

Results:

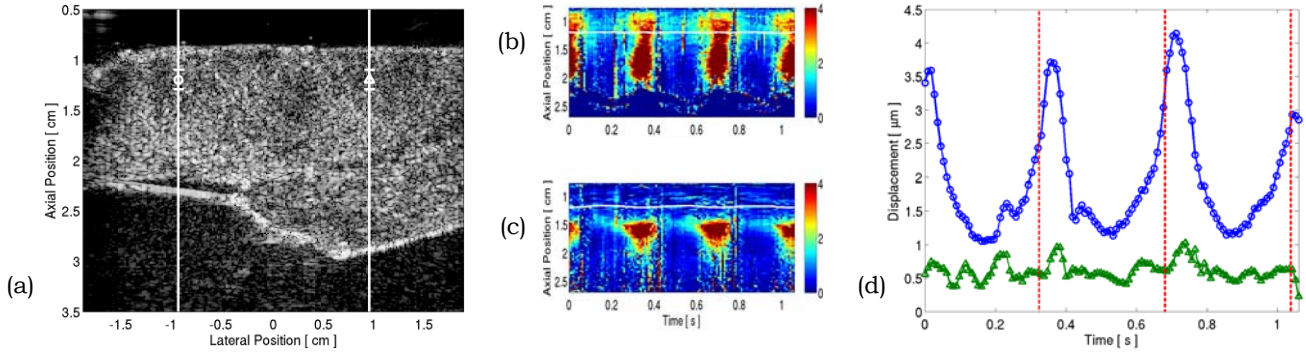

Figure 1: (a) B–mode image of the LV free–wall. Vertical white lines indicate the locations of the M–mode lines situated outside (circle) and inside the lesion (triangle). M–mode ARFI images showing displacement in microns over time and depth for the (b) line through untreated tissue and (c) the line through the lesion. The stiffness of the lesion is visible by low displacements maintained at the tissue surface throughout the cardiac cycle. The horizontal white lines mark 1–D speckle–tracked lines through time in a region of myocardium at the depth of the lesion. The ARFI–induced displacements along this speckle–tracked line are plotted in (d), where the circle and triangle plots correspond to the M–mode lines outside and inside the lesion, respectively. The red dashed lines indicate the external pacing stimulus time. For each curve, a systolic to diastolic stiffness ratio was calculated.

Conclusions: The analysis of the M–mode ARFI image of the ablation lesion throughout the cardiac cycle indicated that the stiffer ablated tissue displayed only a slight change in elasticity between systole and diastole with a ratio of 1.5:1, while the surrounding untreated myocardium experienced a greater change in elasticity with a ratio of 2.9:1. Once ECG–gated ARFI images are acquired at systole and diastole, these stiffness ratios can be calculated for the entire field and potentially used to automatically demarcate the extent of an ablation lesion.

Acknowledgements: This research was funded by NIH Grant #: R21–EB–007741. We would like to thank Siemens Medical Solutions USA, Inc. for their hardware and system support.

References:

[1] B Fahey, K Nightingale, P Wolf, and G Trahey, Acoustic radiation force impulse imaging of myocardial radiofrequency ablation: Initial *in vivo* results, IEEE Transactions on Ultrasonics, Ferroelectronics and Frequency Control, 52(4):631–641, 2005.
[2] S Hsu, R Bouchard, D Dumont, P Wolf, and G Trahey, *In vivo* assessment of myocardial stiffness with acoustic radiation force impulse imaging, Ultrasound Med Biol, 33(11):1706–1719, Nov 2007.

103 **MOTION TRACKING USING BINARY TECHNIQUES IN TMRI DATA.**

Tareq Alrefae[1], Mohammed D. Alenezy[2].*
[1]Kuwait University, Khaldia, KUWAIT; [2]Universiy of Kansas, Lawrence, KS, USA.

Background: Tagged magnetic resonance imaging (tMRI) has found wide–spread applications in various clinical and research areas [1–3]. The strength of this imaging modality lies in its ability to reveal regional motion and deformation of tissue, such as that observed in cardiac studies [1–3]. To quantify motion, post–processing algorithms are developed to track the tissue for a user–selected region of interest (ROI). Examples of such algorithms include harmonic phase analysis [1] and others [2]. To further enrich the library of tracking algorithms, we present an automated method that utilizes binary image processing techniques to follow tissue motion of user–selected ROI in tMRI data.

Aims: The goal of this work is to implement automated software that enables users to track tissue motion in a sequential tMRI data set.

Methods: Figure 1 shows a flow chart describing the developed algorithm which was implemented in a MATLAB code. The procedure starts by uploading the first image frame (I1) of the tMRI data set before converting it into binary form. Next, connected regions in the image frame are defined as areas of values of one (tissue) surrounded by strips of value zero (tags) and are uniquely labeled. The user is then prompted to select an ROI before a calculation of the ROI's centroid is executed. When the next image frame (I2) is uploaded, the software locates the coordinates of the ROI centroid of I1 in the currently uploaded image frame, I2. Under small motion approximation, the location of the ROI centroid of I1 should lie in the same connected region in I2, and, hence, the ROI is tracked. Next, the third image frame, I3, is uploaded, and the procedure is repeated. It is noteworthy that prompting the user to select an ROI occurs once in the entire procedure.

Results: Figure 2 shows synthetic data of a tagged donut undergoing deformation mimicking that observed in the myocardium of left ventricle [3]. A user–selected ROI (red) was tracked throughout the simulated motion. Figure 3 shows experimental cardiac tMRI data of a rat's left ventricle captured in the short axis view. The user–selected ROI (red) was successfully tracked.

Conclusions: We have developed a fully automated algorithm that is capable of tracking cardiac motion in tMRI data sets. The algorithm operates under the small motion assumption and is successfully applicable in cardiac studies. Future work includes strain and strain rate calculations.

References:

[1] Osman NF, McVeigh ER, Prince JL, Imaging heart motion using harmonic phase MRI, IEEE Trans Med Imaging, 19(3):186–202, 2000.
[2] Axel L, Montillo A, Kim D, Tagged magnetic resonance imaging of the heart: a survey, Med Image Anal, 9(4):376–393, 2005.
[3] Alrefae T, Smirnova IV, Cook LT, Bilgen M, A model–based time–reversal of left ventricular motion improves cardiac motion analysis using tagged MRI data, BioMedical Engineering OnLine, 7**:**15, 2008.

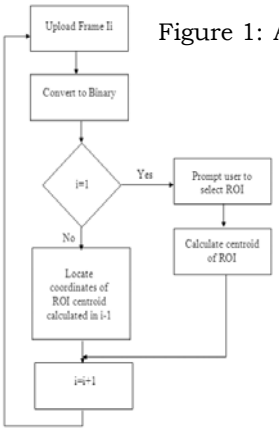

Figure 1: Algorithm procedures

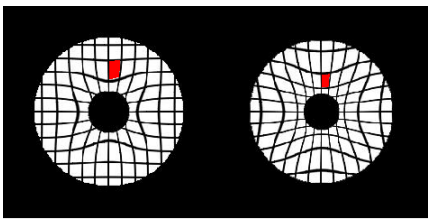

Figure 2: ROI (red) successfully tracked in a simulated motion in synthetic data.

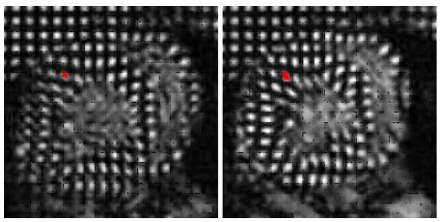

Figure 3: ROI (red) successfully tracked in experimental data of systolic motion of a rat.

* *indicates Presenter*

050 **INCREASING THE ACCURACY OF NON–INVASIVE ESTIMATION OF SHEAR STRAIN IN THE ARTERIAL WALL.**

Tim Idzenga[1], Hendrik HG Hansen[1], Richard G.P. Lopata[1], Chris L de Korte[1].*
[1]Clinical Physics Laboratory, Radboud University Nijmegen Medical Center, Nijmegen, THE NETHERLANDS.

Background: Stroke is a major cause of death and is often caused by rupture of plaques in the carotid artery. Some of these plaques are vulnerable and prone to rupture, while other plaques are stable. Vulnerable plaques mostly consist of a large lipid pool covered by a thin fibrous cap. It is hypothesized that shear stresses induced by the pulsating blood flow change the biochemical compounds of the plaque and make it more prone to rupture [1]. Furthermore, it has been hypothesized that the pulsating blood flow induces strain in the vasa vasorum surrounding the artery. These strains might be related to the vulnerability of plaques. Shear strain in the arterial wall is calculated as the gradient of the longitudinal (the direction of blood flow) displacement in radial direction. At an insonification angle of zero degrees, longitudinal corresponds to lateral direction, and estimation of displacement in this direction is known to be inaccurate. The estimates of axial displacement are more accurate. At larger angles, the displacement estimate in the longitudinal direction can be constructed from axial and lateral estimates or from axial estimates only. The contribution of the axial estimate increases for larger angles, which could increase the accuracy of longitudinal displacement and subsequently shear strain estimates.

Aims: This study aims at increasing the accuracy of estimating shear strain between the arterial wall and the surrounding tissue.

Methods: Radiofrequency (RF) data of a three layered carotid arterial wall were simulated using Field II©. The surrounding tissue (outer layer) remained fixed, and the arterial wall intima (inner layer) was displaced in the longitudinal direction. This resulted in a shear strain in the adventitia (middle layer). RF data were acquired using a simulated linear array transducer (11–3L, f = 7.5MHz, pitch = 135μm). We acquired images of the "pre–" and the "post–compression" state at angles of 0, 15, 30 and 45 degrees. At 0 degrees we applied 1, 5, 10 and 100μm longitudinal displacements, resulting in shear strain of 0.1, 0.5, 1 and 10%. Subsequently, we cross–correlated the rf data using a coarse–to–fine method [2] with a fine window size of 0.158x1.215mm. At 15, 30 and 45 degrees we repeated this for applied displacements of 1, 5 and 10μm. We constructed the shear strain and longitudinal displacement from the axial and lateral displacement estimates (Method A) or from the axial displacement estimate alone (Method B) using the rotation matrix [3]. For each combination of angle and applied displacement we calculated the mean values, the elastographic signal–to–noise-ratios (SNRe) and the root–mean–square error (RMSE) in a selected Region of Interest (ROI).

Results: At an angle of 0 degrees, the SNRe of the shear strain (longitudinal displacement) estimates, constructed from lateral displacement, increased from -12dB (3dB) at 5μm displacement to +10dB (+29dB) at 100μm. The SNRe of the shear strain (longitudinal displacement) estimated at three angles with Method A ranged at 5μm from -20dB (-23dB) to -10dB (6dB), whereas using Method B the SNRe ranged from -8dB (11dB) to -5dB (14dB). Using Method A the RMSE of the longitudinal displacement was higher than at 0 degrees, whereas with Method B the RMSE was lower. Furthermore, the values, estimated using Method A, decreased with increasing angle, whereas those estimated, using Method B were comparable to the applied values or slightly increased with increasing angle.

Conclusions: At zero degrees, the SNRe increased with increasing displacement. At larger angles the SNRe, using Method B, was higher than with Method A and at zero degrees. Also at larger angles the estimated values, using Method B, were comparable to the applied values, and the RMSE was lower than with Method A. Therefore, using insonification angles larger than zero and constructing displacement and strain estimates from axial estimates can only increase the accuracy of shear strain estimation.

Acknowledgements: The support of the Dutch Technology Foundation (STW) and Philips Medical Systems is acknowledged.

References:

[1] Slager, CJ, et al., The role of shear stress in the generation of rupture–prone vulnerable plaques, Nat. Clin. Pract. Cardiovasc. Med., 2(8); 401–07, 2005.
[2] Lopata RG, et al., Performance Evaluation of Methods for two–Dimensional Displacement and Strain Estimation Using Ultrasound Radio Frequency Data, Ultrasound Med Biol., 10–3–2009.
[3] Fung–Kee–Fung SD, et al., Angle–independent strain mapping in myocardial elastography, IEEE Ultrasonics Symposium, 516–519, 2005.

011 **IMAGE REGISTRATION IN ELASTICITY IMAGING: A FEASABILITY STUDY.**

A Costet[1], L Morris[2], WE Svensson[2], DW McRobbie[2].*
[1]Imperial College London–Faculty of Engineering, London, England, UK; [2]Imperial College Healthcare NHS Trust–Imaging Directorate, London.

Background: Some modern commercial US systems allow automated region of interest (ROI) drawing on a single frame of the elastographic video clip to be compared with the B–scan area. However, this is heavily subjective and relies on the user selecting a correct frame from a series of potentially hundreds.

Aims: The aim of this feasibility study is to semi–automate diagnosis by assessing the elastograms throughout the whole image clip and automatically comparing this with a user defined B–Scan ROI (b–ROI).

Methods: In this study, 19 image sequences, obtained freehand using a SONOLINE ANTARES system with a VFX13–5 array transducer were selected with known pathology. The processing code was MatLab. Image frames were pre–processed to remove any frames unsuitable for use before registration processing and diagnostic analysis. These were: correlation between two successive elastogram frames, the average difference per pixel between successive frames and the mean pixel value. The user then manually draws the b–ROI on the selected B–scan frame.

Thresholding and Sobel Masks were used to of detect the elastogram ROIs (e–ROI) are used to identify areas as regions of stiffness, i.e. malignancy appearing darker and larger than benign regions. Properties of the e–ROIs which are used to assess the elastogram are: area of the e–ROI, length of the major axis, length of minor axis, percentage of the e–ROI that exists outside of the b–ROI and distance of the b–ROI centroid to the e–ROI centroid. The mean, maximum and minimum values for each of these properties are displayed and the selection criteria adjusted. The overall quality of the clip can be assessed using these and the previous quality factors (Figure 1) as well as the overall percentage of frames removed from the clip. This allows some evaluation of the sensitivity and specificity of the results.

Results: Sensitivity and specificity of the software were assessed using each criterion individually and combined, each giving differing results. Then our results were compared with results from previous studies [1,2] against which our results were found to be inferior. Combining criteria gave specificity of 60% sensitivity of 73%. Once the poor clips were removed from the study, results improved to specificity of 100% sensitivity of 80%.

Conclusions: While the results of this study appear disappointing in the first instance, removal of the poorer video clips yields more impressive results. As a first pass feasibility study these results are encouraging, although more work is required in the selection criteria, both before and during the processing stages. For example, problems with more than one poor frame during the correlation stage of the selection process require attention.

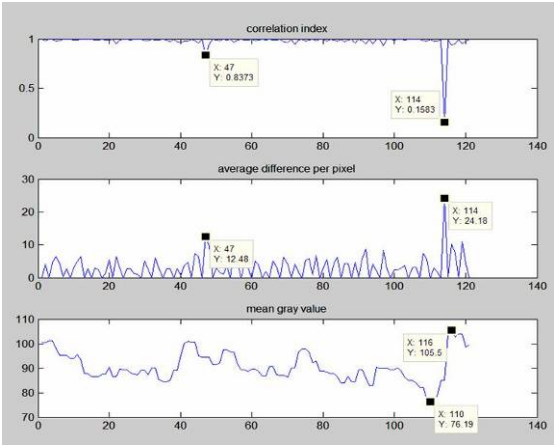

Figure 1: Quality criteria used for frame selection during pre–processing

References:

[1] Tan, et al., Improving B–mode ultrasound evaluation of breast lesions with real–time ultrasound elastography – A clinical approach, Breast, 17(3): p252–257, 2008.
[2] Burnside, et. al., Differentiating benign from malignant solid breast masses with US strain imaging, Radiology, 245:p.401–410, 2007.

* *indicates Presenter*

004 **FREEHAND STRAIN IMAGE NORMALIZATION FOR CONVEX PROBES.**

R. James Housden[1], Andrew H. Gee[1], Graham M. Treece[1], Richard W. Prager[1].*
[1]Engineering Department, University of Cambridge, Cambridge, England, UK.

Background: In freehand quasi–static strain imaging, the applied stress is varied by manually moving the ultrasound probe. This results in significant variations in the magnitude and shape of the observed strain distribution. In addition, the magnitude of the stress field tends to decrease with depth in the tissue, resulting in the well–known depth–hardening artifact. Normalization is a process that compensates for these variations by scaling the observed strain data by an appropriate value, possibly varying over the image according to the expected shape of the stress field [1,2]. Existing work on normalization has concentrated on linear array transducers with flat compression surfaces. A convex probe has a curved compression surface, which applies stress with a very different profile to that of a flat compressor [3]. As a result, different normalization functions may be needed for convex probes.

Aims: To develop normalization functions appropriate for use with a convex probe.

Methods: We used Abaqus FEA software to determine a typical shape for the observed radial strain field. Uniform–stiffness results are shown in Figure 1: (a) is for normal compression, while (b) is a combination of normal compression and a lateral shift. From the general shape of these results, we developed several possible normalizations as a function of radial and angular position, $f(r,\theta)$. These functions approximate the observed strain field, while having as few parameters as possible. This is important, since very flexible functions may remove genuine stiffness variations and are sensitive to noise in low–quality data. The functions tested were $f_1 = a.(1+br).(1+c(\theta+d)^2)$ which has a linear variation with r and a quadratic variation with θ; $f_2 = a.\exp(-br).(1+c(\theta+d)^2)$ which has a more realistic variation with r, and $f_3 = a.\exp(-br).(1+c(\theta+d+er)^2)$, which allows the quadratic's peak position to vary with r. The functions were fitted to the data using the Levenberg–Marquardt algorithm. For comparison, we also normalized to $f_0 = a$.

Results: Figure 2 shows the results of applying these various normalizations to two sample strain images of a uniform–stiffness phantom. Clearly, any of the suggested functions are preferable to normalizing by the mean strain (f_0). Among the other three, f_2 and f_3 are marginally better than f_1, particularly at the bottom of the images. This is mainly due to the exponential, instead of linear, variation with r. Finally, there is very little difference between f_2 and f_3, even in the first example, which has a higher strain at the top right than the top left. This suggests that the extra flexibility provided by f_3 is unnecessary.

Conclusions: Any of the three suggested functions produce reasonably uniform images, although allowing an exponential variation with depth offers a slight improvement. These results suggest that f_3 is best avoided, since its greater flexibility means that it is more likely to incorrectly fit to the data and offers no clear benefit. f_2 is therefore the preferred normalization function, although further experimentation with more data sets is necessary to confirm these conclusions.

Acknowledgements: This work was supported by EPSRC grant number EP/E030882/1.

References:

[1] Ponnekanti H, et al. Ultrasonic imaging of the stress distribution in elastic media due to an external compressor. UMB 20:27–33, 1994.
[2] Lindop J, Treece G, et al. An intelligent interface for freehand strain imaging. UMB 34:1117–28, 2008.
[3] Galin L. Contact problems in the theory of elasticity. Raleigh, NC, 1961.

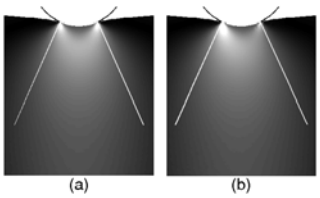

Figure 1: Observed radial strain images from FEA. White is high strain.
(a) Normal compression.
(b) As (a) with lateral shift to the left. White lines indicate the extent of the contact region.

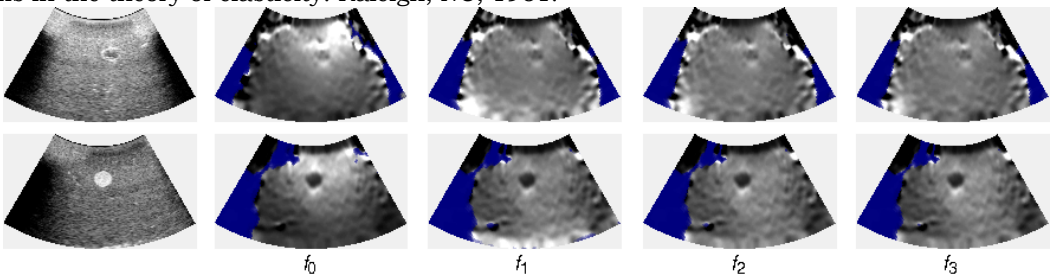

Figure 1: Axial strain images recorded by a convex probe on a uniform–stiffness breast biopsy phantom and normalized by the various functions. The blue areas in the images mask regions with low–precision strain estimates.

019 **METHODS FOR THE ESTIMATION OF THE SUB–SAMPLE MOTION USING DIGITIZED ULTRASOUND ECHO SIGNALS IN THREE DIMENSIONS.**

R Zahiri–Azar[1], O Goksel[1], SE Salcudean[1].*
[1]The University of British Columbia, Vancouver, BC, CANADA.

Background: Motion estimation lies at the heart of many ultrasound–based applications including elastography. We have previously presented pattern matching function interpolation techniques that accurately determine the sub–sample motion in 2D. In these techniques, a 2D polynomial is fitted to the maximum of the discrete pattern matching coefficients and its neighboring lags. A joint estimation of the sub–sample axial and the lateral motion is then achieved by finding the maximum of this 2D polynomial.

Aims: In this work, the sub–sample interpolation technique is extended to 3D where the axial, lateral and elevational components of the motion are determined with sub–sample accuracy.

Methods: Following the coarse estimation of the motion within the sampling accuracy by locating the maximum of the discrete 3D pattern matching function, the quadric, cubic and quartic polynomials with three variables $f(x,y,z)$ with 10, 17 and 23 coefficients, respectively, resulting from multiplying $[1,x,x^2]$, $[1,y,y^2]$ and $[1,z,z^2]$ terms, are fitted to the maximum of the discrete 3D pattern matching function and its neighboring lags in the axial (x), the lateral (y) and the elevational (z) directions using least squares fit. The sub–sample accuracy is then achieved by locating the maximum of this fitted 3D polynomial (i.e. $\nabla f(x,y,z) = 0$) using the closed form solution for the quadric and Newton's method for cubic and quartic polynomials.

Results: A 50x60x10mm^3 virtual phantom was simulated and displaced over a 5x5x5 3D grid with a spacing of ¼ of a sample in each direction. This grid spans ±0.5 of a sample in all three axes. RF echoes corresponding to each of these configurations were generated using the Field II simulation software. Several sub–sample motion estimation algorithms were then applied to these simulated RF volumes in order to evaluate the performance of the proposed 3D polynomial fitting methods comparing these to the conventional methods in the literature, i.e. independent 1D parabola and cosine fitting. The comparison in terms of bias and standard deviation is shown in Figure 1. The mean absolute axial, lateral and elevational bias of the proposed 3D quartic polynomial fitting was found to be 0.0060, 0.0075 and 0.0047 of a sample (corresponding to 120nm, 2.24µm and 710nm), respectively, for simulated axial sampling of 40 MHz (≈20µm), lateral sampling of 300µm, and elevational sampling of 150µm. Experimental results from a commercial breast phantom (CIRS Model 052A, Virginia, USA) are shown in Figure 2 demonstrating the viability of the proposed method. A Sonix RP (Ultrasonix Corp, Richmond, Canada) ultrasound machine with a motor driven 4D transducer was used to acquire the data.

Conclusions: A novel pattern–matching function interpolation scheme suitable for accurate estimation of 3D motion has been presented. Its performance has been evaluated in both simulations and experiments in terms of bias and standard deviation. The proposed 3D interpolation method significantly outperforms techniques based on interpolation in each of the axial, lateral and elevational directions. Specific applications in medical ultrasound include fine 3D tissue motion tracking, blood flow estimation, motion vector estimation, strain tensor estimation and tissue elasticity estimation.

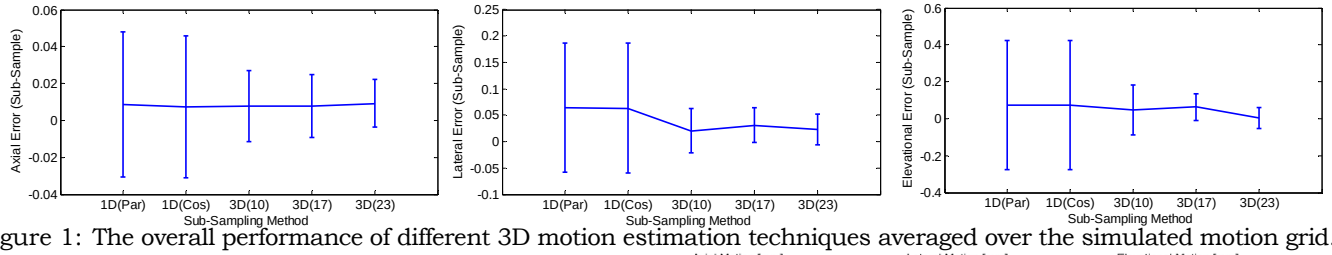

Figure 1: The overall performance of different 3D motion estimation techniques averaged over the simulated motion grid.

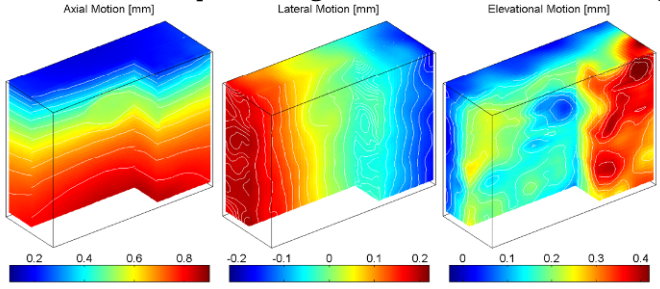

Figure 2: Estimated axial, lateral and elevational components of the motion resulted from axial compression of a commercial breast phantom. Multi-planar view is used to visualize the results in 3D. Equal-cost contours are also drawn to show the direction of displacements.

* *indicates Presenter*

021 **STRAIN IMAGING OF BREAST USING TWO LINEAR ARRAY TRANSDUCERS.**

Mok–Kun Jeong[1], Sung–Jae Kwon[1], Moo–Ho Bae[2].*

[1]Electronic and Communication Engineering Departments, Daejin University, Pocheon, Gyeonggi, 487–711, KOREA; [2]Electronic Engineering Department, Hallym University, Chuncheon, Gangweon, KOREA.

Background: Mammography is routinely used in the diagnosis of breast cancer, but it may cause radiation hazard. Although ultrasound scanners cannot provide very high resolution, they may aid in breast diagnosis by estimating parameters such as the speed of sound, attenuation, harmonics, or elasticity, in addition to the B–mode imaging.

Aims: We previously reported a method of performing both compound and speed of sound imaging by placing protruding objects such as a breast between two linear array transducers [1]. In this presentation, we obtain elasticity images using the same configuration.

Methods: In a configuration where a protruding object such as the breast is placed between two linear arrays that face each other, compound imaging can be achieved by separately obtaining and combining B–mode images from each of both arrays. If one array is used as a transmitter and the other as a receiver, the speed of sound distribution can also be obtained by measuring the time of flight. This imaging configuration is advantageous in that the amount of compression applied to the breast can be adjusted as desired by finely controlling the spacing between both arrays and that the strain image quality can be improved accordingly. In order to do strain imaging, we fabricated an elasticity phantom containing a 10 mm diameter cylinder that was five times harder than the background. Two 7.5 MHz linear array transducers are placed at the top and bottom of the 40 mm high phantom so that they face each other through it. The spacing between both arrays, connected to a clinical ultrasound scanner (Medison, Korea), was finely controlled by using a stepper motor. Using I and Q data sets acquired from both arrays, strain images were produced by employing a correlation–based strain estimation method. The images were compensated for motion from frame to frame based on the available information on the amount of compression applied. The quality of the strain image was improved by averaging over multiple strain images or by persistence processing.

Results: Figure 1 displays strain images that were obtained using data from one array (a) and compounded data from both arrays (b). We observed that the elastographic signal–to–noise ratio, SNRe, and the elastographic contrast–to–noise ratio, CNRe, increased by more than about 2.5 dB after compounding two strain images obtained from each of the arrays.

Conclusions: A method is presented for imaging the strain of a breast that is placed between two opposing linear array transducers. Strain images using data from one array and compounded data from both arrays, respectively, were obtained by phantom experiments. The strain image quality was found to be improved by the compounding technique.

Acknowledgements: This work was supported by Medison.

References:

[1] Jeong MK, Kwon SJ, Cho SM, Bae MH, Kim YG. Ultrasound breast imaging technique using two opposing transducer arrays. Proc IEEE Ultrason Symp, 1274–1277, 2008.

Figure 1: Strain image obtained using one array (a) and compounded image using two arrays (b).

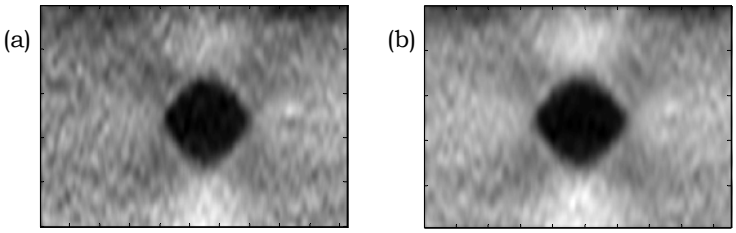

082 **LIVE ESTIMATION AND VISUALIZATION OF 4D×3D ULTRASOUND MOTION VECTORS.**

ER Pospisil[1], R Zahiri–Azar[1], R Rohling[1], SE Salcudean[1].*
[1]The University of British Columbia, Vancouver, BC, CANADA.

Background: There has been considerable research on real–time axial and lateral motion estimation, but only recently have there been efforts to obtain a time series of volumes (4D) where each volume contains full 3D motion vectors, which we term 4D×3D [1].

Aims: To measure and display 4D×3D vector data using a motorized curvilinear transducer at the native rate of volume acquisition.

Methods: This work utilizes several of the fastest and most accurate techniques employed in the real–time production of 2D elastography images and extends these techniques to 3D. In scan conversion and filtering, this extension resultes in novel approaches to resolving the additional complexities arising in 3D processing. The SonixRP ultrasound machine (Ultrasonix Corp, Richmond, BC, Canada) is used so that the motion estimation operates on live streams of radiofrequency data. The C++ implementation is based on the most common type of transducer for obtaining 3D data: a motorized curvilinear transducer. Once two volumes of data have been collected, a 3D version of Time Domain Cross–Correlation with Prior Estimates [2] is used for 3D motion estimation. The code outputs displacement estimates in an R, θ and φ coordinate system, where R and θ are taken about the transducer array foci, while φ is taken about the motor's axis of rotation. As such, a 3D extension of backwards mapping [3], trilinear interpolation, scan conversion is implemented which accurately converts the data to Cartesian positions and displacement components using the transducer's geometry. The algorithm also utilizes the scan geometry to determine if the output resolution will result in aliasing, and if so, performs 1D separable Gaussian filtering on each dimension, where the θ and φ filter distributions are a function of R to maintain a uniform spatial filter size. The output data is stored in a 3D vector volume format for further processing or display. If display is desired, 2D cross sections of the volume are taken and rendered on the screen. For strain imaging, OpenGL texture mapping techniques are used for real–time rendering of a breast mass phantom (CIRS Model 059, Virginia, USA) shown in Figure 1. The 3D displacement data can also be shown as vectors projected onto each cross section, allowing full 4D×3D motions to be visualized (Figure 2). The speeds of each step of the process are measured to fine tune and validate performance.

Results: Several optimizations were needed to achieve the speed requirements, including the use of pre-compiled lookup tables for static computations of trigonometry, the Gaussian filters and backwards mapping. The resulting program can analyze and render 3D volumes at 5.7 volumes per second for a 9 frame volume with 80 scanlines and a 5 cm imaging depth (80 motion estimates per scanline).

Conclusions: It is feasible to obtain geometrically correct 3D Cartesian displacements from a motorized curvilinear transducer and process the data at the native rate of volume acquisition. Moreover, this has been achieved on the standard SonixRP PC hardware. This software is a key step in our ongoing efforts to obtain real–time 3D elastography using FEM techniques or inversion of the wave equation.

Acknowledgements: The contributors would like to thank NSERC and CIHR for their support of this research.

References:

[1] R. Lopata, M. Nillesen, I. Gerrits, J. Thijssen, L. Kapusta, C. de Korte, 4D Cardiac Strain Imaging: Methods and Initial Results IEEE Ultrasonics Symposium, pp 872–875, 2007.
[2] R. Zahiri–Azar, S.E. Salcudean, Motion Estimation in Ultrasound Images using Time Domain Cross Correlation with Prior Estimates, IEEE Transactions on Biomedical Engineering. Vol 53, no. 10, pp. 1990–2000, 2006.
[3] Q. Duanl, E. Angelinil, T. Song, A. Laine, Fast Interpolation Algorithms for Real-Time Three-Dimensional Cardiac Ultrasound, Proceedings of the IEEE, EMBS Conference, pp 1192–1195 Vol.2. 2003.

Figure 1: GUI showing real–time 3D axial strain of a breast mass phantom.

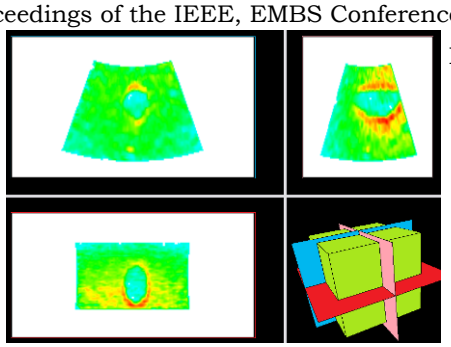

Figure 1: Stress–stra (solid line) The slope was calcu (0.23 to 0. obtain elas and signal-

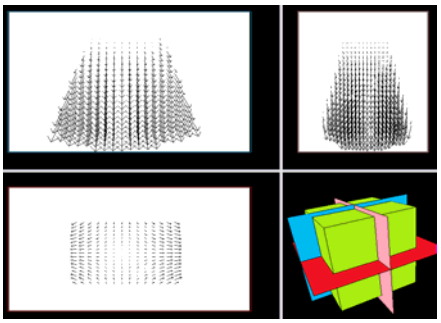

* *indicates Presenter*

029 **QUANTITATIVE CORNEA ELASTICITY MAPPING USING HIGH FREQUENCY SUPERSONIC SHEAR IMAGING.**

M. Tanter[1], J–L. Gennisson[1], D. Touboul[3], T–M. Nguyen[1], J. Bercoff[2], M. Fink[1].*
[1]Langevin Institute, Laboratoire Ondes et Acoustique, ESPCI Paris Tech, CNRS UMR 7587, INSERM, 10 rue Vauquelin, 75005, Paris, FRANCE; [2]SuperSonic Imagine, Les jardins de la Duranne – Bât E & F510, rue René Descartes 13857, Aix en Provence, FRANCE; [3]Service d'ophtalmologie, Hôpital Pellegrin, place Amélie Raba–Léon, 33000, Bordeaux, FRANCE.

Background: High–resolution measurements of cornea elasticity could have many applications in ophthalmology. It could help to understand corneal pathologies, such as Keratoconus, to evaluate the biomechanical response of the cornea after refractive surgeries (LASIK) and to estimate the efficiency of new cornea treatments, such as cornea transplant using femtosecond laser or Riboflavin/UV–A induced corneal collagen cross–linking (UVA CXL). It could also provide the first tool enabling a precise and non–invasive measure of the intraocular pressure.

Aims: In this work, the Supersonic Shear Imaging technique (SSI) is proposed for mapping the biomechanical properties of the cornea.

Methods: The SSI technique is based on the radiation force induced by a conventional ultrasonic probe to generate a planar shear wave into tissue. Then shear wave propagation throughout the corneal layer is caught in real–time due to an ultrafast ultrasound scanner (up to 10,000 frames/s) driving a high–frequency ultrasonic probe (15 MHz central frequency). A study has been conducted *ex vivo* on 10 porcine eyes in order to correlate corneal elasticity measurements with intraocular pressure and to estimate corneal elasticity changes after UVA CXL. *In vivo* data, quantitative elasticity maps, have also been acquired from sheep's eyes.

Results: The results obtained *ex vivo* show a variation of corneal elasticity while changing the intraocular pressure (from 13 to 40 mmHg). Besides, a significant corneal elasticity increase of 50% has been measured after UVA CXL treatment (Young's modulus mean value: 890 +/-250 kPa). The phase velocity of the shear wave has also been extracted to investigate the shear wave dispersion. The results were compared to 3D finite differences simulations. The mechanical wave propagation corresponds to a leaky Lamb wave. Analytical and numerical dispersion curves are compared to experimental results and exhibit very good agreement in the 400 – 3000 Hz range.

Conclusions: This initial investigation demonstrates the ability of ultrafast and high resolution echographic systems to provide a real–time and quantitative mapping of corneal elasticity. Quantitative elasticity maps were acquired *ex vivo* on porcine cornea using the SSI technique. The acoustic intensity induced during the SSI sequence remained lower than the recommendations provided by the FDA for Ultrasonic imaging devices (510k recommendations). This technique can perform real–time, high resolution and quantitative maps of corneal elasticity. It could be adapted straightforwardly for *in vivo* investigations.

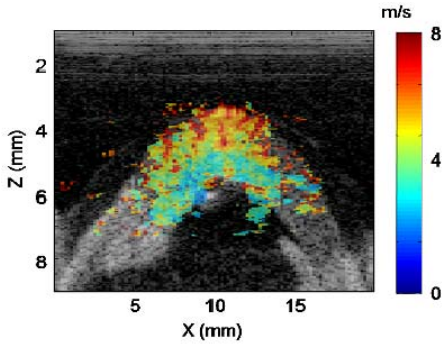

Figure: 2D mapping of shear wave speed of an excised porcine eye whose cornea had been partially burned. The SSI modality is clearly able to image a very stiff 200 µm first layer in the cornea.

096 **BIAXIAL CHARACTERIZATION OF HUMAN FETAL MEMBRANES.**

J Egger[1], A Mallik[2], C Haller[2], M Jabareen[3], A Zisch[2], E. Mazza[1].*

[1]Center of Mechanics, Swiss Federal Institute of Technology, Zurich, SWITZERLAND; [2]Obstetrics and Gynecology Department, University Hospital, Zurich, SWITZERLAND; [3]Technion Israel Institute of Technology, Haifa, ISRAEL.

Background: The fetal membranes, chorion and amnion, form a bi–layer that serves as barrier and bio–container through out gestation. Mechanical rupture of fetal membrane is part of the natural sequence of term delivery, but has serious complications when rupture occurs prior to term. Understanding the mechanical behavior of the chorioamniotic tissue and its dependence on micro–structural components is essential for rupture prevention and for development of repair methods.

Aims: The mechanical properties of the chorioamniotic tissues were determined using a new "inflation test" providing biaxial (physiological) loading conditions. For each membrane biochemical and histological investigation provided information on the microstructure. Correlations are investigated between mechanical and histological data. This study complements the research work presented in [1] that was based on uniaxial tests.

Methods: The inflation test is realized by clamping a sample of fetal membrane on a water filled cylinder. The water pressure is increased according to a predefined loading profile using a peristaltic pump. The membrane is progressively stretched (Figure 1) until bursting. The pressure history and the corresponding displacement history of the highest point of the deformed tissue, obtained through image analysis of the pictures taken at regular time intervals from the side, were obtained for each experiment (Figure 2). An inverse finite element analysis allows determining constitutive model parameters from these data. Elastin content of the fetal membranes was estimated following a commercial elastin assay kit (Fastin elastin assay). Total collagen content was determined based on the amount of one of its known marker, the 4–hydroxyproline. Thickness of amnion and chorion were measured according to the protocol described in [1].

Results: Mechanical as well as histological data were determined from measurements on 18 membranes (about 100 samples). Thickness varied between 250 and 750 µm. Elastin and collagen content were between 15% and 22%, respectively 9% and 27% of the dry weight. Burst over–pressure varied between 30 and 250 mbar. Constitutive model parameters are currently being extracted using a finite element inverse procedure. Corresponding correlations with the histological parameters will be presented.

Conclusions: A protocol for biaxial testing of human fetal membranes was established. Procedures for the determination of elastin and collagen content of membrane samples were successfully applied. This study thus provides quantitative results on (1) the mechanical response of fetal membranes subjected to physiological deformations and (2) the corresponding micro–structural characteristics.

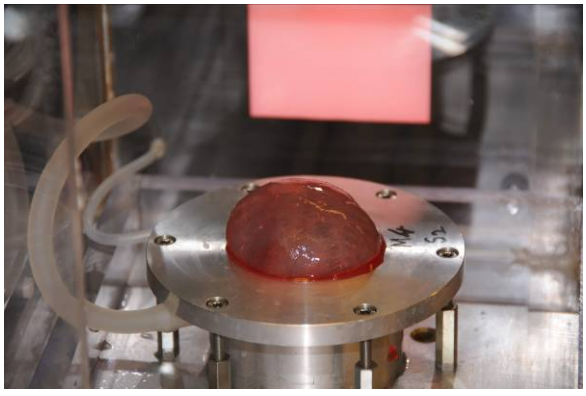

Figure 1: Fetal membrane in the inflation device

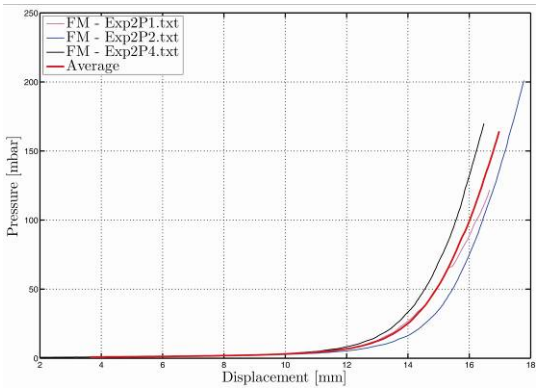

Figure 2: Example of measured curves

References:

[1] M. Jabareen, A.S. Mallik, G. Bilic, A.H. Zisch, E. Mazza, Relation between mechanical properties and microstructure of human fetal membranes: An attempt towards a quantitative analysis, International Journal of Obstetrics & Gynecology and Reproductive Biology, 144, 134–141, 2009.

* *indicates Presenter*

005 **MEASURING THE NONLINEAR ELASTIC PROPERTIES OF LIVER TISSUES *IN VITRO* AND *EX VIVO*.**

Jérémy Chenot[12], David Melodelima[12] and Jean–Yves Chapelon[12].*
[1]Inserm, U556, Lyon, F–69003, FRANCE; [2]University of Lyon, Lyon, F–69003, FRANCE.

Background: Biological tissues are generally very nonlinear elastically. The nonlinearity may be more important for *in vitro* samples compared with *in vivo* tissues [1]. Characterizing this behavior can significantly contribute to better elasticity imaging algorithms. This presentation discusses the nonlinear elastic behavior of *in vitro* and *ex vivo* samples of pig liver.

Aims: To evaluate differences in elastic properties of livers between *in vitro* and *ex vivo* measurements.

Methods: Three livers from butchery (*in vitro* case) and three livers removed just after pig euthanasia (*ex vivo* case) were used for this study. The *in vivo* hepatectomy was performed with vena cava and triad clamping to keep all the fluids (blood and biliary) inside the liver. Livers were placed on a balance. A 12MHz ultrasound imaging linear array was fixed on a motorized mechanical arm. This probe was placed just on the surface of the liver such that no compression was created. A series of displacements of 0.5 mm increments were then produced in the vertical direction. To average fluctuations, the weight measured on the balance and allowing determining the applied force was noted after each step of displacement and at 5 and 10 seconds after the compression. A waiting period of 15 sec was used between displacement increments. The induced displacements were known using the motorized arm. This process was repeated until the applied stress was 3 $N.cm^{-2}$. This limit was used to prevent damage to the liver. Strain was measured based on 1D cross–correlation.

Results: In total, 11 and 17 measurements were performed on *in vitro* and on *ex vivo* livers respectively. Data obtained allowed the visualization of the stress applied as a function of the strain produced in the livers. It was shown (see Figure 1) that the non–linearity of the stress–strain relationship was obtained more rapidly in the *in vitro* case. The range of strain necessary to obtain elastograms with contrast (>15 dB) and signal–to–noise ratio (>1) was defined between 0.23 and 0.33. In this region the gradient was $17.9N/cm^2$ in the *in vitro* case and $7.5N/cm^2$ in the *ex vivo* case signifying that it is easier to deform the tissue in the *ex vivo* case. The pre–compression necessary to stress the liver for doing elastography with this probe is 2.4 times higher in the *in vitro* case when compared to the *ex vivo* case.

Conclusions: These data obtained from uniaxial measurements showed that liver tissue deforms differently *in vitro* when compared to *ex vivo* conditions. The main difference between *in vitro* and *ex vivo* livers was the presence of fluid (blood and biliary) that changed the elastic properties of the liver. Therefore, the necessary stress for elastography is modified, and this can modify the quality of *in vitro* elastograms. Applying nonlinear processing may address strain–hardening problems in conventional elasticity imaging and produce images of the elastic nonlinearity itself.

Acknowledgements: This work was partly supported by funding from EDAP TMS (N° EDAP 88513 B45).

References:

[1] Chui et al., "Combined compression and elongation experiments and non–linear modeling of liver tissue for surgical simulation", Med. Biol. Eng. Comput., 42, 787–798, 2004.

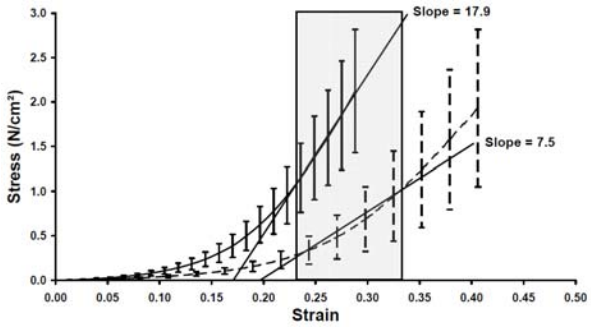

Figure 1: Stress–strain relationship for *in vitro* liver (solid line) and *ex vivo* liver (dashed line). The slope of the stress–strain relationship was calculated in the range of strain (0.23 to 0.33, grey region) necessary to obtain elastograms with contrast >15dB and signal–to–noise ratio >1.

* *indicates Presenter*

023 **THERMAL EFFECTS ON MUSCULAR SHEAR MODULUS ASSESSED BY ULTRASOUND.**

E. Sapin[1], J.L. Gennisson[1], M. Pernot[1], M. Tanter[1], M. Fink[1].*
[1]Langevin Institute, Laboratoire Ondes et Acoustique, ESPCI Paris Tech, CNRS UMR 7587, INSERM, Paris, FRANCE.

Background: A growing interest is given to ultrasound–based techniques that combine temperature and elasticity mapping to monitor HIFU treatments. However, these ultrasonic methods require better understanding of the thermal effects on elasticity of soft tissue.

Aims: The study aims to evaluate the temperature dependence of the shear modulus of *ex vivo* bovine muscles.

Methods: 20 *ex vivo* samples of bovine muscle were slowly heated in a thermally–controlled saline bath (only 2 samples are presented in Figure 1 for clarity). Thermocouples assessed temperatures in both water and muscles. Firstly, samples were heated from 20°C to 70°C by steps of 10°C for 20 minutes then cooled back to room temperature. Elasticity assessment was achieved every minute, either along the muscular fibers or perpendicular to the fibers. Secondly, to identify reversibility/irreversibility thresholds, samples were heated from 20°C to 70°C by steps of 10°C for 20 minutes and cooled back at 20°C for 20 minutes. Local elasticity was assessed using Supersonic Shear Imaging. By successively focusing ultrasonic "pushing" beams for 200µs at 4 different depths (probe L7–4, 5 MHz), shear waves were created and interfered constructively along a Mach cone to generate two quasi–plane shear wave fronts propagating in the opposite direction. The shear wave propagation was acquired with 30 images at 5000 frames/s. 4 successive shear waves were created at different lateral locations, and data were combined to provide the elasticity map of the medium. Finally, shear modulus was computed as the median of the local values into a manually chosen region of interest.

Results: Shear moduli decreased linearly with increasing temperature up to about 45°C, with a change in slope around 45–50°C, and then exponentially increased for higher temperatures (Figure 1). Cool down behavior depended on the ratio: shear modulus at the end of the heating/initial shear modulus. A ratio of <1 led to a quasi–constant modulus during cool down whereas a ratio of >1 led to increasing modulus (Figure 1). 55–65°C was the range of temperatures above which the changes in modulus were irreversible (Figure 2). Initial modulus perpendicular to the fibers was about 1.5 times lower than the longitudinal along the fibers.

Conclusions: Thermal–induced changes in the shear modulus of *ex vivo* bovine muscles were consistent with changes in collagen at the micro–scale [1]. Firstly, the shear modulus decreased with increasing temperatures up to 60°C, probably because of the collagen unfolding process. A change in slope was observed around 45–50°C for all samples. Secondly, muscular elasticity increased with temperatures higher than 60°C likely because collagen was irreversibly transformed into a random structure. Finally, the cool down behavior depended on the shear modulus at the end of the heating relative to the initial value. Effects of time and water absorption in the medium need to be explored to complete the data.

References:

[1] Lepetit, J., A. Grajales, and R. Favier, Modeling the effect of sarcomere length on collagen thermal shortening in cooked meat: consequence on meat toughness. Meat Science, 54(3): p. 239, 2000.
[2] Wright, N.T. and J.D. Humphrey, Denaturation Of Collagen Via Heating: An Irreversible Rate Process. Annual Review of Biomedical Engineering, 4(1): p. 109–128, 2002

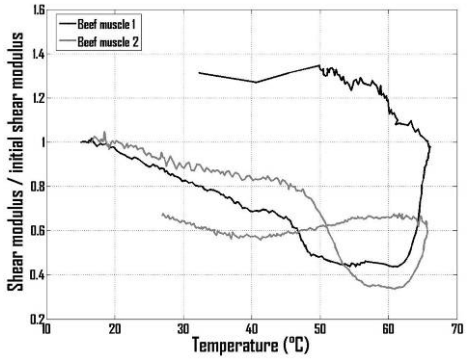

Figure 1: Evolution with temperature of the shear modulus relative to its initial value for only 2 samples.

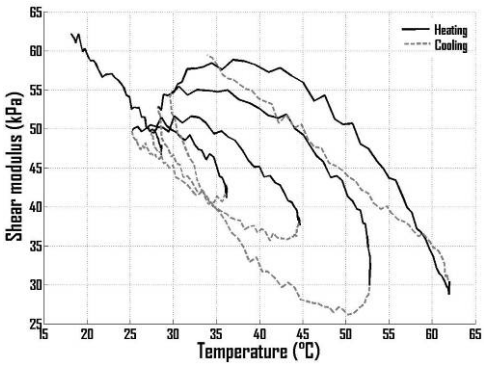

Figure 2: Successive heating and cooling cycles to identify the reversibility/irreversibility threshold.

* *indicates Presenter*

093 **MENSTRUAL CYCLE, SITE AND INDIVIDUAL DEPENDENCES OF BREAST ELASTICITY MEASURED *IN VIVO* USING ULTRASOUND INDENTATION.**

Jia–Wei Li[1], Suk–Tak Chan[1], Yan–Ping Huang[1], Yong–Ping Zheng[1,2].*
[1]Health Technology and Informatics Department, [2]Research Institute of Innovative Products and Technologies, The Hong Kong Polytechnic University, Hong Kong, CHINA.

Background: Recently, the quantification of breast elasticity gained much research attention with the popularity of ultrasound elastography in breast tumor diagnosis. A potential solution was to add a force sensor on the probe to form a 1D or 2D ultrasound indentation system [1,2]. Our preliminary study using this system has demonstrated its feasibility in the elasticity measurement of breast tissue *in vivo* and found some variations of breast elasticity within and among subjects [3].

Aims: This study extends to investigate the changes of breast elasticity arising from the menstrual cycle, breast site and individual subject using the 2D ultrasound indentation system.

Methods: 20 subjects (age: 26.6±3.6; BMI: 20.8±3.0; cycle length: 31.5±5.4) were recruited at an interval of 2 to 3 days for one complete natural menstrual cycle. The measurements were conducted on the four quadrants of both breasts for each subject using an ultrasound scanner (Apogee 3500, Shantou Institute of Ultrasound Instruments Co., Ltd.) with a customized 7.5 MHz probe attached with a force sensor [3]. At each quadrant, five repeated tests were performed, and the values were averaged. The menstrual cycle length of each subject was normalized to 28 days with the help of the ovulation day predicted from the pelvis ultrasound scanning in the mid–cycle. Accordingly, the number of tests for each subject was interpolated to 28 data points by linear interpolation. The data of one test acquired on Days 10–14 was analyzed for the quadrant, and individual dependences with 6 additional subjects were tested, i.e. n=26.

Results: The results indicated that the breast elasticity varied as a function of menstrual cycle days with a trough and peak in the mid–cycle (Days 11–13) and before menstruation (Days 26–28), respectively. All the individual quadrants showed similar trends in elasticity during the menstrual cycle (Figure 1). When the menstrual cycle was staged in the uterine event, breast elasticity in the proliferative phase was significantly lower than that in the menstrual and the secretory phases ($p<0.05$). Breast elasticity presented significant differences among the four quadrants (Figure 2), between the upper and lower parts, and between the inner and outer parts of the breast ($p<0.05$). A significant linear correlation was found between breast elasticity and BMI (n=26, r=0.546, p=0.004), and between breast elasticity and breast thickness (n=26, r=0.53, p=0.005). Significant difference was found in breast elasticity among subjects of bra cup sizes A (n=10), B (n=8) and C (n=8) (p=0.002).

Conclusions: The within– and between–subject differences, arising from the physiological factors of females, were unveiled for breast elasticity. The findings of site, menstrual cycle and individual dependent variations of breast tissue elasticity are expected to provide a meaningful reference and guidance for the clinical generalization of quantitative ultrasound elasticity measurement and imaging.

Acknowledgements: This project is partially supported by the HKSAR Research Grant Council (PolyU5318/05E) and the Hong Kong Polytechnic University (1–BB69).

References:

[1] Zheng, et al., An Ultrasound indentation system for biomechanical properties assessment of soft tissues *in–vivo*, IEEE Transactions on Biomedical Engineering, 43: 912–918, 1996.
[2] Han, et al., A novel ultrasound indentation system for measuring biomechanical properties of *in vivo* soft tissue, Ultrasound in Medicine and Biology, 9:813–823; 2003.
[3] Li, et al., Menstrual cycle dependence of *in vivo* breast elasticity measured using ultrasound indentation, The 7th International Conference on the Ultrasonic Measurement and Imaging of Tissue Elasticity, Austin, USA, 66, 2008.

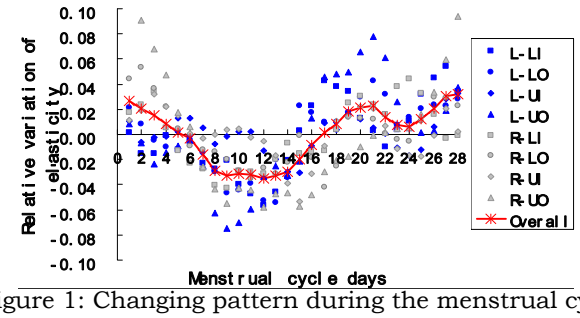

Figure 1: Changing pattern during the menstrual cycle.

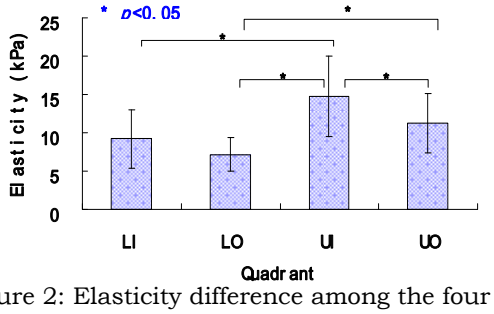

Figure 2: Elasticity difference among the four quadrants.

Notes: L–Left, R–Right, LI–Lower Inner, LO–Lower Outer, UI–Upper Inner, UO–Upper Outer.

083 **SHEAR MODULUS IMAGING OF LIVER USING SPATIALLY MODULATED ULTRASOUND RADIATION FORCE.**

Stephen A. McAleavey[1], Etana Elegbe[1], Manoj Menon[1].*
[1]University of Rochester, 309 Goergen BME/Optics Bldg, Rochester, NY, USA.

Background: Spatially Modulated Ultrasound Radiation Force (SMURF [1]) is a method for shear modulus estimation using ultrasound tracking of shear waves induced by acoustic radiation force [2]. In this method, an acoustic radiation force sequence with multiple, well–defined spatial intensity peaks is used to generate a shear wave of a designed wavelength. The frequency of this wave, tracked along a single A–line, is then used to estimate the shear modulus of the tissue.

Aims: The goal of this study is to demonstrate the capacity of SMURF imaging to generate quantitative shear modulus images in liver tissue.

Methods: All imaging was performed with a Siemens Antares scanner and VF7–3 linear array transducer. SMURF ensembles collect a reference echo, apply a push beam sequences, followed by tracking of the induced shear wave at the same A–line as the reference echo. The push pulse sequence consists of two pushing pulses transmitted in rapid succession along paths adjacent to the tracking beam. The focus of each push beam is at the same depth but translated laterally from each other by a distance ΔP (2.5mm). Tissue motion is then tracked along the same scan line as the reference echo. The period, *T,* of the shear wave motion, tracked by cross–correlation processing of echo signals, is then used to estimate modulus, *G*, with the relation, $G=\rho(\Delta P/T)^2$, where ρ of $10^3 kg/m^3$ is assumed. Tracking pulses were standard 4.2MHz B–mode-style pulses, while pushing pulses for generating displacements were 200cycle, 4.2MHz tone bursts.

Porcine livers, obtained fresh at slaughter, were kept immersed in 0.9% saline solution and scanned at room temperature. Glutaraldehyde was used to create a stiff lesion to demonstrate the ability to track lesion growth through time. In addition, reference samples of Zerdine (CIRS Inc.) tissue–mimicking material of known modulus were scanned to validate the technique.

Results: Modulus images show parenchyma with a shear modulus of ~3kPa, while glutaraldehyde–induced lesions exhibited shear modulus in excess of 10kPa. Diffusion of glutaraldehyde through the liver is visible in the time–sequence of modulus images obtained.

Conclusions: SMURF generated images of tissue shear modulus exhibit relatively low noise and good resolution, approximately equal to the push beam spacing. Good agreement with expected modulus of healthy liver is obtained, and agreement within 8% in the Zerdine samples is found.

Acknowledgements: This work was supported by NIH/NIBIB grants R21 EB008724 and R01 EB008368 and by the Stanford Center for Longevity. In–kind support was provided by Siemens Medical Solutions, USA, Ultrasound Group.

References:

[1] Stephen A. McAleavey, Manoj Menon and Jarrod Orszulak, "Shear–modulus estimation by application of spatially modulated impulsive acoustic radiation force." Ultrasonic Imaging, 29:87–104, April 2007.
[2] Armen P. Sarvazyan, Oleg V. Rudenko, et al., "Shear wave elasticity imaging: a new ultrasonic technology of medical diagnostics", Ultrasound in Medicine and Biology, 24(9):1419–1435, November 1998.

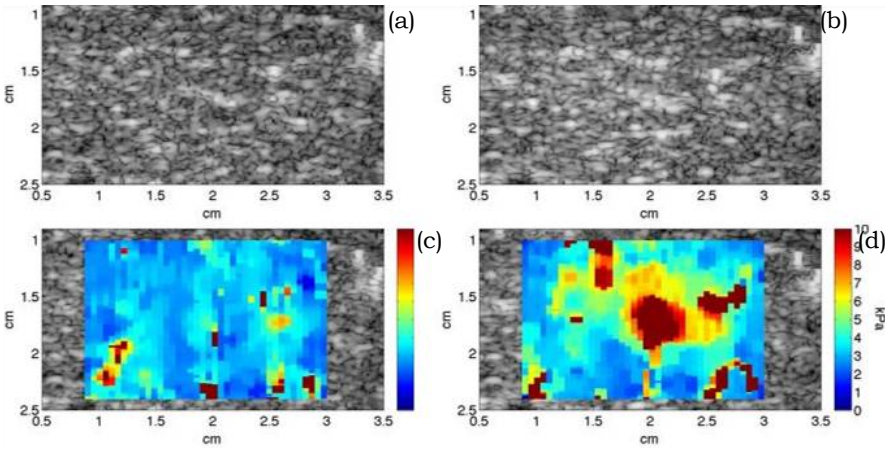

Figure 1: Shear modulus and matched B–scan images of *ex–vivo* porcine liver specimen before (a, c) and four minutes after (b, d) the injection of 0.5ml of 10% glutaraldehyde solution.

* *indicates Presenter*

072 **ON THE FEASIBILITY OF LONGITUDINAL WAVE VISCOELASTICITY IMAGING.**

H. Eskandari[1], A. Baghani[1], S. E. Salcudean[1], R. Rohling[1].*
[1]University of British Columbia, 2332 Main Mall, Vancouver, BC, CANADA.

Background: A mechanical wave in a viscoelastic medium can be decomposed into a shear and a longitudinal component. For the case of nearly incompressible materials, it is often assumed that the longitudinal component travels at a speed much faster than that of the shear component; thus, pulse–echo ultrasound should not be able to track tissue deformations due to a longitudinal excitation. That is why shear waves have received significantly more attention than longitudinal waves in the field of tissue characterization. Although it is generally assumed that any low speed wave that is tractable by ultrasound should be primarily a shear wave, we have previously used ultrasound to track the motion of the medium induced by longitudinal waves [1,2].

Theory: It can be shown that the propagation speed of longitudinal waves is highly dependent on the boundary conditions [3]. Depending on the geometry and the applied boundary conditions, this speed may be as low as the shear wave speed or as high as the acoustic wave speed in the medium. For example, for a nearly incompressible material, a compressive indentation with a point source exciter produces a longitudinal wave that travels at a speed of $\sqrt{\mu/\rho}$, where μ is the shear modulus and ρ is the density. If a finite block of material is allowed to bulge laterally while compressed axially with a plate, the longitudinal wave speed is $\sqrt{E/\rho}$, where E is the Young's modulus. In the same setting, if the volume is preserved and bulging is not permitted, the speed is approximately $\sqrt{(\lambda+2\mu)/\rho}$, where λ is a Lamé constant.

Results: Harmonic and transient 3D FEM simulations were performed for a viscoelastic medium under different boundary conditions. Based on the simulations, first a primary wave (p–wave) is generated in the medium which travels at a high speed. After the p–wave reaches the boundaries and is reflected back, a low–speed longitudinal wave will start to propagate at a low speed which is determined by the boundary conditions (Figure 1). The effect of viscosity on the wave speed, attenuation and resonance frequency was seen to be negligible at frequencies close to the resonance. Using different exciters, the speed of longitudinal wave was measured in tissue–mimicking phantoms using conventional ultrasound motion tracking. The analytical derivations and simulations were validated with the experimental data.

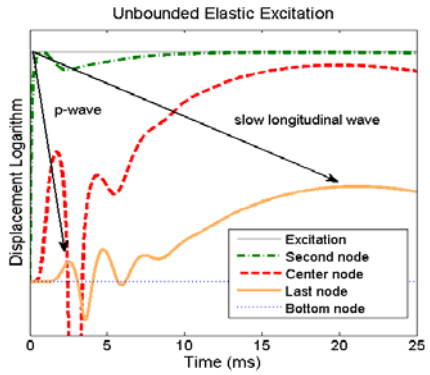

Figure 1: Displacements resulting from a flat step excitation applied from the top to a simulated phantom with E=10kPa and ν=0.495. The phantom was 40mm axially and allowed to bulge laterally while being bounded from the bottom. A fast p–wave propagates first at a speed of 18.2m/s. A second wave starts to travel afterwards at a speed of 2.9m/s. Both speeds confirm with the theoretical values. In this test, the resonance frequency of the phantom is 36Hz. After a step displacement is applied, the 36Hz component of the excitation is attenuated less than other frequencies inside the phantom; therefore the phantom will resonate at this frequency. The arrows show the propagation of the fast and slow longitudinal waves. Note the logarithmic scale of the y–axis.

Conclusion: Depending on boundary conditions, and especially when the total volume is unconstrained, longitudinal waves can be generated in a medium that travel at much lower speed than conventional ultrasound imaging pulses. Thus, the measurement of longitudinal waves traveling in the axial direction of an ultrasound transducer may also be used to measure viscoelastic properties of soft tissue phantoms.

Acknowledgements: This research is supported by NSERC.

References:

[1] H. Eskandari, S. E. Salcudean and R. Rohling, "Viscoelastic Parameter Estimation Based on Spectral Analysis", IEEE Trans. Ultras., Ferr. Freq. Cont., 55 (7), pp. 1611–1625, July 2008.
[2] A. Baghani, H. Eskandari, S. E. Salcudean and R. Rohling, "Measurement of Viscoelastic Properties of Tissue Mimicking Material Using Longitudinal Wave Excitation", IEEE Trans. Ultras., Ferr. Freq. Cont., 56 (7), 2009.
[3] H. Eskandari, A. Baghani, S. E. Salcudean and R. Rohling, "The influence of the Boundary Conditions on Longitudinal Wave Propagation in a Viscoelastic Medium", Phys. Med. Bio., 54, pp. 3997–4017, 2009.

067 **ON THE IMAGING OF SLIP BOUNDARIES USING 3D ELASTOGRAPHY.**

L Garcia[1], C Uff[1], J Fromageau[1], J Bamber[1].*
[1]Institute of Cancer Research, Sutton, Surrey, England, UK.

Background: A method of extracting the location of slip boundaries from elastographic data was proposed in the form of slip elastography [1], which seeks to differentiate between non–slip and slip shear strains in tissue and so locate and characterize slip boundaries. It is hypothesized that 3D elastography [2], may aid this assessment through reduction in image noise due to out–of–plane displacements and volumetric visualization.

Aims: To study the appearance of a tumor's slip boundary in elastographic displacement and strain data via experiments conducted in 3D finite element simulation in comparison with experimental 3D ultrasound data acquired from an approximately equivalent phantom, such that, firstly, we may have confidence in our simulations and, secondly, find additional parameters which may be used as indicators of slip.

Methods: COMSOL Multiphysics v3.5a (COMSOL, USA) was used to generate a 3D model of a sphere in a cube intended to approximate a stiff tumor surrounded by healthy tissue. The Young's modulus contrast was 4, and the tumor was made to adhere or to slip (no boundary friction) against its surroundings. A quasi–static axial compression of 1% the model height was applied at the upper model surface, and the resulting displacements and strains predicted. Gelatin phantoms (of equal dimensions to the model) were manufactured both with an adhered inclusion and with an inclusion that could slip freely against its surroundings through the injection of water onto the inclusion surface and compressed (as above) whilst its displacement was monitored with a 3D ultrasound probe utilizing 3D elastography software Stradwin 3.6 (University of Cambridge, UK).

Results: FEM simulation results are presented in Figure 1. Experimental data is displayed in Figure 2.

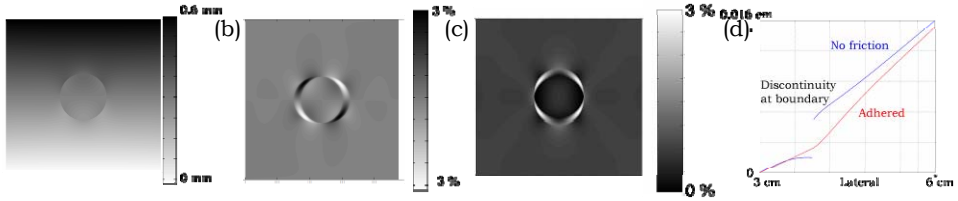

Figure 1: Simulated (a) axial displacement, (b) axial shear strain and (c) axial strain. In (d), a lateral cross section of elevational displacement from the model centre to its edge is displayed for a mobile (blue) and adhered (red) tumor.

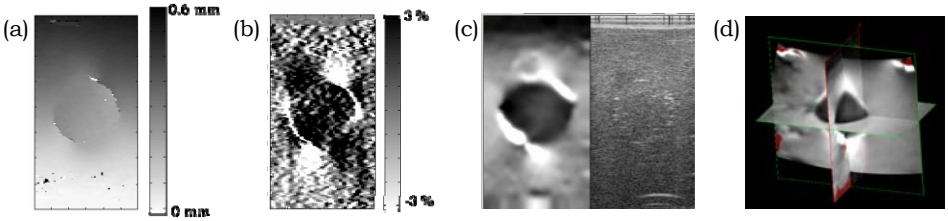

Figure 2: Experimental results showing (a) axial displacement, (b) axial shear strain, (c) axial strain and accompanying B–mode and (d) 3D view of data.

Conclusions: There is good agreement between the simulated and experimental axial displacement data (Figures 1 & 2(a)). Both show discontinuity in data at the tumor slip boundary. A region of high axial strain surrounding the tumor (Figures 1 & 2(c)) is a result of this sharp spatial gradient in axial displacement. Hence, the presence of such high axial strain, correctly interpreted with reference to displacement data, could be a potential indicator of slip in conventional axial strain imaging. In this way, 3D visualization, as in Figure 2(d), could help identify regions of tumor mobility over the entire tumor surface. Figure 1(d), a cross section plot through elevational displacement in the FE model shows that elevational displacement is slightly greater in the mobile tumor. 3D elastography may improve image quality for mobile tumor cases due to its ability to monitor out–of–plane displacements. Whilst axial shear strain images, Figure 1 and 2 (b), show a positive and negative strain 'quadrant' feature; the presence of noise and the strain estimator window size in the experimental data are the main sources of their difference. Further work is required to implement slip indication parameters into a reliable mobility imaging method.

Acknowledgements: This work was supported by the Engineering and Physical Sciences Research Council, UK.

References:

[1] Konofagou E, Harrigan T, Ophir J. Shear strain estimation and lesion mobility assessment in elastography. Ultrasonics., Vol. 38, pp. 400–404, 2000.
[2] Treece G, Lindop J, et al. Freehand ultrasound elastography with a 3–D probe. UMB 34:463–474, 2008.

* *indicates Presenter*

045 **AXIAL–SHEAR STRAIN DISTRIBUTIONS IN AN ELLIPTICAL INCLUSION MODEL (PART I): A SIMULATION STUDY.**

B Galaz[1], A Thitai Kumar[1] and J Ophir[1].*
[1]The University of Texas Health Science Center Houston, Houston, TX, USA.

Background: Axial–shear strain elastography (ASSE) was described recently as a method to visualize the state of bonding at an inclusion boundary [1]. Further, it was demonstrated that it may be feasible to use metrics from ASSE to classify breast tumors into benign or malignant [1]. In the prior studies, the shape of the tumors was assumed to be circular in a plane strain model. However, it is known that benign tumors tend to be more elliptical than perfectly circular [2]. Therefore, it may be important to understand the influence of shape of the inclusion on the axial–shear strain distribution. Furthermore, the orientation of the elliptical inclusion with respect to the axis of compression may be an important factor that influences the axial–shear strain distribution.

Methods: A 2D model containing an elliptical inclusion, either firmly–bonded or loosely–bonded to the background, was used for this study. At each of the two bonding conditions, the effect of the following parameters on axial–shear strain distribution was studied: 1) Orientation of inclusion with respect to the axis of compression, and 2) Eccentricity. The loosely–bonded inclusion was modeled by assigning a coefficient of friction to the contact elements in the finite element (FE) software ANSYS®. The inclusion was twice as stiff as the background, and the applied axial compression was 1%. The nodal displacements from the FE model were used to obtain the post–compression locations of acoustic point scatterers. RF–data were obtained by simulating a linear ultrasound transducer with a 10MHz center frequency, 50% fractional bandwidth and a constant -6dB beamwidth of 1mm. The axial–shear strain was estimated as the gradient of the axial displacements in the lateral direction. A threshold of 25% of applied axial strain was used to segment the area of axial–shear strain distribution. This area was normalized to the inclusion area, as was done for the circular inclusion model [1]. This normalized feature was used to study the effect of the parameters listed above.

Results: Results indicate that the axial–shear strain distribution for firmly–bonded elliptical inclusion was very similar to that of firmly–bonded circular case, i.e., the axial–shear strain is distributed only in regions that are outside the inclusion (see Figure1). However, axial–shear strain distribution for a loosely–bonded elliptical inclusion was similar to its circular counterpart only when the inclusion is oriented normally to the axis of compression (Figure 2a and b). When the long axis of the inclusion is oriented non–normally to the axis of compression, the axial–shear strain fills in the interior of the inclusion (Figure 2c) even at small angles (e.g. ~5°). It was noted that this axial–shear strain fill–in effect was present even in the absence of any modulus contrast.

Conclusions: This simulation study suggests that the presence of the axial–shear strain distribution inside an inclusion may be unique to elliptical or elongated inclusions that are loosely–bonded to the host material and which are non–normally orientated to the axis of compression. Since benign breast tumors tend to be elliptical and loosely bonded, we may expect axial–shear strain to fill–in the interior of such a tumor depending on its orientation. By contrast, the interior of malignant breast tumors is expected to be devoid of axial–shear strain. Phantom and *in–vivo* demonstrations are shown in the companion Part II.

Acknowledgements: This work was supported in part by NIH grant R21CA135580–01 and by the John S. Dunn Foundation.

References:

[1] Thitaikumar A, Krouskop TA, Garra BS, and Ophir J, Visualization of bonding at an inclusion boundary using axial–shear strain elastography: a feasibility study, Physics in Medicine and Biology 52, 2615–33, 2007.
[2] Stavros AT, Thickman D, Rapp CL, et al., Solid breast nodules: use of sonography to distinguish between benign and malignant lesions, Radiology 196, 123–34, 1995.

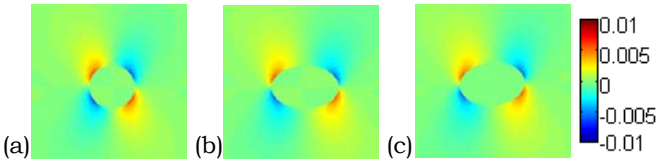

Figure 1: Axial–shear strain elastogram of a firmly–bonded stiff inclusion is shown for (a) circular (b) elliptical at orthogonal orientation and (c) elliptical with 5° orientation to axis of compression.

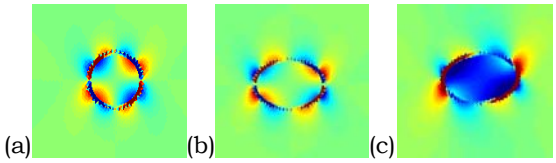

Figure 2: Axial–shear strain elastogram of a loosely–bonded stiff inclusion is shown for (a) circular; (b) elliptical at orthogonal orientation; and (c) elliptical with 5° orientation to axis of compression.

046 **AXIAL–SHEAR STRAIN DISTRIBUTIONS IN AN ELLIPTICAL INCLUSION MODEL (PART II): EXPERIMENTAL VALIDATION AND *IN VIVO* EXAMPLES WITH IMPLICATIONS TO BREAST TUMOR CLASSIFICATION.**

A Thitai Kumar[1], B Galaz[1] and J Ophir[1].*
[1]The University of Texas Health Science Center Houston, Houston, TX, USA.

Background: In the companion Part I presentation [1], we reported on the axial–shear strain fill–in of the interior of loosely–bonded stiff elliptical inclusions in a soft background at non–normal orientations. In this presentation, we report on the experimental validation of the simulation studies using tissue–mimicking phantoms. Further, we show a few confirmatory examples of the existence of this phenomenon in benign vs. malignant breast lesions *in vivo*.

Methods: Experiments performed on gelatin–based phantoms with embedded cylindrical ellipsoidal/oval–shaped inclusions were used to validate the simulation study reported in Part I. The inclusions were either firmly–bonded or loosely–bonded to the background and were oriented at different angles. A stiffer inclusion was obtained by increasing the gelatin concentration in the inclusion relative to that of the background. The ultrasonic data were acquired using a Sonix 500RP ultrasound machine (Ultrasonix Medical Corporation, BC, Canada) with a linear array transducer operating at 10MHz center frequency. A compression plate was attached to the transducer that was attached to a digital motion controller for precise movement/compression. Pre– and post–compression RF data sets were acquired from each phantom at 10 different planes along the elevational direction. Each plane was separated by at least 3mm (~elevational beam width) to obtain independent frames for averaging. Further, we identified from our previous database of pathologically–confirmed *in vivo* breast tumor, those cases that were approximately elliptical and at a non–normal orientation. Since we reprocessed these data retrospectively, we had no control over the orientation angle between the axis of compression and major axis of the elliptical inclusion. However, we did find several cases of tumors that had shapes and orientations similar to our simulation model.

Results: We found that the phantom experiments corroborated the simulation results. The axial–shear strain due to firmly–bonded elliptical inclusions occurred only outside the inclusion, as predicted by the simulation (Figure 1a and b). More importantly, the phantom experiments confirmed that axial–shear strains filled–in the interior exclusively in loosely–bonded elliptical inclusions at non–normal orientations. The axial–shear strain distributions were very sensitive to even slight non–normal orientation of the inclusion (Figure 1c and d) with respect to the compression axis. The axial–shear strain elastograms obtained from the *in vivo* cases appeared to be in general agreement with our simulation and experimental results (Figure 2).

Conclusions: In summary, the experimental validation of the simulations shown in the companion Part I, and initial examples from *in vivo* data suggests that generating axial–shear strain elastograms at different orientations between the inclusion and axis of compression may have important implications. Specifically, axial–shear strain fill–in inside an elliptical inclusion may be a unique signature of loosely–bonded conditions at non–normal orientations of ellipsoidal or elongated inclusions. Thus, it may be used as a sign of benignity of benign breast lesions (e.g. fibroadenomas) that are known to be stiff, elongated and loosely bound to the host tissues.

Acknowledgements: This work was supported in part by NIH grant R21–CA135580–01 and by the John S. Dunn foundation. The *in-vivo* cases were reprocessed from original B–mode data collected by Brian Garra, MD at the University of Vermont, with funding from NIH Program Project P01–CA64597.

References:

[1] Galaz B, Thitai Kumar A and Ophir J, Axial–shear strain distributions in an elliptical inclusion model (part I): a simulation study, Proc. 8th Int. Conf. on the Ultrasonic Meas. and Imaging of Tis. Elast., p. 99, 2009.

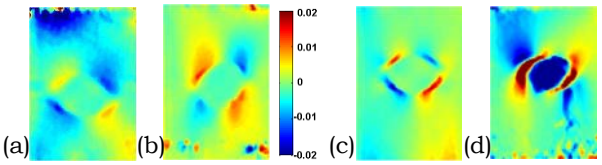

Figure 1: Axial–shear strain elastograms of a firmly–bonded inclusion (a, b) and a loosely–bonded inclusion (c, d) is shown at different orientation: normal (a, c) and non–normal (b, d) to axis of compression.

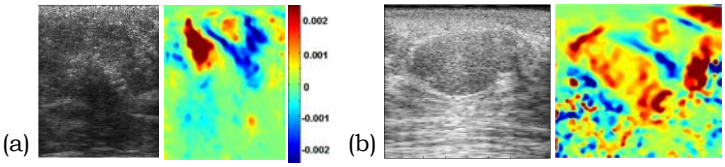

Figure 2: Sonogram (left) and axial–shear strain elastogram (right) from two pathologically confirmed breast lesion cases: (a) malignant, (b) benign. Observe that the fill–in is present only in the benign case. Note that the red (Figure 2b) or blue (Figure 1d) fill–ins and contrasting margins indicate the respective orientation of the lesion with respect to the compression axis.

* *indicates Presenter*

044 **DIFFERENTIATION OF BENIGN AND MALIGNANT BREAST LESIONS BY MECHANICAL IMAGING: CLINICAL RESULTS.**

Vladimir Egorov[1], Thomas Kearney[2], Stanley B Pollak[3], Chand Rohatgi[4], Noune Sarvazyan[1], Suren Airapetian[1], Stephanie Browning[5] and Armen Sarvazyan[1].*
[1]Artann Laboratories, 1459 Lower Ferry Rd., Trenton, NJ 08618, USA; [2]The Cancer Institute of New Jersey, New Brunswick, NJ 08901, USA; [3]Mercy Medical Center, Rockville Centre, NY 11510, USA; [4]The Breast Care Center & General Surgery Practice, Easton, PA 18045, USA; [5]New Jersey Institute of Technology, University Heights, Newark, NJ 07102, USA.

Background: Mechanical imaging [1] yields tissue elasticity map and provides quantitative characterization of a detected pathology. The changes in the surface stress patterns as a function of applied load provide information about the elastic composition and geometry of the underlying tissue structures.

Aim: The objective of this study is the clinical evaluation of breast mechanical imager for breast lesion characterization and differentiation between benign and malignant lesions.

Methods: The breast mechanical imager includes a probe with pressure sensor array, an electronic unit providing data acquisition from the pressure sensors and communication with a touch–screen laptop computer. We have developed an examination procedure and algorithms to provide assessment of breast lesion features such as hardness related parameters, mobility and shape [2]. A statistical Bayesian classifier was constructed to distinguish between benign and malignant lesions by utilizing all the listed features as the input.

Results: Clinical results for 179 cases, collected at four different clinical sites, have demonstrated that malignant breast lesions (histologically confirmed) had increased hardness and strain hardening as well as decreased mobility and longer boundary length in comparison with benign lesions. Statistical analysis of differentiation capability for 147 benign and 32 malignant lesions revealed an average sensitivity of 91.4% and specificity of 86.8% with a standard deviation of ±6.1% (Figure 1). The area under the receiver operating characteristic (ROC) curve characterizing benign and malignant lesion discrimination is 86.1% (Figure 2) with the confidence interval ranging from 80.3% to 90.9%, with a significance level of P = 0.0001 (area = 50%).

Conclusions: The multi–site clinical study demonstrated the capability of mechanical imaging for characterization and differentiation of benign and malignant breast lesions. We hypothesize that the breast mechanical imager has the potential to be used as a cost effective device for cancer diagnostics that could reduce the benign biopsy rate, serve as an adjunct to mammography and to be utilized as a screening device for breast cancer detection.

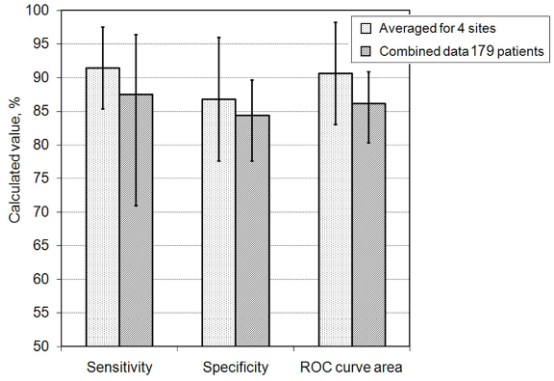

Figure 1: Performance of differentiation between benign and malignant lesions with the use of the Bayesian classifier.

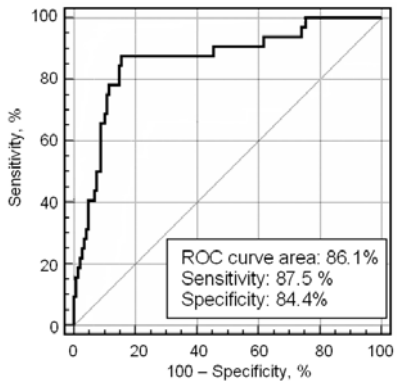

Figure 2: ROC curve for performance of discrimination between benign and malignant lesions for the Bayesian classifier output. The calculated features for all 179 patients were used as input data of the classifier.

Acknowledgements: This work is supported by NIH grant R44 CA091392.

References:

[1] A. Sarvazyan, Mechanical Imaging: A new technology for medical diagnostics, Int. J. Med. Inf., 49:195–216, 1998.
[2] V. Egorov, AP Sarvazyan, Mechanical Imaging of the Breast, IEEE Trans. Med Img, 27(9):1275–1287, 2008.

008 **VIBRO–ELASTOGRAPHY OF THE PROSTATE: METHOD EVALUATION.**

S. S. Mahdavi[1], M. Moradi[1], X. Wen[1], W. J. Morris[2], S. E. Salcudean[1].*

[1]Electrical and Computer Engineering Department, University of British Columbia, Vancouver, BC, CANADA; [2] Vancouver Cancer Centre, BC Cancer Agency, Vancouver, BC, CANADA.

Background: Accurate visualization and segmentation of the prostate is important in treatment planning of prostate cancer and can reduce possible side effects such as impotence, rectal bleeding and urinary incontinence. Ultrasound (US) is the primary imaging modality used for radiation treatment. While safe, and real–time, it does not provide reliable delineation of the prostate. In our prior work [1,2], we have introduced ultrasound vibro–elastography (VE) to generate viscoelastic models of the prostate region.

Aims: In this presentation, we evaluate VE–based segmentation of the prostate quantitatively. Prostate volumes created from VE images are compared to that of US, using MRI as the gold standard. The image contrast and quality of the prostate boundary is also evaluated using various measures.

Methods: Preceding low dose rate brachytherapy treatment, transverse MR and US B–mode images of the prostate were collected. A brachytherapy stepper was modified to enable motorized rotation and vibration of the US probe. Synchronized with the probe motion, RF data was acquired and processed to provide transverse strain images of the prostate. Data from seven patients has been used in this study.

Four measures have been used in this evaluation. To compare the 3D shape of the gland created by manual delineation in VE and US images with the corresponding MR images, the difference of the total volumes and the percentage volume error in the mid–gland is calculated. The latter is the non–overlapping volume between rigidly registered VE (US) and MR surfaces of the prostate, divided by the sum of the total volumes. The contrast–to–noise ratio (CNR) provides a measure of visibility of the prostate in the image. The target and background regions of interest are regions with the best visible contrast inside and outside the prostate respectively. The quality and visibility of the prostate boundary is also evaluated using a correlation–based index and a model–based statistical approach. In the correlation–based method, 'continuity' is the desired characteristic of an edge. For each small region on the edge, three edge profiles are extracted along rays extending from the prostate center. The cross–correlation between the center edge profile and the two neighboring profiles is averaged. In a continuous and strong edge, this average should have a shape similar to a Gaussian distribution with a large peak (P) and small standard deviation (σ). The value $K=P^2/\sigma$, calculated for each point on the edge, is the measure of edge continuity. Our statistical approach is based on the observation that the existence of a strong edge requires the edge profile to be non–stationary. Our analysis showed that edge profiles can be sufficiently described as first order autoregressive (AR(1)) processes. Therefore, the Augmented Dickey Fuller (ADF) unit root test is performed to determine the stationarity of the edge profiles.

Results: The VE–MRI and US–MRI percentage volume error in the mid–gland is similar (5%). However, the total volume difference is larger in the US–MRI case (9% vs. 5%) indicating better delineation of the base and apex in VE images. The average CNR in VE images is 10 times higher than that of B–mode. A higher K of VE is observed in the apex region, whereas a higher K, but also higher σ is seen in the base and mid region of B–mode images. This shows that the edge in VE images is more consistent whereas in B–mode, the boundary is very strong in some regions but not visible in others. Based on the ADF test, stationarity was rejected in 94% ($p<0.1$) of the profiles in VE images and only 19% of those extracted from B–mode images. This is an indication of high strength of edges in VE images.

Conclusions: Quantitative comparison of VE and B–mode ultrasound images shows that VE imaging is a promising modality for prostate delineation, with implications for treatment planning.

Acknowledgement: This work was supported by NIH grant R21 CA120232–01.

References:

[1] Salcudean, S.E., French, D., Bachmann, S., Zahiri–Azar, R., Wen, X., Morris, W.J.: Viscoelasticity modeling of the prostate region using vibro–elastography. MICCAI, 9(Pt 1), 389–396, 2006.

[2] Zahiri–Azar, R., Salcudean, S.E.: Motion estimation in ultrasound images using time domain cross–correlation with prior estimates. IEEE Trans Biomed Eng 53(10), 1990–2000, 2006.

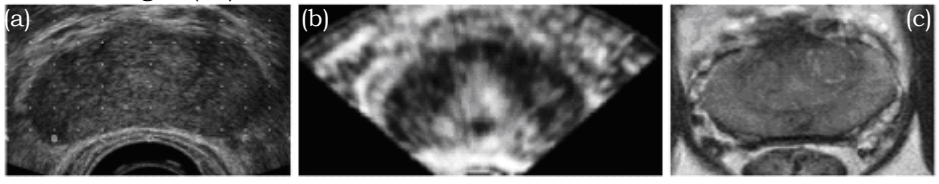

Figure 1: Transverse B–mode (a), VE (b) and MR (c) prostate images of a patient.

* *indicates Presenter*

034 **PERFORMANCE OF *EX VIVO* PROSTATE CANCER DETECTION USING 3D SONOELASTOGRAPHY.**

Benjamin Castañeda[1,2], Liwei An[2], Jorge Yao[3], Laurie Baxter[3], Leeann Kushner[3], Jean Joseph[3], Kenneth Hoyt[4], John Strang[3], Deborah J. Rubens[3], Kevin J. Parker[2].*

[1]Pontificia Universidad Católica del Perú, Av. Universitaria 1801, San Miguel, Lima, PERÚ; [2]University of Rochester, 206 Hopeman Building, Rochester, NY, USA; [3]University of Rochester Medical Center, 601 Elmwood Ave., Rochester, NY, USA; [4]University of Alabama at Birmingham, 817 Boshell Building, 1808 7th Avenue South, Birmingham, AL, USA.

Background: Prostate cancer is the most prevalent type of cancer in men, and it is second only to lung cancer in cause of death among adult males. Preliminary work in a limited number of *ex vivo* prostate glands [1] has shown that sonoelastography is a promising imaging technique for tumor detection.

Aims: This work evaluates the performance of three–dimensional sonoelastography for prostate cancer detection *ex vivo* in a larger number of cases.

Methods: Thirty prostate glands were examined *ex vivo*. The specimen was received after radical prostatectomy and embedded in a 10.5% gelatin mold. An external piston was used to vibrate the embedded gland at low frequencies (chords composed of 105, 140, 175 and 210 Hz). A GE Logiq 9 US scanner was used in conjunction with a positioning device to acquire B–mode and sonoelastographic volumes. The surface of the gland was segmented from the US images and the tumors from sonoelastographic images using a 3D segmentation algorithm [2]. After imaging, the gland was step–sectioned following a whole–mount histological procedure [1]. From these histological images, a volume was reconstructed and registered to the US and sonoelastographic volume using the surface of the gland as a marker. To assess detection performance, both 3D US and sonoelastographic findings were compared in size and position to 3D pathology.

Results: Sonoelastography found fifty–one deficits in the thirty *ex vivo* glands that were examined. Twenty–eight of the deficits corresponded to cancerous masses, eleven to BPH nodules and twelve were unexplained false positives. Seventeen tumors were missed entirely. The average diameter of the detected tumors was 8.0 ± 2.8 mm measured in the sonoelastographic images versus 8.5 ± 3.3 mm measured in the histological images. The minimum estimated diameter of a detected tumor was 2.51 mm. The undetected tumors measured in average 4.8 ± 2.1 mm in diameter. When tumors over 2.8 mm in diameter were considered for the analysis, Sonoelastography showed 75% accuracy, 63% sensitivity and 79% specificity. If only tumors larger than 4 mm in diameter (as measured on histology) were considered, the performance of sonoelastography improved up to 82% accuracy, 72% sensitivity and 85% specificity. Figure 1 shows a representative case in 3D.

Conclusions: Sonoelastography demonstrated an accuracy of over 80% for finding tumors larger than 4 mm in diameter and slightly underestimated their volumes. These results are an improvement over B-mode but not yet sufficient to replace biopsy.

Acknowledgements: This study was partly supported by NIH grants 5 RO1 AG016317 and 5 RO1 AG29804.

References:

[1] Taylor et al., "Prostate cancer: three–dimensional sonoelastography for in vitro detection", Radiology Dec; 237(3):981–5, 2005.

[2] Castañeda et al., "Semiautomatic measurement of thermally ablated lesions in sonoelastographic images", Journal of Ultrasound in Medicine, 26:S87–S88, 2007.

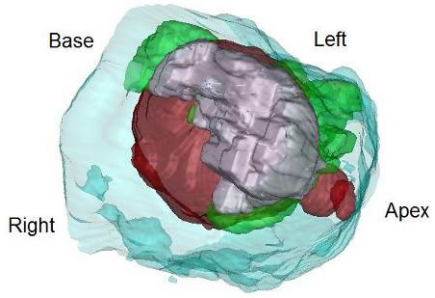

Figure 1: 3D comparison between sonoelastographic and histological findings. The surface of the gland is depicted in cyan, sonoelastographic findings in green, histological findings in red and the intersection between sonoelastography and histology is shown in white.

056 **VIBROGRAPHY AND FREE HAND ELASTOGRAPHY FOR RESECTION OF GLIOMAS AND OTHER BRAIN TUMORS.**

M Scholz, S Möller[1], J Thissen[1], C Löhnert[1], P Spangenberg[1], A Harders[1].*
[1]Neurosurgery Department, Ruhr–University Bochum, GERMANY.

Aims: The aim of this study was to determine whether elastography, an ultrasound–based real–time strain imaging method for registering the elastic properties of tissue, can be used in brain tumor surgery and especially for resection of gliomas.

Methods: From 2004 to 2008, elastography was first applied in 63 cases in our clinic in vibrography mode [1, 2]. The real–time vibrography system consisted of a conventional ultrasound system (Siemens Sonoline Omnia) with a custom–designed RF interface and a 6.5MHz endocavity curved array (Siemens 6.5EC10). The RF data were digitized using a 50MHz, 12–bit PCI analog/digital (A/D) converter for real–time or offline processing. Static compression was replaced by low-frequency axial vibration of the probe. A special applicator equipped with a stepping motor moved the ultrasonic probe and produced a low frequency mechanical vibration of ~ 5–10Hz with a vibration amplitude of 0.3mm and slight preliminary compression (total <1mm). The maximum application time was 60sec. A pneumatic holding device (Unitrac, Aesculap, Tuttlingen, Germany) was used.
Since April, 2008, elastography was used in 10 glioma patients in a free hand fashion during brain tumor surgery. A conventional ultrasound system (Hitachi, EUB 8500HV, Wiesbaden, Germany) with a custom designed radio frequency (rf) interface was used. Ultrasound–rf-data was acquired with an endocavity phased array (5–9MHz; Hitachi, EUP–V53W, Wiesbaden, Germany). The study was conducted with the approval of the Ethics Commission of the Ruhr–University Bochum (No.: 3139–08). Elastography was performed immediately after dura opening (Figure 1). MR–neuro–navigation was used to precisely determine the position of the ultrasound probe.

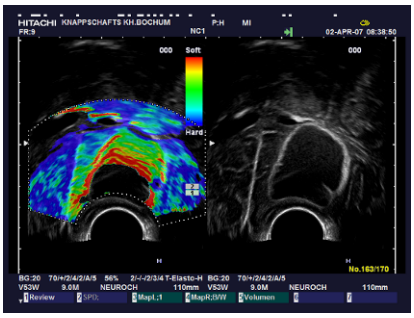

Figure 1: Free hand elastography in a cystic intracerebral metastasis.

After resection of the tumor, elastography and conventional sonography was again applied to localize residual tumor. This was done several times until the neurosurgeon stated that the resection was finished. Then the resection cave was additionally controlled with elastography by introducing the small probe. If residual tumor could be visualized, further resection was performed. Biopsies were done in areas of unknown histology. An early postoperative MRI was done.

Results: With the free hand method, detection of tumors was possible in all cases. Different relative tumor strains could be detected. Especially in huge gliomas, control of tumor resection is difficult because the neurosurgeon needs healthy brain tissue to compare to the tumor tissue. Two residual tumors (one oligoastrocytoma and one recurring glioblastoma) could not be seen with conventional ultrasound, but could be seen with elastography and could be successfully resected with microsurgery. Average sonographic application time was between 5–7.5 minutes.

Conclusion: These findings indicate that free hand elastography is feasible in surgery of gliomas for control of resection and may have numerous potential applications in neurosurgery if further improvements are performed. Application of this method can be taught and performed faster in comparison to concurring methods.

Acknowledgements: The authors would like to thank the staff of our operation room especially Eva Marie Fischer for her patience during application of the presented method. This project was a project of the Ruhr Center of Excellence for Medical Enineering (KMR) and was supported by the Federal Ministry of Education and Research, No. 13N8079.

References:

[1] Scholz M, Fricke B, Mönnings P, Brendel B, Schmieder K, Siebers S, Düring von M, Ermert H, Harders A, Vibrography: First experimental results in swine brains. Min Invas Neurosurg, 47: 1–7, 2004.
[2] Scholz M, Noack V, Pechlivanis I, Engelhardt M, Fricke B, Linstedt U, Brendel B, Schmieder K, Ermert H, Harders A, Vibrography during tumor neurosurgery, J Ultrasound Med, 24 (7): 985–92, 2005.

* *indicates Presenter*

059 **MONITORING DEMYELINATING PROCESSES BY HIGH RESOLUTION MAGNETIC RESONANCE ELASTOGRAPHY IN THE MOUSE BRAIN.**

E Diguet[1], B Larrat[1], R Sinkus[1], M Fink[1].*

[1]Institut Langevin, CNRS UMR 7587, Univ. Paris 7, ESPCI Paristech, Laboratoire Ondes et Acoustique, 10 rue Vauquelin, 75005 Paris, FRANCE.

Aims: Magnetic Resonance Elastography (MRE) is able to non–invasively map and quantify the viscoelastic properties of tissue *in vivo*. A change in elasticity often reflects a pathological change in tissue. The investigation of the effect of different brain pathological processes such as neurodegeneration, protein aggregation or demyelination on viscoelastic properties of cerebral tissue appears to be essential to evaluate the interest of this imaging technique to help diagnosis and/or to evaluate therapeutics. The aim of the present work was to measure the interest of MRE in the detection of demyelinating processes within the central nervous system. The effect of cuprizone exposition on viscoelastic properties of C57Bl/6 mouse corpus callosum was studied. High–field MRI measurements at 7T were made and animals were followed longitudinally.

Methods: Waves were transmitted into the mouse brain with a mechanical transducer consisting of a coil driven by a programmable pulse generator. A sinusoidal excitation at 1000Hz was used to optimize the wavelength within the brain. Wave propagation into the brain was recorded with a phase-locked spin-echo sequence on a 7T animal MRI scanner. Elasticity maps were calculated using a home-made 3D local inversion algorithm. A total of 20 brain sections of 300µm slice thickness and 300µm isotropic in-plane resolution were acquired. In addition, high-resolution T2-weighted images were acquired with identical slice positioning but increased in-plane resolution (150µm). Eight-week-old male C57BL/6 mice were placed on diet of 0.2% cuprizone thoroughly mixed into milled chow. Mice were maintained on the cuprizone diet for 12 weeks (n=6). Brains were then perfusion fixed for histological analysis. A control group consisted of 8-week-old male C57BL/6 mice (n=6) that were not fed cuprizone.

Results: High resolution T2 images and MRE data were obtained after 0, 3, 6, 9 and 12 weeks of demyelinating diet. Mean elasticity and viscosity were calculated over 6 adjacent brain sections where the corpus callosum was clearly visible on high resolution anatomical images. Data reproducibility was tested on a group of 5 C57Bl/6 mice each one scanned 3 times over 3 weeks. The viscoelastic properties of their corpus callosum were measured: <Gd> = 7.36±0.5kPa (7%); <Gl> = 3.33±0.8kPa (25%), with $G^*=Gd+i^*Gl$, the complex shear modulus. The elasticity was found to decrease with time in the corpus callosum of C57Bl/6 mice treated with cuprizone (Figure 1B). The control group did not present significant changes (Figure 1A). In the thalamus area, the elasticity remained constant for both groups suggesting that elasticity changes could be linked to changes in myelin concentration. Correlation with histology is currently ongoing (Figure 1C and D).

Conclusions: The elasticity of the brain of C57Bl/6 mice was reproducibly measured (only 7% variance). The well–established cuprizone–challenged mouse model was used for a longitudinal MR elastography study. The decrease of myelin content in white matter structures seems to quantitatively change the viscoelastic parameters as measured via MRE. A methodology based on mechanical measurements of brain structures such as MRE might open new possibilities for the early detection and the management of central demyelinating disorders such as multiple sclerosis or Alzheimer's disease.

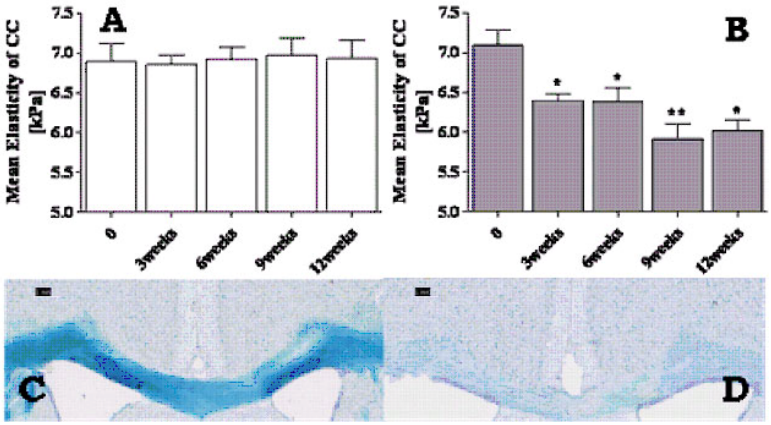

Figure 1: Time evolution of the mean elasticity (* p<0.05, ** p<0.005) in the corpus callosum of control mice (A and C) and cuprizone treated mice (B and D). Demyelination of the corpus callosum is visible on axial brain sections stained with Luxol Fast Blue (C and D).

102 **ARFI MEASUREMENTS ON THE HUMAN UTERINE CERVIX USING A NOVEL INTRACAVITARY TRANSDUCER.**

H Feltovich[1], L Reusch[1], JJ Dahl[2], ML Palmeri[2], JM Harter[1], M Kliewer[1], TJ Hall[1].*
[1]University of Wisconsin–Madison, Madison, WI, USA; [2]Duke University, Durham NC, USA.

Background: Understanding uterine cervical microstructure is critical to understanding dysfunction that leads to preterm delivery. A long, slow process of cervical softening associated with collagen fibril reorganization occurs prior to delivery (preterm or term). Acoustic Radiation Force Impulse (ARFI) imaging techniques are a promising approach to evaluation of cervical microstructure. Using three–dimensional finite element method models of tissue heating and dynamic tissue displacement in response to acoustic radiation force excitation, we have previously performed mechanical simulations of peak shear wave displacement. We found it possible to achieve adequate displacement magnitudes at the excitation focus without exceeding the FDA heating threshold of 1ºC for fetal ultrasound imaging. Also, the simulated dynamic displacement fields demonstrated that shear wave propagation over 8mm with adequate displacement SNR is possible to characterize cervical compliance during pregnancy.

Aims: To determine whether we can apply our modeled ARFI imaging techniques to human tissue and to compare performance between a 64–element and 128–element version of the prototype transducer.

Methods: Experiments were performed using the Siemens Sonoline Antares imaging system and either the 64–element (6.4mm aperture) or 128–element (13mm aperture) version of the prototype intracavity transducer operating as a linear array. Initial experiments involved a phantom with acoustic attenuation and elastic modulus that mimics the normal nonpregnant cervix but has randomly distributed spherical scatterers. Current work involves hysterectomy specimens of 'normal' cervix (expected to contain dense, aligned, cross–linked collagen fibers) where we sample spatially from the lower uterine segment to the external os.

Results: The 64–element prototype transducer produced displacements as large as 35microns in the cervix–mimicking phantom. These displacements are well in excess of that needed to produce robust shear sound speed estimates. Smaller displacements were expected in the aligned and cross–linked microstructure of the cervix. However, the 128–element prototype transducers produced displacements in hysterectomy specimens as large as 40–50microns in the lower uterine segment (the stiffest part of the normal cervix).

Conclusions: These data confirm that the displacement estimate simulations reported last year provided accurate performance expectations for estimating shear wave speed in the human cervix with these novel prototype transducers. Characterization of the biological variability in cervix shear sound speeds continues and will be reported. Current results suggest that the prototype transducers generate adequate displacement SNR to characterize cervical compliance during pregnancy.

Acknowledgements: We are grateful to Siemens Medical Solutions Ultrasound Division and Siemens Corporate Research for their technical support and equipment loans in this support of this effort.

* *indicates Presenter*

055 **VALIDATION OF MAGNETIC RESONANCE ELASTOGRAPHY WITH DIRECT MECHANICAL MEASUREMENT.**

Patricia Debergue[1], Peter Latta[2], Valérie Pazos[1], Christopher Bowman[2].*
[1]Industrial Materials Institute, National Research Council of Canada, Boucherville, Québec, J4B 6Y4, CANADA; [2]Institute for Biodiagnostics, National Research Council of Canada, Winnipeg, Manitoba, R3B 1Y6, CANADA.

Background: Palpation has long been used in clinical practice for diagnosing pathologies based on changes in tissue stiffness. However, some organs, like the brain, are not accessible to the palpating hand. Furthermore, mechanical properties of tumours are patient–specific, depending on their type, size and stage. Magnetic Resonance Elastography (MRE), a non–invasive MR–based approach, is very well–suited to obtain patient–specific biomechanical properties of tumour tissue. It can provide relevant pre–operative information on the consistency of brain tumour and surrounding healthy tissue. Correlations between direct mechanical measurements and MRE are necessary to quantitatively evaluate the MRE–based results.

Aims: This work aims to validate MRE–based results against direct mechanical measurements obtained over an overlapping frequency range using Poly (vinyl alcohol) cryogel (PVA–C) tissue–mimicking gel phantoms.

Methods: In this study, dynamic elastography results are compared with rotational rheometry and dynamic compression measurements obtained on different samples of the PVA–C gel phantom. The phantom used for the MRE experiments is a 10cm diameter x 10cm height cylinder containing inclusions of different sizes and stiffness values. It demonstrates tissue–mimicking mechanical and MR imaging properties, similar to brain tissues. The MRE tests were performed on a 3T Siemens TIM TRIO system. Shear waves were generated in the phantoms using a pneumonic actuator. The resulting displacement field was then measured using gradient echo (GE) and echo planar imaging (EPI) pulse sequences. In addition to the standard imaging gradients, the MRI sequence incorporated oscillating motion–sensitizing gradients that were synchronized with the acoustic shear wave. The resulting standing wave displacement field was then analyzed to compute the shear modulus of the phantom by using local frequency estimates of the displacement field [1]. The MRE experiments were conducted at frequencies ranging from 50–100Hz. Dynamic compression tests, as well as, oscillatory shear tests were conducted in an effort to overlap with the MRE frequency range.

Results: Figure 1 shows the propagating shear waves together with the MRE computed shear modulus (in kPa) in a mid–sagittal slice of the PVA–C phantom obtained at 100Hz. It clearly depicts the presence of the inclusion together with the difference in stiffness between the bulk of the phantom and the inclusion. Those MRE measurements obtained on phantoms with tumour–mimicking inclusions demonstrate that the calculated shear modulus for the bulk of the phantom is in good agreement with the directly measured values (~2kPa).

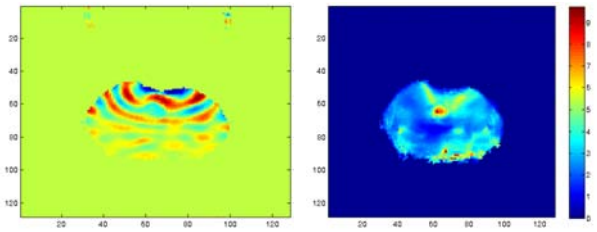

Figure 1: MRE wave propagation and computed shear modulus in kPa.

Conclusions: Direct mechanical measurement of shear modulus validates the estimates produced with MRE for the brain tissue-mimicking PVA–C gel phantoms. Work is proceeding to extend this validation methodology to more PVA–C phantoms as well as *in vivo* human brain tissues.

Acknowledgements: The authors would like to acknowledge Gord Campbell and Christian de Grandpré for the phantom fabrication.

References:

[1] Muthupillai R, Lomas DJ, Rossman PJ, Greenleaf JF, Manduca A, Ehman RL, Magnetic resonance elastography by direct visualization of propagating acoustic strain waves, Science, 269:1854–1857, 1995.

068 **DEMONSTRATING MAGNETIC OPTICAL COHERENCE ELASTOGRAPHY (M–OCE).**

A Grimwood[1], L Garcia[2], J Bamber[2], Q Pankhurst[1], J Holmes[3].*
[1]Davy–Faraday Research Laboratories, Royal Institution of Great Britain, 21 Albermarle Street, London, England, UK; [2]Institute of Cancer Research, 15 Cotswold Road, Sutton, Surrey, England, UK; [3]Michelson Diagnostics Limited, 11A Grays Farm Production Village, Orpington, Kent, England, UK.

Background: Optical coherence tomography (OCT) is a micron resolution imaging modality with the ability to acquire noninvasive images in real time [1]. Previous research into optical coherence elastography (OCE) has been undertaken and shown clinical potential [2]. Whilst conventional elastography relies on controlled applied physical compression, we aim to develop a minimally invasive and non–contact method of tissue actuation we call magnetic optical coherence elastography (M–OCE). We propose that instead of applying pressure to the tissue surface, a magnetic metal implant <1mm in size embedded in the tissue can be actuated using an external magnetic field, thus producing the displacement necessary to generate useful strain contrast in regions of inhomogeneous Young's modulus distribution from within the tissue.

Aims: To assess the potential of producing internal tissue displacements through non–contact remote magnetic actuation through simple yet clinically relevant finite element models (FEM) with experimental verification in tissue-mimicking phantoms.

Methods: Commercial FEM software Comsol Multiphysics 3.4 (COMSOL, USA) was used to generate a cylindrical 3D FE model (radius 20mm; height 5.8mm; Young's modulus 20kPa) with a rigid spherical inclusion of diameter 0.79mm (whose mechanical properties mimicked that of a high strength alloyed steel ball bearing) embedded inside, such that the ball bearing's centre was 3mm from the lower surface of the model. Forces were applied to the ball bearing such that it moved axially away from the upper model surface, and the resulting displacements predicted. A room temperature vulcanizing (RTV) silicone rubber phantom containing a chrome steel ball bearing was constructed to the same specifications as above and was actuated using an external magnetic field from a Halbach array, generating the same forces on the ball bearing as in the simulation. The resulting phantom displacements were monitored using an OCT system (EX 1301, Michelson Diagnostics Ltd., UK) from pre– and post–applied force images through cross–correlation based 2D speckle tracking algorithms.

Results:

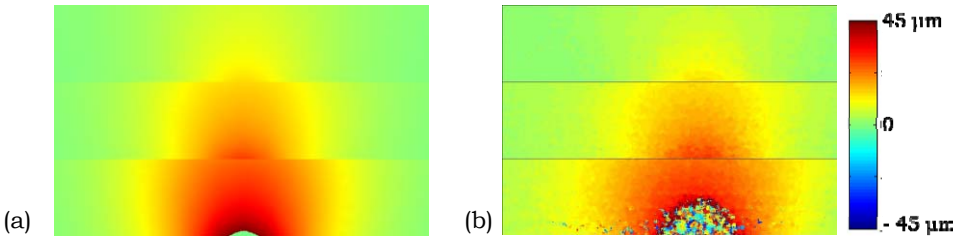

Figure 1: Axial displacements generated through (a) FE analysis and (b) experimental OCT data for applied forces of 2.3mN, 4.8mN and 7mN (upper, middle and lower images). Note that downward axial displacements are taken to be positive.

Conclusions: It has been possible to map the axial displacement field of a series of experimental OCT images when magnetically actuating a small metallic implant. The experimental results show good agreement with the simulation data, thus providing confidence in future FE analysis of the problem. This work has enabled the authors to demonstrate proof of principle for M–OCE, which will form the basis for further work into the quantification and extraction of the elastic behavior of tissue. In the future we hope that clinically useful mechanical properties of tissue on the micron scale may be determined using this non-contact modality.

Acknowledgements: This work was supported by the Engineering and Physical Sciences Research Council, UK.

References:

[1] Tomlins P.H., Wang R. K., Theory, developments and applications of optical coherence tomography, J. Phys. D: Appl. Phys. 38, 2519–2535, 2005.
[2] Rogowska J, Patel N.A, Fujimoto J. G., Brezinski M.E., Optical coherence tomographic elastography technique for measuring deformation and strain of atherosclerotic tissues, Heart 90(5), 556–562. 2004.

* *indicates Presenter*

070 **DYNAMIC VISCOELASTIC PROPERTIES OF SOFT TISSUES MEASURED BY HARMONIC MOTION IMAGING (HMI): PRELIMINARY RESULTS OBTAINED ON NORMAL AND CANCEROUS BREAST TISSUES.**

Jonathan Vappou[1], Caroline Maleke[1] and Elisa E. Konofagou[1].*
[1]Ultrasound and Elasticity Imaging Laboratory, Biomedical Engineering Department, Columbia University, New York, NY, USA.

Background: Harmonic Motion Imaging (HMI) is an acoustic radiation force–based method that was originally developed for both mechanical characterization and ablation of cancerous tissues [1]. An HMI–based technique has been proposed recently for measuring dynamic viscoelastic properties by using the local shear wave number, *k*, and the phase shift, Φ, between the oscillating radiation force and the measured shear strain [2]. This method has been validated through numerical simulations and comparison with mechanical testing [3].

Aims: This study aims at measuring dynamic viscoelastic properties of breast tissue *in vitro* using the aforementioned method. Preliminary results obtained on both normal and cancerous human breast tissues are presented.

Methods: Experiments were performed on two samples, (1) normal breast tissue and (2) invasive ductal carcinoma (IDC). Both samples were excised during breast surgery and were tested within one hour following the operation. The shear storage modulus G' and the shear loss modulus G" were measured versus the excitation frequency within the 10–80Hz frequency range.

Results: Figure 1 illustrates the frequency–dependent behavior of the shear storage modulus G' and of tan(Φ)=G"/G'. The IDC was found to be almost 2 orders of magnitude stiffer than normal tissue. A significant difference was also found in the dynamic behavior of tan(Φ), as the relative viscosity of healthy tissue was much higher than the one of IDC at a given frequency.

Conclusions: Feasibility of using HMI for quantitative measurement of frequency–dependent viscoelastic properties of soft tissues was demonstrated in this study. Preliminary results obtained on breast tissue suggest significant differences between healthy and cancerous tissues regarding viscoelastic values but also regarding the overall dynamic viscoelastic behavior. Ongoing work involves assessing reproducibility on a larger number of samples and on different types (e.g., fibroadenoma).

Acknowledgements: The authors would like to acknowledge the National Institutes of Health (NIH grant #1R21EB008521–01) for supporting this study.

References:

[1] Konofagou and Hynynen, Localized harmonic motion imaging: Theory, simulations and experiments, Ultrasound Med. Biol., 29: 1405–1413, 2003.
[2] Vappou, et al., Harmonic Motion Imaging (HMI) Compared to Rotational Rheometry for the Measurement of Soft Tissues Viscoelasticity, Proc. 7th International Conference on Tissue Elasticity Imaging, p 73, 2008.
[3] Vappou, et al., Quantitative viscoelastic parameters measured by harmonic motion imaging, Phys. Med. Biol., 54(11):3579–94, 2009.

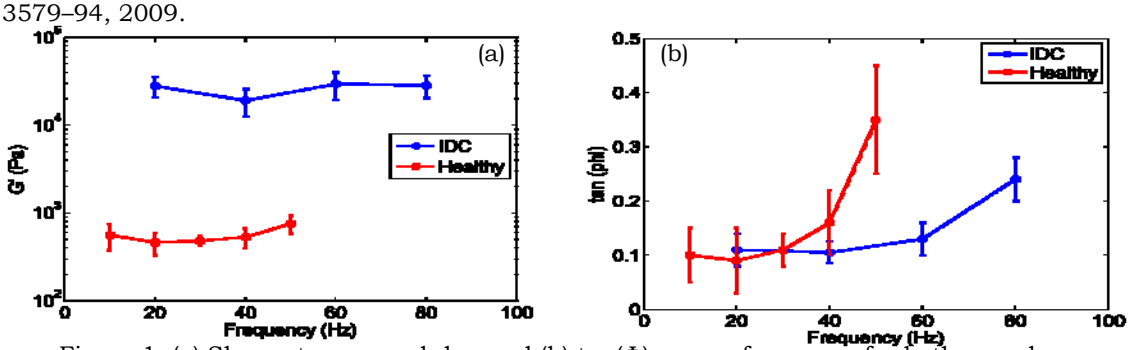

Figure 1: (a) Shear storage modulus and (b) tan(Φ) versus frequency for both samples.

073 **ITERAIVE RECONSTRUCTION OF TISSUE ELASTICITY AND VISCOSITY USING FINITE ELEMENTS.**

H Eskandari[1], I Bell[1], SE Salcudean[1], R Rohling[1].*
[1]University of British Columbia, Vancouver, BC, CANADA.

Background: Solving the inverse problem of calculating elasticity from displacement measurements, with the goal of tissue characterization, has been widely addressed in recent literature. In a finite element framework, a linear system of equations can be defined to relate nodal displacements, elasticity, viscosity and density parameters and the boundary conditions. This problem has been tackled in the quasi–static regime in several ways. If the problem is discretized and formulated such that Young's moduli are the unknowns, with known displacements and strains, a forward solution technique can be applied to estimate the parameters [1]. In another approach, the inverse problem of elasticity is solved by minimizing a functional which is often the quadratic norm of the difference between the measured displacements and the displacements resulting from an assumed distribution of elasticity [2].

Method: In this work, the inverse problem of elasticity and viscosity is solved using a dynamic finite element approach. A model is proposed that incorporates the Voigt model for the viscoelastic deformation of soft tissues in a dynamic finite element formulation. Using the Voigt's viscoelastic model for soft tissue, the relationship between the tensors of stress and strain–rate is integrated into an FEM discrete system to obtain the damping matrix for individual elements. The inverse problem is solved based on harmonic measurements of the axial displacements. The resulting complex–valued equations are separated into real and imaginary components to constitute a linear system of equations. The problem is then solved using an iterative Gauss–Newton approach. The algorithm is devised such that by knowing the parameters on the boundaries, their distribution can be estimated inside the medium, without needing to know the force on the boundaries or the lateral displacements inside the region of interest.

Results: The sensitivity of the solutions to noise, model and boundary conditions has been studied through numerical simulations. By comparing the results to traditional strain images, it has been shown that the artifacts can be reduced and accurate measurement of the parameters can be obtained. While a 3D model accounts for the deformations in all directions, to comply with conventional ultrasound imaging and phantom experiments, a 2D plane stress assumption was made. For a 20×20 mesh, the processing time of each iteration was 4.2s on a 2.33GHz Intel© Core–2 Quad processor. A gelatin–based tissue–mimicking phantom was made with a soft PVA sponge inclusion to act as both an elasticity and viscosity inclusion. The displacements resulting from a 10.7Hz external vibration were estimated. Based on rheometric measurements, the background gelatin had a Young's modulus and a viscosity of 15kPa and 30Pas respectively. Using these initial values for the entire medium, the inverse problem has been solved, and the parameters have been reconstructed (Figure 1). The average estimated elasticity and viscosity inside the inclusion were 85kPa and 176Pas respectively, while those parameters were 35kPa and 40Pas in the background. These results were in agreement with independent rheometry measurements.

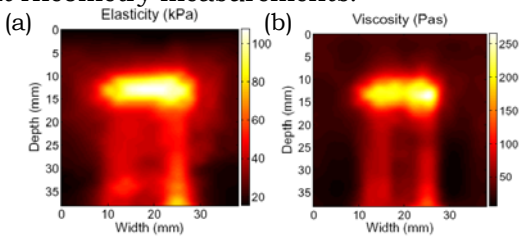

Figure 1: Young's modulus (a) and Viscosity (b) reconstruction of a gelatin based phantom with a PVA sponge inclusion. The location of the inclusion and the relative values of the parameters are consistent with the B–mode observations and the rheometry.

Conclusion: The feasibility of reconstructing the elasticity and viscosity in a non–homogeneous medium based on a finite elements analysis has been studied in this work. An accurate knowledge of the boundary parameters and the lateral forces or displacements at the boundaries would help to assure uniqueness and convergence and to obtain accurate parameter images. The proposed method has shown promise in reconstructing the 2D distribution of the viscosity and elasticity in simulations and experiments.

Acknowledgements: This research is supported by NSERC.

References:

[1] Y. Zhu, T. J. Hall, and J. Jiang, "A finite–element approach for young's modulus reconstruction," IEEE Transactions on Medical Imaging, vol. 22, no. 7, pp. 890–901, Sept. 2003.
[2] F. Kallel and M. Bertrand, "Tissue elasticity reconstruction using linear perturbation method," IEEE Transactions on Medical Imaging, vol. 15, no. 3, pp. 299–313, June 1996.

* *indicates Presenter*

018 **THE ROLE OF REAL–TIME ELASTOGRAPHY IN THE NON–INVASIVE ASSESSMENT OF FIBROSIS IN DIFFUSE HEPATOPATHIES.**

Dan Ionuț Gheonea[1], Adrian Săftoiu[1], Florin Gorunescu[2], Marina Gorunescu[3], Tudorel Ciurea[1]*
[1]Gastroenterology Department, [2]Biostatistics Department, University of Medicine and Pharmacy Craiova, Dolj, ROMÂNIA; [3]Biostatistics Department, University of Craiova, Craiova, ROMÂNIA.

Aim: Ultrasound elastography was recently reported to offer supplemental information that appears to yield a better characterization of liver tissue [1]. The principle of real–time elastography (RTE) is that tissue compression produces displacement within the tissue and that the strain is smaller in harder tissue as compared to softer tissue [2]. The aim of the study was to analyze whether computer–enhanced dynamic analysis of RTE movies is able to better characterize the degree of fibrosis in chronic hepatic diseases.

Methods: We included in this prospective study 97 consecutive patients examined in the Research Centre of Gastroenterology and Hepatology Craiova by RTE, with a Hitachi 8500 US system with an embedded SonoElastography module. Patients with alcoholic fatty liver disease (n=21), viral B, C or B+D hepatitis (n=26), cirrhosis (n=29) and healthy volunteers (n=21) were examined. RTE was performed through the right intercostal space, during breath holding at end–expiration phase (Figure 1). Two examinations consisting of three distinct ten second elastography movies were consecutively recorded by two different operators, blinded to each other and to the liver biopsy information. Each acquired elastography movie was subject to computer–enhanced dynamic analysis using a public domain Java–based image processing tool (ImageJ). The final diagnosis was based on the results of liver biopsy, with liver fibrosis quantified according to the Metavir scoring system.

Results: Due to the limitations of the method, we obtained high–quality elastography information in only 73.48% of the patients. The k–means clustering method was applied to assess the inter–observer diagnosis variability, showing good variability values in concordance with the experience in ultrasound examination of every observer. Cohen's kappa test indicated a moderate agreement between the study observers (kappa=0.4728). Furthermore, we compared the way the two observers have clustered the patients, using the test for comparing two proportions (t–value, two–sided test). Thus, we obtained that there is no statistical significant difference (p=0.54, 0.85, 0.81 and 0.78 respectively) between the two physicians, regardless of the patients' real status.

Conclusions: Real time elastography is a new and promising method for the characterization of liver fibrosis in chronic hepatic diseases, but it should be compared with other non–invasive markers, transient elastography and liver biopsy results in large multi–centric studies with improved methodology.

Acknowledgements: This presentation was partially supported through the research grant no.2076/2007 financed by the Romanian Ministry of Education and Research.

References:

[1] Friedrich–Rust M, Ong MF, Herrmann E, Dries V, Samaras P, Zeuzem S, Sarrazin C, Real–time elastography for noninvasive assessment of liver fibrosis in chronic viral hepatitis, AJR Am J Roentgenol., 188:758–764, 2007.
[2] Saftoiu A, Gheonea DI, Ciurea T, Hue histogram analysis of real–time elastography images for noninvasive assessment of liver fibrosis, AJR Am J Roentgenol., 189:W232–233, 2007.

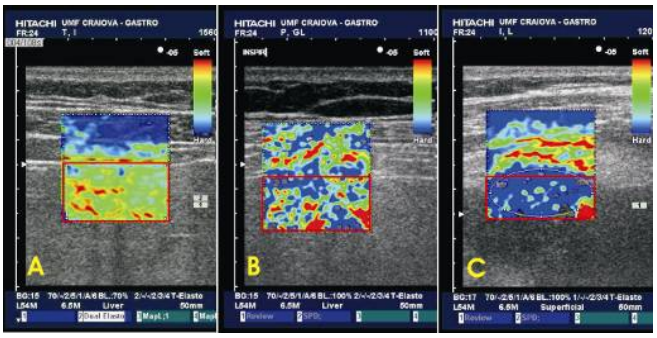

Figure 1: Comparative elastography aspects of (A) alcoholic fatty liver disease, (B) chronic viral hepatitis and (C) cirrhosis.

* *indicates Presenter*

024 **ULTRASOUND TRANSIENT ELASTOGRAPHY OF THE BRAIN: AN *IN VIVO* FEASABILITY STUDY IN SMALL ANIMALS.**

E Macé[1], I Cohen[2], JL Gennisson[1], R Miles[2], M Tanter[1], M Fink[1].*
[1]Institut Langevin - Laboratoire Ondes et Acoustique, ESPCI ParisTech, CNRS UMR 7587, INSERM, Université Paris VII, Paris, France ; [2]Cortex et Epilepsie, INSERM EMI 0224, CHU Pitié–Salpêtrière, Université Paris VI, Paris, FRANCE.

Background: Imaging damaged tissues in the brain *in vivo* is a major issue in neurology and neurosurgery. New imaging techniques could help improve clinical follow–up and diagnosis of neurodegenerative diseases. It would also be of great interest in the development of HIFU brain therapy that requires precise monitoring of necrosis during treatment.

Aims: Brain elasticity imaging is a promising approach, given that the mechanical properties of neural tissues are likely to be altered when damaged. In this work, the ability of Ultrasound Transient Elastography to quantitatively map brain elasticity is demonstrated *in vivo* on rats using the Supersonic Shear Imaging technique (SSI).

Methods: Experiments are performed on adult rats placed in a stereotaxic frame. A 15x25mm^2 cranial window is opened to expose the brain. A standard high frequency (15MHz) ultrasound linear probe is set in the coronal plane and controlled with a micromanipulator system. For coronal slices every 500µm, shear waves induced by radiation force are imaged at very high frame rate (10kHz) with an ultrafast ultrasound scanner. Ultrafast movies are then post–processed to reconstruct a 3D elasticity map of the brain. A high resolution ultrasonic scan of brain anatomical structures is also acquired and superposed with elasticity images. To estimate artifacts due to physiological motion such as pulsatility, 3D transient dynamics of brain vibrations are measured during a whole cardiac cycle using ultrafast imaging at a 400Hz. Electrocardiogram signals are recorded for all ultrasound sequences.

Results: The high resolution ultrasonic scan of the brain allows a clear identification of anatomical regions. The 3D map of the shear modulus shows a mean value of 3.2 ± 0.7kPa in the cortex and the thalamus and a higher value of 18.8 ± 7.0kPa in the corpus callosum. Mechanical waves induced by the ultrasonic radiation force exhibit higher frequencies (50–1000Hz) than pulsatile waves (5–15Hz). The measurement of motion during a whole cardiac cycle shows a pulsatile movement peaking approximately 60ms (30% of cycle) after systole, with a maximum amplitude of 5–30µm depending on regions where radiation force generates smaller displacements (1–5µm).

Conclusions: In this study, we proved the feasibility of elasticity imaging of the brain *in vivo* in rats. We observed a correlation between elasticity heterogeneities and anatomical structures. Furthermore, we showed that pulsatility induces important movements in the brain which are coherent with the localization of blood vessels. Small animals were chosen for the perspective offered by existing models of neurodegenerative diseases such as Alzheimer and Parkinson diseases. Next experiments will concentrate on applying this new technique in those models to quantify the effect of damaged tissues on elasticity. HIFU experiments coupled with elastography could also be easily set up in small animals to address the monitoring of necrosis. Concerning transition to clinical use, this technique could be evaluated intra–operatively in the context of surgery of brain lesions.

015 **INTRAVASCULAR ULTRASOUND PALPOGRAPHY AS AN IMAGING BIOMARKER IN CLINICAL TRIALS.**

Antonius FW van der Steen[1], Johannes A Schaar[1], Frits Mastik[1], Hector Garcia[1], Mike G Danilouchkine[1] and Patrick W Serruys[1].*
[1]Biomedical Engineering, Thorax Centre, Erasmus Medical Center, Ee23.02 P.O. Box 2040 3000 CA, Rotterdam, The NETHERLANDS.

Background: The composition and morphology of an atherosclerotic lesion are currently considered more important determinants of acute coronary ischemic syndromes that the degree of stenosis. When a lesion is unstable, it can rupture and cause an acute thrombotic reaction. An unstable plaque can be characterized by a lipid core that is covered by a thin fibrous cap, which has been locally weakened by inflammatory cells [1]. Cardiovascular drugs aim at lowering the risk for events by lowering the instability of lesions. Traditionally, efficacy of these drugs is tested in incidence trials, which take tens of thousands of patients and many years of follow up. Imaging biomarkers can lower the number of patients and follow up time dramatically. Intravascular Ultrasound Palpography is an intravascular ultrasound based technique that is capable of detecting unstable atherosclerotic lesion with a sensitivity and specificity of 90% [2].

Aims: This study aims to evaluate Intravascular Ultrasound Palpography as an imaging biomarker in clinical trials.

Methods: Intravascular Ultrasound Palpography is an intravascular ultrasound based technique that is capable of measuring the local strain in coronary and atherosclerotic plaques. This strain is induced by varying intraluminal pressure. By mapping the coronary tree, the condition of the vessels can be assessed by Palpography. Palpography has been applied in 2 different clinical trials: the integrated imaging and biomarker study (IBIS) [3] and the integrated imaging and biomarker study II (IBIS II) [4]. IBIS was an investigator driven study in which three different patient groups were recorded at intake and 6 months follow up. In IBIS II, the efficacy of Darapladip, an LpPLA2 inhibitor, to improve the condition of the vessel wall was studied; patients with standard of care were compared with patients that received Darapladip in addition to standard of care.

Results: IBIS showed that patients who were less stable had more unstable lesions as shown by Palpography. This confirmed earlier findings. Furthermore, it showed that patients who had suffered from an acute myocardial infarction had a dramatic improvement at 6 months follow up. This could be attributed to the fact that most of those patients did not use any medication before they had their infarction, but they were put on maximum medication when their intervention was started. IBIS II showed a significant improvement in the patients with unstable lesions and used Darapladip plus standard of care. The standard of care group, however, also showed a slight improvement. Therefore, the actual additional treatment effect of Darapladip had a positive trend but did not reach significance.

Conclusions: Palpography can show the condition of the vessel wall and is suited as an imaging biomarker in clinical trials.

Acknowledgements: This work is financially supported by the Dutch Technology Foundation, The Dutch Heart Foundation and research grants from Volcano Corporation and Glaxo Smith Kline. AFW van der Steen is the 2000 NWO PIONIER for Technical Sciences and the 2007 Simon Stevin Meester.

References:

[1] Schaar JA, van der Steen AFW, et al., Terminology for high–risk and vulnerable coronary artery plaques, Report of a meeting on the vulnerable plaque, June 17 and 18, 2003, Santorini, Greece, Eur Heart J. 25(12):1077–82, 2004.
[2] Schaar, J. A., de Korte, C.L., van der Steen, AFW, et. al., Characterizing vulnerable plaque features with intravascular elastography, Circulation, 108(21), 2636–2641, 2003.
[3] Van Mieghem CA, van der Steen AFW, et al., Noninvasive detection of subclinical coronary atherosclerosis coupled with assessment of changes in plaque characteristics using novel invasive imaging modalities: the Integrated Biomarker and Imaging Study (IBIS), J Am Coll Cardiol., 47(6):1134–42, 2006.
[4] Serruys PW, van der Steen AFW, et al., Effects of the direct lipoprotein–associated phospholipase A(2) inhibitor Darapladib on human coronary atherosclerotic plaque, Circulation, 118(11):1172–82, 2008.

090 **SONORHEOMETRY FOR CLINICAL ASSESSMENT OF HEMOSTASIS.**

William F. Walker[1,2,3], Xiefan Lin–Schmidt[1], F. Will Mauldin[1], Michael B. Lawrence[1,3] and Francesco Viola[1,3].*

[1]Biomedical Engineering Department, [2]Electrical and Computer Engineering Department, University of Virginia, Charlottesville, VA, USA; [3]HemoSonics, Charlottesville, VA, USA.

Background: Hemostasis is the physiological process by which blood clots form to stop bleeding. Uncontrolled hemostasis represents the leading cause of mortality in the developed world through conditions including heart attack, stroke and pulmonary embolism. During surgery and trauma hemostasis may be suppressed, enhanced or even alternate between the two, making proper diagnosis critical to guide patient care. Existing clinical tools are unable to provide rapid monitoring of hemostasis at the point of care and, therefore, cannot guide therapy in the most critical situations.

Aims: Our team is developing and evaluating a novel instrument to assess hemostasis at the point of care. The system performs an *in vitro* test on a small volume of blood. Our instrument will be placed at the patient's bedside to provide rapid quantitative information in a matter of minutes. The system is designed to be easy to use and provide results which are easy to interpret.

Methods: Our instrument for measuring hemostasis uses sonorheometry, an ultrasound radiation force based method, to measure the elasticity of a forming blood clot. Approximately 1ml of blood is added to kaolin (a clot inducer) in a disposable test chamber. Measurements of viscoelastic properties are performed every six seconds. The current prototype consists of a temperature control and acoustic coupling unit, two piston transducers, a custom printed circuit board and a laptop computer. Experiments are performed in real–time. The system utilizes advanced signal processing methods to filter out both electronic noise and echo decorrelation and a spline–based time delay estimator to estimate displacements of less than one micron.

Results: We show data indicating that our system can dynamically measure stiffnesses covering five orders of magnitude. We show characteristic time–stiffness curves from over 40 subjects, including both healthy subjects and patients undergoing cardiac surgery. These characteristic curves provide clear indication of a given patient's propensity to bleed or clot and the relative function of the hemostatic subsystems including platelets, coagulation factors and fibrinolytic proteins. In tests with healthy subjects, we show that the time to clot measured by our system has a coefficient of variation of less than 5% in repeated trials. Time to clot among healthy subjects varies by less then 10%. The functional effects of heparin (an anticoagulant), ReoPro (a platelet inhibitor) and urokinase (an thrombolytic) are clearly indicated in time–stiffness curves. Initial data from over 30 Cardiopulmonary Bypass patients suggests that sonorheometry can predict bleeding in this fragile clinical population.

Conclusions: Sonorheometry represents a valuable new tool for the clinical and laboratory assessment of hemostasis. Early laboratory and clinical data show that the instrument performs as well as or better than existing clinical laboratory tests.

Acknowledgements: This work was supported by NIH/NIBIB Grant R01EB005433, the Wallace Coulter Foundation for Translational Research, and the Investors of HemoSonics.

075 **TUMOUR SIZE MEASUREMENT OF BREAST CANCER USING ULTRASOUND ELASTOGRAPHY: A CLINICAL STUDY.**

Junbo Li[1], J. Alison Noble[1], Ying Chi[1], Ruth E. English[2], Rosie F. Adams[2], Vaishali Parulekar[2] and Jane E. Baldwin[2].*

[1]Institute of Biomedical Engineering, Engineering Science Department, University of Oxford, Oxford, England, UK; [2]Oxford Radcliffe Hospitals NHS Trust, Oxford, England, UK.

Background and Objective: Breast cancer is the most common cancer in women. Precise measurement of the size of an invasive breast cancer is critical for accurate diagnosis and effective treatment. Ultrasound elastography, as a novel imaging technique to characterize the mechanical parameters of soft tissues, can provide additional clinically relevant information and has been used successfully in clinic to detect and classify breast tumour [1–3].

Methods: We have developed an Assisted Freehand Ultrasound (AFUSON) system for breast ultrasound elasticity imaging [4], in which automated, measurable external compression has been applied to the breast by a compression plate to improve ultrasound data acquisition and reduce operational variability. This system consists of a real-time digital acquisition ultrasound engine (Analogic AN2300, MA, USA), support computer, ultrasound transducer (Type 8805, B–K Medical, Denmark), linear actuator and force probe (Mini 40, ATI Industrial Automation, NC, USA). Software was written in Matlab to interface with the hardware components, control the acquisition and provide a user–friendly GUI. Thirty–two (32) patients with breast tumours were examined and their histological reports and wide local excision (WLE) pathology slides were obtained after biopsy and operation. Tumour contours were drawn independently by three radiologists on US B–mode images and elastograms. Maximum pathology tumour dimensions in the same study planes were correlated for B–mode image, elastogram and pathology slide, with dimensions from the pathology slide as the gold standard (Figure 1).

Results and Conclusion: Results shows tumour size measured from elasticity images is closer to the gold standard. The measurement accuracy is increased from 72% by using a B–mode image alone to 85% by combining B–mode and elasticity images together. The size and location of the tumour may affect the measurement accuracy and confidence.

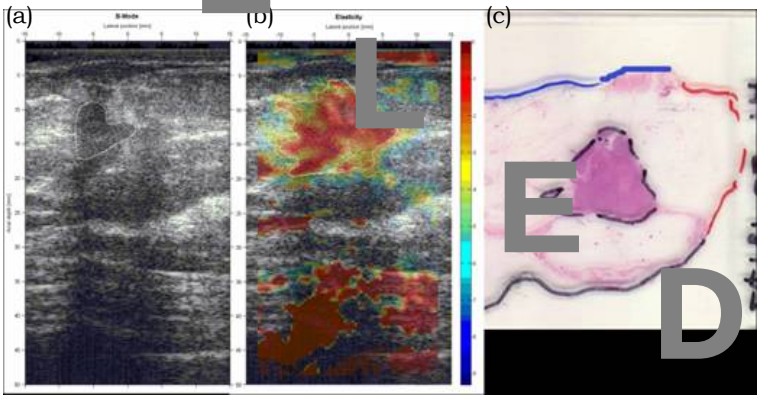

Figure 1: (a) US B mode (b) Elastography and (c) Wide local excision (WLE) specimen of a grade 3 invasive ductal carcinoma.

Acknowledgements: This work was funded by NIHR Biomedical Research Centre Programme, Oxford, UK.

References:

[1] K. M. Hiltawsky, M. Kruger, C. Starke, L. Heuser, H. Ermert and A. Jensen, "Freehand ultrasound elastography of breast lesions: clinical results", Ultrasound in Med. & Biol., Vol. 27, No. 11, pp. 1461–1469, 2001.

[2] A. Itoh, E. Ueno, E. Tohno, H. Kamma, H. Takahashi, T. Shiina, M. Yamakawa, T. Matsumura, "Breast Disease: Clinical Application of US Elastography for Diagnosis", Radiology: Vol. 239, No. 2, pp. 341–350, May 2006.

[3] J. Li, Y. Cui, M. Kadour, and J. A. Noble, "Elasticity Reconstruction from Displacement and Confidence Measures of a Multi–compressed Ultrasound RF Sequence", IEEE Trans. on Ultrasonics, Ferroelectrics, and Frequency Control, vol. 55, no. 2, pp. 319–326, 2008.

[4] M. J. Kadour and J. A. Noble, "Assisted–Freehand Ultrasound Elasticity Imaging", IEEE Trans. on Ultrasonics, Ferroelectrics, and Frequency Control, vol. 56, no. 1, pp. 36–43, January 2009.

091 **QUANTITATIVE VISUALIZATION OF MUSCLE MOTION USING ELASTOGRAPHY TECHNIQUE.**

Yongjin Zhou[1,2], Yongping Zheng[1,2], Jing–Yi Guo[1].*

[1]Health Technology and Informatics Department, [2]Research Institute of Innovative Products and Technologies, The Hong Kong Polytechnic University, Hong Kong, CHINA.

Background: Ultrasonography and Electromyography (EMG) have been widely used for skeletal muscle assessment. Traditionally, ultrasound imaging is only used for qualitative visualization about muscle morphology and its movement pattern during contraction. Recently, sonomyography (SMG) is proposed to obtain real–time signals about muscle morphological change during contraction for control and assessment purpose [1]. However, the detailed motion pattern of skeletal muscle during contraction has seldom been visualized in 2D, though such technique has been used to study cardiac muscle motions.

Aims: To quantitative visualize the muscle motion during contraction based on elastography technique.

Methods: Ultrasonic image sequences of rectus femoris, vastus lateralis and vastus medialis muscles of the right thigh were recorded dynamically during knee extension–flexion movements. During the experiment, the subjects were instructed to sit on Humac/Norm Testing and Rehabilitation System with a calibrated dynamometer (Computer Sports Medicine, Inc., MA, USA). Then an ultrasound probe was attached to the front of the thigh (Figure 1). The subjects were required to produce their torques increasing from 0–100% maximum voluntary contraction (MVC) of their own and then decreasing to 0% linearly by following a template showed on a computer screen. The recorded cross–sectional images of muscles were processed by a coarse–to–fine motion tracking method to assist the visualization of the local motion field. The motion tracking algorithm comprises two steps of calculation based on B–mode images. For two consecutive sonogram frames, the coarse motion field was first estimated using a block matching algorithm. The motion estimates obtained was then used to warp the first frame towards the second one, thus, the frame warped became more spatially correlated to the second one. Next, an optical flow method was employed to compute the "residual" motion between the warped first frame and the original second frame, with an inherent sub–pixel precision. Finally, the 2–D displacement fields obtained from the two steps were combined. The result could be displayed in a pseudo color map or vector field to represent the 2-D motion patterns of muscle components.

Results: Figure 2 shows a frame of the motion field estimated during a repeated muscle contraction where the region of interest is marked out with a bright rectangle. The results demonstrated that the motion pattern of muscles during contraction was very complicated. The obtained motion field can clearly view the translational as well as rotational movements of muscle components at different locations.

Conclusions: The proposed motion estimation method can visualize the cross–sectional muscle motion, and it may have potential clinical values for the quantitative functional assessment of muscles. The relationship between the motion pattern and other quantitative measures for muscle contraction needs to be studied further.

Acknowledgements: This work was supported by The Hong Kong Polytechnic University (G–YE22, J–BB69) and the Grant Council of Hong Kong (PolyU 5331/06E).

References:

[1] Zheng YP, et al., Sonomyography: Monitoring morphological changes of forearm muscles in actions with the feasibility for the control of powered prosthesis, Medical Engineering and Physics, 28: 405–415, 2006.

Figure 1: Experimental setup.

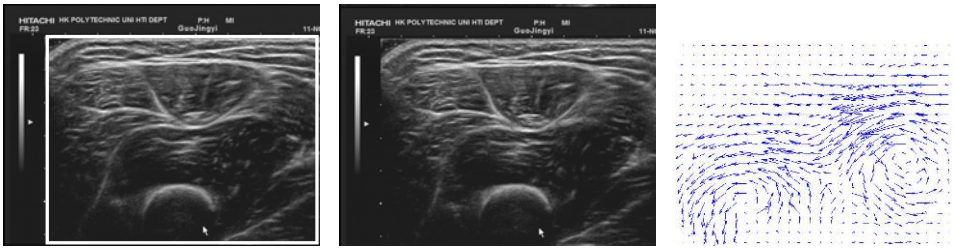

Figure 2: Original two frames of muscle transverse cross–section and the motion vector field estimated during muscle contraction. The region of interest is marked out in the first frame with the bright rectangle.

* *indicates Presenter*

097 **MEASUREMENT OF THE MECHANICAL RESPONSE OF THE VAGINAL WALL.**

B Röhrnbauer[1], M Bajka[2], C Betschart[2], D Peruncchini[2], D Fink[2], E Mazza[1], D Scheiner[2].*
[1]Center of Mechanics, Swiss Federal Institute of Technology Zurich, Tannenstrasse 3, 8092 Zurich, SWITZERLAND; [2]Obstetrics and GynecologyDepartment, Division of Gynecology, University Hospital of Zurich, Rämistrasse 100, 8091 Zurich, SWITZERLAND.

Background: The biomechanical characterization of the diaphragma urogenitale and, in particular of the vaginal wall, has gained increased interest in the descensus surgery. Recently, Epstein et al. performed tissue elevation measurements on the vaginal side–wall applying the dermalab skin probe (Cortex Technology, Hadsund, Denmark) [1]. They succeeded in correlating a scalar stiffness–like parameter with the severity of the pelvic floor disorder as well as with quality of life scales. These efforts should help to find indications of potential predispositions, genetic or due to traumatic events, to pelvic organ prolapse (POP) and allow for patient–specific therapies.

Aims: A preliminary study has recently been concluded, showing the feasibility of applying the aspiration device [2], in order to quantify the compliance of the anterior vaginal wall. The study aims at identifying mechanical parameters that correlate with the throphic conditions and stage of vaginal prolapse.

Methods: A new version of the aspiration device was developed for application on the vaginal wall. The measurement probe is a slender tube with a modular tip, serving as a vacuum cavity. Through a laterally placed elliptical aperture of 12x19mm^2, the tissue is sucked into the cavity. A control unit allows realizing a defined vacuum pressure history. The current pressure is acquired by a pressure sensor and the current tissue deformation is recorded by a digital camera. The apex displacement and the change of the area occupied by the projection of the aspirated tissue are scalar measures of tissue deformation, which are evaluated from the gray–scale images by contour extraction. Elastic, viscoelastic and strain history dependent parameters are calculated from the deformation history.
The measurements are performed at the University Hospital Zurich during normal urodynamics examinations. The measurement site is situated 1–2cm proximal with regard to point Aa on the anterior vaginal wall, according to the POP–Q standard. During the preliminary study, for safety reasons, the vacuum pressure was applied as a flat ramp, reaching 25mbar vacuum pressure within 14 seconds. For the upcoming study, the pressure history is defined as cyclic step functions, with plateaus of several seconds at alternating vacuum pressures of 25 and 0mbar respectively. The duration of one measurement is approximately 60 seconds.

Results: 11 women took part in the preliminary study. The mean age was 67.9 years (22–86 years). 3 women (parity >2) suffered from cystoceles of Stage II–III according to the POP–Q standard. 5 women (parity 1–3) had cystoceles of Stage I, and 3 women of Stage 0. The measured maximum deformations were 60% larger for the group of women with either POP–Q Stage II–III or with age <55 years, and, thus, with good trophic conditions compared to the rest. Moreover, the preliminary study suggested significant variances in the strain history dependence of the tissue related to its trophy. Strongly atrophic tissue was seen to soften during cyclic loading, whereas tissue of good or medium trophy tended to stiffen. No pain, no irritations, no bleeding and no damage were found after the measurements.

Conclusions: The preliminary study proved the feasibility of correlating biomechanical parameters to the tissue conditions of the vaginal wall. This provides the basis for the definition of a clinical study which will include evaluation of histological data and shall provide insight on the usefulness of specific therapies that influence the anatomy of pelvic floor.

Figure 1: (a) Aspiration probe: Modular tip with the aspiration cavity. (b) Camera view of the aspirated tissue.

References:

[1] Epstein L., Graham C., Impact of sacral colpopexy on *in vivo* vaginal biomechanical properties, American Journal of Obstetrics & Gynecology, 199, 664.e1–664.e6, 2008.
[2] Nava A., *In vivo* characterization of the mechanical response of soft human tissue, ETH Zurich, Dissertation No. 17060, 2007.

* *indicates Presenter*

048 **CHARACTERIZATION OF STRAIN DURING SIMULATED ANGIOPLASTY USING ULTRASOUND ELASTOGRAPHY.**

William F. Weitzel[1], Prashant P. Patel[1], Rohan Biswas[1], Dae Woo Park[1,2], Thomas J. Cichonski[1], Michael S. Richards[3], Jonathan M. Rubin[3], Sem Phan[4].*

[1]Internal Medicine Department, [2]Biomedical Engineering Department, [3]Radiology Department and [4]Pathology Department, University of Michigan, Ann Arbor, MI, USA.

Background: Sonography with phase–sensitive speckle–tracking is increasingly used as a noninvasive tool with the potential to distinguish tissue translation from deformation. In vascular tissue, angioplasty results in detectable changes in the anatomy of arterial fibers of the tunica media as the balloon expands. Therefore, we sought to investigate if high–resolution speckle tracking could accurately distinguish translation from strain occurring in vascular tissue during balloon expansion in a laboratory model of angioplasty.

Aims: This study aimed to assess the accuracy of ultrasound strain imaging in detecting the onset of vessel wall strain during angioplasty. Ultrasound strain measurements of bovine artery specimens were compared to the physical characteristics of the vessel obtained from pathology tissue specimen examination.

Methods: Elasticity Imaging Data: Ultrasound data and video B–scans were obtained from bovine carotid artery specimens and an inserted angioplasty balloon (10mm diameter by 4cm length) using a 7.5MHz linear ultrasound transducer. The transducer was fixed in a harness while the angioplasty balloon was inflated linearly from 0–5atm of pressure in all specimens but the control. The balloon–inflated vessels were fully expanded at 2atm. After data collection, off–line data processing of four regions of interest (ROIs) were selected on the leading edge of each specimen. Respective strain values were determined by numerically calculating the derivatives (gradients) of the displacement values frame by frame. Because the diameter of the balloon had a known value, it was possible to use a comparison between the n^{th} frame, where there was an inflection point (change in slope) and the final frame to obtain the elasticity imaging circumference in millimeters from the ultrasound B–scan image. Pathology Data: Five histologic slides were prepared by Masson's trichrome staining of a cross–section of each of the five bovine carotid artery specimens (for collagen) to observe the extra–cellular matrix composition and architecture. The slides were magnified and the folded fibers within the tunica media were traced and measured using Adobe Illustrator CS2 and Pathlength software to trace and measure the circumference.

Results: In the *in vitro* model of angioplasty, the vessel wall fibers exhibited folding prior to balloon inflation. As the balloon inflated, the vessels expanded and underwent tissue deformation, which was observable using tissue strain imaging. The inflection point (change in slope) of the longitudinal strain versus time (frame) graph, as seen in Figure 1, indicated the point at which the fibers of the artery had unfolded and begun to undergo strain (deformation) induced by the angioplasty balloon. This was common among all four ROIs, and the inflection point corresponded to the "imaging circumference" of the expanded vessel. These elasticity imaging circumference values were compared to the pathology circumference values in Table 1. Although the sample size was not large, statistical analysis found that the data were highly correlated, with an R^2 value of 0.9364.

Conclusions: Although further study is needed, these results suggest ultrasound elasticity imaging can detect highly localized mechanical changes of the vessel wall during angioplasty.

Acknowledgements: This work was supported in part by NIH grant DK62848.

Table 1

Specimen	Pathology Circumference	Elasticity Imaging Circumference
Control	21.44 mm	N/A
Artery 1	22.34 mm	23.04 mm
Artery 2	23.59 mm	24.37 mm
Artery 3	23.69 mm	24.12 mm
Artery 4	23.25 mm	23.92 mm

Figure 1

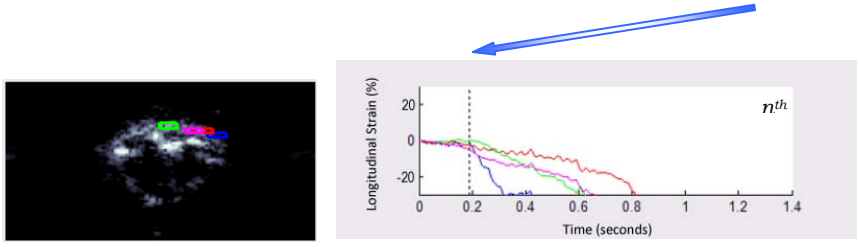

* *indicates Presenter*

058 ***IN VITRO* CHARACTERIZATION OF MECHANICAL PROPERTIES OF HUMAN MESENCHYMAL STEM CELLS BY TIME–RESOLVED ACOUSTIC MICROSCOPY.**

Cornelia Hildebrandt[1], Wolfgang Bost[1], Hagen Thielecke[1], Robert M. Lemor[1].*
[1]Fraunhofer Institut fuer Biomedizinische Technik, Ensheimer Str. 48, St. Ingbert, GERMANY.

Background: The application of human mesenchymal stem cells (hMSCs) in cell–based therapies depends on well characterized cells and tissues in an unperturbed environment. Developmental processes of hMSCs are reflected by changes in the cytoskeleton and extracellular matrix compounds, which in turn leads to changes in the mechanical properties of hMSCs during differentiation. Ultrasound is a non–invasive technique, and using a frequency of 1 GHz provides the resolution to investigate the local mechanical properties of individual cells by measuring acoustic attenuation and impedance [1]. Accordingly, these values can be used as a lineage specific marker.

Aims: The aim of this investigation was to test the hypothesis that specific changes of the cellular structure related to developmental processes into the adipogenic, chondrogenic and osteogenic lineage of hMSCs show variations in mechanical properties that can be detected by acoustic microscopy at 1 GHz.

Methods: Cells for investigation of the differentiation in cell layers were cultured on cover glass chambers at a density of $2x10^4$ cells/cm^2. The differentiation of hMSCs into the adipogenic, chondrogenic and osteogenic lineage was induced as previously described [2]. Cells were imaged under vital conditions using an acoustic microscope (SASAM–System, kibero GmbH, Germany). The differentiation was determined by oil red staining for adipocytes, alician blue staining and anti–proteoglycan immunostaining for chondrocytes and alkaline phosphatase staining for osteoblasts. Acoustic reflectance and attenuation images were generated from the recorded ultrasound data and subsequently analyzed. The experiment was conducted on triplicates; the scanned area was 100 μm^2.

Results: The acoustic properties were found to be specific for every differentiation lineage. For instance, adipogenic cells have a low acoustic attenuation coefficient (0.07 a.u.; deviation 12%) and exhibit a higher reflectivity (0.35 a.u.; dev. 20%), while chondroblasts as well as osteoblasts showed a higher acoustic attenuation coefficient (osteoblasts: 0.038 a.u.; dev. 4%, chondroblasts: 0.037; dev. 7%) and differed in their sound reflectivity (osteoblasts: 0.2 a.u.; dev. 10%, chondroblasts: 0.125 a.u.; dev. 8%). In the attenuation and reflectivity images, structural differences not seen by optical microscopy can be observed. High acoustic reflectivity can also be seen in regions without cells and can be attributed to the extracellular matrix.

Conclusion: Acoustic microscopy is highly suitable for investigation of mechanical properties of hMSCs. It can be used to non–invasively test the differentiation status of stem cells during cell or tissue maturation. Further studies using specific markers for cytoskeleton and extracellular matrix proteins and synchronous optical and acoustic microscopy will help to link the changes in mechanical parameters to the underlying biology of the cells.

Acknowledgements: This work was partly funded by EU under the framework VI project OsteoChord.

References:

[1] O. Wagner, et al.: Viscoelastic Properties of f–actin, Microtubules, f–actin /a–actinin, and f–actin / Hexokinase Determined in Microliter Volumes with a Novel Nondestructive Method, Biophysical Journal Vol. 76, 2784–2796, May 1999.
[2] Pittenger M.F., et al.: Multilineage potential of adult human mesenchymal stem cells, Science 284, 143–147, 1999.

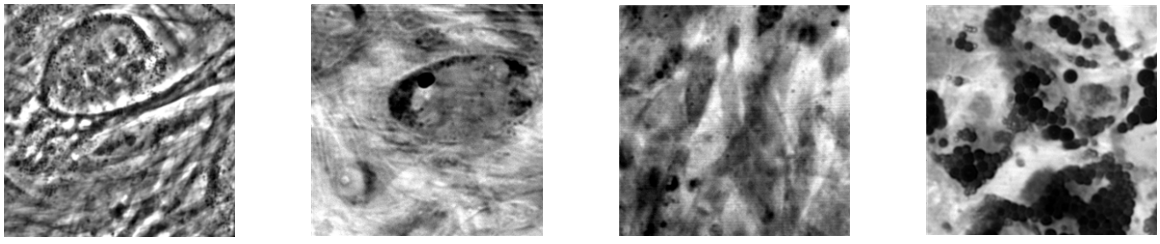

Figure1: (a) Phase contrast image of chondrocytes. (b) Acoustic attenuation image of chondrocytes. (c) Acoustic attenuation image of osteocytes. (d) Acoustic attenuation image of adipocytes. (all images 100μm^2)

027 **NON–INVASIVE LIVER FIBROSIS STAGING USING SUPERSONIC SHEAR IMAGING: A CLINICAL STUDY ON 150 PATIENTS.**

E. Bavu[1], J–L. Gennisson[1], B–F. Osmanski[2], J. Bercoff[2], M. Fink[1], V. Mallet[3], P. Sogni[3], A. Vallet–Pichard[3], B. Nalpas[3], M. Tanter[1] and S. Pol[3].*

[1]Langevin Institute, Laboratoire Ondes et Acoustique, ESPCI Paris Tech, CNRS UMR 7587, INSERM, 10 rue Vauquelin, 75005, Paris, FRANCE; [2]SuperSonic Imagine, Les jardins de la Duranne – Bât E & F510, rue René Descartes 13857, Aix en Provence, FRANCE; [3]Service d'hépatologie, Hôpital Cochin, 27, rue du Faubourg Saint–Jacques 75014, Paris, FRANCE.

Background: Fibrosis staging can be assessed by a rough estimation of liver stiffness averaged along an ultrasonic A–line. Providing a complete 2D map of liver stiffness would thus be of great clinical interest for the diagnosis of hepatic fibrosis and help prevent upcoming cirrhosis. However, such measurement requires both quantitative value of shear elasticity and great precision to discriminate between different fibrosis levels.

Aims: In this work, the Supersonic Shear Imaging technique (SSI) is proposed for mapping the *in vivo* viscoelastic parameters of liver in patients with hepatitis C and deriving a mean elasticity of liver tissue. The results are compared to biological tests (Fib4, Apri, Forns) and Fibroscan® (Echosens, Paris, France) measurements. Beyond the scope of non–invasive fibrosis quantification, it is also envisioned that quantitative elasticity imaging of liver will have potential interest for liver cancer diagnosis.

Methods: The SSI technique is based on the radiation force induced by a conventional ultrasonic probe to generate a planar shear wave deep into tissue. The shear wave propagation throughout the medium is caught in real–time due to an ultrafast ultrasound scanner (up to 5000 frames/s). Using modified sequences and post–processing, this technique is implemented with curved arrays in order to get a larger field of view of liver tissue. A study on 142 HCV patients with different stage F fibrosis has been conducted to investigate the accuracy of the technique ($F \in [0;4]$). Quantitative maps of liver elasticity are produced for each volunteer with a linear and a curved array (5 MHz and 2.5 MHz central frequency respectively).

Results: B–mode images of 120x75 mm^2 and corresponding elasticity maps were obtained using a curved ultrasonic probe with a good reproducibility and accuracy. The shear wave phase velocity dispersion was also calculated (Figure 1b). This study shows a good correlation between the values obtained by SSI and the fibrosis levels diagnosed by biological tests (p–index $<10^{-8}$) and allows a good differentiation of fibrosis level F (Youden's index Y> 0.9 for F>3 and Y> 0.8 for F>2). Results are also compared ($r^2 > 0.92$) to the Fibroscan® elasticity measurement by fitting the velocity dispersion curves obtained by SSI at 50 Hz.

Conclusions: This real–time elasticity mapping using an ultrasonic curved probe offers better signal–to–noise ratio than linear arrays and a larger area in the patient's liver (13.3 ± 2.8 cm^2 versus 9.1 ± 1.1 cm^2 in estimation areas). This gives more confidence about the accuracy of the diagnosis of the fibrosis stage. Furthermore, the elasticity parameters obtained with SSI give access to the shear wave group velocity and the phase velocity. As a consequence, the SSI assessment of liver stiffness could potentially give more information on the viscoelasticity properties of the liver.

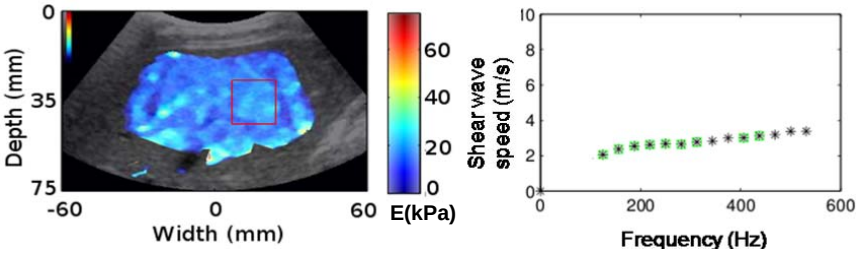

Figure 1: a) Elasticity map and B–Mode image of the liver and
b) shear wave speed dispersion curve, calculated in the red box displayed on the elasticity map, for a patient diagnosed as F3.

* *indicates Presenter*

099 **CHANGES OF MECHANICAL PROPERTIES OF ARTICULAR CARTILAGE WITH ENZYMATICALLY-INDUCED DEGRADATION DETECTED USING AN OCT–BASED AIR JET INDENTATION *IN VITRO*.**

Shu–Zhe Wang[1], Yan–Ping Huang[1], Yong–Ping Zheng[1,2].*
[1]Health Technology and Informatics Department, [2]Research Institute of Innovative Products and Technologies, The Hong Kong Polytechnic University, Hong Kong, CHINA.

Background: The mechanical properties of articular cartilage play an important role in its daily function. It is well known that in the commonly seen osteoarthritis (OA) disease, the quality of the cartilage significantly deteriorates, and its mechanical properties severely degrade. On the other hand, ultrasound indentation is a very important and popular method for the measurement of mechanical properties of cartilage *in vivo* [1,2]. To improve the detection accuracy and avoid a rigid contact indentation, we had previously developed a non–contact air jet indentation system based on optical coherence tomography (OCT) for measuring the mechanical properties of soft tissues [3]. This system has potential in the detection of early OA related to articular cartilage.

Aims: This study aims to apply the OCT–based air jet indentation for measuring the change of stiffness in articular cartilage induced by enzymatic degradations.

Methods: 40 bovine osteochondral disks with articular cartilage attached to the subchondral bone were tested using the OCT–based air jet indentation system before and after degradations using two enzymes: collagenase (n=20) and trypsin (n=20). The stiffness obtained by regression of the indentation pressure with the deformation ratio (deformation/initial thickness of the cartilage) was used for comparison. The initial thickness of the cartilage was measured by a high frequency ultrasound system. The cartilage samples were also indented with a standard mechanical testing machine (Instron 5569) using a similar protocol as that of the air jet indentation. Histological analysis was conducted to analyze the change of proteoglycan (PG) content in the case of trypsin digestion.

Results: The cartilage stiffness measured by the OCT–based air jet indentation was significantly reduced after both the collagenase and trypsin treatments ($p < 0.05$, Figure 1). A fairly good correlation ($r^2=0.69$, $p<0.05$, Figure 2) was also found for the stiffness obtained from the air jet indentation and the standard mechanical indentation test. The histological study showed that PG content was almost completely digested in the trypsin treatment group.

Conclusions: The OCT–based air jet indentation system could be used to detect the change of mechanical properties in articular cartilage in an osteoarthritic process simulated by enzyme treatments *in vitro*. Further research work is being conducted to develop a miniaturized probe for arthroscopic use.

Acknowledgements: This project was partially supported by Hong Kong Research Grant Council (PolyU5318/05E, PolyU5245/03E) and The Hong Kong Polytechnic University (J–BB69).

References:

[1] Zheng YP, Mak AFT. An ultrasound indentation system for biomechanical properties assessment of soft tissues *in–vivo*. IEEE Trans Biomed Eng 43: 912–918, 1996.
[2] Laasanen et al. Novel mechano–acoustic technique and instrument for diagnosis of cartilage degeneration. Physiol Meas 23: 491–503, 2002.
[3] Huang et al. An optical coherence tomography (OCT)–based air jet indentation system for measuring the mechanical properties of soft tissues. Meas Sci Technol 20: 15805, 2009.

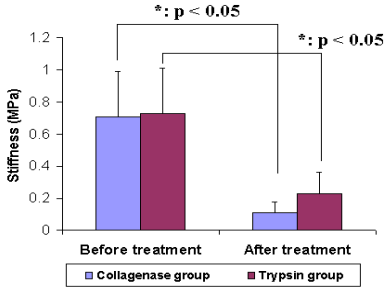

Figure 1: Stiffness measured using the air jet indentation system before and after enzyme treatments.

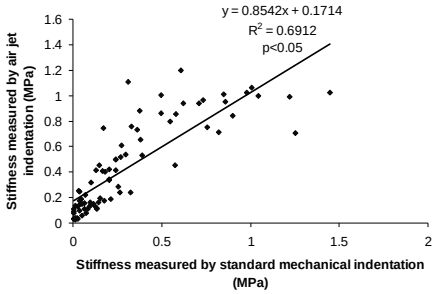

Figure 2: Stiffness measured with the air jet indentation and the standard mechanical indentation methods.

* *indicates Presenter*

100 ***IN VIVO* MONITORING OF DIABETIC FOOT ULCER HEALING USING OCT AIR-JET INDENTATION.**

Clare Yuet–Lan Chao[1,4], Yong–Ping Zheng[2,3], Yan–Ping Huang[2], Gladys Lai–Ying Cheing[4].*
[1]Physiotherapy Department, Queen Elizabeth Hospital, Hong Kong, CHINA; [2]Health Technology and Informatics Department, [3]Research Institute of Innovative Products and Technologies, [4]Rehabilitation Sciences Department, The Hong Kong Polytechnic University, Hong Kong SAR, CHINA.

Background: Chronic wounds such as diabetic foot ulcers and pressure ulcers are growing challenges for the health care system. In UK, an estimated population of 500,000 people is diagnosed with a chronic wound each year, and the total cost of the health service is estimated to be 3% of the total health care budget [1]. The evaluation of wound status and monitoring of wound healing have become a priority from both research and clinical perspectives. Accurate evaluation of the physiologic status of a chronic wound provides important information to guide appropriate treatment decisions and monitoring treatment effectiveness. So far, there is a lack of accurate quantitative methods to assess wound tissue properties. The status of a wound should not be judged by its appearance only. A critical outcome of the wound repairing process is the restoration of the mechanical properties of tissue strength [2].

Aims: Firstly, to measure the mechanical properties of diabetic ulcer tissues by a newly developed non–contact optical coherence tomography (OCT)–based air–jet indentation system [3]. Secondly, to examine the test/retest reliability of the system for measuring the mechanical properties of diabetic ulcer tissues.

Methods: Figure 1 shows the experimental setup. Five male subjects with diabetic foot ulcers were recruited. Their mean age was 57±9 yrs. The mean duration of diabetes was 14.0±4.7 yr. A total of 7 wounds from the subjects was examined. All ulcers were located below the ankle, and the mean duration of the ulceration was 6.0±8.2 months. A total of 23 measuring sites at both the central wound bed (n=13) and peri–ulcer areas (n=10) were evaluated with the OCT–based air–jet indentation system. Four cycles of loading and unloading, with approximately 36 s duration at an indentation rate of 0.03 to 0.06 mm/s, were carried out for each indentation trial. Test/retest reliability was performed at all measuring points.

Results: Our results indicated that the peri–ulcer area tended to be stiffer than the central wound bed area (stiffness coefficient: 0.47±0.18 vs. 0.40±0.29 N/mm, respectively), but not significantly (p=0.47). Figure 2 shows a typical indentation curve along with time obtained on one subject. A high value of test/retest reliability was demonstrated (ICC: 0.986; Pearson's correlation: r=0.972, p<0.001).

Conclusions: Our preliminary findings demonstrated that the peri–ulcer showed a higher stiffness than the ulcerated tissues, but further study with more subjects is needed to confirm these findings. We found that the novel air–jet system is a reliable tool for characterizing the biomechanical properties of tissues around the wound in a non–contact way, which will allow better monitoring of wound tissues during the healing process *in vivo*. However, small sample size is a limitation of the study.

Acknowledgements: This project is partially supported by the HKSAR Research Grant Council (PolyU5318/05E, PolyU 5126/07E) and the Hong Kong Polytechnic University (J–BB69).

References:

[1] Pollard T. A new research focus for skin breakdown. J Wound Care 16: 281, 2007.
[2] Gamelli RL, He LK. Incisional wound healing. Model and analysis of wound breaking strength. Methods Mol Med 78:37–54, 2003.
[3] Huang, et al. An optical coherence tomography (OCT)–based air jet indentation system for measuring the mechanical properties of soft tissues. Meas Sci Technol 20: 15805, 2009.

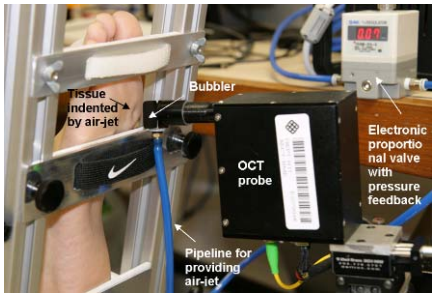

Figure 1: The experimental setup for the plantar tissue assessment using the OCT air–jet indentation system.

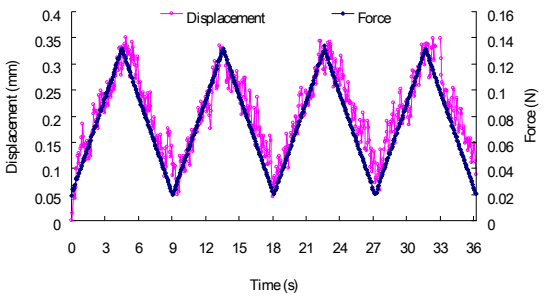

Figure 2: A typical indentation curve obtained on one subject at the central wound bed area.

* *indicates Presenter*

071 **THE IMPACT OF PHASE ENCODING ON LATERAL DISPLACEMENT ESTIMATES.**

S. Korukonda[1], M. M. Doyley[1].*
[1]Electrical and Computer Engineering Department, University of Rochester, Rochester, NY, USA.

Background: Ultrasound elastography visualizes the mechanical properties of soft tissues. Images of internal tissue strains (i.e., strain elastograms) are typically produced by analyzing pre– and post–deformed radio–frequency (RF) echo frames using the cross–correlation method. Strain elastograms can be viewed as a first order approximation of the relative modulus distribution by assuming that the internal stress is constant, albeit at the expense of degrading elastographic contrast transfer efficiency and introducing image artifacts. We can improve contrast transfer efficiency by considering elastography within the framework of solving an inverse problem, but this approach to elastography is not without problems: it is sensitive to measurement errors, and it requires reliable estimates of all three components of displacements to produce accurate modulus elastograms, which is generally difficult to achieve with ultrasound. Specifically, including noisy lateral and elevational displacement estimates in the image reconstruction process could reduce the benefits of this approach to elastography. In this presentation, we report the results of experiments that we have conducted to assess the extent to which encoding modulations in the lateral direction during beam forming will improve the precision of lateral displacement estimates.

Aims: In this presentation, we assess the impact of phase encoding on quality of lateral displacement estimates.

Methods: In this study, we simulated a phantom (20mm (w) x 40mm (h)) that had a homogeneous shear modulus of 20kPa. We synthesized RF echo frames when the simulated phantoms were deformed using applied strains in the range of 0.1–5%. All echo imaging was performed using a 128 element linear transducer array that had centre frequency of 5MHz. During beam–forming, we encode phase in the lateral direction by employing apodization functions that we constructed by convolving Gaussian pulse with a two delta functions [1]. It is important to note that we increase the modulation by increasing the distance between the delta functions. In all cases, we estimated lateral displacement elastograms by performing two–dimensional cross–correlation analysis on the pre– and post–deformed RF echo frames obtained with different apodization functions. We computed strain images from the displacement images by employing a radial basis function strain estimator and evaluated the quality of the resulting strain elastograms using conventional measures of image quality that were derived from an experimentally determined strain filter.

Results: Figure 1 shows a representative example of lateral strain maps obtained when the lateral wavelength λ_x was reduced from 4.5mm (no phase encoding) to 0.76mm. For small applied strains (<1%), increasing the lateral modulation improved the peak SNR of the lateral strain elastograms from 4dB (no phase encoding) to 67dB (for λ_x); whereas, SNR decreased noticeable for larger applied strains.

Conclusions: Encoding lateral phase through customized beam–forming will improve lateral displacement estimates, but, because of lateral phase decorrelation, other noise reduction methods will have to be employed when estimating larger internal lateral displacements.

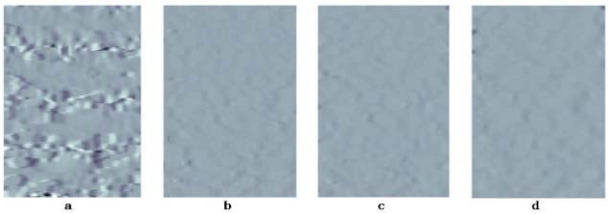

Figure 1: Lateral strain maps obtained with PSFs of lateral wavelength (a) 4.5mm (b) 2.28mm (c) 1.14mm and (d) 0.76mm

Acknowledgements: This work was supported by startup funds provided by the University of Rochester.

References:

[1] H Liebgott, et al., PSF Dedicated to Estimation of Displacement Vectors for Tissue Elasticity Imaging with Ultrasound, IEEE transactions on Ultrasonics, Ferroelectrics, and Frequency Control, Vol. 54, No. 4, April 2007.

086 **APPLICATION OF 2D POLYNOMIAL FITTING TO BEAM STEERING FOR MOTION ESTIMATION WITH SUB–SAMPLE ACCURACY.**

R Zahiri–Azar[1], O Goksel[1], SE Salcudean[1].*
[1]The University of British Columbia, Vancouver, BC, CANADA.

Background: Several methods for measuring both axial and lateral motion components in ultrasound images have been proposed in the literature including techniques based on (1) 2D pattern matching functions and (2) 1D pattern matching functions combined with beam steering (Figure 1). Sub–sample motion estimation lies at the heart of both of these techniques. We have recently introduced a novel method for 2D sub–sample motion estimation using polynomial fitting and showed that it significantly improves the performance of (1) [1].

Aims: Our goal is to improve the accuracy of 2D tracking when beam steering is employed by using polynomial interpolation for sub–sample motion estimation.

Methods: The previously proposed method for 2D sub–sample motion estimation is performed as follows: First, a coarse estimation of motion between two echo frames is found by locating the maximum of a discrete pattern matching function. Then, a quartic 2D polynomial $f(x,y)$ is fitted to the matching coefficients at this maximum and its neighboring lags. The sub–sample motion is found next as the maximizer of this fitted polynomial using Newton's method. For motion estimation utilizing beam steering, the above mentioned process is repeated on two sets of frames, acquired at steering angles +θº and -θº. The motion can then be estimated accurately by using the components of motion along the axial directions of the steered beams, because axial resolution, even when beam steering is employed, is higher than lateral resolution.

Results: A virtual phantom was simulated and displaced over an 11×11 2D grid with 1/10 sample distance in each direction spanning ±0.5 of a sample in both axes. The RF frames corresponding to each of these configurations were then generated for multiple steering angles (0º, ±2.5º, ±5º… ±15º) using Field II simulation software. Using these RF echoes, the performance of motion estimation with beam steering was studied in terms of estimation biases and standard deviations. As expected, the performance depends on the steering angle employed (Figure 2). For the steering angles of ±10º, the mean absolute axial and lateral biases were found to be 0.0067 and 0.0050 of a sample (corresponding to 134nm and 1.50um, respectively), using the proposed motion–estimation method (similar to the results reported for (1) in [1]) and 0.0113 and 0.0253 using the conventional 1D sub–sample estimation method using cosine fit. The mean axial and lateral standard deviations were 0.021 and 0.011 for the proposed method and 0.042 and 0.019 of a sample for the 1D cosine fitting method for the same steering angles (i.e. ±10º).

Conclusions: The proposed method significantly improves the performance of 2D tracking using beam steering in terms of bias and standard deviation. The results show that the proposed 2D sub–sample estimation provides better accuracy compared to common 1D sub–sample estimation techniques even when only the component along the beam propagation is used. The proposed method has several potential applications in medical ultrasound namely motion vector imaging, strain tensor imaging and tissue elasticity imaging.

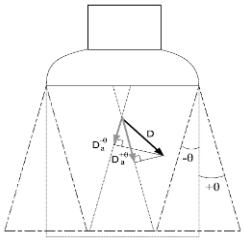

Figure 1: Schematics for 2D motion estimation using beam steering. Data from ROI are acquired with two different steering angles. The 2D displacements are reconstructed using 1D measurement from the two steering angles.

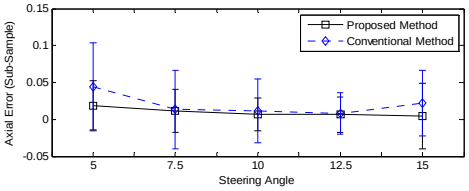

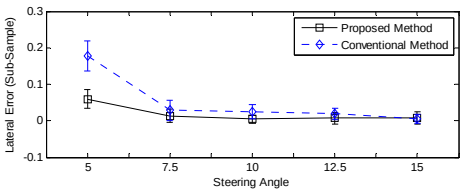

Figure 2: The overall performance of 2D motion tracking using beam steering using the proposed 2D and the conventional 1D sub–sample estimation technique averaged over the entire simulated motion grid.

Reference:

[1] R. Zahiri–Azar, et al., "Methods for the Estimation of Sub–Sample Motion of Digitized Ultrasound Echo Signals in Two Dimensions", 30th International IEEE EMBS, Vancouver, Canada, pp 5581–5584, 2008.

* *indicates Presenter*

088 **PRELIMINARY EXPERIMENTS ON NEW VIRTUAL SOURCE FOR LATERAL MODULATION.**

C. Sumi[1], N. Matsui[1], K. Shimizu[1], Y. Takanashi[1].*
[1]Sophia University, 7–1, Kioicho, Chiyodaku, Tokyo 102–8554, JAPAN.

Background: We have realized beamformings [1,2], by using steering of multiple beams and apodization, for B–mode imaging and accurate measurement of tissue or blood displacement vectors or strain tensors using the multidimensional cross–spectrum phase gradient method (MCSPGM) and autocorrelation and Doppler methods (MAM and MDM). In [1,2], we reported lateral cosine modulations (LCMs) that use several apodization functions. As shown, the coherent superimposition of the steered beams performed in LCM has a higher potential for realizing a more accurate measurement of a displacement vector than the synthesis of the displacement vector using the accurately measured axial displacements performed in the multidirectional synthetic aperture method (MDSAM) and the multiple transmitting method (MTM). However, recall that in LCMs, MDSAM and MTM can also be used.

Aims: When dealing with deeply situated tissues, LCM requires the use of a large physical aperture [2]. This confines the applications of LCM. To overcome this limitation, we propose to use a new virtual source [2]. That is, regardless of the focal position of an individual element aperture, proper scatters are used as virtual sources. For instance, by setting virtual sources in tissue, an arbitrary vision of field (VOF) will be obtained regardless the aperture geometry (convex, linear etc). A proper random scattering medium will also be installed in the transducer [2] or between the transducer and a target body. In addition, virtual sources (or receivers) will also be realized in null spaces aside the short physical array aperture by searching for the corresponding echo data in acquired echo data set. In this report, preliminary experimental results are presented.

Methods: Experiments are performed using the same agar phantom as that used in [1,2]. The target agar phantom [40 (axial, x) x 96 (lateral, y) x 40 (elavational) mm^3] had a central circular cylindrical inclusion (diameter, 10mm; depth, 19 mm) with a shear modulus different from that of the surrounding region and shear moduli of 2.63 and $0.80x10^6 N/m^2$ in the inclusion and surrounding regions, respectively (i.e., relative shear modulus, 3.29). The phantom was compressed manually by 2.0mm in the lateral direction. The contact surfaces of the linear array transducer (7.5MHz, 0.2mm pitch, 2.4mm for acoustic lens, etc.) and phantom were separated by less than 0.3mm by immersing them in water in a tank, and a sponge was put under the phantom to allow the phantom to elongate in the axial direction by lateral uniform compression from the right–hand side using a large plate. The left surface was fixed to a wall. A rectangular ROI [13.7 (axial, x) x 13.2 (lateral, y) mm^2] was centered on the inclusion (depths from 12.2 to 25.9 mm). The depth of virtual source line was changed from -38.1–99.1mm with respect to the linear array surface (0.0mm). MAM was used to measure a displacement vector. 2D shear modulus reconstruction was also performed under a 2D stress condition.

Results and Conclusions: Figure 1 shows the images of axial and lateral displacements, axial, lateral and shear strains, and 2D shear modulus reconstruction obtained for (a) –5, (b) 0 and (c) 5 mm virtual source depths only. In this range, the accurate shear modulus reconstructions were obtained. Figure 2 shows the means and standard deviations (SDs) of shear moduli evaluated in the central square region in the inclusion. Aforementioned other applications of the virtual source will also be reported.

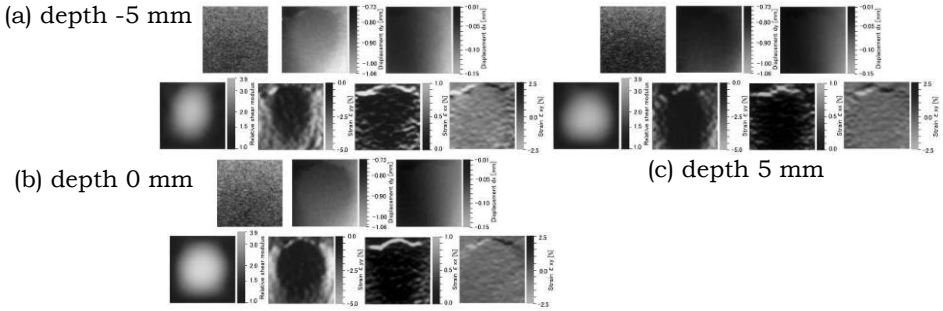

Figure 1: Measurements and reconstructions.

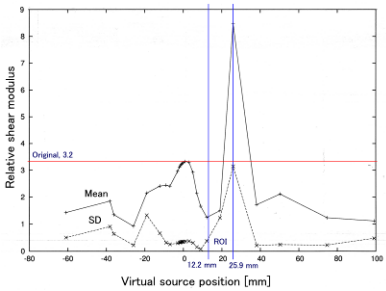

Figure 2: Reconstructed relative shear modulus vs virtual source depth.

References:
[1] C. Sumi et al., Jpn J Appl Phys, vol. 47(5B), 4137, 2008.
[2] C. Sumi et al., IEEE Trans UFFC, vol. 55, pp. 2607, 2008.

* *indicates Presenter*

095 **COMPARATIVE ANALYSIS OF TWO COMPOUNDING TECHNIQUES FOR IVUS PALPOGRAPHY.**

MG Danilouchkine[1], F Mastik[1], AFW van der Steen[1,2].*
[1]Erasmus Medical Center, Rotterdam, THE NETHERLANDS; [2]Interuniversity Cardiology Institute of the Netherlands, Utrecht, THE NETHERLANDS.

Background: Recent validation studies [1] proved the diagnostic value of IVUS palpography in semi–invasive characterization of atherosclerotic plaques in coronary arteries. The neighboring high and low strain regions are frequently associated with rupture–prone locations. However, IVUS probe motion hampers accurate determination of the mechanical properties at each location of the luminal surface and results in regions of void strain estimates.

Aims: This study aims at the quantitative assessment and comparison of two compounding techniques for IVUS Palpography.

Methods: In order to overcome the detrimental effect of catheter motion, Doyley et al. proposed a compounding scheme for IVUS Palpography [2]. The neighboring IVUS frames, acquired during diastole of a cardiac cycle, are paired to compute the luminal strain profiles or partial palpograms. Subsequently, the obtained strain maps are averaged to form a final compounded strain profile for a given cross–section of a coronary artery. This first scheme is further referred to as the classical compounding. The second scheme explicitly takes into account that the measured strains are only partially available. It attempts to reconstruct the missing elasticity values by using the available strain information in its direct vicinity. The reconstruction algorithm is based upon the earlier proposed Normalized Convolution method [3]. The improved partial strain profiles are subsequently averaged in the same manner as in classical compounding. This scheme was coined as reconstructive compounding.

Results: Eight *in–vivo* IVUS pullbacks were used for the comparative analysis. The percentage of valid strain was 28.6±13.7% for the scheme without compounding (the partial strain profiles at end diastole represent the elastic properties of the coronary surface), 94.3±4.4% and 99.7±0.2% for the classical and reconstructive compounding, respectively. Figure 1 shows the luminal strain distribution for a cross–section of a coronary artery with an atherosclerotic burden, computed with the classical (A) and reconstructive (B) compounding scheme. Due to the missing information about the cap stiffness, plaque vulnerability cannot be assessed with classical compounding. Reconstructive compounding restores the missing strain values and allows for more accurate assessment of its rupture–proneness.

Conclusions: Implementation of the compounding schemes significantly boosts the diagnostic information coming out of IVUS Palpography with the reconstructive scheme being the best.

Acknowledgements: Volcano Corp. (Rancho Cordova, CA, USA) for the financial support.

References:

[1] Schaar, J. A. et al., Circ. 108(21), 2636–2641, 2003.
[2] Doyley M.M. et al., UMB 27(11), 1471–1480, 2001.
[3] Andersson K. et al., Sign. Proc. J. 87(3), 353–365, 2007.

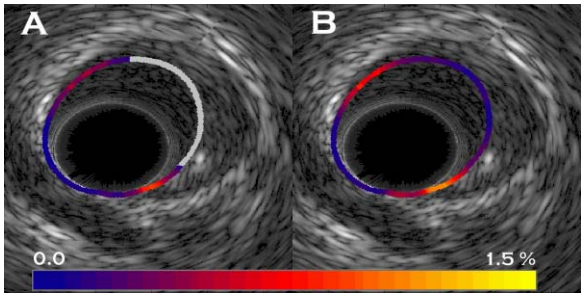

Figure 1: Examples of luminal strain profiles computed for a cross–sectional view of a coronary artery with an atherosclerotic burden (between 12 and 5 o'clock) for the classical (A) and reconstructive compounding (B) scheme.

* *indicates Presenter*

042 **STUDY OF CONTRAST DETAILS OF HETEROGENEOUS PHANTOMS BASED ON CRAWLING WAVE SONOELASTOGRAPHY.**

L An[1], DJ Rubens[2], YT Cho[1], Z Hah[1], KJ Parker[1].*
[1]University of Rochester, Rochester, NY, USA; [2]University of Rochester Medical Center, Rochester, NY, USA.

Background: The crawling wave (CrW) technique [1] for local tissue shear velocity estimation was recently introduced into the sonoelastographic field. It has been applied to depicting the elastic properties of biological tissues including radiofrequency ablated hepatic lesions *in vitro* [2], human skeletal muscle *in vitro* [3] and excised human prostate [4].

Aims: The objective of this study is to quantify contrast details for heterogeneous elastic phantoms and evaluate frequency dependence, bias and spatial resolution of lesion detection based on CrW sonoelastography. We focus on parameters of particular interest in prostate cancer detection.

Methods: Heterogeneous elastic phantoms were prepared by embedding stiff spherical inclusions (11% gelatin) with diameter of 1cm and 6mm in otherwise soft homogeneous backgrounds (6% gelatin) separately. Two vibration sources were positioned at each side of the phantom with the ultrasound transducer scanning from the top of the cross–section to be observed. CrWs at 70Hz, 100Hz, 120Hz, 140Hz, 200Hz and 300Hz were acquired by offsetting a small frequency difference between two sources. Independent reference measurements were obtained in homogeneous specimens. The elastic contrast of the lesions, $E_{lesion}/E_{background}$, was 1.52, similar to the ratio found in prostate cancer [5].

The CrW movies were first normalized to compensate for the gain difference at different depth level of the image. Sinusoidal curve fitting over one cycle of crawling waves was then applied to improve the SNR. A 2D local shear velocity estimator was employed with the CrW phase pre–conditioned to a favorable range of the estimator. Finally, the shear velocity information from both the hard region and the soft region was extracted from the estimation map and was compared against the reference values obtained from homogeneous phantoms.

Results: The separation of the shear velocity values of the lesion and the background is shown in Figure 1. The 1cm inclusion phantom gives the highest contrast of hard and soft regions at 1.29 averaged over frequency, followed by the 6mm case at 1.15. The estimations followed an upward tendency with frequency increase due to the finer resolution of CrW at higher frequencies. The effect of under–estimation and loss of contrast was revealed, which is caused by noise and the spatial support of the estimator.

Conclusions: In this study, contrast details were demonstrated for phantoms with stiff inclusions of different sizes. The experiment showed the ability of shear velocity estimator to distinguish the lesion from the background. Lesions similar in elastic contrast to prostate cancer that are 6mm in diameter or larger are resolvable at frequencies above 100Hz, using our current system and methods.

Acknowledgements: This study was partly supported by NIH grants 5 RO1 AG016317 and 5 RO1 AG29804.

References:

[1] Zhe Wu, et al., Sonoelastographic imaging of interference patterns for estimation of shear velocity distribution in biomaterials, JASA, 120(1), pp. 535–545, 2006.
[2] Kenneth Hoyt, et al., Two–dimensional sonoelastographic shear velocity imaging, UMB, 34(2), pp. 276–288, 2008.
[3] Kenneth Hoyt, et al., Muscle tissue characterization using quantitative sonoelastography: preliminary results, Proceedings of the IEEE Ultrasonics Symposium, pp. 365–368, 2007.
[4] B Castaneda, et al., Prostate cancer detection using crawling wave sonoelastography, SPIE, 7265, 726513, 2009.
[5] Man Zhang, et al., Congruence of imaging estimator and mechanical measurements of viscoelastic properties of soft tissues, UMB, 33, pp. 1617–1631, 2007.

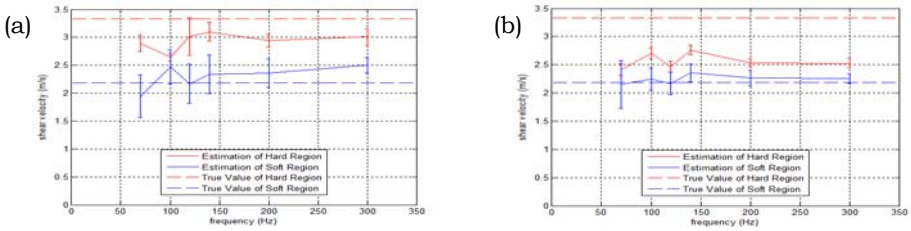

Figure 1: Contrast detail curves for heterogeneous phantoms with inclusions of diameters of (a) 1cm, (b) 6mm.

051 **RADIATION FORCE INDUCED CRAWLING WAVES.**

Zaegyoo Hah[1], Yong Thung Cho[1], Christopher R. Hazard[2], Deborah J. Rubens[3], Kevin J. Parker[1].*
[1]Electrical and Computer Engineering Department, University of Rochester, Rochester, NY, 14627, USA; [2]GE Global Research, One Research Circle, Niskayuna, NY, 12309, USA; [3]Imaging Science Department, University of Rochester, Rochester, NY, 14627, USA.

Background: Crawling waves can be easily imaged using conventional color Doppler scanning and can be readily analyzed to estimate local elastic properties of tissues and lesions [1]. Crawling waves can be produced by two vibration sources. These can be mechanical sources or radiation force excitation using focused ultrasound.

Aims: The present study aims to characterize the trade–offs as crawling waves are created with longer sinusoidal radiation force excitation versus shorter, periodic impulsive forces.

Methods: Both results of numerical simulation using finite element analysis, and actual phantom measurements are shown. The influence of different frequencies, duty ratios, shapes of pulses, distances between sources and properties of material are investigated.

Results: For imaging applications, crawling wave excitations from 70–150Hz with radiation force duty cycles from 50–2% are shown to provide crawling waves in the range of 1–20 microns over limited ROIs.

Conclusions: It was confirmed that the crawling waves can be imaged by the appropriate processing of displacement data. It was also observed that there are cases with favorable parameters in which crawling waves can be generated more effectively.

Acknowledgements: This study was partly supported by NIH grants 5 ROI AG016317 and 5 RO1AG29804.

References:

[1] Zhe Wu, Kenneth Hoyt, Deborah J. Rubens, Kevin J. Parker, Sonoelastographic imaging of interference patterns for estimation of shear velocity distribution in biomaterials, Journal of the Acoustical Society of America, vol. 120, no. 1, pp. 535–545, July, 2006.

* *indicates Presenter*

074 **MEASURING THE EXTENT OF TIME–HARMONIC SHEAR DEFORMATION USING THE OCTAHEDRAL SHEAR STRAIN.**

Matthew DJ McGarry[1], Elijah EEW Van Houten[2], Phillip R Perrinez[1], Adam J Pattison[1], John B Weaver[1,3], Keith D Paulsen[1].*

[1]Thayer School of Engineering, Dartmouth College, 8000 Cummings Hall, Hanover, NH, USA; [2]University of Canterbury, Private Bag 4800, Christchurch, 8410, NEW ZEALAND; [3]Radiology Department, Dartmouth–Hitchcock Medical Center, Lebanon, NH, USA.

Background: Time–harmonic actuation of tissue *in–vivo* encounters problems when the applied excitation fails to propagate completely through the tissue due to damping and/or insufficient coupling of the actuation device to the tissue of interest. Inducing shear waves in the brain is particularly problematic due to the cushioning effect of the skull, meninges and cerebrospinal fluid [1], which can result in rigid body motion of the brain with little shear deformation, therefore limited elasticity information.

Aims: The average value of octahedral shear strain [2] amplitude is used to quantify the "quality" of data collected in a time–harmonic MRE feline brain study, and this measure is compared with the effectiveness of material property reconstruction. In addition, images of the octahedral shear strain distribution are investigated as a means of extending the reach of strain imaging to time–harmonic data.

Methods: The octahedral strains are derived by transforming a general 3D state of strain onto the octahedral planes (planes forming an equal angle with each of the three principal strain directions). The total strain energy of the system is then equal to the sum of the individual strain energies resulting from the octahedral shear and normal strains, therefore these strains give a measure of the effective shear and volumetric deformation occurring at a point. A phase contrast MRI pulse sequence with motion sensitizing gradients [3] is used to measure full volume, complex–valued 3D motion amplitudes which are interpolated onto a tetrahedral finite element mesh. Each of the six individual strain components, ε_{xx}, ε_{yy}, ε_{zz}, γ_{xy}, γ_{xz} and γ_{yz}, is calculated as a constant value over each element to allow calculation of the octahedral shear strain, γ_{os}, and normal strain, ε_{on}, using:

$$\gamma_{os} = \frac{2}{3}\sqrt{(\varepsilon_{xx}-\varepsilon_{yy})^2+(\varepsilon_{xx}-\varepsilon_{zz})^2+(\varepsilon_{yy}-\varepsilon_{zz})^2+\frac{3}{2}(\gamma_{xy}{}^2+\gamma_{xz}{}^2+\gamma_{yz}{}^2)}, \text{ and } \varepsilon_{on} = \frac{1}{3}(\varepsilon_{xx}+\varepsilon_{yy}+\varepsilon_{zz}).$$

The magnitude of the complex valued γ_{os} was used in all subsequent analysis.

Results: MRE datasets from *in–vivo* feline brains with unstable reconstructions were identified as having significantly lower levels of octahedral shear strain compared to datasets with high quality reconstructions. This indicates the quality of the reconstruction is related to the level of shear deformation present. Images of the octahedral strain show good definition of areas of differing stiffness in both gelatin phantoms and in the brain.

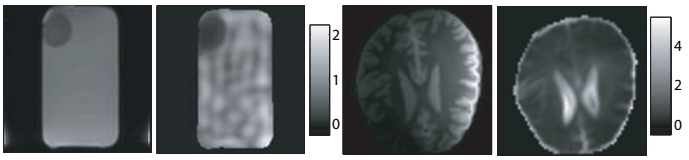

Figure 1: Images of a gelatin phantom with a hard inclusion (a), and formalin fixed *ex-vivo* human brain (b). MR magnitude images (left) and relative octahedral shear strain images (right)

Conclusions: Calculating the octahedral shear strain can be used as an indicator of the expected reconstruction quality of a time–harmonic MRE dataset. The method has extremely low computational overheads, therefore, could be used during an MRE exam to identify cases where the induced shear deformation is insufficient for reconstruction, and the setup could be altered accordingly. Images of the octahedral shear strain distribution are free of harmonic motion patterns, which pollute individual strain component images, show good definition of areas of higher stiffness and are of similar quality to quasi–static strain images. The ease of computation means they could be used as *a priori* elasticity information for a more sophisticated elastography algorithm, as has been suggested in the quasi–static case [4].

Acknowledgements: We gratefully acknowledge support from NIH/NIBIB R01-EB004632-03.

References:

[1] I. Sack, et. al., Non–invasive measurement of brain viscoelasticity using magnetic resonance elastography. NMR Biomed., 21: 265–271, 2008.
[2] N. Polakowski, E. Rifling, Strength and Structure of Engineering Materials, Prentice–Hall, New York, 1966.
[3] J Weaver, et. al., Magnetic resonance elastography using 3D gradient echo measurements of steady–state motion, Med. Phys, 28 :1620–1628, 2001.
[4] M. Doyley, et. al., Enhancing the performance of model–based elastography by incorporating additional *a priori* information in the modulus image reconstruction process Med Phys. Med. Biol., 51 95–112, 2006.

080 **A ROBUST REAL–TIME SPECKLE TRACKING ALGORITHM FOR ULTRASONIC ELASTICITY IMAGING.**

J Jiang[1] and TJ Hall[1].*
[1]Medical Physics Department, University of Wisconsin–Madison, Madison, WI, USA.

Aims: Ultrasonic strain imaging systems are rapidly gaining attention for breast tumor differentiation, despite the fact that consistently obtaining high quality *in vivo* strain images is a persistent challenge. To enhance the clinical usfulness of such systems, much research effort has been devoted to developing more sophisticated motion tracking algorithms. Our objective of this study is to develop a robust speckle tracking algorithm that can be used not only for real–time strain imaging but also potentially for high–quality displacement data acquisition during elastic modulus imaging in a clinical setting.

Methods: The proposed algorithm is a novel combination of our regularized speckle tracking algorithm [1] and a competitive (i.e. quality–based) seeding strategy proposed by Chen et al. [2] as a two step process. In the first step, displacement vectors in a coarse grid (typically every half centimeter) were obtained by optimizing using a cost function combining correlation and motion continuity constraints. Ultrasound echo data were often down–sampled by a factor of 4 in this step. To solve the optimization problem with a reasonable computational load, a dynamic programming technique that does not require iterations (i.e. Viterbi Algorithm) was used. [1] In the second step, only displacement vectors have sufficiently high correlation values in the initial search grid will be used as seeds for the subsequent predictive search for the entire region of interest (ROI) with a much reduced search range (i.e. a 3 by 3 sample grid). As demonstrated by Chen et al. [2], the competitive seeding in the second step will ensure that high–quality seeds carry priority. Radiofrequency (RF) echo data acquired from a Siemems Elegra unit with freehand scanning of *in vivo* breast and thyroid lesions were used to validate this method.

Results: Through processing of *in vivo* breast and thyroid tissue data (10 sets with different types of thyroid and breast lesions and roughly 1000 RF echo frames in total), our findings demonstrated that the new algorithm provides more consistent displacement estimates than our previous real–time algorithm [3] for *in vivo* clinical data. In particular, among five sets of thyroid lesion data with the presence of complex anatomy, the new algorithm is capable of tracking larger frame-average tissue deformation (0.5–1%) and increasing strain image consistency in a sequence of images. For instance, based on Displacement Quality Metric (DQM>0.6; [4]), a significantly longer sequence of high contrast strain images (e.g. 45 vs. 15 in one cancer dataset) could be obtained with the new algorithm compared to the our previously reported real–time algorithm [3]. We project that the new algorithm can achieve more than 15 frames/second with a 3cm by 3cm region of interest, which is sufficient to provide real–time feedback during *in vivo* elasticity imaging.

Conclusions: A modified block–matching algorithm integrated with dynamic programming (Viterbi algorithm) and a competitive seeding strategy [2] for motion tracking is presented. These preliminary results support the hypothesis that this novel algorithm may potentially make ultrasound–based elasticity imaging more easy to use by providing high quality strain imaging data in real–time. Our future work will be focused on extending this novel framework to full 3D motion tracking and to test that with *in vivo* volumetric breast lesion data.

Acknowledgements: This work was supported in part by the U.S. National Institutes of Health under Grants R01CA100373 and R21CA133488.

References:

[1] J. Jiang and T.J. Hall, "A Generalized Speckle Tracking Algorithm for Ultrasonic Strain Imaging Using Dynamic Programming", Ultrasound in Medicine & Biology, provisionally accepted, 2009.
[2] L. Chen, G.M. Treece, J.E. Lindop, A.H. Gee, and R.W. Prager, "A quality–guided displacement tracking algorithm for ultrasonic elasticity imaging", Med Image Anal, pp. 286–96, Apr 2009.
[3] J. Jiang and T.J. Hall, "A regularized motion tracking algorithm using dynamic programming for Ultrasonic Strain Imaging", IEEE Ultrasonics Symposium, Vancouver, Canada, 2006.
[4] J. Jiang, T.J. Hall and A.M. Sommer, "A novel performance descriptor for ultrasonic strain imaging: A preliminary study", IEEE Trans. UFFC, 2006.

* *indicates Presenter*

076 **HIGH QUALITY LATERAL STRAIN ESTIMATION USING TWO BEAM STEERING ANGLES.**

Hendrik HG Hansen[1], Tim Idzenga[1], Richard GP Lopata[1], Chris L de Korte[1].*
[1]Clinical Physics Laboratory, Radboud University Nijmegen Medical Center, Nijmegen, The NETHERLANDS.

Background: Strain imaging has been performed using 1D, 2D and 3D ultrasound data. In general, strain estimates along the ultrasound beam are more accurate than strain estimates perpendicular to the beam. This is mainly due to the lack of phase information in the directions perpendicular to the ultrasound beam. The beam direction can be changed by using beam steering. In this way, different projections of the 2D displacement field can be accurately measured since phase information remains available. Also using many of these projections, the lateral displacements and strains can be derived [1]. The choice of the projection angles is crucial. Large beam steering angles seem favorable, since more lateral information is contributing to the projections at those angles. On the other hand, the quality of the ultrasound data is lower for large beam steering angles due to the directional sensitivity of the transducer elements and the larger amount of filtering that is required for the removal of grating lobe artifacts [2].

Aims: This study investigates which combination of two beam steering angles enables deriving the most accurate horizontal (lateral) strain estimates.

Methods: A cube ($4x4x4cm^3$) with a cylindrical inclusion was constructed from polyvinyl alcohol (PVA) solutions. The cylindrical inclusion was centered in the cube, had a diameter of 1cm and a three times higher Young's modulus than the cube. 1% by weight SiC particles were added for scattering. Radiofrequency (rf) data of the inclusion phantom were acquired with a Philips SONOS 7500, equipped with a linear array transducer (11–3L, f_c = 8.7) and an rf–interface. Rf data were acquired for beam steering angles ranging from -30º to +30º with an incremental angle of 5º before and after application of 1%, 2%, 3% and 4% vertical compression. A coarse–to–fine 2D cross–correlation based algorithm was used to estimate the axial displacements in the various beam directions. For each possible combination of beam steering angles, horizontal displacements were reconstructed by using a projection formula. A 1D least squares strain estimator was applied to derive horizontal strains. Elastographic signal–to–noise and contrast–to–noise ratio's (SNR_e and CNR_e) were calculated for the horizontal strain images constructed for each angle combination and strain level to determine the most optimal angle combination.

Results: The most accurate horizontal strain estimates were observed when using data from beam steering angles that were symmetric around the vertical axis. SNR_e values were highest for beam steering combinations that used data from 15º to 20º. CNR_e values were highest for combinations that used data from 20º to 25º. Both observations were found for all strain levels. Data acquired at -20º and 20º at a compression of 2% revealed an increase of 5.0dB in SNR_e and 11dB in CNR_e with respect to a standard 0º acquisition for the horizontal strain images.

Conclusions: The quality of lateral displacements and strains can be increased by performing acquisitions at two large beam steering angles that are opposite in sign. Beam steering angles of -20º and 20º result in the most accurate results. The addition of a 0º acquisition for the determination of the axial strain components, would enable an accurate assessment of the full 2D strain tensor at an effective frame rate of about 40Hz, suggesting that the technique can be applied for actively deforming tissue as well.

Acknowledgements: The support of the Dutch Technology Foundation (STW) and Philips Medical Systems is acknowledged.

References:

[1] M. Rao, T. Varghese, "Estimation of the Optimal Maximum Beam Angle and Angular Increment for Normal and Shear Strain Estimation", IEEE Transactions on Biomedical Engineering, 2009, in press.
[2] H.H.G. Hansen, R.G.P. Lopata, C.L de Korte, "Non–invasive Carotid Strain Imaging Using Angular Compounding at Large Beam Steered Angles: Validation in Vessel Phantoms", IEEE Transactions on Medical Imaging, 2009, in press.

089 **A STUDY ON REGULATION FOR RECONSTRUCTION OF PHYSICAL QUANTITIES – MECHANICAL SOURCE AND THERMAL SOURCE/PERFUSION.**

C. Sumi[1], Y. Takanashi[1], K. Shimizu[1], R. Yamashita[1], Y. Ishii[1].*
[1]Sophia University, 7–1, Kioicho, Chiyodaku, Tokyo 102–8554, JAPAN.

Background: A robust non–invasive technique for reconstructing the thermal properties of living tissues – thermal conductivity, thermal capacity and thermal diffusivity – and thermal quantities such as thermal source/sink and perfusion for diagnosis, and monitoring and planning thermal treatments such as a high-intensity focused ultrasound (HIFU) and interstitial rf or microwave electromagnetic coagulation therapy have been reported by us [1,2]. Internal tissue temperatures can be measured using ultrasonic strain imaging [3] or magnetic resonance imaging. Previously, we dealt with the case of performing reconstruction after stopping heating and perfusion [4]. However, the region of interest (ROI) may include a thermal source, and the perfusion cannot always be stopped. In such cases, by increasing the independent temperature data, the thermal source and perfusion can be reconstructed together [1,2].

In conjunction with HIFU, we also perform reconstruction of the mechanical source together with that of a shear modulus [5]. Although by performing the estimation of a point spread function at the focus position, such thermal source or mechanical source will be estimated; we also extended our previously developed shear modulus reconstruction methods (A to F [6]) such that arbitrary internal mechanical sources can be reconstructed together (i.e., expressed as a static or dynamic pressure or a force vector). Although all the original methods can deal with arbitrary mechanical sources existing outside an ROI (e.g., HIFU, static compressor, vibrator, heart motion, pulsation, etc.), if a mechanical source exists in the ROI, reconstruction of shear modulus cannot be achieved. Thus, this extension will also increase the application of shear modulus reconstruction.

Aims: Through the simulations, the reconstruction accuracies are improved for thermal source/perfusion and mechanical source together with those for thermal and mechanical properties. In this study, the effect of regulation parameter [1] specifically is examined. That is, when the orders of magnitudes of the coefficients multiplied by thermal and mechanical properties and target physical quantities markedly differ from each other, a constant is multiplied by the respective coefficient such that the orders become the same (i.e. eigenvalues of matrix to be inverted are regulated).

Methods: Thermal: The same cubic tissue phantoms (50.0mm sides) were simulated as those used in [2]. It contained a spherical region (dia=6.0mm), which had a conductivity and a specific heat twice those of the surrounding medium, i.e., 1.0 vs 0.5W/(mK), and 8,400 vs 4,200J/(Kkg) (uniform density, 1,000kg/m^3). The phantom had a uniform temperature of 36.0. The time series of temperature distribution was calculated by the successive over–relaxation (SOR) method. (I) As shown in Figure 1a in [2], a spherical heat source Q of 0.1 to 1.0W (dia=6.0mm) was set at t=0sec such that it overlapped with the inclusion. (II) Next, the spherical heat source was changed by perfusion. Pennes' model was used (blood temperature, 36.0; specific heat cb, 3,770J/Kkg). The temperature of one surface of the phantom was increased by 6.0. For each perfusion coefficients w=0.1 to 10kg/m^{3}K, the reconstruction of wcb was performed. Mechanical: Similarly to [5], a tissue phantom (e.g., 50mm/side cube) and mechanical sources were also simulated using SOR method. For instance, a spherical source (5mm dia.) that partially overlapped a spherical region having a different shear modulus from that of the surrounding region was used (e.g., 2 vs 1 x 10^{5}N/m^2). For both simulations, noise was not added to temperatures nor were strains.

Results and Conclusions: For all reconstructions, proper regulations increased the reconstruction accuracies and stabilities together with the convergence speeds of iterative solutions (conjugate gradient method). For instance, when w=1.0kg/m^{3}K, Table I shows the relationships between the regulation parameter used for unknown wcb and statistics (means and SDs) obtained in the spherical region (1.e4 is the best). Effects of the regulation on measurement noise will be examined as well as those of regularization [1] in the near future.

Table 1: Regulation Parameter vs Means and SDs.

Regulation parameter	Conductivity [W/mK] Org., 1.000	Capacity e6 [J/m^{3}K] Org., 8.40	Perfusion wcb e3[J/m^{3}sK] Org., 3.77
1.	0.799 (0.057)	4.49 (0.02)	1.66 (3.08)
1.e3	0.914 (0.047)	8.20 (0.94)	4.06 (1.31)
1.e4	0.951 (0.045)	8.23 (0.88)	3.80 (1.74)

References:

[1] C. Sumi et al., Phys. Med. Biol. 52, 2845, 2007.
[2] C. Sumi et al., "Thermal property reconstruction –Reconstruction of thermal source and perfusion", Proc. 7th ITEC, full paper version, 2008.
[3] C. Sumi et al., Jpn. J. Appl. Phys. 46(7b), 4790, 2007.
[4] C. Sumi et al., Acoust Imag 29, 153, 2008.
[5] C. Sumi et al., "Mechanical source reconstruction", Proc. 7th ITEC, full paper version, 2008.
[6] C. Sumi et al., Acoust Imag 29, 59, 2008.

* *indicates Presenter*

112 **DETERMINATION OF ELASTIC PROPERTIES AND HEIGHT PROFILE OF LAYERED BIO–MATERIALS WITH VECTOR–CONTRAST SCANNING ACOUSTIC MICROSCOPY USING POLAR DIAGRAM IMAGE REPRESENTATION.**

Esam T. Ahmed Mohamed[1], Albert Kamanyi[1], Moritz von Buttlar[1], Reinhold Wannemacher[1], Kristian Hillmann[1], Wilfred Ngwa[2] and Wolfgang Grill[1].*

[1]Institute of Experimental Physics II, University of Leipzig, Leipzig, GERMANY; [2]Physics Department, University of Central Florida, Orlando, Florida, FL 32816, USA.

Reprinted from 2008 Proceedings:

Background: Acoustic phase and magnitude contrast data represented in a polar plot have been shown to provide a direct way to elucidate the elastic properties of sufficiently planar and homogenous biomedical samples of variable thickness [1]. The method is also applied to get non–contact mapping of the topography of thin film layered biomedical samples.

Aims: Non–contact mapping of the height and determination of the elastic properties of thin layered biomedical samples using phase and magnitude data represented in a polar graph.

Methods: An In–focus image of chitosan thin film deposited on glass substrate was taken using a vector contrast phase–sensitive acoustic microscope (PSAM) [2] working at 1.195 GHz.

Results: The variation in the grey value of the reflected signal was taken along the horizontal straight black line across the phase and amplitude images (Figure 1). These data were plotted in a polar graph (Figure 2). The reflectivity of the different points along the surface of the sample depends spatially on the thickness of the sample. Highest reflectivity comes from bare glass and is represented at the top of the polar graph by a point corresponding to zero phases. The reflectivity decreases along the spiral curve till its minimum value near the center of the polar plot which corresponds to maximum thickness. The attenuation increases with increased thickness. The interferences between reflections from interfaces and reflections within the sample are represented by the spirals at which the polar graph reverses its direction to delineate zones of equal acoustic path lengths and then continues toward the direction of increased thickness. The experimental data were fitted with a model based on the geometrical ray theory to get the acoustic velocity, attenuation and density of the material. These parameters were then used to calculate the shear viscosity and the elasticity (Young's) modulus of a chitosan thin film. Since the variation of the reflectivity depends basically on the variation of the thickness, the thickness of each point is deduced resulting in the height profile of the sample (Figure 3).

Conclusions: The method provides a direct way to find the acoustic parameters from which the elastic properties are derived. In addition, it allows height profiling of the thin films.

References:

[1] Ahmed Mohamed. E, et al., Determination of mechanical properties of layered materials with vector contrast scanning acoustic microscopy using polar diagram image representation. Proc. SPIE Vol. 6935, 69351Z, 2008.

[2] Grill. W, Hillmann. K, Würz. K and Wesner. J, Advances in Acoustic Microscopy, Springer Publisher, New York, 168–175, 1996.

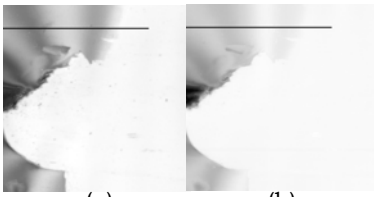

(a) (b)

Figure 1: Images in magnitude contrast (a) and phase contrast (b) of a chitosan layer of variable thickness on a glass substrate. Magnitude and phase data were taken along the horizontal black line indicated in the images and are displayed in a polar representation in Figure 2.

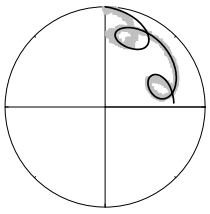

Figure 2: Polar diagram of the magnitude and phase of the reflected signal along a horizontal straight line across the images of a thin film of chitosan (grey squares) and the fit of the experimental data (black solid line).

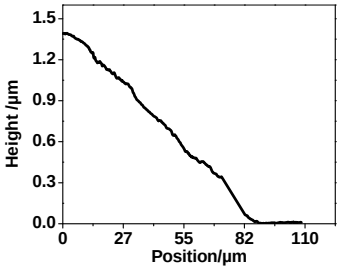

Figure 3: Height profile of the chitosan thin film drawn from the data represented in the polar graph in Figure 2.

Westduin Conference Center Floor Plan

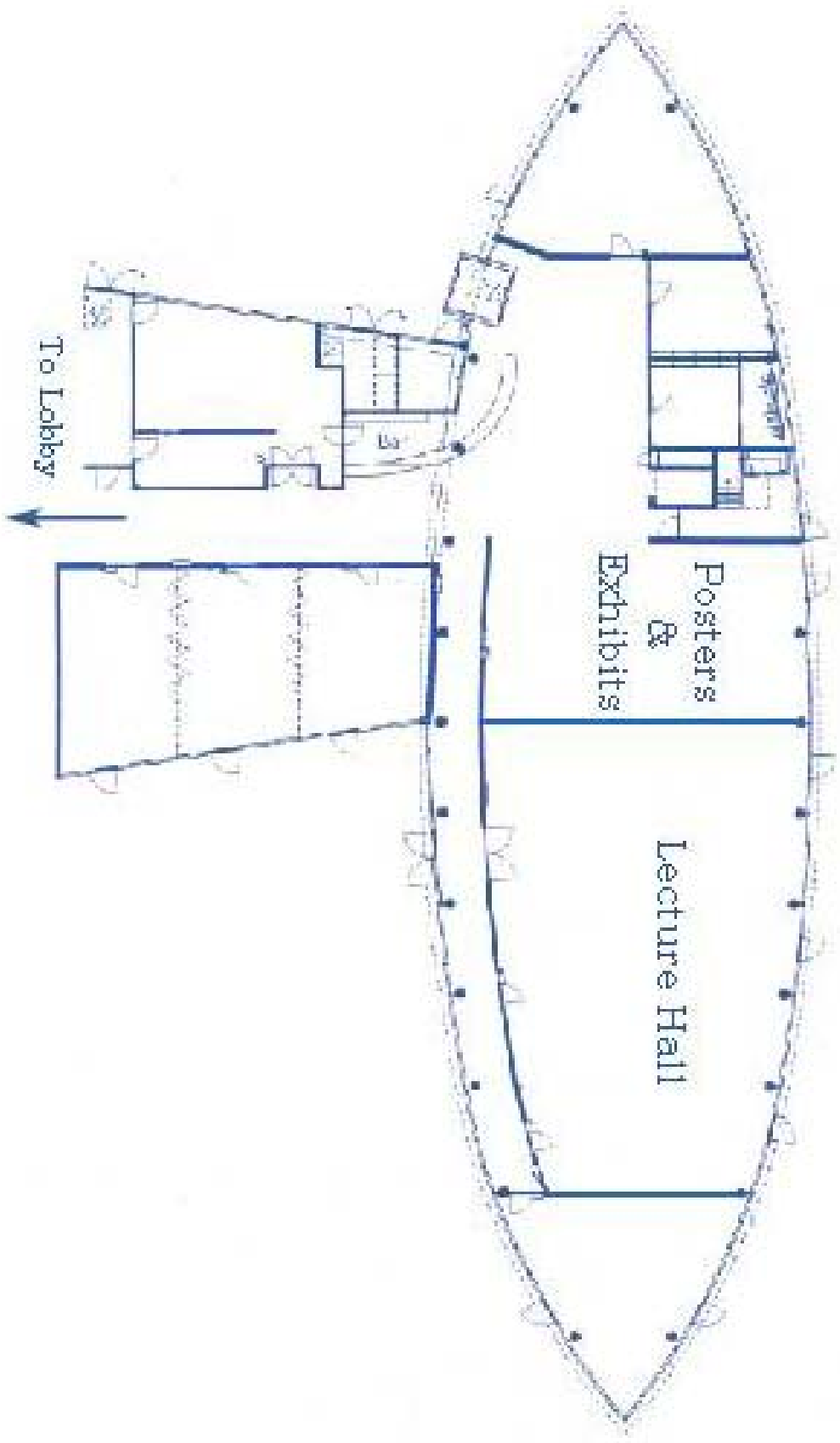

Please Fill Out Both Sides

Conference Evaluation and Questionnaire

OVERALL CONFERENCE

	Poor		Mid		Excellent
Overall Conference Evaluation	1	2	3	4	5
General comments:					

SCIENTIFIC PROGRAM

	Poor		Mid		Excellent
Quality of the Presentations	1	2	3	4	5
Relevance of Presentations to the Conference's Theme	1	2	3	4	5
Time Allotted for Presentations	1	2	3	4	5
Time Allotted for Discussion	1	2	3	4	5
Poster Session	1	2	3	4	5
Tutorials	1	2	3	4	5
Equipment Exhibit	1	2	3	4	5
Student Participation	1	2	3	4	5
Additional comments:					

CONFERENCE MATERIALS

	Poor		Mid		Excellent
Printed Proceedings Book	1	2	3	4	5
CD Proceedings	1	2	3	4	5
Other Registration Materials	1	2	3	4	5
Additional comments:					

CONFERENCE FACILITIES & SOCIAL PROGRAM

	Poor		Mid		Excellent
Lecture Hall	1	2	3	4	5
Registration Desk	1	2	3	4	5
Meals: Dining facilities	1	2	3	4	5
Conference Breakfasts and Lunches	1	2	3	4	5
Conference Dinner and Concert	1	2	3	4	5
Coffee Breaks	1	2	3	4	5
Opening Dinner Reception	1	2	3	4	5
Closing Pizza Party	1	2	3	4	5
Audio–Visual: Screen Visibility	1	2	3	4	5
Sound Level	1	2	3	4	5
Presentation Transition	1	2	3	4	5
Wireless Internet Connectivity:	1	2	3	4	5
Additional comments:					

Please Fill Out Both Sides

Conference Evaluation and Questionnaire

VENUE AND HOTEL

	Poor		Mid		Excellent
Venue – Vlissingen, The Netherlands and Environs	1	2	3	4	5
Would you return to this city?	Yes		Perhaps		No
Area Attractions	1	2	3	4	5
Hotel: Overall	1	2	3	4	5
Reservations	1	2	3	4	5
Transportation and Accessibility	1	2	3	4	5
Reception and Check–In	1	2	3	4	5
Accommodations	1	2	3	4	5
Facilities	1	2	3	4	5
Parking	1	2	3	4	5
Would you return to this hotel?	Yes		Perhaps		No
Additional comments:					

CONFERENCE ADMINISTRATION

	Poor		Mid		Excellent
Website	1	2	3	4	5
Registration off–site	1	2	3	4	5
Registration on–site	1	2	3	4	5
Administrative staff	1	2	3	4	5
Correspondence	1	2	3	4	5
Additional comments:					

GENERAL INFORMATION

I am a Returning Delegate	Yes		No
I plan to attend the next conference	Yes	Perhaps	No
and present a paper(s) / poster(s)	Yes	Perhaps	No
Other(s) from my lab would attend the next conference	Yes	Perhaps	No
and he/she / they would present a paper(s) / poster(s)	Yes	Perhaps	No
How did you learn of this conference? (Check all that apply)	☐ Email Announcement		
☐ Internet	☐ Website		
☐ Other	☐ Colleague		
Tutorial Topic Suggestions for next year:			
Additional Comments:			

If you would be willing to host the Conference in your city, please give your name to the Conference Staff.

Questions or comments are welcome at any time at <elasticity.conference@uth.tmc.edu>

Thank You!